2021

Carbon Nanotube-Coated Scaffolds for Tissue Engineering Applications

Soham Dipakbhai Parikh
Wright State University

CARBON NANOTUBE-COATED SCAFFOLDS FOR TISSUE ENGINEERING APPLICATIONS

A Dissertation submitted in partial fulfillment of the
requirements for the degree of
Doctor of Philosophy

by

SOHAM DIPAKBHAI PARIKH

M.S. Sardar Patel University, India, 2013

2021

Wright State University

WRIGHT STATE UNIVERSITY

GRADUATE SCHOOL

April 21, 2021

I HEREBY RECOMMEND THAT THE DISSERTATION PREPARED UNDER MY SUPERVISION BY Soham Dipakbhai Parikh ENTITLED Carbon Nanotube-Coated Scaffolds for Tissue Engineering Applications BE ACCEPTED IN PARTIAL FULFILLMENT OF THE REQUIREMENTS FOR THE DEGREE OF Doctor of Philosophy.

_____
Sharmila M. Mukhopadhyay, Ph.D.
Dissertation Director

_____
David R. Ladle, Ph.D.
Program Director

_____
Barry Milligan, Ph.D.
Vice Provost for Academic Affairs
Interim Dean of the Graduate School

Committee on Final Examination:

_____
Sharmila M. Mukhopadhyay Ph.D.

_____
Courtney E.W. Sulentic, Ph.D.

_____
David R. Cool, Ph.D.

_____
Saber Hussain, Ph.D.

_____
David R. Ladle, Ph.D.

_____
Tyler Nelson, Ph.D. (non-voting)

ABSTRACT

Parikh, Soham Dipakbhai, Ph.D., Biomedical Sciences Ph.D. Program, Wright State University, 2021. Carbon Nanotube-Coated Scaffolds for Tissue Engineering Applications

Carbon Nanotubes (CNTs) have beneficial properties for cell scaffolding, which has translated into effective growth of bone, muscle, and cardiac cells. However, loose carbon nanotubes can cause *in vivo* toxicity. To reduce this risk, our team has developed biomimetic scaffolds with multiscale hierarchy where carpet-like CNT arrays are covalently bonded to larger biocompatible substrates. In this study, we have tested such scaffolds in two distinct types of biomedical applications involving glioblastoma and keratinocyte cells.

The growth of glioblastoma (GBM) cells on our CNT-coated biomimetic scaffolds was evaluated to check their suitability as a potential chemotherapy-loaded implant for GBM patient treatment. We utilized CNT carpets on flat carbon fiber cloths and porous carbon foams and identified differing effects on cell growth by altering the surface features, such as hydrophilicity. Synthesized CNT-coating is naturally superhydrophobic and prevents GBM cell growth initially, but over time cell proliferation increases to normal levels. When the CNT surface was modified to be hydrophilic, GBM cells followed a normal growth curve. These findings

support the feasibility of developing a CNT-coated chemotherapy-loaded implant for post-surgical resection in GBM patients.

Keratinocyte cell growth on CNT-coated carbon fiber cloth was investigated to assess its compatibility as a skin graft material for wound healing applications. Due to its covalently linked structure, biocompatibility, functionalizable topological features, and extensive surface area, CNTs could provide a suitable surface for skin cell proliferation. CNTs can also provide directionality, which can be important for supporting scaffolds used in wound healing applications. This project aimed to determine whether the use of CNTs attached to carbon scaffolds are capable of sustaining keratinocyte growth for future development of novel skin graft development. Studies demonstrated biocompatibility for keratinocyte growth as shown by cell proliferation, cell migration, and cytotoxicity analysis. Moreover, the CNT-coated scaffolds provided cytoprotection against environmental stressors such as Ultraviolet-B rays. We also found that keratinocyte cell growth can be tailored through the length of CNT coating and wettability control. These results point to the benefits of designing CNT-coated scaffolds for strategic wound healing applications. These results strongly support the future potential of these bio-mimetic scaffolds in tissue engineering.

TABLE OF CONTENTS

FIGURES

TABLES

Acknowledgments

This work would have been impossible without the guidance and support of many people who have helped me throughout my journey.

I would like to first thank my advisor, Dr. Sharmila Mukhopadhyay who guided me throughout my Ph.D. program and helped me with every step of the way. Advise and opportunities from Dr. Mukhopadhyay has helped me become a better researcher. I also would like to thank Dr. Debra Mayes for guiding me through my research project. Furthermore, I was fortunate to have a fantastic committee and the work wouldn't have been possible without their guidance and feedback. I really owe them a lot. Thank you, Dr. Cool, for your helpful discussions; Dr. Saber for helping me when I needed it the most; Dr. Ladle for being a great microscopy advisor and Dr. Nelson for helping me with some of the essential reagents for the project. Without Dr. Nelson's help, some of the experiments would not be possible. Lastly, I want to thank Dr. Courtney Sulentic, who not only helped me improve my critical thinking and research acumen but went above and beyond to ensure my research project gets conducted in the best way possible. She not only helped me become a better scientist but also a better person and I can't thank her enough for the support.

I would also like to thank the Biomedical Sciences Program, Graduate School, Graduate Student Assembly, and the Material Advantage program for their financial support. I would particularly like to thank Dr. Mill Miller and Karen Luchin for making

the transition from a different country very easy and helping me throughout the program. I also would like to thank neighboring labs, especially Dr. Travers Lab and Dr. Kemp lab for all the help and for letting me use their equipment for the project.

I would like to also thank all my past and present lab members. I am especially thankful to Dr. Wenhu Wang, Kimia Kiaei, Mili Bhakta. Clayton Allex-Buckner who supported me every step of the way and helped me refine my research project. It is really a privilege to know all my lab-mates. I also thank Gregory Wilt for his assistance in the department. Also, I thank Raji, Polash, Ishita, Sara, Hannah, Jenanie, and all other friends and colleagues. Without them, I would not be where I am right now.

Lastly, my deepest thanks to my wife, Krushangi Shah who always put everything aside and helped me when I needed it. She has helped me with every step of the way, and I can't imagine how difficult it may have been without her. I would also like to thank my parents, Dr. Deepak Parikh and Geeta Parikh, and my brother, Madhav Parikh for supporting me mentally and financially and for supporting my decision to go study abroad. I would also like to mention and thank my grandma who is no longer with us. I also would like to thank my in-laws; I sincerely convey my gratitude to them. Thank you Krushangi and all my family members for your unconditional love and support!

Dedication

This dissertation is dedicated to Dr. Courtney Sulentic and Krushangi Shah for their endless support and encouragement.

OVERVIEW

The objective of this study is to understand the potential of using biomimetic carbon scaffolds with multiscale hierarchy for tissue engineering applications. More specifically, we have tested such scaffolds in two distinct types of biomedical applications involving glioblastoma and keratinocyte cells. This thesis is divided into two sections:

Section-1 focuses on how the hierarchical CNT-coated scaffolds were prepared, functionalized, and characterized. We prepared CNT-coated scaffolds using two types of substrate materials: reticulated vitreous carbon (RVC) foams, which are rigid porous solids with three-dimensionally connected struts, and carbon fiber fabric (CFC) which is a flexible woven fiber cloth. These hierarchical materials were surface functionalized to modify their water wettability and tested for two distinct types of biomedical applications.

Section-2 focuses on assessing the effects of carbon nanotubes and their surface functionalization on cell growth, cytotoxicity, and biocompatibility in order to understand the surface features that can modulate cell growth for the two targeted applications. In the first study, the hierarchical scaffolds were assessed for glioblastoma interaction,

which can help us understand the disease pathophysiology and to prepare targeted chemotherapy-containing scaffolds after tumor incision. In the second study, CNT-coated fiber cloths were investigated to understand their potential use in band-aid-like wound healing applications.

Section 1: HIERARCHICAL NANO-STRUCTURED CARBON SCAFFOLDS

1.1 Introduction and Background

1.1.1 Carbon Nanotubes

Carbon can react with oxygen, silicon, sulfur, and other metals at extremely high temperatures, but it is essentially inert at room temperature. For example, Silicon Carbide can be formed at temperatures above 1400°C. Because of its unique bonding properties, carbon has many different forms including carbon nanostructures.

Orbital hybridization is the concept that explains the bonding of electrons in molecules. The electronic configuration of carbon is $1s^2$ $2s^2$ $2p^2$ and it can acquire either sp, sp^2, or sp^3 hybridization which essentially determines its molecular geometry. When sp^2 hybridized carbon atoms are arranged hexagonally, they make tube-like graphene cylinders called nanotubes as shown in *Figure 1*. Single rolled-up graphene sheets construct long, nanoscale cylinders with diameters of 0.4 nm (inner) and 2 nm (outer) known as single-walled carbon nanotubes SWCNTs. Multiple coaxial and concentric rolled-up graphene sheets make up the Multi-Walled Carbon Nanotube (MWCNT) structures with 1-3 nm (inner) and 2-100 nm (outer) diameter (*Figure 1*) [1,2].

Carbon nanostructures, mainly CNTs are very commonly used as sensors, electronics, energy storage, and drug delivery systems [3,4]. Due to their hollow structure, CNTs can encapsulate the drugs and can be used for targeted drug delivery [5]. Sidewalls and tips are also the surfaces where cargo can be attached to CNTs. For example, CNTs have been used as a vaccine delivery system by linking peptides on the sidewalls [6]. CNTs have also been used as a nanoinjector system to deliver quantum dots into live cells by utilizing tips of carbon nanotubes without causing any cell damage [7].

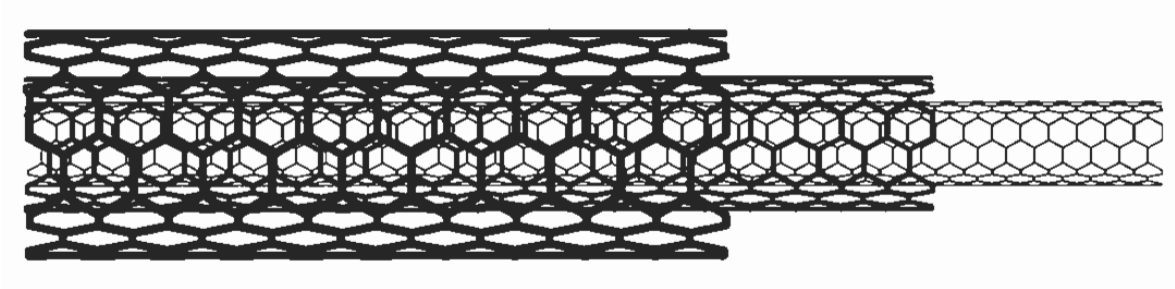

Figure 1 ***Structure of multi-walled carbon nanotubes***

1.1.2 Properties and Applications of Carbon Nanotubes

1.1.2.1 Mechanical Properties

In addition to their flexible nature, carbon nanotubes provide approximately 100 times more tensile strength (200GPa) than steel of the same thickness [8]. Carbon nanotubes are large structures and the atoms are interlinked through covalent bonding, making them extremely strong in nature. CNTs are also extensively lighter than steel and have roughly 1/6th density compared to steel. Young's modulus of a material is indicative of the stiffness of a material and CNTs have similar Young's modulus as diamond and have almost 500% higher Young's modulus than steel [9,10].

CNTs are resistant to damage through physical stresses and are also resistant to chemical stresses, making them mechanically robust and chemically inert material. Such unique properties make CNTs a very appealing candidate as a lightweight structural material.

1.1.2.2 Electrical Properties

Carbon nanotubes have extremely low longitudinal resistivity as electrons can only move in the axial direction in CNTs. As described earlier, CNTs are rolled-up sheets of graphene atoms. How this rolling-up direction takes place decides the orientation and electrically conductivity of the CNTs. Depending on such orientations, CNTs can be either metallic or semiconducting. All CNTs with armchair orientation are of metallic species and some armchair CNTs even have superior electrical conductivity compared to other metals [11]. A 30-degree rotation of the graphene sheets would result in an altered orientation and CNTs could acquire the zigzag orientation. Two-thirds of the chiral and zigzag nanotubes are semiconducting in nature [12–14]. Research is also being done on the separation of metallic and semiconducting CNTs to be used for specific electrical applications [15,16].

1.1.2.3 Thermal Properties of CNTs

Similar to electrical conduction, thermal conduction in CNTs also happens through the axial direction and limited heat exchange occurs perpendicular to the axis [17]. The thermal conductivity of CNTs ranges around 3000-3500 W mK^{-1} [18,19]. The thermal conductivity of CNTs is better than bulk diamond and graphite at room temperature and it makes CNTs the first nanostructures with a higher thermal conductivity than bulk diamond and graphite. In a periodic, elastic configuration of atoms or molecules, collective oscillation or vibrational motion takes place in all the

atoms or molecules in a corresponding lattice. This vibration of the atomic lattice is measured as phonons. Due to the graphene arrangement in CNTs, thermal energy transport through CNTs is believed to be predominantly through phonons [20]. These phonons can scatter in the case of crystallographic defects or external contamination such as catalyst used for CNT preparation or amorphous carbon and can create resistance in thermal conductivity at higher amounts inducing increased thermal resistance [19,20]. Our lab has also shown that increased thermal resistance is also observed with increasing the height of the CNT carpet [21]

1.1.2.4 Adsorption Properties of CNTs

Adsorption is the process in which a solid adsorbent receives either gas, solution, or solute and the molecules attach on the surface as a thin film. CNTs due to their hollow tubular morphology and substantially high surface area provide exceptional adsorption capacity [22,23]. Carbon nanotubes are easier to use, provide increased adsorption, quicker equilibrium times, and more efficient reuse potential than activated carbon which is widely used for adsorption applications [24,25]. In addition to that, CNTs can also be used to capture microorganisms or a specific contaminant and can provide a better alternative for future adsorption and water purification devices [26]. Due to their functionalizable properties and inert nature, CNTs can be used in a wide variety of adsorption-based applications.

1.1.3 Prior Work on Applications of CNTs

Due to the aforementioned properties, CNTs have the potential to be used in a wide variety of applications including but not limited to catalysis, field emission, energy storage, biosensors, flexible electronics, air filtration, water purification, conductive

tapes, thermal conductors, energy storage, thermal materials, structural applications, and biomedical applications.

1.1.3.1 Biosensors

Biosensors are usually comprised of a sensing element and a signal transducer. Sensing elements usually are biological elements such as protein, antibodies, enzymes, nucleic acid, bacteria, microorganisms, etc. For a biosensor, the transducing device is a crucial feature that produces the output signal which could be in electrical, magnetic, optical, or thermal forms. In recent years, advances in the world of nanotechnology have given rise to new and advanced transducers for biosensors. Carbon nanotubes due to their high aspect ratio, enhanced surface area, high electrical conductivity, and ability to be functionalized with different functional groups are very sought after for electrochemical biosensors. CNT-based biosensors have been successfully used for a wide range of applications ranging from the detection of drugs in biological samples and blood glucose monitoring to the detection of bacteria and microorganisms [27–29].

1.1.3.2 Water Purification and Catalytic Support

There has been a growing trend to use materials with a high surface area for water treatment applications. Nanoparticles are being increasingly used in conjugation with porous materials in order to provide increased surface area for the potential adsorption of contaminants. Carbon-based materials such as activated carbon, carbon fibers, and carbon-based nanomaterials due to their increased surface area nature can be extremely useful for applications such as water purification or decontamination. In addition to the increased surface area, CNTs can also enhance the adsorption and desorption properties of a material [30]. CNT-based materials can also be used with

nanoparticles to achieve substantially increased catalytic effects for water treatment [31,32].

1.1.3.3 Composites

CNTs make an excellent addition to composites due to their mechanical strength, high aspect ratios, and easy to functionalize nature, which can increase their interaction with the material. Additionally, CNTs can also provide some extremely unique material properties as they can be very flexible in nature and have excellent thermal and electrical conductivity. Plus, they are also non-corrosive. Due to such advantages, CNTs can be used in a wide variety of composites as additives and can be combined with various materials based on the type of application. Due to its advantages for structural applications, CNTs can be used to reinforce various materials, particularly carbon-based for lightweight yet high-performance structural materials. Some of the examples include the use of CNTs in the aerospace, railroad, automotive, and sporting goods industries [33,34]. In addition to this, CNTs can also be aligned and bundled as a fiber to manufacture carbon nanotube high-performance fibers with superior properties even on a macroscopic level [35].

1.1.3.4 Electronics

Electronics based on carbon nanotubes have been identified to be one of the most suitable candidates for advancement in energy efficiency and computing power [15]. In terms of electrical conductivity, CNTs can either be metallic or semiconducting, based on the configuration of the CNTs. In the case of armchair orientation, there is no gap in between conduction and valence bands and CNTs acquire electrical properties similar to metals. In the majority of chiral and zigzag forms, there is an energy gap in between the conduction and valance bands and the CNTs have

semiconducting properties. Ever since an integrated circuit was built around a single CNT [36], its use in flexible electronics has increased tremendously. CNTs are being used in integrated circuits [37], light-emitting diodes [38], touch panels [39], supercapacitors [40], and many more flexible electronic devices. Traditionally used silicon-based transistor systems can be made with CNTs, which can drastically improve the performance and energy use of the device. Novel CNT-based transistors are also reported to be potentially used in the manufacturing of next-generation computer systems [16].

1.1.4 Fabrication Methods used for CNT Deposition

By attaching a layer of carbon nanotubes to a substrate, an enhanced hierarchical interface can be created. This will allow for a structure that can be modified both at micro and nano levels. However, creating a hierarchical structure using CNTs could also be a huge challenge considering the geometry and composition of a substrate can highly alter the growth of CNTs [41,42]. There are various ways CNTs can be fabricated: arc discharge, laser ablation, flame synthesis, high-pressure carbon monoxide, and chemical vapor deposition. The three most common methods of producing CNTs are discussed below.

1.1.4.1 Arc Discharge

The first CNTs were made using arc discharge in 1993 [43]. In this method, a closed chamber filled with inert gas is used. Inside the chamber, two graphite electrodes are placed, and DC current is applied at extremely high temperatures around 4000°C to make an arc between the two electrodes. As a result, one graphite electrode gets vaporized and newly generated CNTs deposit on the other electrode.

Generally, by this method, MWCNTs can be produced without any catalyst but mixed metal catalysts will be required for making SWCNTs.

1.1.4.2 Laser Ablation

This method was first utilized in 1995 by the Smalley lab to produce CNTs [44]. As the name suggests, a high-power laser pulse is used in this technique in order to ablate and vaporize carbon at high temperatures around 1200°C from a target made up of graphite. This is done inside a flow tube and the resultant CNT vapors are collected on the walls of the tube. By this method, very high purity (~90%) SWCNT can be manufactured, and the diameters of the nanotubes generated are also consistent. Similar to arc discharge, by this method, MWCNTs can be made without metal catalysts and SWCNT production requires metal catalysts.

1.1.4.3 Chemical Vapor Deposition (CVD)

This is one of the most widely used methods to produce CNTs due to the simplicity, versatility, low cost, higher CNT yields, and various controllable optimization steps [45]. This method uses a liquid or gaseous form of hydrocarbon source, metal catalyst, and inert gas along with high temperature in a tube furnace. The metal catalyst decomposes the hydrocarbon source into CNTs, and the nucleation begins from the metal catalyst particles. This CVD method can be used for the production of both SWCNTs and MWCNTs and the yield can be optimized to be high or low. In addition to that, both aligned and non-aligned forms of CNTs can be produced by optimizing catalysts used in the method. Hence, the desired morphology of CNTs can be achieved and optimized on pre-defined surfaces by using the CVD technique.

The Mukhopadhyay lab identified that the growth of the CNTs on irregular surfaces can be enhanced and made more uniform by coating the surface with a silica

buffer layer first. This SiO_2 buffer layer was achieved by Mukhopadhyay *et.al.* [46] using oxygen plasma-enhanced chemical vapor deposition (PECVD) and then subsequent CNT-coating was done by floating catalyst-based thermal chemical vapor deposition method. This process could lead to increased impurities but that can be addressed by additional purification steps [47]. The other disadvantage of using this method is the substrate size is limited by the chamber area. This mode of CNT-coating was used for this work. More details about the method are discussed in the materials and methods section of this chapter.

1.1.5 Wettability

Wettability is the interaction of a liquid to sustain contact with a solid. When a liquid interacts with a solid surface, there are two kinds of forces that determine how the interaction will take place. These forces are adhesive and cohesive in nature. The adhesive force is between the affinity of the liquid to interact with the solid surface and the cohesive force is within the liquid itself. Liquid always adjusts its shape to expose the smallest surface area possible. In the case of strong adhesive forces, the liquid will spread out and form a thin sheet over the solid surface. This process is also called wetting (*Figure 2*). If the cohesive forces predominate, the liquid will minimize the surface interaction with the solid surface and will form spherical beads instead.

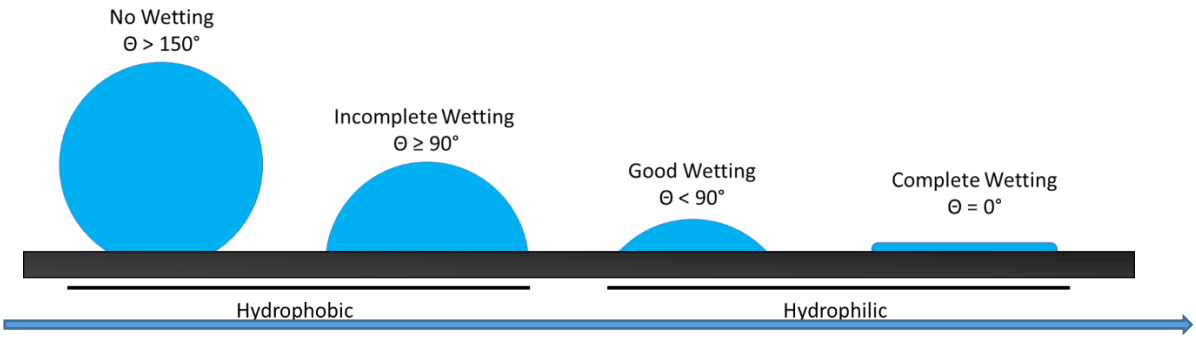

Figure 2 ***Wetting and contact angle.***

Decreasing contact angle due to decreasing cohesive forces and/or increasing adhesive forces

1.1.5.1 Wetting on a Surface

When the contact angle is high (>90°), it indicates that surface wetting by liquid is not favorable, and the liquid may thus remain in a droplet and minimize surface interaction. This is also known as incomplete/partial wetting or non-wetting. If the liquid is a water droplet, it can also be termed as a hydrophobic surface (repels water). If the contact angle is beyond 150°, the surface can be termed superhydrophobic. In such a case, there is almost no contact between the droplet and the surface. A lower contact angle (<90°) on the other hand is representative of wetting, and it can also mean that the liquid-surface contact is favorable. Such surfaces with high water affinity are called hydrophilic.

Surface tension can be defined as the cohesive force between molecules at the material surface. Due to surface tension, liquid always assumes a configuration where it occupies the lowest surface area. Surface energy is the intermolecular force between the molecules at the solid surface. The determination of how the interaction between liquid and solid surface will take place can be done by the spreading parameter, which can be calculated using the following equation:

$$S = [E_{substrate}]_{dry} - [E_{substrate}]_{wet}$$

Here, S is the Spreading parameter, $[E_{substrate}]_{dry}$ is surface energy when the substrate is dry and $[E_{substrate}]_{wet}$ is the surface energy when the substrate is wet.

If the spreading parameter is positive, liquid spreads to lower its surface energy and wetting will take place. If S is negative, there will be incomplete/partial or no wetting.

1.1.5.2 Young's Equation for Contact Angle

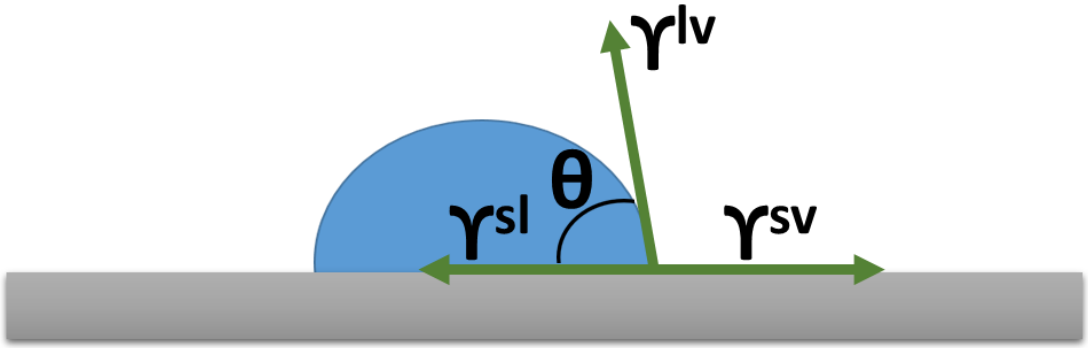

Figure 3 ***Young's contact angle model.***

Contact angle measurement of a drop on an ideal solid surface. The young equation assumes that the surface topography is smooth and it is chemically homogenous. Reprinted from "Multi-walled carbon nanotube carpets as scaffolds for U87MG glioblastoma multiforme cell growth" by Parikh, S. D., Dave, S., Huang, L., Wang, W., Mukhopadhyay, S. M., & Mayes, D. A. (2020). Materials Science and Engineering: C, 108, 110345. Copyright by Elsevier

The wettability of a solid surface for a liquid can be determined by measuring the contact angle of the liquid droplet onto the substrate. For an ideally smooth surface, Young's equation [48] determines this inherent contact angle of a liquid drop which can be calculated by using this formula:

$$cos\theta = (\gamma_{SV} - \gamma_{SL}) / \gamma_{LV}$$

where θ is apparent contact angle, γ_{SV} is solid–vapor interfacial tension; γ_{SL} is solid-liquid interfacial tension; γ_{LV} is liquid-vapor interfacial tension. Young's equation

recognizes equilibrium between all three phases: solid, liquid, and gas. As these forces come in contact, the liquid assumes a shape where all three phases are balanced. Hence, this equation is very important to describe the wettability of a surface.

1.1.5.3 Wenzel's Equation

Although Young's equation gives us a fair idea of the inherent contact angle of a liquid, it assumes that the solid surface is smooth, rigid, and homogenous, which is not usually the case. Surface roughness is a property that is omnipresent in most of the used surfaces. Taking account of that, Robert Wenzel came up with a modified version of Young's equation [49].

$$cos\theta = rcos\theta_i, \text{ (r>1)}$$

Where r is surface roughness factor and θ_i is the inherent contact angle of the liquid.

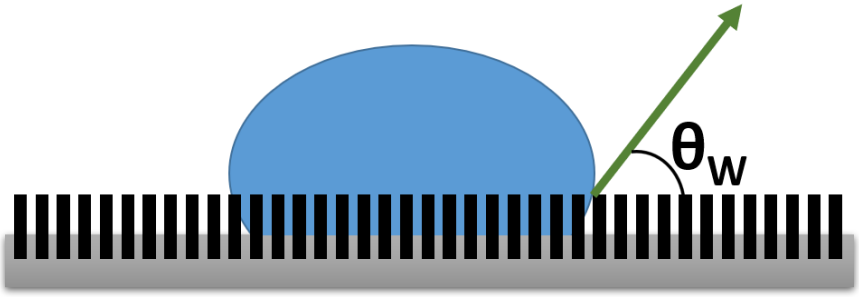

Figure 4 ***Schematic of a drop on a solid surface in the Wenzel model.***

In the Wenzel model, the liquid is homogenously in contact with the solid surface. Reprinted from "Multi-walled carbon nanotube carpets as scaffolds for U87MG glioblastoma multiforme cell growth" by Parikh, S. D., Dave, S., Huang, L., Wang, W., Mukhopadhyay, S. M., & Mayes, D. A. (2020). Materials Science and Engineering: C, 108, 110345. Copyright by Elsevier

1.1.5.4 Cassie-Baxter Equation

When the surface roughness is extremely large, it may trap air inside the structure. The presence of air pockets in the surface may avert liquid contact with the full surface and the droplets in that scenario are only in contact with the top of the asperities. In such a case, the top surface is made up of air and solid. In such a case, the fakir drop regime (*Figure 5*) follows the Cassie-Baxter equation [50] and the apparent contact angle is calculated as in the below equation.

$$cos\theta_{CB} = rf\ cos\theta_i + f - 1$$

Here r is surface roughness, f is the surface fraction of solid and liquid in contact.

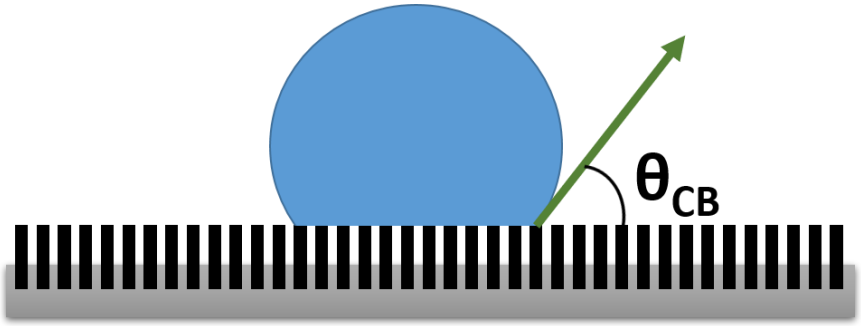

Figure 5 ***Schematic of a drop on a solid surface in the Cassie-Baxter model.***

In this model, the liquid is in heterogenous contact with the solid surface and due to air pockets within the surface, full liquid contact is avoided. Reprinted from "Multi-walled carbon nanotube carpets as scaffolds for U87MG glioblastoma multiforme cell growth" by Parikh, S. D., Dave, S., Huang, L., Wang, W., Mukhopadhyay, S. M., & Mayes, D. A. (2020). Materials Science and Engineering: C, 108, 110345. Copyright by Elsevier

Wenzel and Cassie-Baxter equations are the most commonly used models to estimate contact angles and to estimate surface wettability. The carbon scaffold CNT coating preparation used in these studies creates superhydrophobic structures with

the fraction of liquid-solid interface (f) being extremely low and follows the Cassie-Baxter model (*Figure 5*).

$$cos\theta_{CB} = rf\ cos\theta_i + f - 1$$

As previously reported, our hierarchical CNT-coated scaffolds have an f as low as 0.0462 [51]. As a result, whenever the inherent contact angle range (θ_i) is in the hydrophobic range, the same scaffolds coated with vertically aligned CNT carpets will exaggerate this effect and become superhydrophobic. Alternatively, when the inherent contact angle is in the hydrophilic range, those values are also exaggerated and become extremely hydrophilic after CNT-coating. Theoretically, this would shift cell adhesion and cell scaffold interactions into a Wenzel model (*Figure 4*).

1.1.6 Prior Work on CNT Surface Functionalization for Wettability Modification

Carbon nanotubes are hydrophobic in nature and cannot be suspended in water. CNTs can be functionalized by either noncovalent or covalent modifications for making them hydrophilic for biomedical applications [52]. CNTs can be functionalized noncovalently by surfactants, hydrophilic macromolecules, and repulsive forces [53]. Covalent CNT functionalization can be achieved by an acid oxidation reaction. For example, strong acids like nitric acid are generally used to oxidize CNTs. CNTs can also be conjugated by functional groups by treating them with chemicals or amino acids. For instance, by reactions such as 1,3-dipolar cycloaddition, functional groups can be attached to side-walls as well as on tips of CNTs [52,54].

Other advantages of using CNT-coated carbon scaffolds for potential biological therapies include the ability to modify CNTs. The CNT length and density upon these multiscale hierarchical carbon foam or fiber supports can be modified according to the

tissue of interest and the surface chemistry can also be modified and functionalized with moieties of interest for future possible therapeutic development. Because of such unique functionalization capabilities, CNTs can be effectively used for drug delivery purposes by forming stable complexes in molecular therapeutics such as siRNA and drug molecules [112,113].

1.2 Materials and Methods

1.2.1 Chemicals

Xylene (PTI chemicals) was used as a carbon source, ferrocene (99%) (Alfa-Aesar Ltd) as a catalyst, hexamethyldisiloxane (HMDSO) (99.5%, Sigma-Aldrich chemicals) for silicon oxide plasma treatment, and commercially available sodium hypochlorite solution for surface wettability treatment. Ethanol (200 proof) (Decon Laboratories), methanol (≥99.9%) (VWR chemicals), isopropanol (Fisher Bioreagents), and deionized water (DI water) were used for surface treatment. Hydrogen gas (99%) was used as a reducing gas. Oxygen (99.5%), and argon gases (99.999%) were used as inert gases in the chemical vapor deposition process.

1.2.2 Substrates

Carbon substrates were coated with Carbon Nanotube forests. The substrates used in the study are highly porous Reticulated Vitreous Carbon (RVC) foam and highly aligned carbon fiber mats. *Figure 6* shows low-resolution scanning electron microscopy pictures of the substrates used.

1.2.2.1 Reticulated Vitreous Carbon Foam (RVC Foam)

RVC foam is generally manufactured by pyrolysis of thermosetting foam in an inert environment. RVC foams have open porous three-dimensional structures and thus have a very high surface area and have less fluid resistance. Due to their surface properties, the RVC foams can be used in a wide variety of applications including thermal, catalysis, filtration, aerospace, semiconductor, and biomedical devices. This

foam was generously supplied by Ultramet Inc., USA. The foams had 97% open porosity, interconnected carbon solid struts, and 80 pores per inch. These RVC foams also have very low density (0.045 g/cc), are thermally insulating, electrically conductive, and chemically inert. These features are useful when choosing a biomaterial for cell scaffolding. The detailed material properties of the RVC foam are listed in *Table 1*.

Standard Properties of the RVC foam	
Micro Porosity (%)	97
Bulk density (g/cm^3)	0.045
Average Pore Size (μm)	300
Compression Strength at 20°C (MPa)	0.763
Flexural Strength (MPa)	58.6
Electrical conductivity (S/cm)	1.33
Bulk Thermal conductivity at 200°C (W/m.K)	0.085

Table 1 ***Summary of important material characteristics of RVC foam used in the study (from the manufacturer)***

1.2.2.2 Aligned Carbon Fiber Mats

Carbon fiber mats are generally manufactured by heating carbon at extreme temperatures and then interweaving the carbon fibers to make a carbon cloth. Two-dimensional carbon fiber mats were generously gifted by Hexcel (ACGP206-P-50). These fibers are flexible yet very strong, which is a unique property. They are used for

a wide variety of applications in different fields including aerospace, automotive, reinforcing composite and biomedical engineering.

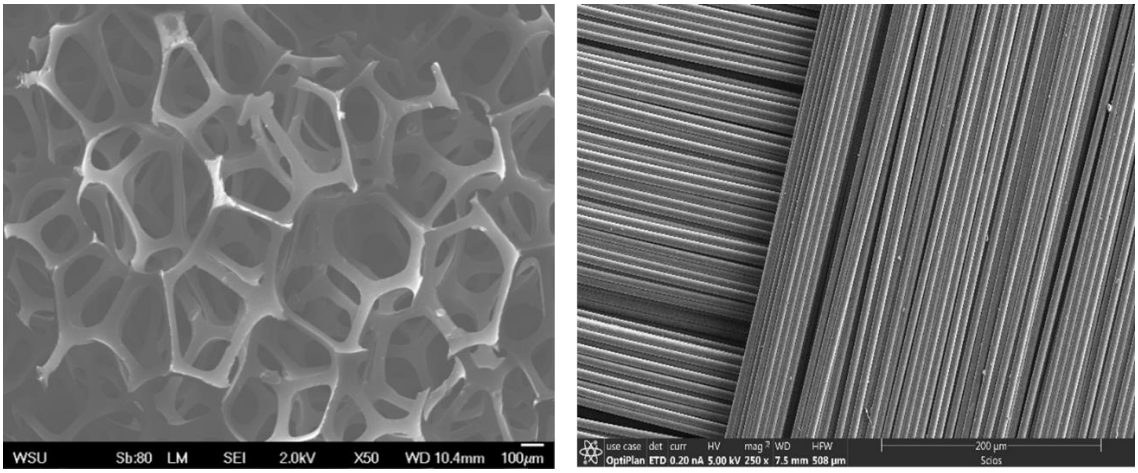

Figure 6 ***Low-resolution scanning electron microscopy (SEM) micrographs of reticular vitreous carbon (RVC) foam (L) and aligned carbon fiber mats (R).***

The porous 3D morphology and interconnected carbon solid struts for the RVC foams are evident from the SEM micrographs. Aligned and perpendicular carbon fibers of the carbon fiber mats can be observed.

1.2.3 Experimental Methods

1.2.3.1 Preparation of nanotube-coated scaffolds

Both aligned carbon fiber mats and RVC foam samples were nano-functionalized by covalently bonding carbon nanotubes to their surface using a previously optimized two-step method developed by the Mukhopadhyay group [30,55,56]. The first step involves oxygen plasma layer deposition by Microwave Plasma Enhanced Chemical Vapor Deposition (MPE-CVD). In the second step, the oxygen plasma layer-treated substrates are subjected to a carbon source, which in turn creates carbon nanotube-coated scaffolds. This step is done through Thermal Chemical Vapor Deposition. In our set-up, it was previously established that to form a

uniformly coated layer of CNTs, iron metal catalysts are critical and hence were used along with the carbon source [57].

1.2.3.1.1 Microwave Plasma Enhanced Chemical Vapor Deposition (MPE-CVD):

This process is executed by treating carbon fiber and carbon foam samples to form a silicon oxide plasma/buffer layer. This is done by exposing the samples to the plasma of hexamethyl-di-siloxane (HMDSO, 99.5%, Sigma Aldrich) and oxygen (99.9%) as a precursor in a microwave plasma reactor (V15GL, PlasmaTech Inc.).

In the beginning, the substrates are cut in appropriate sizes and placed on a wire mesh holder, and then sealed from the sides by a plastic wrap to ensure the gas treatment only passes through the substrates. MPE-CVD is a three-step process. The first step, Etching is done by flowing oxygen at 50 ml/minute for 3 minutes at 48 Pa chamber pressure and microwave power of 225 watts. This step is for cleaning up and activation the substrates for the next step.

In the second step, Silica Coating controls the oxygen plasma layer thickness. In this step, HMDSO (2 ml/min) is also introduced for 5 minutes with oxygen at a microwave power of 250 watts and 60 Pa chamber pressure.

The last step, also known as Stabilizing step, is conducted to stabilize the oxide coating formed in the silica coating step. In this step, oxygen is passed at 50 ml/minute for 1 minute at 50 Pa chamber pressure and low microwave power of 150 watts.

Microwave Plasma Enhanced Chemical Vapor Deposition step (*Figure 7*) forms the Si-C bond that covalently binds the oxygen plasma layer on the substrate. Mukhopadhyay lab has already characterized and optimized the oxygen plasma treatment steps for different substrate types [46,55,58]. Each substrate is plasma treated on the front as well as on the backside.

For carbon fiber cloths (CFC), the procedure used for front oxygen plasma coating is done by following steps 1,2,3,2, and 3. For back coating, steps 3,2,3,2, and 3 are followed. For RVC foams, the plasma coating is the same as fiber cloths, with the modification that the front coating is repeated twice. These steps are preoptimized [55,58] and yield a stable plasma layer on the substrate, which is then treated with floating catalyst chemical vapor for CNT deposition.

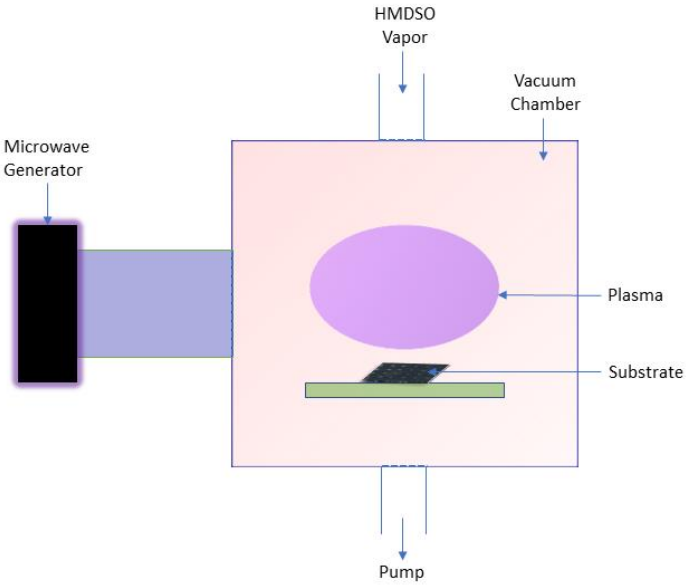

Figure 7 ***Set-up for Microwave Plasma Enhanced Chemical Vapor Deposition step used in this study for plasma layer coating on foam and fiber substrates.***

Briefly, the substrate (fiber cloth or carbon foam) is placed on a wire mesh in a vacuum chamber and treated with microwave plasma along with HDMSO vapor under pressure. This yields a covalently bonded SiO2 plasma layer onto the substrate.

1.2.3.1.2 Floating-Catalyst Chemical Vapor Deposition of Carbon Nanotubes (CNT)

The Thermal Chemical Vapor Deposition of Carbon Nanotubes using a floating catalyst technique was adapted from previous research [59,60]. For this technique, a quartz tube with a three-zone furnace (MTI Corporation Ltd.) was used (*Figure 8*). The quartz tube has an outer diameter of 80 mm, an inner diameter of 72 mm, and a length

of 1400 mm, and its temperature is controlled by a computer control module (OTF-1200X-III, MTI). The quartz tube is sealed with stainless-steel caps on both ends, which has openings for gas flow as well as carbon precursor and catalyst injection on one end and an outlet for exhaust on the other. The tube was insulated by two cylindrical disc supports (diameter ~70mm) and sealed on both ends.

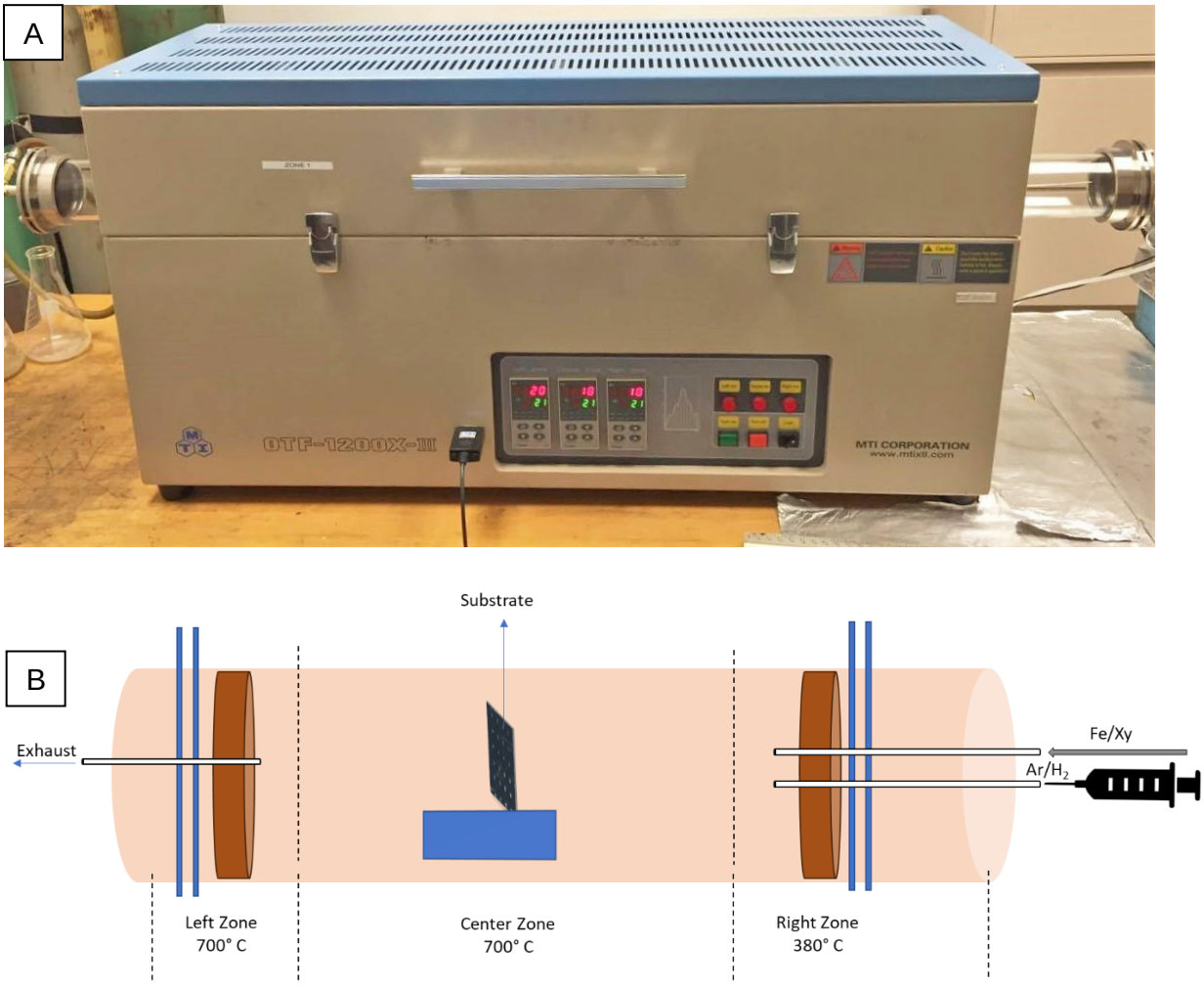

Figure 8 ***Chemical Vapor Deposition set-up used in this study for the preparation of carbon nanotubes.***

CVD Furnace (A) and graphical representation of three-zone furnace set-up (B) used for Thermal Chemical Vapor Deposition of Carbon Nanotubes using a floating catalyst technique. Briefly, catalyst (Fe) and carbon source (Xy) are passed in presence of argon and hydrogen gases at high temperatures. This leads to the chemical deposition of carbon nanotubes which strongly bind to the plasma layer.

The three-zone furnace set-up is shown in *Figure 8*. Three zones will be referred to as left, center, and right zones. The right zone is termed as a catalyst or pre-heat zone as the freshly mixed catalyst and the carbon source is introduced in the system from the right zone which heats the mixture at 380°C which turns the liquid into vapor form. The left and center zones are also called growth zones as the catalyst starts binding on the substrates and carbon nanotubes start growing.

This method has been based on previous work [59,61] and it takes place in presence of an Ar/H_2 environment. Argon (Ultra-high purity) is provided to keep the environment inert while hydrogen (99.999%) facilitates the growth of CNTs. The flow rate of Argon is maintained at 1200cc/min and hydrogen is maintained at 240cc/min. The growth zone is kept at 700°C during the entire reaction phase. In this process, ferrocene is used as a catalyst, and xylene is used as a carbon source. Ferrocene powder (99%, Alfa Aesar) is dissolved in pure xylene (99%, Alfa Aesar) with a concentration of 10mg/L. The prepared solution is injected using a stainless-steel syringe (Harvard Apparatus) and needle (Small Parts) set up through an infusion pump (Pump 11 Elite, Harvard apparatus). The flow rate is maintained at 12.5 ml/hour.

The process runs for a pre-defined time for desired CNT growth and once the reaction is over, hydrogen flow is turned off, argon flow is lowered and the furnace cooled down with the rate of 5℃/min and brought back to room temperature. This is the established process for growing CNT on different porous supports in the Mukhopadhyay lab. Following optimization studies, 2h growth was chosen for Long CNT-coated scaffolds and 20-minute growth for Short CNT-coated scaffolds.

1.2.4 Surface Treatment of CNT-modified Surfaces

Inherently, the produced CNT arrays exhibit superhydrophobic nature, and the water contact angle on such surfaces is >160°. However, it may vary, and the contact angle may decrease if the CNT alignment is disturbed or the oxygen-containing groups covalently bind to the surface [62]. The CNT-coated scaffolds were treated with different chemicals to evaluate surface wettability.

1.2.4.1 Chemical Oxidation with Acid and Base

Functionalization with acids is one of the commonly reported methods to make the carbon nanotubes hydrophilic. The scaffolds were treated with nitric acid, hydrochloric acid, or ammonium hydroxide and evaluated for changes in wettability. Scaffolds were treated with different concentrations of HNO_3 for 10 minutes or 30 minutes, HCl for 10 mins or 90 minutes, and NH_4OH for 1h. Following the chemical treatment, scaffolds were washed with deionized water multiple times to remove any remnant acid and the contact angle of water droplets on the treated scaffolds was analyzed.

1.2.4.2 Oxygen Plasma Treatment

To convert the superhydrophobic surface to a more hydrophilic surface, oxygen plasma treatment functionalization was also evaluated. Previous studies have shown that water wettability can be regulated by repeated plasma and air annealing treatments [51]. Therefore, the CNT-coated scaffolds were treated in a microwave plasma reactor (V15GL, PlasmaTech Inc.) at 115W at 50ml/min oxygen flow rate for 6 seconds as previously optimized [63] and the treatment was applied to one side of CNT-coated fibers and both sides of CNT-coated foams due to the thickness of foams.

1.2.4.3 Bleach Treatment

For bleach treatment, samples were first treated with 1M nitric acid at room temperature to remove metal impurities and amorphous carbon. This low concentration nitric acid treatment also mildly oxidizes the surface. Samples were then treated with ethanol and the dried scaffolds were autoclaved at 121°C for 20 minutes in the keratinocyte study. For the GBM study, the autoclave step was not used. Scaffolds were then treated for 1h with 70% isopropanol (in presence of UV light in the GBM study) followed by a 1h treatment with 15% v/v sodium hypochlorite-based bleach-containing solution at room temperature and finally washed three times with autoclaved deionized water.

1.2.5 Characterization of CNT-coated Hierarchical Scaffolds

1.2.5.1 Contact Angle

Contact angles for samples with or without CNT functionalization were measured using a lab-made contact angle goniometer assembly. 5µl drop of DI water was added to the carbon scaffolds using a micropipette (Eppendorf). Water-droplet image processing and contact angle measurements were calculated using SolidWorks® software. The measurement was repeated for at least 3 different samples and for each sample, at least 5 different spots were analyzed to yield accurate results. For hydrophilic surfaces, some of the representative values are qualitative, despite the repeated measurements due to the very small value of contact angle and gradual wicking of the water droplet into the surfaces of carbon scaffolds.

1.2.5.2 Scanning Electron Microscopy (SEM)

Scanning electron microscopy (SEM) was used to observe micro as well as nano features of the scaffolds used in the different experiments. For this, a field emission scanning electron microscope, JEOL 7401F was used. The images were acquired using secondary (1-2kV) and a mixture of secondary and backscatter (5-10kV) modes with variable accelerating voltages and working distances depending on the sample type. Backscatter mode allows identifying structural as well as the composition of various samples just below the outer surface. Transmission mode allows for high magnification images, which were used for understanding the surface topography of CNTs grown over different time periods.

1.2.5.3 Energy Dispersive X-Ray Spectroscopy (EDS)

Using SEM, characteristic X-rays are emitted from the samples, which were also used for Energy-dispersive X-ray spectroscopy (EDS) of the samples. This was done using the Ametek Inc. EDAX system, which is attached with a field emission scanning electron microscope, JEOL 7401F. This system provides qualitative data of elements present in a sample at the surface level and up to a surface depth of several microns.

1.2.5.4 X-ray Photoelectron Spectroscopy (XPS)

X-ray photoelectron spectroscopy (XPS) was performed to understand the detailed surface chemical composition of the CNT-coated scaffolds and to understand the surface chemical changes pre- and post-chemical modifications. The XPS evaluations are based on exposing the material to an X-ray source and measuring the kinetic energy of ejected photoelectrons emitted from the samples. XPS is a surface-

sensitive technique and gives insights into the elemental composition, bonding, and chemical state of the top 1-7nm of the outer surface.

Each atom produces unique binding energy and it is also specific to the overall molecule. XPS was carried out using the Kratos (Axis Ultra) system and was performed in an ultra-high vacuum environment (UHV, ~10-9 Torr), with a monochromatized Al Kα (1486.6 eV) source. The acquired data was processed with Casa XPS software (Casa Software Ltd).

1.3 Results

1.3.1 Nano-functionalization of Carbon Foam and Carbon Fiber Scaffolds with MWCNT.

Reticulated Vitreous Carbon (RVC) foam and aligned carbon fiber mats were used as carbon substrate scaffolds for carbon nanotube growth. These materials are made of carbon and have very different structural properties. Carbon foam and fiber substrates were processed through a two-step process as previously reported and were coated with CNT carpets [64–66]. Non-coated carbon structures are defined here as ‘pristine’ and carbon fiber cloths are denoted as CFC. All prepared foam samples were cut into cylinders of 0.5 cm diameter and 0.5 cm height (*Figure 9 A1, B1*). Surface characteristics of scaffolds were measured using scanning electron microscopy. *Figure 9* displays representative images of pristine and CNT-coated carbon foam and fiber scaffolds whereas CNT-coated scaffolds show vertically grown carbon nanotube carpets onto and inside the porous foam substrates (*Figure 9 B2–B3*). The nano-scaled cross-links form a 3D architecture in CNT-coated scaffolds (*Figure 9 C*).

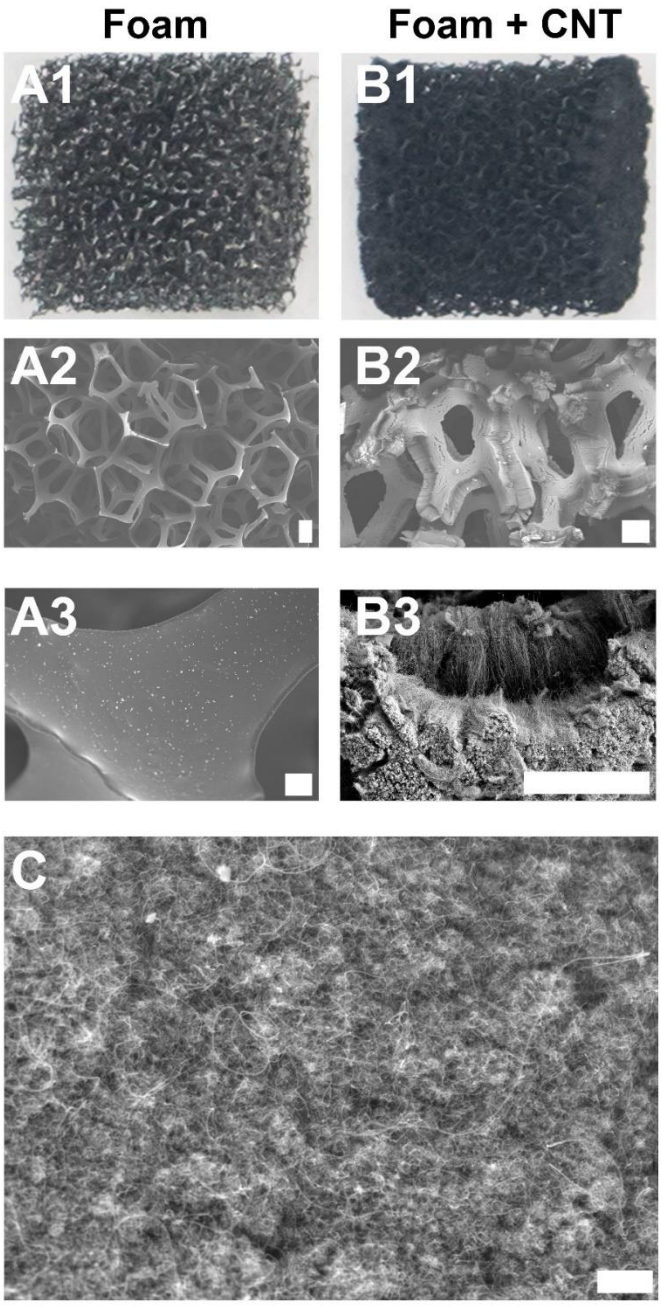

Figure 9 ***Nano-functionalization of carbon foam with MWCNT****.*

Representative images of the multiscale hierarchical structure of carbon foam with or without the addition of 120 minute CNT coating. Optical images of cylindrical-shaped 0.5×0.5 cm carbon foam (A1) and CNT-coated carbon foam (B1). Representative SEM images of foam (A2-A3), carbon nanotube-coated foam (B2–B3), Representative high magnification images show nanoroughness contributed by CNTs in foam (C) scaffolds. Representative scale bars: A2, B2, & B3=100μm; A3 = 10μm; C =1μm.

Reprinted from "Multi-walled carbon nanotube carpets as scaffolds for U87MG glioblastoma multiforme cell growth" by Parikh, S. D., Dave, S., Huang, L., Wang, W.,

Mukhopadhyay, S. M., & Mayes, D. A. (2020). Materials Science and Engineering: C, 108, 110345. Copyright by Elsevier.

All the prepared fiber scaffolds were cut into 1 cm×1 cm squares unless stated otherwise (Figure 10 *A1, B1*). Representative SEM images show the detailed microstructural alignment of the fibers and hierarchical multiscale architectures of pristine (*Figure 10 A2–A3*) and CNT-coated carbon fibers (CNT-CFC) and how CNTs coat along with the weave of fiber cloth (Figure 10 *B2-B3*) supports.

From *Figure 9* and Figure 10, it can be observed that carbon substrates are smoother in their structural morphology before coating and get fuzzier after the CNT-coating. Tube-like clusters on the supports can be visualized, contributing to an increase in nano-roughness in the CNT-coated foam and fiber structures when compared to their pristine counterparts. The individual nanotubes in these carpets are multi-walled CNT of uniform size and shape with an outer diameter in the range of 30 nm and lengths of the order of 200μm [67]. The CNTs also appear to be clustered as a carpet on CNT-coated carbon fiber structures (*Figure 9 C*).

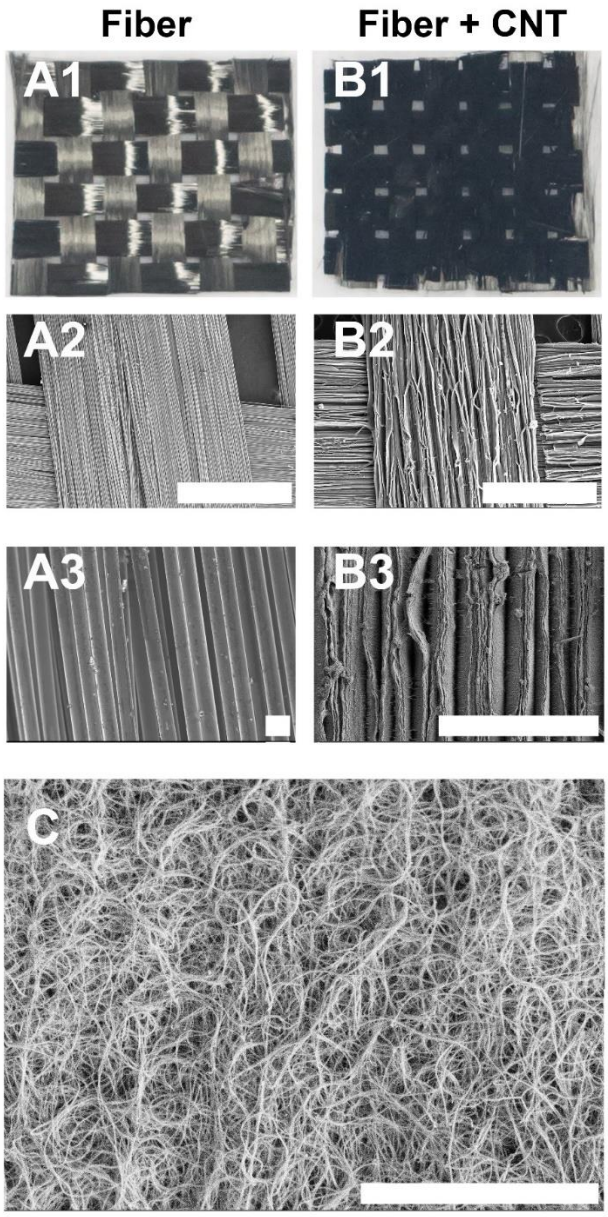

Figure 10 ***Nano-functionalization of carbon fiber with MWCNT.***

Representative images of the multiscale hierarchical structure of carbon fiber with or without the addition of 120-minute CNT coating. Optical images of 1×1cm carbon fiber (A1) and CNT-coated carbon fiber scaffolds (B1). Representative SEM images of carbon fiber (A2–A3), and CNT-coated fiber (B2-B3) scaffolds. Representative scale bars: A2 & B2=1 mm; A3=10μm; B3=20μm; and C=5 mm. Reprinted from "Multi-walled carbon nanotube carpets as scaffolds for U87MG glioblastoma multiforme cell growth" by Parikh, S. D., Dave, S., Huang, L., Wang, W., Mukhopadhyay, S. M., & Mayes, D. A. (2020). Materials Science and Engineering: C, 108, 110345. Copyright by Elsevier

Carpet length using this method can be tailored, which could be important for future bio-implant development. To achieve a shorter length of CNTs to analyze the effects on cell growth applications, in addition to the 120-minute floating catalyst CVD method, we also analyzed different time points to achieve the desired characteristics of the CNTs. Nano-tailored surfaces of the aligned carbon fiber mats after 6, 10, 20, 30, and 40 minutes of floating catalyst chemical vapor deposition were assessed in this study to optimize the timing for preparing short CNTs that with uniformly distributed and interconnected CNT clusters (*Figure 11*-*14*). For long CNTs, a pre-optimized 120 minute deposition time was chosen (*Figure 15*) [66].

For the 6-minute coating and 10-minute coating (*Figure 11*), it can be observed that the attachment and growth of the CNTs are random and nonaligned. This could be due to a lack of nucleation sites available as the time may not be enough to provide sufficient deposition of the catalyst particles. Hence the CNT clusters can only be observed in several areas in a non-uniform manner. For this topography, there are not enough CNTs available on the surface and the characteristic uniform and dense carpet-like structures are not formed and not all CNTs are in contact with the adjacent tubes.

From 20-minute coating and onwards, enough nanotubes can be observed to be uniformly distributed throughout the fiber cloth substrate and we see the characteristic CNT-forest covering the entire surface of the substrate. As the coating time increases, more entangled CNT structures can be observed. With increasing times, the underlying carbon fibrils start becoming indistinguishable due to increased lengths. This is consistent with the previous studies that the length of the CNTs increases with time [57]. The calculated values for the lengths of the CNTs have also been documented before on graphite substrates [57]. Graphite has a flat surface,

which is an ideal geometry as its cross-section can be observed and the measurements can be accurately performed. As the fiber cloths and foams have a non-uniform topography, the measurements become extremely difficult and we have used the graphene calculations for approximate length estimation. As the CNT carpet growth is directly formed and is dependent on the plasma buffer layer [64,68], and the buffer layer used for all the substrates is the same, we can use the graphite calculations for CNT length measurement on fiber cloths.

For our study, the 6- and 10-minute growth do not give uniform CNT-coating and lengths cannot be accurately measured due to the sporadic growth (Table 2). However, from previous reports [57], CNT length is known to be 14.5μm for a 20-minute coating on graphite. Therefore, CNT length can be predicted to be around 32.3μm for 30-minute coating, 54μm for 40-minute coating, and 210μm from the 120-minute coating. Also, from the work of Wang *et al.* [32], it was also proved that CNT diameter remains consistent with different growth times. Hence, by keeping the same substrate material and varying only the CNT coating times, we achieve CNTs with consistent diameters. Since CNT formation is dependent on the buffer layer and the nucleation sites of the CNTs on the substrate are limited, we can elucidate that CNT morphologies for different growth times remain the same and the primary differentiating factor between them is their length.

From the SEM images, consistent with our previous studies [30,60] it was evident that the growing CNTs have entangled structures and resemble a carpet-like structure on the substrates. In our previous studies [57], using even surfaces like graphite, our lab has also shown that the CNT carpets have micro-scaled roughness, represented by hills and valleys. There are millions of nanotubes on a small 1x1 cm fabric and they all can be tailored for their height and hence we can optimize a

hierarchical structure by selecting the right underlying substrate and by controlling the CNT properties. This could be very advantageous for bioscaffolding applications.

Our lab has already done an extensive amount of work on analyzing the CNT properties with increased growth time. In this study, we aimed to modify the fiber cloth using two different times of the floating catalyst method so that the CNTs coated on the substrate are of short (*Figure 12*) and long (*Figure 15*) lengths which can potentially lead to different cellular interactions. Section 2 evaluates the biological effects of short vs. long CNTs. Through different coating times, we were able to achieve different CNT growth on the same base substrate consistent with the previous studies in our lab [57]. It was also shown in the previous work that no measurable CNT growth occurs up to the first 5 minutes of the coating times and the CNT length linearly increases with time for up to 120 minutes. Hence we opted to test 6 minutes and above times up to 120 minutes for the coating step to determine the shortest time point for CNTs where the coating on the fiber cloth is uniform but not isolated [57].

Consistent with previous results, we were also able to generate uniform but significantly less entangled and shorter forests with 20-minute coating, referred to as ‘short CNTs’ (*Figure 12*) due to their shorter lengths, and extremely entangled and longer CNT forests for 120-minute coating, referred to as long CNTs (*Figure 15*). These two growth settings were used to identify the effects of cell growth of skin cells in Section 2.

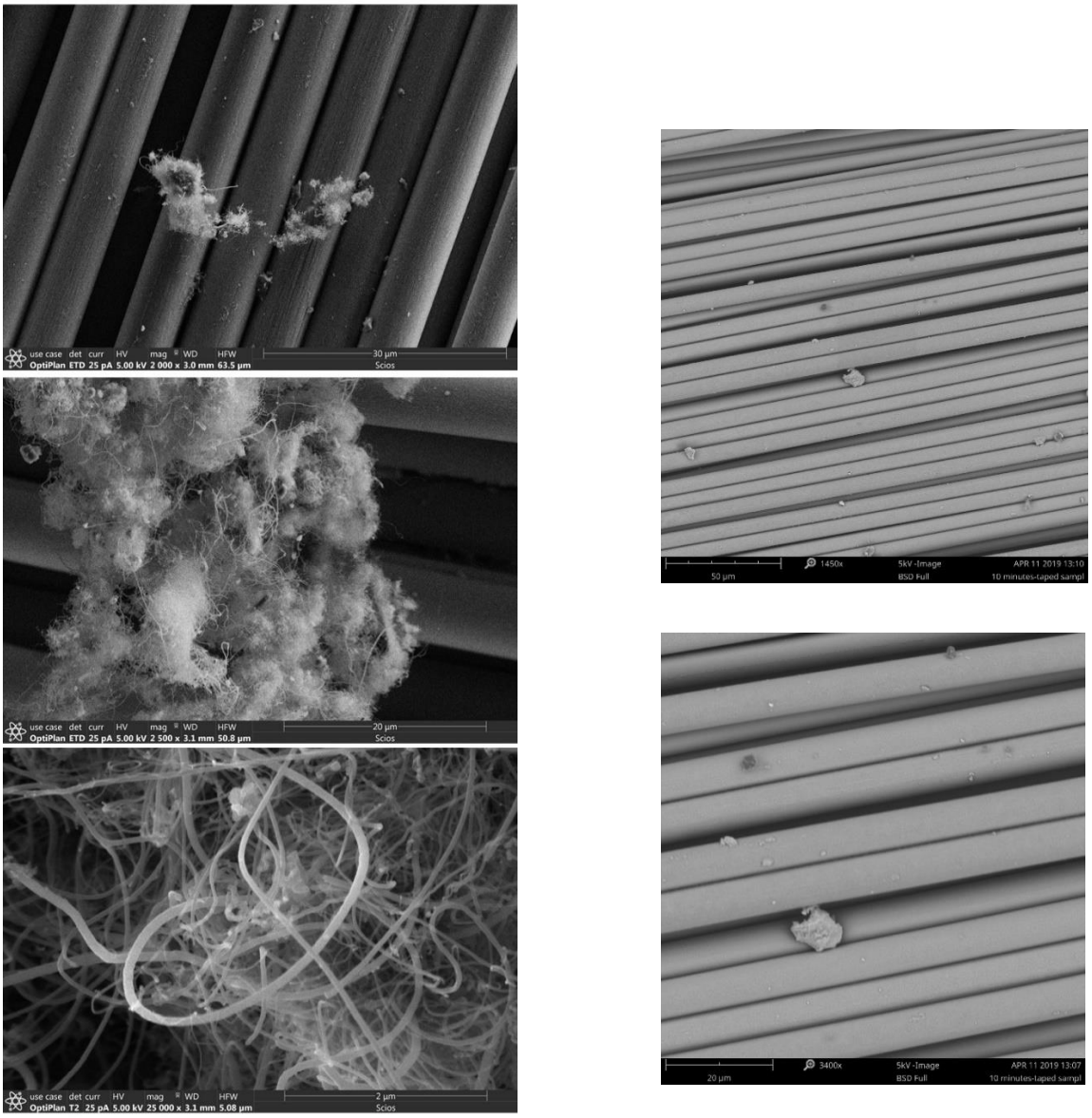

Figure 11 ***Representative images of the multiscale hierarchical structure of carbon fiber with 6 minutes (L) and 10 mins (R) of Floating-Catalyst Chemical Vapor Deposition of CNTs.***

CNTs are random and nonaligned most likely due to the initial nucleation phase. Bare carbon cloth fibrils are visibly present as there are not enough CNTs available on the surface and the characteristic uniform and carpet-like structures are not formed.

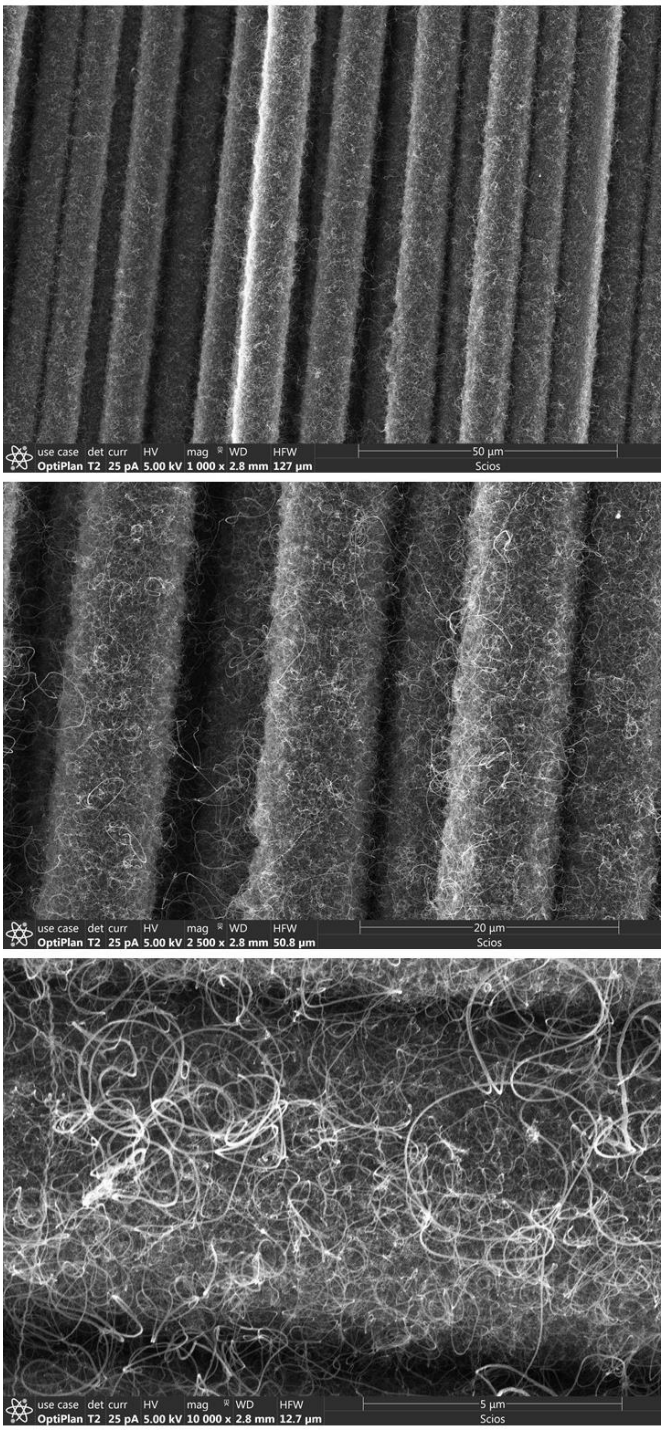

Figure 12 ***Representative images of the multiscale hierarchical structure of carbon fiber with 20 minutes of Floating-Catalyst Chemical Vapor Deposition of CNTs.***

Uniformly distributed and interconnected nanotube structures throughout the fiber cloth substrate can be observed. The underlying fibrils are visibly covered with CNTs.

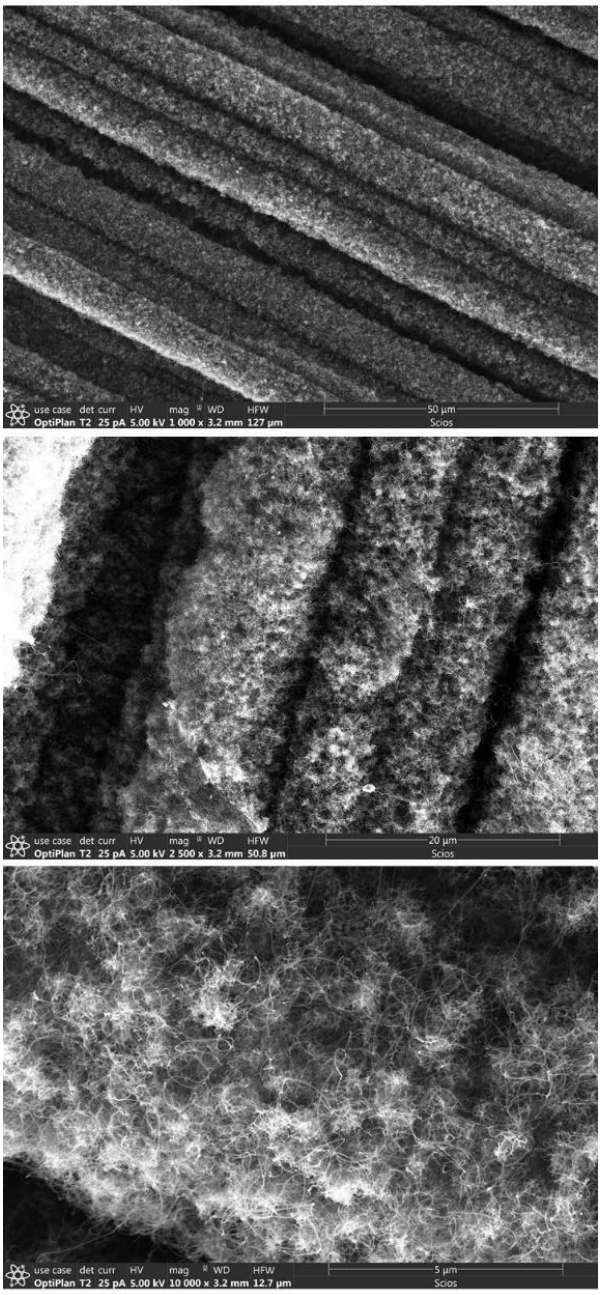

Figure 13 ***Representative images of the multiscale hierarchical structure of carbon fiber with 30 minutes of Floating-Catalyst Chemical Vapor Deposition of CNTs.***

Uniformly distributed and interconnected nanotube structures throughout the fiber cloth substrate are observed. The underlying fibrils are visibly covered with CNTs.

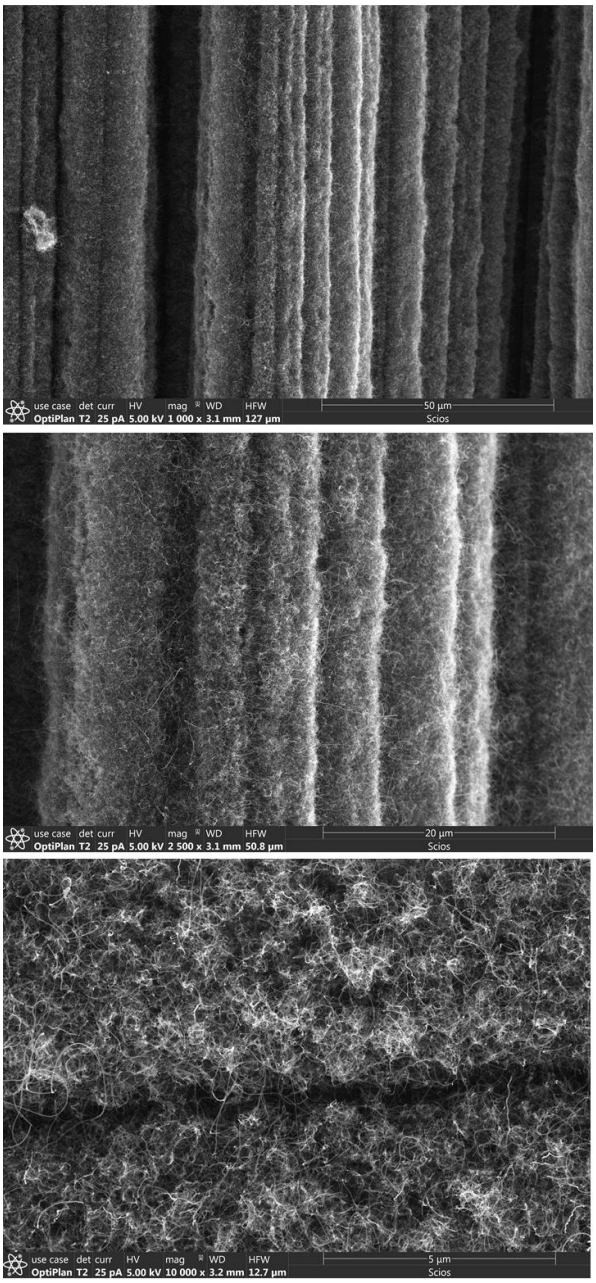

Figure 14 ***Representative images of the multiscale hierarchical structure of carbon fiber with 40 minutes of Floating-Catalyst Chemical Vapor Deposition of CNTs.***

Uniformly distributed and extremely thick layers of CNTs are visible over the fiber cloth substrate.

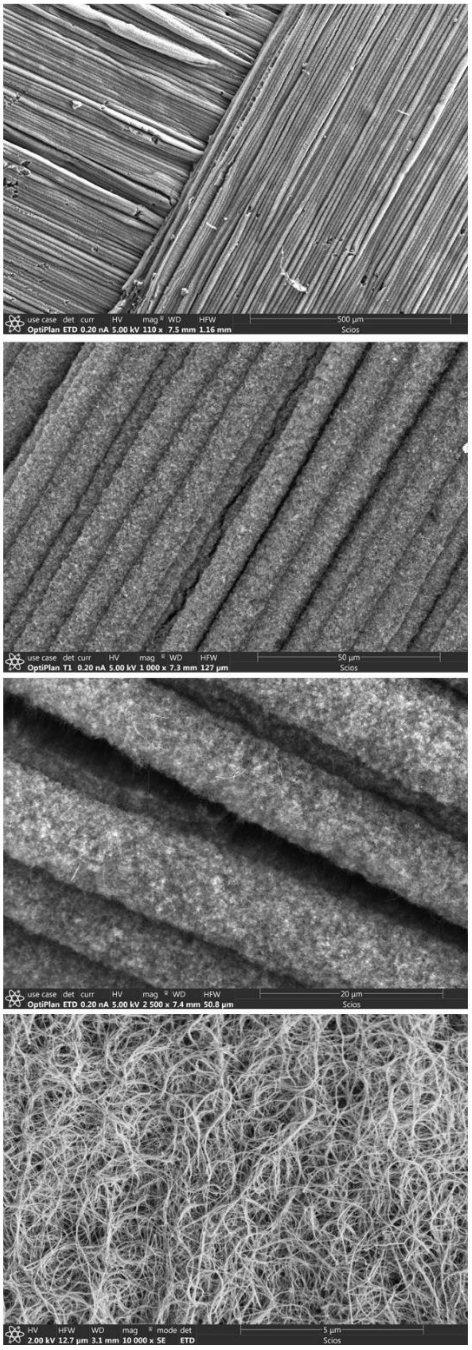

Figure 15 ***Representative images of the multiscale hierarchical structure of carbon fiber with 120 minutes of Floating-Catalyst Chemical Vapor Deposition of CNTs.***

Uniformly distributed and extremely thick layers of CNTs are visible over the fiber cloth substrate. The underlying fibrils are not visible due to the extensive growth time.

CNT-coating duration (minutes)	**Expected CNT Length**	**Observation**
6	N/A	Sporadic and isolated CNT clusters. Probably due to the initial nucleation process not being complete. Length cannot be estimated due to the irregularity
10	N/A	Sporadic and isolated CNT clusters. Probably due to the initial nucleation process not being complete. More clusters compared to 6-minute coating. Length cannot be estimated due to the irregularity
20 (Short CNT)	14.5μm	Well distributed and entangled CNT clusters. Underlying carbon fibers are coated with short CNTs. The chosen time point for short-CNT analysis.
30	32.3μm	Well distributed and entangled CNT clusters. Underlying carbon fibers start becoming indistinguishable due to increased CNT length
40	54μm	Well distributed and entangled CNT clusters. Very packed CNTs due to increased length. Carbon fibers visibly coated with CNT carpets
120 (Long CNT)	210μm	Well distributed and Intertwined CNT clusters. Very thick layers of CNTs observed over underlying carbon fibers and the underlying fibrils are not

		visible due to the extensive growth time. The chosen time point for Long CNT analysis

Table 2 ***CNT growth time and observations***

1.3.2 Wetting and Contact Angle Measurements of Surface-modified CNT-Coated Scaffolds

Nano-functionalization with carbon nanotube surfaces provides nanoroughness, which has been linked with improved cellular adhesion [65,66,69,70]. The wettability of these surfaces, which is important for cell proliferation, can be influenced very strongly by surface chemical attachments, as demonstrated in earlier studies [51]. We chemically modified the inherently superhydrophobic scaffold surfaces (water contact angle of >150°), with different methods to assess their potential to turn the surfaces hydrophilic.

1.3.2.1 Chemical Oxidization to Alter the Wettability

Chemical functionalization is one of the commonly reported methods to make carbon nanotubes hydrophilic. The degree of functionalization of CNTs is also inversely linked with cellular cytotoxicity [71]. Metallic impurities have been linked strongly with *in vitro* as well as *in vivo* toxicity [72,73]. The overall aim of this experiment was to identify a suitable functionalization method to achieve hydrophilicity and eliminate the metal catalyst impurity from the surface that could induce cytotoxicity in the cell-culture experiments. The wettability of the scaffolds was measured using a contact angle goniometer.

Nitric acid is known to modify the surface by functionalizing it with -COOH groups [74,75]. Apart from the wettability change, it can also help by the removal of

amorphous carbon and by removing remnant catalysts from the surface. We used different concentrations of nitric acid and measured the contact angles of the scaffolds. We found out that even at higher concentrations of 10M HNO_3, a short 10-minute treatment is not enough to alter the surface wettability. However, a 30-minute reaction with 8M HNO_3 successfully modified the CNT-coated scaffolds to be extremely hydrophilic and the contact angles of the CNT-coated scaffolds were ~30° post-treatment (*Table 3*).

Hydrochloric acid refluxing is often used to remove impurities, metal catalysts and does not directly form oxygen-containing groups. However, it exposes the amorphous carbon and this leads to increased oxygen-bearing sites on CNTs, which leads to its increased wettability [75]. Similar to nitric acid, a short 10-minute treatment of HCl was not enough to alter the surface wettability of the CNT-coated scaffolds. The scaffolds required prolonged treatment with HCl for the wettability modification and the superhydrophobic CNT-containing scaffolds turned to hydrophilic when treated with 12M HCl for 90 minutes. The surfaces however did not turn extremely hydrophilic in this reaction as they did with the nitric acid treatment (*Table 3*).

Ammonium hydroxide treatment is also known to yield mild oxidation treatments [76] and also was attempted in this study to check its effect on the surface wettability of CNT-coated scaffolds. This base treatment was not as successful as the other treatments and yielded moderate changes in wettability (*Table 3*). However, this result was expected as this reaction only leads to partial oxidation of the surfaces as evidenced by the superhydrophobic to the hydrophobic transformation of the surfaces at higher concentrations.

In summary, the chemical treatments, particularly acid treatments were moderately successful in altering the surface wettability of CNT-coated scaffolds at

higher concentrations and at longer reaction times. However, acid treatments at higher concentrations have been known to damage the morphology of CNTs [77] and such CNTs will have inferior structural properties and may not be suitable for scaffolding applications. Because of that, the acid treatments were not further utilized in our studies. Similarly, commonly used chemical reactions such as 'piranha' solution (a mixture of sulphuric acid/hydrogen peroxide) [76], and reactions performed with concentrated acids at higher temperatures were also not attempted in this study.

Contact Angle Measurements	
Treatments	**Contact Angle**
10M Nitric Acid 10 minutes	Extremely hydrophobic >130°
8M Nitric Acid 10 minutes	Extremely hydrophobic >130°
6M Nitric Acid 10 minutes	Extremely hydrophobic >130°
4M Nitric Acid 10 minutes	Extremely hydrophobic >130°
10M HCl for 10 minutes	Extremely hydrophobic >130°
6M HCl for 10 minutes	Extremely hydrophobic >130°
12M HCl for 90 minutes	Hydrophilic <90°
6M HCl for 90 minutes	Hydrophobic, 90°- 130°
3M HCl for 90 minutes	Extremely hydrophobic >130°
16M HNO_3 for 30 minutes	Extremely hydrophilic ~30°
8M HNO_3 for 30 minutes	Extremely hydrophilic ~30°

4M HNO_3 for 30 minutes	Hydrophilic <90°
7M NH_4OH for 60 minutes	Hydrophobic, 90°- 130°
3.5M NH_4OH for 60 minutes	Hydrophobic, 90°- 130°
1.7M NH_4OH for 60 minutes	Hydrophobic, 90°- 130°

Table 3 ***Contact angles of a water droplet on CNT-coated scaffolds after chemical functionalization.***

1.3.2.2 Surface Plasma Treatment to Modify the Hydrophobicity

To assess the potential for plasma treatment modification, scaffolds were treated with 115w oxygen plasma for 6 seconds and wettability was measured. Plasma-treated CNT-coated scaffolds quickly turned from superhydrophobic to extremely hydrophilic and modified water contact angles were in the range of 20°- 30°. Such plasma-treated samples can also be turned to superhydrophobic by treating them with heat in presence of air circulation, a process called air annealing treatment. Briefly, samples are placed at 110°C for 3 hours in the presence of an installed fan [62].

However, plasma treatment was not stable enough for performing studies evaluating cell growth applications. The resultant wettability effect was transient and reverted to hydrophobic after 14+ hours of storage. The newly created hydroxyl groups could have also been replaced by oxygen in the air since the hydroxyl groups have low binding energy and the reaction is more thermodynamically favorable.

1.3.2.3 Sodium Hypochlorite-based Bleach Treatment and its Influence on Water Wettability

To identify a wettability reaction step that also sterilizes samples, sodium hypochlorite-based bleach treatment was attempted. Surface modification to attach oxygen and halogen-containing molecular groups through the plasma and liquid treatments has been investigated by our group for the wettability of various polymers, water, oil, epoxy, and biofluids [51,56,78–81]. For this study, we hypothesized that the sodium hypochlorite-based bleach treatment would not only aid in material sterilization but would also alter the nanomaterial surface wettability. This bleach treatment was effective for hydrophilicity modification (*Figure 16*) as well as a sterilization step (Section 2).

Inherent water contact angles on carbon fiber and foam supports are hydrophilic. As shown in Tables 3 and 4, contact angles of the CNT-coated carbon scaffolds are dramatically high compared to pristine fiber and foam supports. As previously described [51], these results also prove that as-synthesized carbon nanotubes make the inherent carbon fiber surface superhydrophobic.

To ensure residual carbon and metal impurities from the manufacturing process are removed, nitric acid treatment is first performed on these materials. CNT-coated fibers treated with 1M Nitric Acid have a slightly lower contact angle than that shown in untreated CNT-coated fibers (*Figure 16 A-B*).

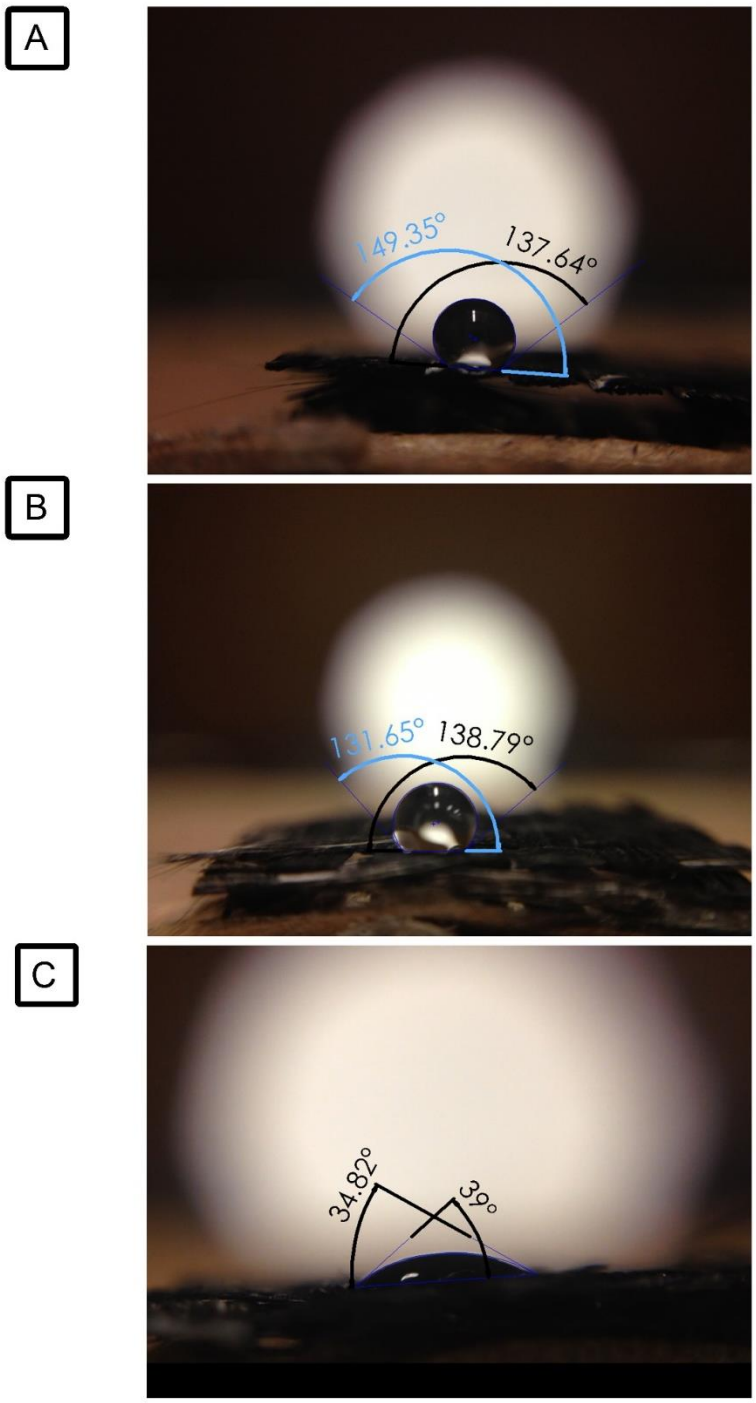

Figure 16 ***Sodium hypochlorite-based bleach treatment and its influence on water wettability.***

Water contact angle on untreated CNT coated fiber scaffold is superhydrophobic (A). After nitric acid treatment, water contact angle on the CNT-coated fiber scaffold is reduced but remains hydrophobic (B). Sodium hypochlorite-based bleach treatment dramatically reduces the water contact angle and the CNT-coated surfaces become hydrophilic (C). Reprinted from "Multi-walled carbon nanotube carpets as scaffolds for

U87MG glioblastoma multiforme cell growth" by Parikh, S. D., Dave, S., Huang, L., Wang, W., Mukhopadhyay, S. M., & Mayes, D. A. (2020). Materials Science and Engineering: C, 108, 110345. Copyright by Elsevier

Composition	Contact Angle (°)
Pristine Foam	65-75
CNT Foam	160
Nitric Acid Treated CNT Foam	140-150
Sodium hypochlorite treated CNT Foam	0-30

Table 4 ***Mean contact angle measurements for foam coated scaffolds***

Composition	Contact Angle (°)
Pristine Fiber	40-45
CNT Fiber	140
Nitric Acid Treated CNT Fiber	135
Sodium hypochlorite treated CNT Fiber	0-30

Table 5 ***Mean contact angle measurements for fiber coated scaffolds***

After sodium hypochlorite-based bleach treatment, the contact angle decreased significantly (*Figure 16 C*).

However, to have an additional measure of sterilization, in the keratinocyte study, we introduced an autoclave step after the initial nitric acid treatment. The autoclave step also makes the scaffolds extremely hydrophobic and contact angles of the CNT-coated scaffolds go above 130° after the autoclave step. Such scaffolds are treated with isopropanol to reintroduce some oxidation groups on the surface to enhance the subsequent interaction with the bleach solution.

In summary, sodium hypochlorite-based bleach, which can provide stable surface hydrophilicity modification without considerable structural damage and sterilization for cell growth applications was selected as the method of the choice for wettability modification. The subsequent effect(s) of such sodium hypochlorite-based bleach treatment on cell growth are discussed in chapter 2.

1.3.3 Surface Chemistry of Bleach treated CNT-CFC (XPS)

To analyze the chemical state of the bleach-treated CNT-coated scaffolds, we performed XPS analysis which is represented in *Figure 18* Analysis of the samples was carried out by using duplicate samples, selecting multiple spots in each sample, and optimizing the scan location for maximum output counts.

We first performed a semi-qualitative elemental analysis through a survey scan (general scan) which gives a low-resolution outlook of all the surface elements through XPS. The characteristic spectra for CNT-coated and uncoated CFC samples have been published previously [32,59,62] and suggests the pristine samples have both oxygen and carbon components on their surface (*Figure 17 A*). However, when coated with CNT, the CNT-CFC only has carbon on its surface due to the nanotube formation (*Figure 17 B*). Once the CNT-CFC sample gets treated with sodium hypochlorite-based bleach, due to surface oxidation, we again see the characteristic peaks at 533 eV and 285 eV indicating the presence of oxygen and carbon, respectively (*Figure 18*). The survey scan suggests that the bleach-treated scaffold has carbon as its main component and also has some amounts of oxygen on the surface. This is different than the CNT-coated scaffold without functionalization [32,59,62], which only has carbon and minimal traces of oxygen on the surface.

To gain insights into the carbon and oxygen presence, we performed fine scans of carbon as well as oxygen. Each fine scan represents a high-resolution step with a small scanning step such as 0.1eV and multiple scans are averaged to increase the signal-to-noise ratio.

C 1s fine scan (*Figure 19*) shows a characteristic carbon peak at 284.5 eV. Carbon bonding patterns were understood by following the deconvolution step which resolves different components within the element. The most prominent peak is at 284.5 eV. It can be attributed to the sp^2 hybridization of carbon-carbon bonding in a graphitic structure making up the carbon nanotube structure. The peak at 290.6 eV represents the pi-pi peak and the second-largest peak at 285.2 eV represents the C-CH sp^3 hybridization and could be partly due to structural defects. Lastly, the peak at 286.8 is characteristic of the C-O/OH functionalization. This is a peak that is directly associated with the oxygen functionalization and wettability of the material [62].

O 1s fine scan (*Figure 20*) reveals the oxygen 1s peak to be at 532.7 eV. Upon deconvolution, two distinct peaks at 532.7 eV and 531 are identified. The predominant peak at 532.7 indicates O/OH=C functionalization by the sodium hypochlorite modification. The second peak at 531 eV could be indicative of the carbonyl C=O bonding introduced by the surface oxidation.

It is already established that CNT-coated scaffolds prepared in our lab show iron signal from the CVD preparation step due to the iron catalyst used [59]. We identified that after nitric acid treatment, there are no iron catalyst particles left on the surface of the CNT-coated scaffolds (*Figure 18* and *Figure 21*) indicating that it can be utilized for cell growth applications without metal catalyst toxicity-related implications.

Fine scans of chloride show that the sodium hypochlorite treatment does not leave any unwanted chloride moieties on the surface (*Figure 21*) indicating the washing steps resulted in effective rinsing and successful elimination of any remnant surface chloride moieties

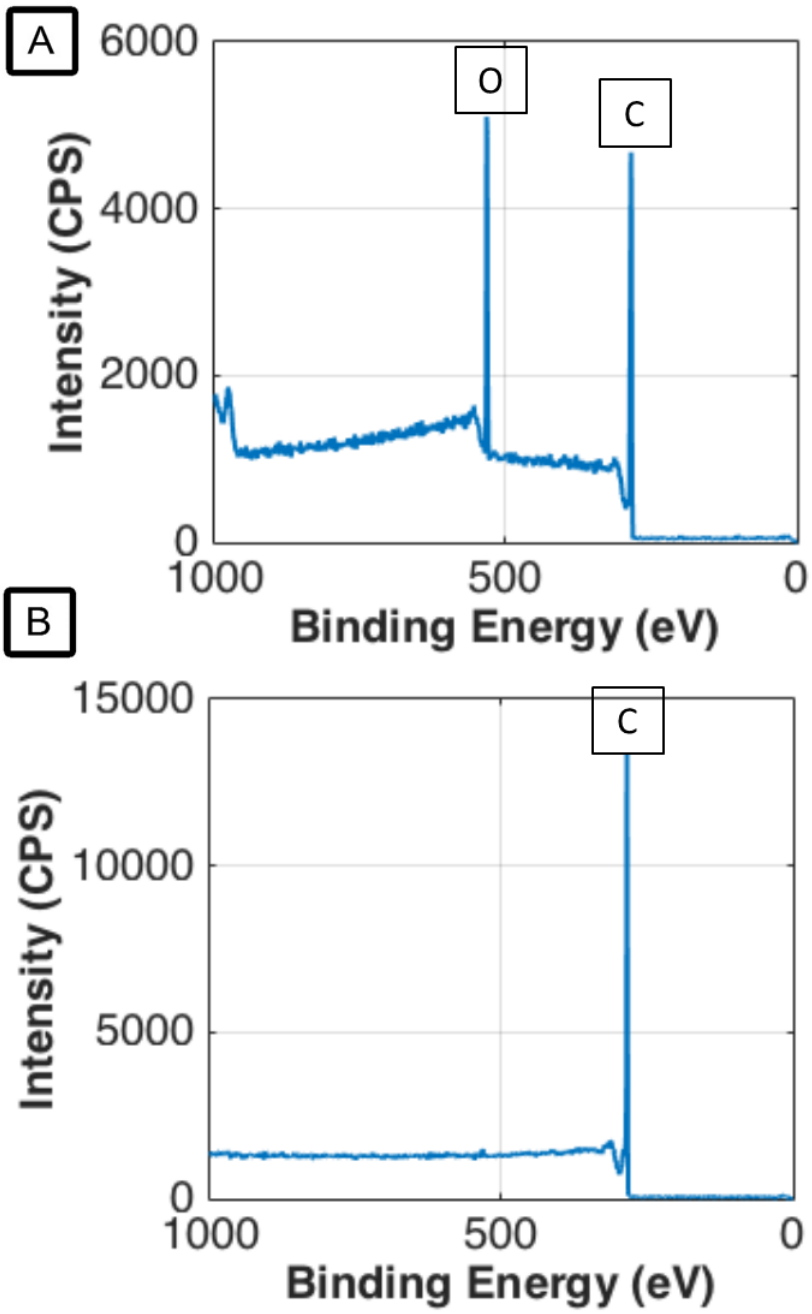

Figure 17 ***Survey scan of CFC (A) and CNT-CFC (B)****.*

Pristine CFC has both oxygen and carbon on its surface. However, the same fiber cloth coated with CNTs has carbon as its only surface composition. Figure 17 reprinted from "Hierarchical Hybrid Materials from Flexible Fabric Substrates" by Wang, W. (2020).

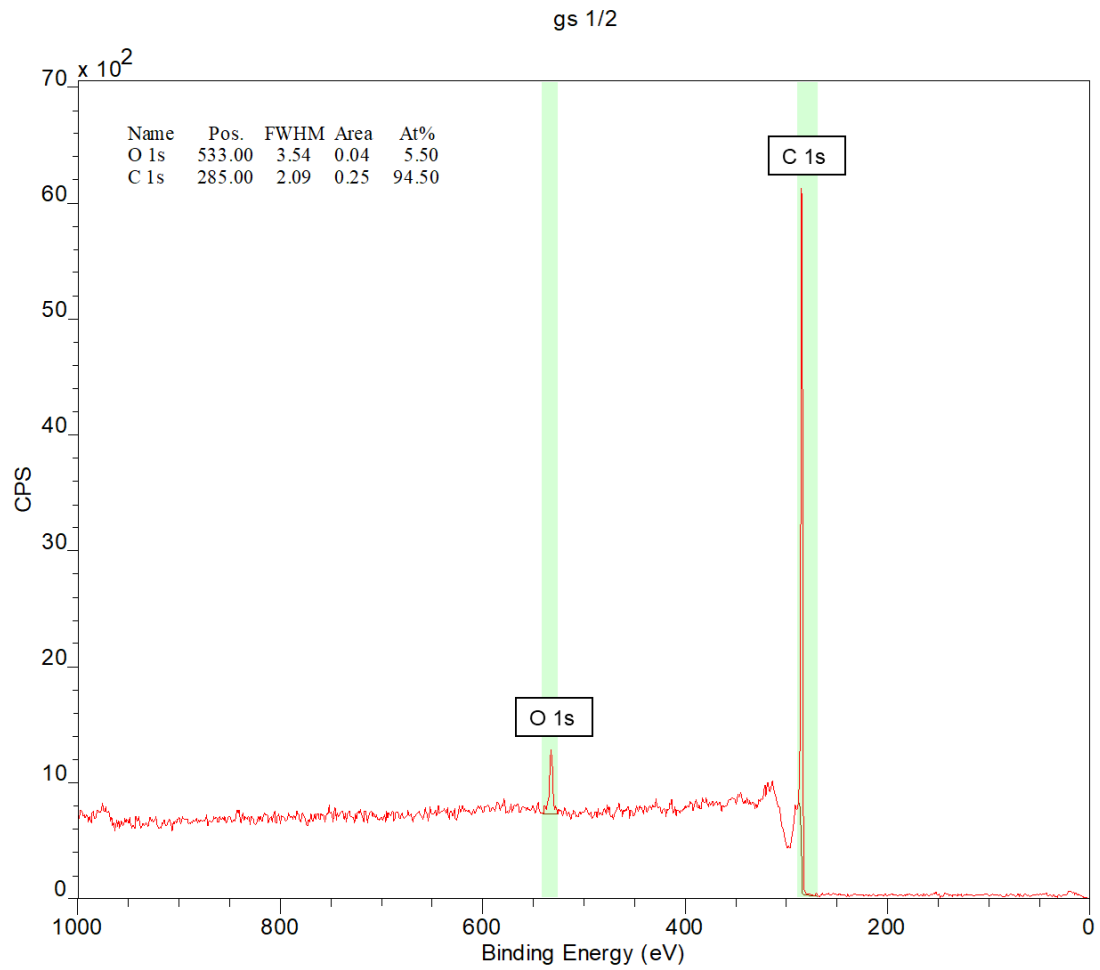

Figure 18 ***Survey scan of bleach treated CNT-CFC scaffold***.

Survey scans were performed between 0-1000 eV binding energy range to identify elements at the surface. The characteristic peaks at 533 eV and 285 eV represent the presence of oxygen and carbon on the scaffold, respectively.

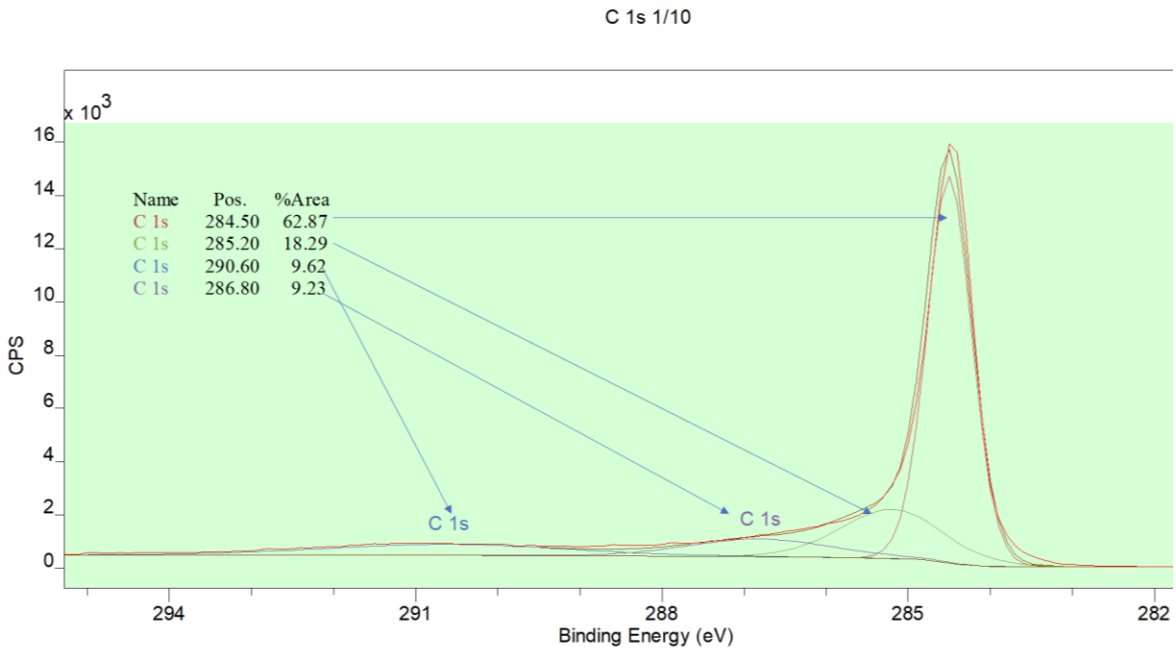

Figure 19 ***XPS fine-scan spectra of C 1s after bleach treatment of CNT-CFC.***

The most prominent peak at 284.5 eV is indicative of the sp^2 hybridization of graphitic carbon-carbon bonding. The second-largest peak at 285.2 eV represents the C-CH sp^3 hybridization and could be partly due to structural defects. The peak at 290.6 eV represents the pi-pi satellite peak and the 286.8 eV peak is characteristic of the C-O/OH functionalization and indicative of the wettability of the material.

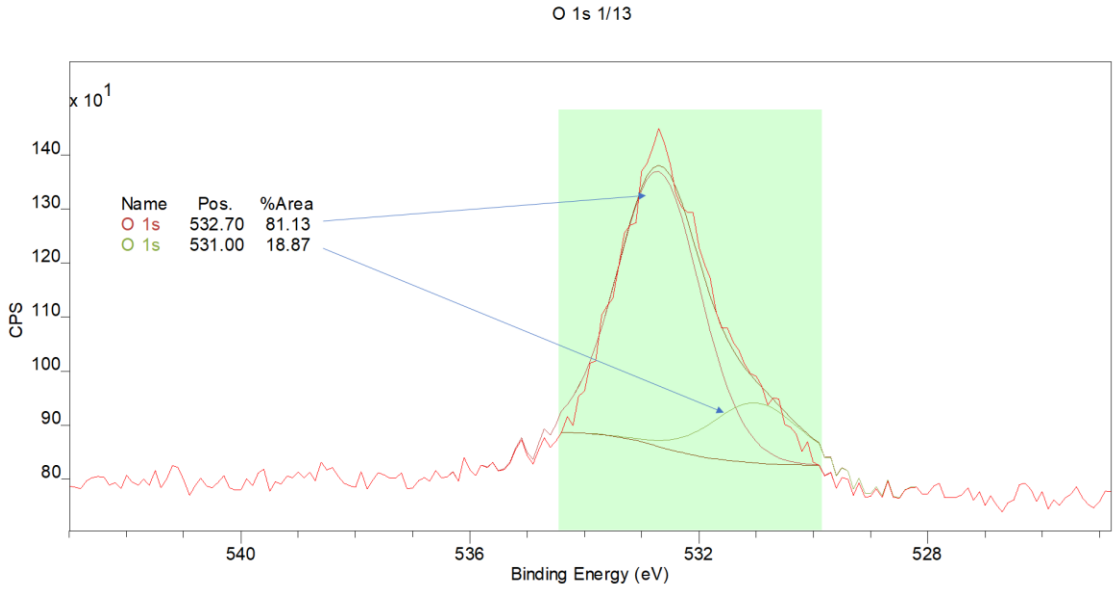

Figure 20 ***XPS fine-scan spectra of O 1s after bleach treatment of CNT-CFC.***

The predominant peak at 532 represents O/OH=C functionalization by the sodium hypochlorite modification. The second peak at 531 could be indicative of the carbonyl C=O bonding introduced by the surface oxidation.

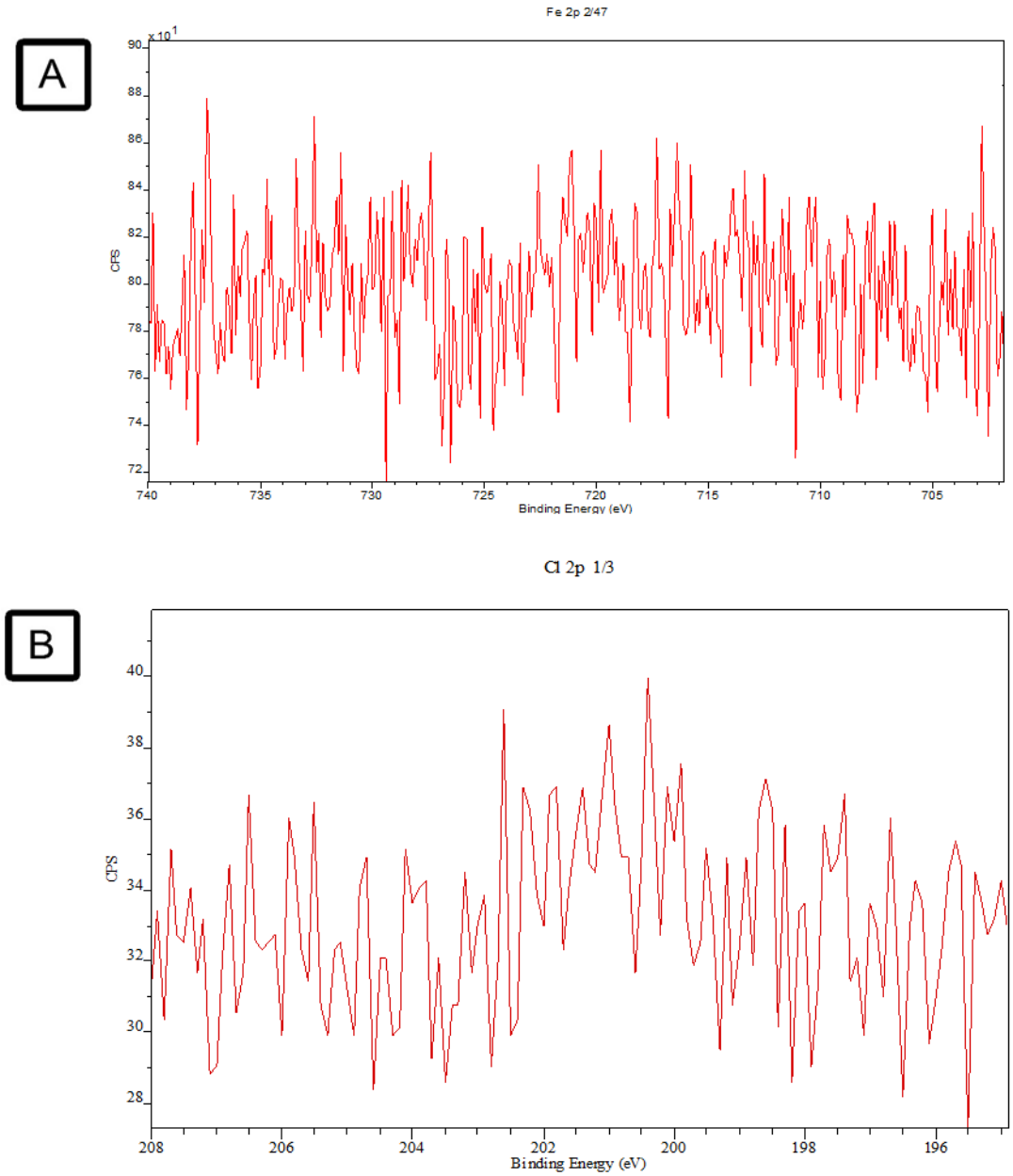

Figure 21 ***XPS fine-scan spectra of Fe after nitric acid treatment (A) and Cl after bleach treatment of CNT-coated CFC samples (B).***

After nitric acid treatment, surface iron was removed and no surface iron was detected. Any distinct peak for chloride was also not found indicating the washing steps resulted in effective rinsing and successful elimination of any remnant surface chloride moieties after sodium hypochlorite-based bleach treatment.

1.3.4 Elemental Characterization

The elemental quantification of various scaffolds used in the study is shown in *Figure 22*. EDS data was collected by using a probe current of 12 mA and an accelerating voltage of 20 kV. The data from at least two different locations per sample have been averaged and quantified in *Figure 22*. As evidenced from the XPS spectra as well as from the EDS characterization, it is evident that the carbon nanotube functionalization significantly enhances the carbon content on the surface and the main surface element is carbon. From EDS, it can be observed that carbon atomic level is close to 98% in CNT-coated scaffolds. CNT-coated samples also show remnants of the iron (Fe) catalyst used in the production of CNTs. However, it is expected as the CVD method employed in the preparation uses iron particles that are internalized within the CNTs [82].

From *Figure 22* (B) and (C), it is also apparent that the 1M nitric acid treatment reduces the iron content on the surface which is consistent with our prediction as mild nitric acid treatment removes remnant metal catalysts present on the surface. XPS analysis (*Figure 21*) also suggested that there is no surface iron present on the CNTs, meaning the EDS iron results mainly represent the internalized iron. The nitric acid treatment even at 1M concentration could mildly oxidize the surface and the increased oxygen content in the nitric acid scaffold could be due to that. The EDS analysis can capture up to 2000nm of the sample depth. Since it captures a large depth of surface, EDS may not represent accurate chemical state information, however, it provides reliable atomic information of the outer surface. Thus, to understand the molecular details of the surface chemistry of bleach treatment, XPS was utilized.

A

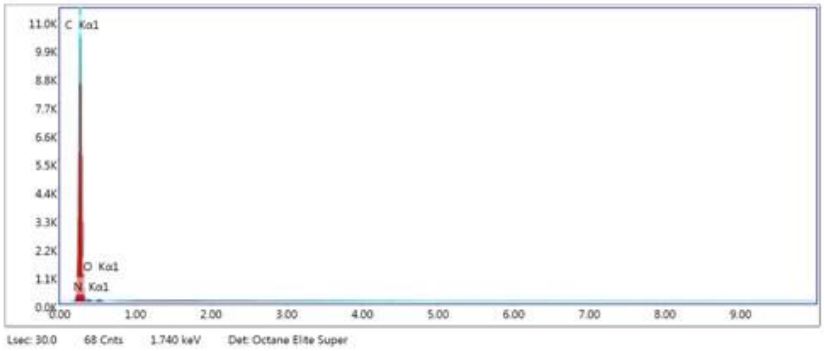

Sample	Atomic %			Weight %		
	C K	N K	O K	C K	N K	O K
CFC	93.133	5.71	1.12	91.883	6.57	1.47

B

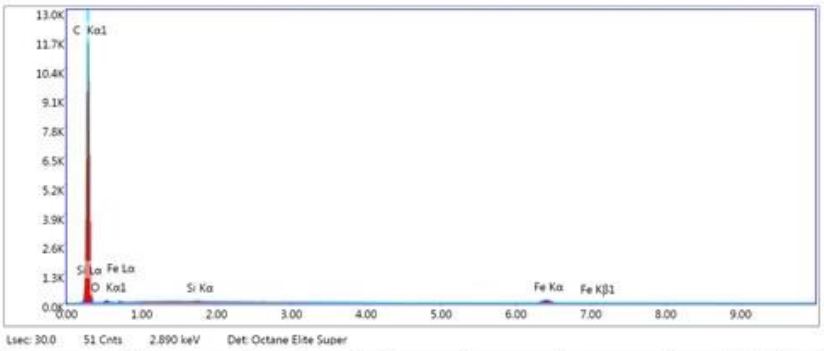

Sample	Atomic %				Weight %			
	C K	O K	Si K	Fe K	C K	O K	Si K	Fe K
CNT-CFC	98.015	1.365	0.04	0.58	95.5	1.77	0.09	2.645

C

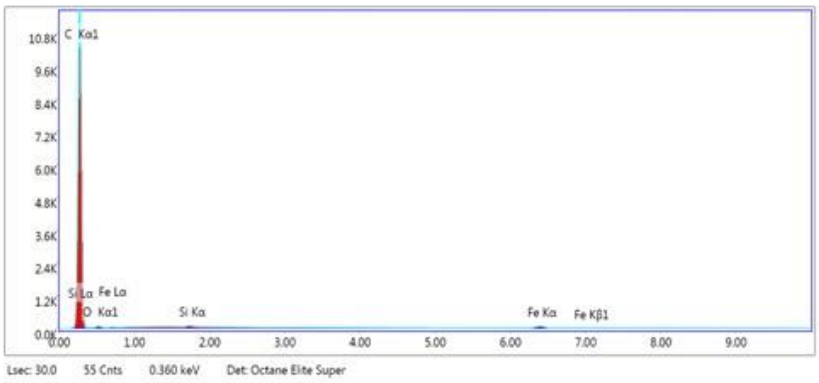

Sample	Atomic %				Weight %			
	C K	O K	Si K	Fe K	C K	O K	Si K	Fe K
CNT-CFC N	97.385	2.06	0.105	0.445	95.05	2.685	0.24	2.025

Figure 22 ***Elemental composition of scaffolds (A) Carbon fiber cloth (B) CNT-coated carbon fiber cloth (CNT-CFC) and (C) CNT-coated carbon fiber cloth after 1M Nitric acid treatment (CNT-CFC N).***

EDS data was collected by using a probe current of 12 mA and an accelerating voltage of 20 kV. Carbon nanotube coating introduces Si and Fe to the surface due to the plasma deposition and catalyst particles. Once surfaces are treated with nitric acid, surface iron content decreases.

1.4 Summary

In summary, we prepared different CNT-coated scaffolds by the floating catalyst CVD method to be utilized for cell growth applications. We prepared the carbon nanotube tailored carpets by coating CNTs on RVC foams with a 3D structure. RVC foams are highly porous which allows them to have a very high surface area (*Figure 9*). Various material properties of the surface of carbon foam scaffolds may assist cell proliferation. For example, the surface of RVC foam has high surface nanoroughness, which can affect biological interaction via adhesion and extracellular matrix modifications. However, while these surface material properties are thought to be important to the biological interaction between nanostructures and cells/tissues (and specifically cell growth), the 3D structure of RVC foam cannot provide directionality and may therefore be a limiting factor where cellular growth in a specific direction is required. The unique macro-micro scale architecture between the interconnected pores found in the carbon foam structures or the aligned fibrils within the carbon fiber supports could also differentiate the cell-interaction potential for these structures [83].

The aligned carbon fiber mats have a 2D structure, have high mechanical strength, and are very flexible. These fiber mats have a multiscale hierarchy where aligned fibrils form a parallel, multilayered band. Bands are then interwoven by other fibrils (Figure 10 A3). Such layers are parallel and highly directional. These structures alone and CNTs woven onto these structures can provide directionality to the growing cells [42]. Besides, both CNT-coated RVC foam and CFC are electrically conductive, which is an important material property for biological interactions with cells and tissues responsive to electrical stimuli such as brain neurons and glia, cardiomyocytes, and

osteocytes. CNT-coated foam and fiber scaffolds are also stable, easily functionalized, and can be utilized as contrast agents [54,84]

We first characterized the CNT-coated scaffolds by scanning electron microscopy and optimized two different lengths of CNTs bound to the fiber mats by changing the duration of the floating catalyst CVD procedure. These surfaces were termed ‘Short CNT’ and ‘Long CNT’ depending on their CNT length.

CNT-modified surfaces are superhydrophobic as the nanoroughness of the structure enhances their inherent hydrophobicity. Water droplet when in contact with such surfaces follows the Cassie–Baxter model where the presence of air pockets in the surface may avert the droplet contact with the full surface. We utilized different chemical functionalization as well as plasma treatment to change the surface wettability to hydrophilic. We also identified that along with air annealing, such hydrophilic surfaces could be reverted to superhydrophobic by autoclaving the scaffolds. Sodium hypochlorite-based bleach treatment to modify the wettability of the scaffolds was chosen due to their effectiveness, ease of use, potential to sterilize the surfaces, and minimal risk to cause structural defects.

Sodium hypochlorite-based bleach-treated hydrophilic scaffolds can be reverted to superhydrophobic by a single-step autoclave reaction. This reversible wettability effect of CNT-coated scaffolds was observed initially in our lab by air annealing where the scaffolds were treated with heat treatment at 110° for 3 hours [62]. Similar to this, by using an autoclave, we can achieve the superhydrophobic nature back. The reversible or switchable wettability of the scaffolds can be very useful for oil-water separation [85], lab-on-chip devices [86], and microfluidic devices [87].

Such bleach-treated scaffolds were also checked for their surface chemistry via X-ray Photoelectron Spectroscopy. The surfaces exhibited greater oxygen content

on the surface compared to as produced CNT-CFC and showed a possible carbonyl and O/OH=C functionalization with the sodium hypochlorite-based bleach treatment. Finally, there were no residues of chloride and iron metal catalyst on bleach-treated CNT scaffold and short CNT scaffold, respectively, indicative of successful treatment steps.

From this study, RVC foam, CNT-coated RVC foam, aligned carbon fiber mats (CFC), and Long CNT-coated aligned carbon fiber mats were chosen for the glioblastoma study as the tumor interaction with such hierarchical 3D and 2D structures could be crucial to understand the disease pathophysiology and to prepare targeted chemotherapy containing scaffolds after tumor incision. For the keratinocyte study and CFC, long and Short CNT-coated scaffolds were chosen due to their flexible and flat nature to be potentially used in band-aid-like wound healing applications and to understand the implication of length of CNTs in cell growth.

Section 2: BIOSCAFFOLDING PROPERTIES: INFLUENCE OF SURFACE TREATMENTS ON CELL GROWTH

2.1 Introduction and Background: Cell Growth on Bioscaffolds

2.1.1 Tissue Engineering and Bioscaffolds

Tissue engineering is a very important part of regenerative medicine. It generally involves three main elements: a scaffolding material, cells, and growth factors [88]. The biomaterial market was at $106 billion in 2019 and is estimated to triple by 2027 [89]. Various forms of bioengineered organs or tissues have been developed to date and so far, the highest success ratios with patients have been achieved in the skin [90], bone [91], bladder [92], and airway [93] based tissue-engineered constructs. Cells are generally allowed to grow into the constructed scaffolds and influence their microenvironment. The main aim and also the major challenge with tissue engineering is to have the engineered tissue mimic the tissues or organs the same way as it exists in nature.

One of the widely used approaches for tissue engineering is to use a matrix or scaffold to support cell adhesion, proliferation, and Extracellular Matrix (ECM) production and provide support to the growing tissue ultrastructure. Such material has to be biocompatible, able to support waste and nutrient exchange, provide a suitable surface for cell adhesion, cell growth, and ultimately tissue regeneration. The scaffold

also has to be mechanically stable to be able to support tissue formation without disintegration or breakage, at least until substantial ECM and growth and cellular factors have been generated and it also needs to be of relevant geometry and size [94]. Lastly, an ideal scaffold should also provide biological and surface cues to support and maintain cell growth [95]. There are various classes of bioscaffolds based on the materials used to produce them. It includes natural biological scaffolds, synthetic polymer scaffolds, composite polymer scaffolds, and nano scaffold materials.

Naturally occurring materials can be obtained from the natural source and then processed to make scaffolds [96]. It can include materials in their natural forms such as ECM or fundamental building blocks such as calcium phosphate or other molecules such as proteins, polysaccharides, lipids. It also can lead to potential immunogenicity as they are derived from natural sources and can be recognized as antigens [97]. To mitigate that risk decellularized ECM-based scaffolds can be used as they are processed from xenogenic or allogenic tissues [98]. The tissues are processed by chemical, physical, and enzymatic methods to remove any present cellular residues. Such scaffolds can also be produced as hybrid or composite scaffolds and are being used in a wide variety of applications. Some of the applications include tissue engineering for cartilage [99], cardiac [100], neuronal [101] regeneration applications. The major limitations of such scaffolds are that they have to be restricted to simple structures [98], cannot provide strong mechanical properties, and cannot be used for load-bearing applications [102]. Lastly, their degradation rates are variable and difficult to control [103].

Synthetic biodegradable polymer materials can be used as scaffolds for structural robustness. Such synthetic polymers can also be better in terms of their

immunogenicity. Their degradation rates can be easier to regulate than natural polymer materials and their mechanical properties are also modifiable [104]. However, they still pose a significant threat in terms of their potential cytocompatibility and toxicity. The contents of synthetic scaffolds are variable and some are unknown [105]. Upon degradation, they also release toxic by-products increasing the toxicity and associated risk [106]. Some synthetic scaffolds are also not very effective in promoting differentiation as there are difficulties with cellular attachment on these synthetic materials and some also increase chances of immune rejection [96,107,108].

Composite scaffold materials are made up of two different materials that can incorporate favorable attributes from different materials. Such materials can be combined to make a scaffold with preferred mechanical and structural properties and cellular compatibility. For example, ceramics have been introduced to polymer materials to give the scaffolds more mechanical robustness [109]. Although composite scaffolds show a great promise due to their properties, they still possess constituents not naturally present in the body and pose a significant threat in terms of their toxicity, biocompatibility, and degradation properties [96].

There has been a growing trend in using nano-scaffold materials as they allow detailed surface manipulation and allow for a hierarchical structure that can mimic naturally available structures [110]. By choosing the right substrates as the structural materials a hierarchical scaffold can be made that is tailored on both nano and micro scales. This can lead to a functional replacement of the naturally found tissue and desired properties characteristic of the tissues can be achieved [111,112]. Carbon nanotube-based scaffolds are extensively being studied ever since their invention [113] as they can undergo biodegradation [114], are biocompatible [115–117], can be

functionalized with different growth factors and molecules [118,119], and have been chosen in this study due to their unique surface properties.

2.1.2 Use of CNTs in Tissue Engineering

In the recent decade, CNTs have shown promise and have been extensively tested as a biomaterial in tissue engineering applications because of their unique properties. CNTs are relatively simple to manufacture and functionalize [120], easy to sterilize, have exceptional strength and stiffness [121], elasticity [122], electrical conductivity, and modifiable wettability [123]. Due to such unique properties, these multiscale scaffolds from our lab have been successfully used as catalysts [124], sensors [125], disinfection devices [60], thermal interface materials [21,64], and bioscaffolds [65,66]. Alongside other applications, there has been a huge interest to use CNT-containing materials for biomedical applications. Due to such properties, the role of CNT has been already investigated in a variety of biomedical applications such as drug delivery systems, gene therapy, biosensors, theragnostic applications, orthopedics, and many more [4,8,27].

CNTs are easy to sterilize [126], they also provide exceptional strength and stiffness to the material [121] and can also provide high elasticity [8]. Such attributes can be leveraged to make a robust and flexible scaffold to provide structural reinforcement for tissue engineering applications. This has been particularly useful for designing scaffolds for bone regeneration applications [8,127]. By controlling CNT functionalization, chances of graft vs host rejection can be significantly diminished and CNTs can be used to make a non-immunogenic and biocompatible scaffold [115–117].

Due to their smaller dimension, extensive surface area, and functionalizable surfaces, CNTs provide more attachment sites for drugs, nanoparticles, and chemicals and it is easier to form stable complexes of CNTs with drugs and small molecular therapeutics such as siRNA to enter mammalian cells [118,119]. Hence, Single-Walled carbon nanotubes (SWCNT) and Multi-Walled carbon nanotubes (MWCNT) have been identified as potential carriers for delivering therapeutics to cells for targeted therapeutic applications. For example, Cirillo *et al*. checked the efficacy of CNT-doped hydrogels for wound healing applications through the electrically tunable release of curcumin and were successfully able to control drug release by a varying voltage applied to the CNT containing hydrogels [128]. Additionally, targeted doxorubicin delivery against gastric cancer cells was achieved using functionalized carbon nanotubes [129].

Biophysical and biochemical stimuli are very important to guide cell alignment. Carbon nanotubes have biophysical contact cues such as electrical conductivity, surface topography, and nanoroughness. CNT can be easily tailored to alter or add a chemical functional group on the surface that can influence their surface wettability [123]. Concurrently, CNTs provide very high nanoroughness. Both wettability and nanoroughness can influence how cell growth takes place on a material. Surface nanoroughness plays an important role in cell adhesion on scaffolds [130,131]. The surface wettability of CNT scaffolds is tailorable [51,78] and it can facilitate cell adhesion and cell growth [66].

Due to their electrical conductivity, CNTs can be well suited for neuronal applications and the Mattson group was one of the first to explore that potential where they successfully used CNTs for neuronal growth applications [132]. Also, because of its electrical conductivity, CNT-based scaffolds can direct cell growth, which is

important for cell scaffold interaction [133]. For example, hierarchically aligned CNT sheets not only were successful in directing the cell morphology but also were useful for promoting the maturation of cardiac muscles of rats through electrical stimulation and improved spontaneous beatings [134].

Due to their unique thermal properties, CNTs have been successfully implemented to selectively induce cell death in cancerous cells by applying near-infrared light and by resultant heat-mediated cytotoxicity [135]. The therapeutic efficacy of CNTs for cancer treatment has also been checked by using SWCNT as photosensitizers for photodynamic therapy [62]. These attributes can be exploited for nanotherapeutics and toxic side effects of the drug cargo can be mitigated using targeted drug delivery utilizing CNT-based systems. These properties can be very useful for reconstructing tissues with physical and/or electrical complications due to their electrical conductivity and structural cues.

Development in the field of nanotechnology has yielded innovative solutions for mimicking the naturally observed hierarchical structures. Nanoscaled features can be used to regulate and positively influence cell growth, migration, proliferation, differentiation, and also to increase targeted drug delivery. A substantial amount of work has already been done in the tissue engineering field using carbon nanotubes as supporting material for cell growth applications due to their unique properties. For example, the Lalwani group [136] compared PLGA (poly(lactic-co-glycolic acid)) alone vs cross-linked SWCNTs/MWCNTs for mesenchymal stem cell growth *in vitro* and found MWCNTs provided the maximum cell growth amongst all utilized materials. The Akasaka group [137] found that CNT-coated cell culture plates provided better support for osteoblastic growth compared to culture plates without nanotube coating. These CNT supports have also been used in *in vivo* applications. MWCNTs have also been

found to be very effective for bone regeneration. The Abarrategi group [138] and Hirata et. al. [139] have analyzed the role of MWCNT supports for bone regeneration in mice and rats, respectively. Both groups have demonstrated that for bone regeneration applications, MWCNT scaffolds are substantially more effective than traditionally used bio-scaffolds.

Free CNT has been known to cross cell membranes due to multiple reasons including CNT length [119], hydrophobic nature [140], and chirality of CNTs [141]. Due to these properties, along with their characteristic shape, free CNTs could get taken up by adsorption [142] or by a 'needle-like' mechanism through cell membrane piercing due to their characteristic shape [118,143]. Reports also suggest that functionalized CNTs are excreted by urine (94%) and feces (6%) in mice [144]. According to recent reports using mouse models, CNT can be biodegraded through enzymatic oxidation *in vitro* as well as *in vivo* by the myeloperoxidase (MPO) enzyme [145–147]. There also have been reports suggesting that CNTs can be also degraded by oxidation as well as by neutrophils and macrophages *in vitro* as well as *in vivo* [145,148–152]. Despite such encouraging findings, the risk associated with the exposure of CNTs is still unclear.

2.1.3 The Gap in Knowledge of Current Work and Potential Solution

Despite its unique advantages for regenerative medicine, the biggest limitation with existing CNT-based studies is that free, detached, or disintegrated CNTs can also cause *in vitro* and *in vivo* cytotoxicity [153–156]. Hence, using CNTs using conventional approaches like using dried CNT suspension, coating, or doping the substrate with loosely attached CNTs could cause substantial toxicity. Numerous

studies have already identified that unconjugated or loose carbon nanotubes from such systems may lead to detachment of CNTs and these loose CNTs can lead to adverse effects on cell growth and promote cytotoxicity [72,157,158]. Also, metal catalysts used in the synthesis of nanotubes have also been strongly linked with the cytotoxic effects observed with the CNTs [159,160]. Certain parameters can be altered to limit the toxicity of CNTs such as purity, functionalization, and the dimension of CNTs; however, the overall toxicity associated with usage of CNTs can still be unpredictable and often lead to adverse effects [72,157,158].

To combat these issues, in the Dr. Mukhopadhyay lab, we have covalently bonded carpet-like arrays of CNTs to larger and more robust biocompatible carbon substrates. The covalent bonds provide robust attachment and an overall hierarchical solid that could provide the morphological and functional advantages of CNTs without the *in vivo* toxicity risks due to dispersion or disassociation of CNTs from the scaffolds [55]. These scaffolds are further processed by acid treatment to remove any metal catalyst impurities to eliminate chances of potential cytotoxicity.

The multiscale hierarchical arrangement of a scaffold could be important as a support for cell growth applications as cells also follow a similar multilayered structural arrangement. However, till now, how covalently bonded CNTs on 2D and 3D scaffolds would impact cell growth is not well understood. This will be one of the first studies assessing the potential of using covalently CNT-coated scaffolds for evaluating cytotoxicity, cell migration, and growth.

2.1.4 Hierarchical Carbon Nanotube-coated Scaffolds

In this project, we have utilized functionalizable topological features and extensive surface area of CNTs for tissue engineering applications while mitigating the potential cytotoxic effects. This is done by covalently linking MWCNTs to underlying carbon substrates. With such modification, we have created novel hierarchical systems to utilize the unique advantages of the carbon nanotube-coated materials as bio-mimetic scaffolds without the associated risks.

In the present study, we have carefully characterized the biological interactions of cells utilizing two different hierarchical systems. To do this, based on their architectural diversity, we have chosen two different base substrates: 1) reticulated vitreous carbon (RVC) foams, which are 3D in shape and have a porous structure and 2) aligned carbon fiber mats, which are 2D, flat and flexible supporting materials. We then modified these supports by growing covalently bonded carbon nanotube carpets. The RVC foams and aligned carbon fiber mats are available in various morphologies, so we can choose them according to the tissue characteristics.

Previous reports suggest that loose CNTs are susceptible to intracellular uptake and are also highly toxic for cellular growth in multiple cell types [154–156,161]. The Mukhopadhyay lab has shown that the attachment of CNTs to a scaffold can provide structural support and increased surface area such that cellular growth is promoted without the toxic effects noted with loose CNTs [64]. So, unlike the previous studies exploring the potential of CNTs for tissue regeneration applications, our MWCNT carpets are covalently attached to foams/fibers, contributing to mechanical strength and yet avoids any chances of detachment and its subsequent limitations.

Also, in our lab, we have control over CNT length and density by controlling the nano and micro features of the scaffolds. We can thus build a controlled multiscale architecture by growing carbon nanotube carpets on highly directional carbon fibers and highly porous carbon foams. This functionalization increases nanoroughness and specific surface area by several orders of magnitude and allows for tailored wettability through the attachment of functional molecular groups containing oxygen, halogen, and selective proteins which are very important for material for their ability to support cell growth. These CNT carpets also offer biocompatibility, permeability, high mechanical strength, and increased nanoroughness [65,66] that can modulate and aid cell attachment. Hence, we can customize the nano and micro-scaled features according to the tissue of interest and use them as bioscaffolds.

This is one of the first studies where such CNT-coated hierarchical scaffolds have been analyzed to evaluate their cell growth potential and the effects of their surface functionalization are assessed to check their potential for tissue engineering applications. We hypothesized that MWCNT-coated scaffolds are noncytotoxic, biocompatible, and can effectively support cell growth and cell migration.

2.1.5 CNT-coated Hierarchical Materials for Cell Growth Applications

To test our hypothesis, we evaluated scaffolds for two different cell lines, glioblastoma and keratinocyte cell lines In a previous study, these nanotube-coated scaffolds were tested with multipotent progenitor cell lines which can further transdifferentiate and nanoroughness was one of the critical factors regulating the differentiation process [66]. In this study, we tested glioblastoma and keratinocyte cell lines, which are already are in a differentiated state to determine the effects of carbon

nanotubes and their surface functionalization on cell growth to understand whether nanoroughness could still be a primary regulating factor for cell growth modulation. The CNT-coated scaffolds prepared for this study due to their unique mechanical and functionalization properties could be a very promising material for biomedical engineering applications.

2.1.6 Glioblastoma and Current Approaches for GBM

Glioblastoma multiforme (GBM) is the highest grade (WHO grade IV) malignant glioma with astrocytic cell features and accounts for more than 45% of all primary malignant brain tumors. GBM is the leading cause of death among brain tumor patients. A majority of GBM develop *de novo* (primary), while a small portion of glioblastoma develops progressively from lower-grade astrocytoma (secondary) over a clinical course of generally 5-10 years [162]. In addition, brain metastasis of other types of cancers occurs in approximately 15% of all cancer patients [163]. For example, brain metastasis occurs in 54% of lung adenocarcinoma patients [164,165].

There has been tremendous advancement in the diagnosis of this disease, but little if any improvement has occurred concerning the development of treatment options and improved morbidity [166]. Current therapies for GBM include surgical resection, chemotherapy, and radiation treatments [167,168]; however, these combined treatments have not proven to be effective at decreasing mortality rates, and the tumor recurrence rate for GBM is about 90% at the tumor location [169].

Despite advances in surgery and radiotherapy, the survival of patients with GBM has not significantly improved over the last 30 years. GBM patients survive an average of 15 months, and fewer than 3% are living 5 years after diagnosis [170–173].

There are several reasons for this high lethality. GBM cells are highly invasive, they aggressively infiltrate nearby healthy tissues making complete surgical resection impossible and giving recurrence a high likelihood. GBM also tends to be resistant to many chemotherapies. Also, many chemotherapies do not permeate the blood-brain barrier (BBB) in sufficient doses to contribute greatly to GBM patient recovery [170–173].

While localized chemotherapy injections post-surgical resection have been attempted, these therapies have not yet allowed for the slow-release, localized treatment necessary to effectively treat this tumor. One therapeutic alternative is the development of an implant that could utilize current nanomaterial properties that would allow slow-release chemotherapy administration directly to post-surgical resection sites.

The lack of curative options for GBM has motivated the field to explore and develop new drug delivery systems. Chemical modifications to current therapeutics utilizing nanocarriers have been explored to improve their ability to penetrate the brain past the blood-brain barrier; however, the efficiency and dose delivery have not been proven to reach therapeutic levels [167]. To bypass the BBB issues, several labs have developed nanostructures such as liposomes, lipid nanoparticles, nanocapsules, nanofibers, and hydrogel injectables that might provide a localized treatment option post-surgical resection [168,169,174–176]; however, therapeutic efficacy has been inadequate – possibly due to limitations in either the nanostructure and/or the chemotherapeutic drug of choice.

Currently, the only drug approved for local treatment of brain tumors is Gliadel®, a biodegradable carmustine wafer, that can be implanted post-surgical resection [161]. However, while this treatment has proven effective in increasing

patient life for 2–3 months [177,178], the wafer has several flaws. These failings include: 1) the flat wafer design does not allow for tumor contact with the complete implant surface; 2) the polyanhydride copolymer is designed to break down and release encapsulated chemotherapy within the first few days and cannot be utilized beyond this limited timeframe; and 3) the half-life of the chemotherapy utilized (carmustine) is only 15 min, which is too short to treat highly migratory cells, such as GBM [161,167]. Moreover, the most common and effective chemotherapies, such as alkylating chemotherapy temozolomide (TMZ), have not been extensively studied for localized therapy.

2.1.7 Potential of using CNT-coated Scaffolds for Glioblastoma

Although it has been well-established that the GBM tumors are resistant against the existing treatments, the reason behind the resistance is still not well studied. It is believed that the tumor microenvironment and ECM promote therapeutic resistance, but the underlying mechanism is still poorly understood [179]. Plus, the current therapeutic models do not provide the relevant microenvironment necessary to maintain the active physiology of the GBM tumors [180]. Most of the studies checking the migratory and invasive potential of these tumors are still being done on a 2D surface, primarily with tissue culture plates. Knowing the tumor cell interaction with the surrounding area is a critical step that is poorly understood [181]. While it is well understood that the tumor interaction on a 3D surface is desired to have a technical understanding of the disease, only a few approaches are being used to look at the same [182,183]. Hence, it can be asserted that while the concept and potential for using a nano-therapy for treatment of GBM post-surgical resection have been

highly sought after; proper design, characterization, and testing will be needed before deciding if it can be a potentially viable treatment option.

To address that, a scaffold that can provide a 3D surface for cells to interact and maintain the physiological, as well as biochemical environment, could be a great step forward for the field to understand the disease and for finding potential ways to mitigate it [184]. Hence, knowledge from this study could give important considerations for chemotherapy conjugated scaffolds aimed to be localized post-surgical resection for GBM treatment.

Ideal scaffolds for this purpose should neither cause cytotoxicity nor increase proliferation and/or migration of glioblastoma cells. In other words, any cytotoxicity should be induced by the attached chemotherapeutic drug and not the scaffold structure. An idyllic implant should also be stable, easy to sterilize, easily reproducible, and non-immunogenic. As bioscaffolds, different CNT conjugated scaffolds have already been examined for various applications and have the potential to fulfill all of the above requirements.

While CNTs are very effective as tumor-targeting agents and for drug delivery applications for tumors [185–187], the bio-interaction between CNT-coated 2D or 3D hierarchical scaffolds and glioblastoma cells is unknown. Because of their unique material properties, CNTs easily allow for alterations in functionalization, which will be necessary for future therapeutic development for this cancer.

2.1.8 Wound Healing and Current Approaches

Skin is the largest organ in the body and is the first line of defense against external insults. The skin protects our internal organs and tissues throughout our

lifetime. The dermis also acts to control temperature and fluid balance; therefore, wounds can increase the risk of infection and dehydration [188–190]. Since 2008, approximately 5 million cases of traumatic injuries involving skin (accidents, burns, firearms, intensive surgeries) are registered every year which causes a financial burden of $25 billion annually in the USA [191]. The World Health Organization (WHO) predicts that every year, over 300,000 deaths are linked to fire-related burns. In India alone, over a million people are affected by burn-related injuries every year [192]. Such physical injuries and emotional trauma affect millions of people worldwide [193]. WHO also predicts that skin traumatic injuries will overtake heart disease and cancer and become the primary cause of death by 2020 worldwide [188].

2.1.9 Wound Healing Process

Human skin mainly is formed of three layers: epidermis, dermis, and hypodermis [194]. Epidermis is the outermost layer and consists of keratinocytes, melanocytes, and epidermal stem cells [192]. The dermis has collagen ECM, elastin, glycosaminoglycans (GAGs), and fibroblast cells. Apart from providing mechanical properties, the dermis also provides sensory properties to the skin and has nerve endings. Dermis also has sebaceous glands, hair follicles, and sweat glands [192]. The hypodermis is mainly comprised of adipose tissue.

Wound healing is a process that involves multiple cell types, vascular systems, and various cytokines and growth factors. Four major phases take place and overlap one another in wound healing.

Hemostasis is the initial stage when an injury happens. Blood and lymphatic fluid outpouring occur, and coagulation pathways are activated, which are necessary

to stop the flow of the blood. There is an initial cascade event of vasoconstriction followed by vasodilation. This vasodilation, in turn, allows for the recruitment of white blood cells and additional thrombocytes [195]. In the next step, the inflammation phase, the newly recruited white blood cells and thrombocytes start releasing more and more cytokines and expedite the inflammation. Platelet activation increases histamine and serotonin secretion which increases vascular permeability. Increased vascular permeability and angiogenesis allow for increased growth factors, cytokines, and metabolites to reach the wound site [195]. Fibroblasts are also recruited in this step which produces collagen, which provides scaffolding for the healing [196]. Inflammatory cells such as monocytes, neutrophils also get activated in this step. Neutrophils play a major role in this step by removing the damaged cells, bacteria, pathogens from the site [197]. This inflammation phase goes on for several days.

The proliferation stage begins and occurs throughout the wound healing process. Fibroblasts begin to produce more collagen and stabilize the wound. In the Re-epithelialization stage, basal and suprabasal keratinocytes migrate towards the wound bed from the wound edge and periphery and start proliferating [198]. Due to increased activation of dermal fibroblasts through growth factors, they also increase their migration and proliferation at the wound site and secrete ECM proteins. Fibroblasts then adopt a different phenotype, myofibroblast, and aid in wound contraction, and physically start closing the wound [199,200]. This process can go on for several weeks, depending on the wound. Maturation is the final maturation and remodeling step that takes place, which strengthens the wound and can go on for a year. Wound contraction peaks after week 3 [195]. The keratinocytes and fibroblasts from the vicinity start the secretion of matrix metalloproteases (MMP), which degrades the excess ECM and collagen. ECM also remodels to resemble the normal tissue

[201]. Keratinocytes and fibroblasts play a key role in the different stages of the wound healing process and have been evaluated in our study with the CNT-coated scaffolds to assess whether the scaffolds can support cell growth and cell migration of keratinocytes and fibroblasts.

2.1.10 Effects of Environmental Stressors on Wound Healing

Wound healing can be affected by multiple factors such as environment, diet, medication, contamination and all these factors can affect the outcome of the skin injury [202]. Environment plays a big role and it can expedite or defer the recovery process [203–205]. The effect of environmental stressors on skin health is also one of the topics that needs more attention [206]. So, in this study, we assessed the effects of two major stressors UVB and TCDD on keratinocytes growing on scaffolds to check if the CNTs can provide cytoprotection against the stressors.

TCDD and UVB have proven to aggravate wound healing and both act through the AhR pathway [207–210]. It is shown that chronic AhR activation can promote skin-related conditions such as premature aging, apoptosis, and carcinogenesis [211–214]. Constitutive activation of AhR in mice also causes inflammatory skin lesions [215]. Hence, in this study, we are focusing on two potent environmental stressors UVB and TCDD that can directly affect skin proliferation, migration, and differentiation and analyzing their effects in presence of the CNT-coated scaffolds.

2.1.10.1 Effects of TCDD on the Skin and Wound Healing

Skin wound healing is aggravated by environmental insults. 2,3,7,8-tetrachlorodibenzo-*p*-dioxin (TCDD) is a type of dioxin that is persistent in the environment and gets produced when organic materials with chlorine are combusted

[216]. Such events include natural events such as forest fires, Australian and California wildfires, the byproduct of industrial processes, and medical waste incineration. TCDD is a potent immunotoxicant [209,217] that enters the body through the skin or ingestion of contaminated animal products and accumulates due to its lipophilic nature. TCDD has a half-life of 2-4 weeks in rodents [218] but has a half-life of around 7-11 years in humans [219,220] and it is resistant to metabolic breakdown.

TCDD is the most potent dioxin [208] and exerts its toxicity mostly through the aryl hydrocarbon receptor (AhR) signaling pathway as a high-affinity exogenous ligand of the AhR [208,209]. The AhR pathway activation induces the production of xenobiotic-metabolizing enzymes [221]. AhR also regulates cell proliferation, cell differentiation, and apoptosis [222,223].

Harmful effects of TCDD exposure are well-reported and can cause cancer [224], immunosuppression and decreased resistance to infection [225,226], developmental defects, and reproductive abnormalities [227]. As potent dioxin, the effects of TCDD have been found as lethal and cytotoxic in animal studies [208,228]. Studies on the same hairless mouse models also show that TCDD disrupts the epithelial cell differentiation process [229]. TCDD has also been linked to pro-inflammatory effects on the wounded tissue and shown to disrupt normal healing in mice [230].

TCDD can halt the cell cycle and reduce the cells in G0/G1 perturbing the cell cycle and slows down cell proliferation [231–233]. It also has adverse effects on the pathology and physiology of human skin including skin lesions and reactions [230]. In HaCaTs, commonly used immortalized keratinocytes, it has been shown that TCDD can lead to a decrease in cell viability and apoptosis [231]. TCDD is also shown to

decrease cell proliferation of HaCaTs, particularly at higher concentrations [231,234], and slows down the cell migration during wound healing [235].

However, the effects of TCDD in studies involving skin are highly variable. For instance, in some studies involving and primary keratinocytes [236] and immortalized keratinocytes HaCaTs [237,238], TCDD did not slow down cell proliferation. In addition to that, some studies also found that TCDD accelerates cell proliferation and differentiation of primary human keratinocytes [239,240].

Hence, both *in vivo* and *in vitro* experiments show that ligand-dependent activation of the AhR pathway through TCDD induces different and sometimes conflicting effects on cell proliferation and differentiation. There is considerable variation in effects dependent on cell type, tissue, and species. However, from the evidence, we wanted to assess whether the TCDD causes a significant impact on keratinocyte cell proliferation and migration and conducted experiments to analyze the same.

2.1.10.2 Effect of UVB on Skin Cell Growth

The ultraviolet (UV) spectrum is divided into Ultraviolet A (315–400 nm), Ultraviolet B (280–315 nm), and Ultraviolet C (200–280 nm) [241]. The shorter range of radiations encompass more energy and also pose a great threat to stability to unprotected organic materials. The most damaging solar radiations, UVC, and extensive amounts of UVB are fortunately absorbed by the stratospheric ozone layer in the atmosphere which blocks almost all wavelengths shorter than 310nm [242].

The UVA can penetrate the dermis of the skin and can produce reactive oxygen species effectively causing skin aging and wrinkles [243,244]. However, UVA is not as harmful as UVB in terms of its biological effects. The fraction of UVB that passes

through the ozone layer can be absorbed by the epidermis and dermis [245]. Moderate and regulated UVB exposure is required to produce vitamin D in the body and promote health [246]**.** However, due to their shorter wavelengths, the fraction of the available UVB is also enough to pose a threat by mediating photochemical damage.

Excess UVB exposure can also lead to dermatitis, inflammatory responses on the skin, skin pigmentation, erythema, weakening of skin barriers [247,248]. In the skin cells, UVB radiation also induces cell death, growth arrest, DNA damage, premature skin aging, and skin cancer [249,250]. Due to their outermost cutaneous position, keratinocytes are particularly vulnerable to UVB radiation. UVB also restricts keratinocyte cell migration and has been shown to delay wound healing response *in vivo* and *in vitro* [251].

2.1.11 Need for a New Implant Material for Wound Healing

Pressure wounds and burns can cause ulcerating lesions that do not close. In these cases, normal cellular tissue regeneration and repair are insufficient. Current therapies for these types of wounds lack both cosmetic satisfaction and functional compatibility [252]. Such approaches include skin substitutes, wound cleaning, infection control, and surgical dressings [191]. However, these therapies only treat the symptoms and the surgical procedures are often complicated and can lead to morbidity [253]. When insufficient donor skin is available, the cultured keratinocytes have allowed for increased donor surface area than conventional methods [254]. Hence, in recent times skin grafts are being extensively studied in an attempt to close these wounds [255]. While this practice can be successful in some circumstances, current approaches to manufacture suitable scaffolds for skin-related injuries are

suboptimal, and grafted skin typically leads to extensive scarring, immune rejection, infection, slow healing and requires substantial post-operative care [192,256–258].

Improved understanding of skin wound healing has opened up a new avenue in terms of preparing new scaffolds, implants, or materials that are cytocompatible as well as cosmetically and functionally viable for skin regeneration. Recent biomedical advances have made significant progress to address this concern by utilizing engineered scaffolds upon which tissue can be artificially grown as a graft and/or utilized as an anti-microbial surgical dressing for wound care. In theory, these skin substitutes could provide faster, more natural healing with less scarring as compared to standard surgical dressings and/or tissue grafts [259]. Chitosan and collagen are the two most widely used materials used as bio-scaffolds for wound healing. Puracol Plus® (Medline Industries), Fibracol Plus® (Systagenix), or BIOPAD® are collagen-based marketed scaffolds for wound healing, but they need to be typically replaced after a few days which do not qualify them as typical scaffolds. Also, it has been argued that a scaffold comprised solely of type I collagen is not enough to provide complete regeneration [260–263]. Hydrogel based formulations, Tegagel™ (3M) and Vigilon® (CR Bard), Xelma® (Mölnlycke Health Care), silicone-based formulations, Integra™ (Integra Life Sciences) and Biobrane® (Smith & Nephew) and natural ECM scaffolds, Matristem®, Primatrix™ (TEI Biosciences), Alloderm® (Lifecell), GraftJacket® (Wright Medical Technology), and DermaMatrix™ (Synthes) have been reported to be effective in treating radiation wounds, venous ulcers, open pilonidal wounds, acute full-thickness wounds, and chronic wounds, due to diabetes [193,264–266]. Although these scaffolds have the supreme advantage of faster repair rate and better tissue remodeling, they are far from being generalized bio-scaffolds for wound healing due to their limitations in effectiveness in varied wound types, handling, preparation,

sterilization, and shelf life [267]. Clinical studies on these bio-scaffolds showed promising results, however many of them are not translatable to real-world applications. Thus, the need for stable and better bio-scaffold arises for wound healing and related treatment [268].

The CNT-coated scaffolds due to their unique properties can be a great fit as wound healing scaffolds, which can potentially address the limitations of the existing implant materials. CNTs provide advantages over other materials in terms of tissue biocompatibility, immune compatibility, cell adhesion (due to nano-roughness and wettability) [130,131], and ease of modification (i.e. ability to chemically 'functionalize' for possible drug delivery) [269]. CNTs have also been implicated as being beneficial in cell growth applications of many cell types including epithelial keratinocytes [270,271]. Three-dimensional structures have been shown to support and maintain normal proliferation while the healing progresses [272] and CNT-coated scaffolds due to their hierarchical nature could be very effective at wound healing applications.

The CNT-coated scaffolds used in this study have been used as excellent adsorbents of aromatic compounds [61] and are also extremely lipophilic structures [63]. The adsorption capacity of a structure is directly proportional to the surface area and carbon nanotube-coated scaffolds due to its substantially large surface area could potentially negate the potentially adverse effects of TCDD. Carbon nanotubes have also been shown very effective to block UV rays, including UVB rays, and have been tested in sunscreen applications against UV radiation [273]. Hence, in aiding the cell growth of keratinocytes and supporting wound healing, CNT-coated scaffolds can also minimize the effects of environmental stressors, and the effectiveness of such scaffolds is checked in this study.

Thus, the objective of the keratinocyte study was to assess cell proliferation and cell migration of keratinocytes on the CNT-coated scaffolds and to check the viability of the scaffolds as future wound healing scaffolds. In addition to that, we also focused on checking the cell growth of keratinocytes on the scaffolds in presence of environmental stressors such as UVB and TCDD to check their potential cytoprotective impact.

2.1.12 Immune Response and Bioscaffolds

The immune response can be broadly categorized into the innate immune response and the adaptive immune response. The innate immune system is also termed as the first line of defense. It will protect against foreign bodies and pathogens through physical barriers such as skin and chemical barriers such as saliva. An innate response against foreign pathogens that evades such barriers will be done through recognition of these elements as non-self materials and by internal defenses, which will involve inflammatory response, complement proteins, phagocytic cells, and natural killer cells [274]. Both innate and adaptive immune responses are dependent on white blood cell activities [274]. There are five major types of white blood cells or leukocytes: lymphocytes, neutrophils, monocytes, eosinophils, and basophils.

A wide range of cells are found in the innate immune system, such as polymorphonuclear cells such as eosinophils, neutrophils, and basophils, mononuclear phagocyte cells such as monocytes, macrophages, and dendritic cells, and lymphocytes such as natural killer cells; while T and B lymphocytes mediate the adaptive immunity.

Adaptive immunity can be categorized into cell-mediated and humoral immunity. Cell-mediated immunity is carried out by T cells. T cells are a type of white blood cells. They originate from bone marrow and move to the thymus for maturation. After leaving the thymus, T cells continue to mature. Different T cells play different roles in the immune system. T cells can mainly be categorized into T helper cells (CD4+) and cytotoxic T (CD8+) cells. All T cells are activated by recognizing antigen present on either major histocompatibility complex (MHC) I or II on other cells. Recognition of MHC I results in activation of the CD8+ T cells into effector T cells or cytotoxic T cells, which are directly able to recognize foreign antigens such as pathogens and viruses. Such T cells can also proliferate and differentiate the effector cytotoxic T cells which can kill the antigens. These CD8+ T cells can also recruit other cells to bolster the immune response against the antigen. The T helper cells or CD4+ T cells recognize MHC II cells on antigen-presenting cells and get activated. Activated T helper cells can provide an adaptive immune response against the specific antigen and also makes long-lived memory cells in the case when the same pathogen attacks again.

B cells also a type of white blood cells. They are derived from hematopoietic stem cells (HSC) and they originate and mature in the bone marrow. B cells mediate humoral immunity through antibody secretion. B cell recognizes antigen through B cell receptors (BCR) present on their cell membrane and they produce antibodies against the same.

B cell antigens can be categorized into thymus-independent (TI) and thymus-dependent (TD) antigens. TI antigens are enough to promote B-cell stimulation and for proliferation and differentiation of B-cells. Alternatively, some antigens require cooperative assistance from B cells and T helper cells to stimulate an antibody

response. Such antigens are called Thymus-Dependent (TD) Antigens. A wide variety of antigens are TD antigens. B cells internalize and present the TD antigen to a helper T cell via MHC II molecules. This leads to subsequent expression of CD40L on the T cell surface, which then, in turn, interacts with the CD40 receptor of the B cells. The T helper cells also increase secretion of IL-4 which triggers B cell proliferation and differentiation and turn them into plasma cells.

Plasma B cells are terminally differentiated and able to uniquely trigger antibody production against a specific antigen. Memory B cells stay in systemic circulation and can only get activated once they encounter their specific antigen. In the case of reinfection with the same antigen, the memory T cells generate a profound antibody response that has more affinity for the antigen than the primary antibodies and the amount of antibodies secreted are also substantially more than the primary response [275,276].

If a foreign scaffold is implanted, the innate immune response will be the first to react. Once the object or implant has been recognized as non-self or foreign, the succeeding adaptive immune reaction will take place which is governed by effector cells, which is specific to the type of the antigens and could potentially lead to implant rejection. The initial studies checking the immune response of external materials characterized the macrophage fusion around the scaffolds to understand the impact of foreign materials on immune function [277,278]. Shortly after that, a study involving a cage implant revealed that foreign body reaction involving scaffolds involves polymorphonuclear cells (mainly neutrophils) as well as lymphocyte involvement besides the monocyte/macrophage response [279]. Now, it is established that biomaterials can induce stimulation of innate [280–282] as well as adaptive immunity

[283–285]. In this study, we focused on understanding the B-cell lymphocyte function to assess the effect of the scaffolds on immune function.

Various immune cells and their cytokine secretion also regulates the wound healing process. For example, IL-4 has been deemed as proliferative and aids liver and skin regeneration [286,287]. So, in this study, we examined whether the scaffolds alter the inherent cytokine response of the keratinocyte cells as well as immune cells.

2.2 Materials and Methods

2.2.1 Chemicals and Reagents

TCDD (308 μM) dissolved in 100% DMSO was purchased from AccuStandard, Inc. DMSO was purchased from Sigma Aldrich. For the B-cell stimulation study, Human interleukin-4 (IL-4) was purchased from Cell Signaling Technology, Inc, and human recombinant CD40 ligand (MEGACD40L®) was purchased from Enzo Life Sciences. For all UVB studies, Philips TL 20W/12 RS SLV/25 light in Dr. Jeffery Travers' Lab at Wright State University was used.

2.2.2 Cell Culture and Cell Seeding on Scaffolds

The U-87MG cell line is derived from a female patient in 1968 [288], has been previously characterized [289], and commonly used cell line for studying glioblastoma [290,291]. Human Glioblastoma cells (U-87MG) were purchased from ATCC (ATCC® HTB14™). Cells were maintained in Eagle's Minimal Essential Medium (EMEM; ATCC, USA), supplemented with 10% Fetal Bovine Serum (FBS; Corning, USA) and 1% penicillin/streptomycin (PenStrep; Gibco, USA). Cells were maintained at 80–90% confluence, split with 0.05% Trypsin-EDTA (Gibco, USA), and the media changed twice a week.

The HaCaT cell line is a spontaneously immortalized keratinocyte cell line that was first isolated from a male epidermis [292]. HaCaT has been further characterized [293] and is a commonly used cell line in skin research [3,4]. Immortalized keratinocytes (HaCaT) were supplied by Dr. Jeffrey Travers at Wright State University. Telomerase-immortalized, normal human foreskin fibroblasts (NHF1) were supplied

by Dr. Mike Kemp at Wright State University and were originally obtained from Dr. William Kaufmann from the University of North Carolina. NHF1 cells were first derived from a neonatal foreskin [294] and immortalized by the ectopic expression of the catalytic subunit of telomerase [295]. Cells were maintained in HyClone Dulbecco's Modified Eagle Medium supplemented with high glucose (DMEM; GE Healthcare Life Sciences), supplemented with 10% Fetal Bovine Serum (FBS; corning), 1% L-Glutamine (200 mM; Gibco), and 1% Antibiotic-Antimycotic (Gibco). Both cell lines were maintained at ~80% confluence. HaCaTs were split with 0.025% Trypsin-EDTA (0.25%; Gibco) and NHF1s were split using 0.05% Trypsin-EDTA (Gibco, USA). Fresh culture media was provided every 48 hours.

For B-cells, suspension cell lines CL-01 cells, and SKW 6.4 cells were used. These cells are derived from different Burkitt lymphoma patients and are EBV-transformed cell lines. CL-01 cells express surface IgM and IgD and can undergo class switch recombination upon stimulation [296], this cell line is further characterized [297] and was purchased from Novus Biologicals. SKW 6.4 (SKW WT) cells were derived originally from the Daudi B-cell line [298]. SKW 6.4 cells express surface IgM and have been previously characterized [299,300] and purchased from ATCC (ATCC® TIB-215™). Both cell lines were maintained in RPMI complete media prepared by RPMI 1640 (HyClone, GE) supplemented with 10% bovine calf serum (Thermo Fisher Laboratories), 13.5 mM HEPES (Sigma), 1.0 mM non-essential amino acids (Corning Cellgro), 1.0 mM sodium pyruvate (Corning Cellgro) and 50μM 2-mercaptoethanol (Fisher) and pH was adjusted using filter-sterilized 1N NaOH. The media was changed every 3 days. CL-01s were maintained around $1x10^5$ cells/ml to $3x10^5$ cells/ml and SKWs were maintained around $2x10^5$ cells/ml to $1x10^6$ cells/ml. For all experiments

except for the glioma study, all cell lines used were incubated under the same conditions and maintained at 37°C in a humidified 5% CO_2 environment.

2.2.3 Surface Treatments of CNT-coated Scaffolds and Cell Seeding

For the glioblastoma study, all cylindrical foam (0.5 cm height, 0.5 cm diameter) or carbon fiber (1 cm × 1 cm) supports with (CNT-coated) or without (pristine) carbon nanotube functionalization were treated with 1M nitric acid at room temperature to remove metal impurities and amorphous carbon. This nitric acid treatment also oxidizes the surface and makes it hydrophilic without destruction of the CNT structure [301,302]. Samples were then transferred to sterile 96-well or 24-well tissue culture plates (foam and fibers, respectively) and were sterilized via ultraviolet (UV) light irradiation for 1 hour in 70% isopropanol. These scaffolds are hydrophobic. For hydrophilicity modification, scaffolds were incubated for 1 hour with 10% sodium hypochlorite-based bleach at 25°C, washed multiple times with deionized (DI) water, and then transferred to sterile tissue culture plates before ultraviolet light treatment. Once air-dried, U87MG cells were seeded at respective densities (96-well: 5×10^3 cells/well; 24-well: 2.5×10^4 cells/well, 12-well: 5×10^4 cells/well) and allowed to grow on the nanomaterial for 1 day, 3 days, 7 days, or 14 days.

For the second part of the study involving keratinocytes, fibroblasts, and B-cells, we used carbon fiber supports with (CNT-coated) or without (CFC) carbon nanotube functionalization. For CNT-coated scaffolds, we used Short CNT-coated hydrophobic scaffolds, Short CNT-coated hydrophilic scaffolds, Long CNT-coated hydrophobic scaffolds, and Long CNT-coated hydrophilic scaffolds. All scaffolds were pre-treated with methanol, 1M nitric acid followed by treatment with 70% ethanol.

When the scaffolds were completely dried, they were autoclaved for 30 minutes at 121°C followed by incubation in 70% isopropanol treatment. After autoclave treatment, all scaffolds remain hydrophobic. For hydrophilicity modification, scaffolds were incubated for 1 hour with 10% sodium hypochlorite-based bleach and subsequently washed with autoclaved DI water. Once dried, all the hydrophilic scaffolds were also pre-wetted overnight by complete media to aid cell attachment [303].

Both adherent cell lines, HaCaTs and NHF1s were seeded in the form of a 100-150µl concentrated cell suspension on top of the scaffold surface. The scaffolds were then incubated for 4 hours for allowing cellular attachment. After 4 hours, culture media was added to the plates. We used seeding densities of 5 x 10^4 cells/well for 12-well plates, 2.5 x 10^4 cells/well for 24-well plates, 0.5 x 10^4 cells/well for 24-well plates, and 1.5 x 10^5 cells/plate for 35mm^2 plates unless otherwise mentioned. To understand how suspension cells interact with CNT-coated scaffolds, SKW and CL-01 cells were first seeded in 12-well plates at 2 x 10^4 cells and 1 x10^5 cells in a 2 ml suspension, respectively. After 24 hours, scaffolds were introduced to each well. For experiments lasting longer than 4 days, cells along with scaffolds were transferred to 6-well plates. In those wells, additional 2ml culture media was added to the wells on days 5 and day 7 to avoid higher cell concentrations which can induce cell-cell activation and also cell death [304].

2.2.4 Immunofluorescence

To visualize GBM cells for morphology, nano-interaction, and cell counts, immunofluorescence was performed. The cells were grown for 1, 3, 7, or 14 days, washed 3 times with cold PBS, then fixed in 4% paraformaldehyde. The cells were

then washed 3 times with PBS and blocked/permeabilized at room temperature with 5% normal rabbit serum in PBS for 30 min with 0.2% Triton X-100. The primary antibody, rabbit Glial Fibrillary Acidic Protein (GFAP, 1:500, Dako North America), was incubated overnight at 4°C. All scaffolds were then washed 3 times with PBS and incubated for 1 hour with a secondary antibody (Alexa Fluor 488-conjugated donkey anti-rabbit IgG, 1:300; Jackson Immunoresearch Laboratories, Inc., USA) at room temperature in the dark. GFAP intermediate filament was chosen as a differential marker for U87MG cell lines as it is highly expressed in astrocytes, the original cell type for glioblastoma tumors, and has been widely used for U87MG cell studies [54,305]. Cell nuclei were stained using 4',6-diamidino-2-phenylindole (DAPI). Images were captured using an AMEFC4300 EVOS fluorescent color inverted microscope.

2.2.5 Elution Test

SWF used in the study was made according to the formula by Bradford *et al.* [306]. Briefly, 0.1M sodium chloride, 40mM sodium hydrogen carbonate, 4mM potassium chloride, 2.5mM calcium chloride, and 3% bovine albumin were added in 100 mL deionized water to prepare SWF. To prepare the extracts for the elution test, we incubated the scaffolds in simulated wound fluid (SWF) for 14 days. These prepared extracts were first checked for their pH and further diluted to 25%, 50%, and 75% in the complete cell culture media as well as quiescent cell culture media.

Briefly, for the elution test, the HaCaTs were first grown in 96 wells until they were confluent. Immediately after that, they were incubated for 3 days in the presence of extracts prepared from the scaffolds in complete media or quiescent media. Quiescent cells were prepared by incubating confluent cells with quiescent media (1%

FBS) for 24 hours [307]. Cell growth was assessed visually by microscopy, and the cytotoxicity was measured with CytoTox-ONE™ Homogeneous Membrane Integrity Assay (Promega). This assay measures LDH from cells with a damaged membrane. When the cells are undergoing apoptosis, necrosis, or any other form of damage, the plasma membrane gets damaged. This, in turn, releases LDH in the cell culture supernatant which can be analyzed by quantifying amounts of resorufin from resazurin in the assay. The amounts of produced resorufin are proportional to the amount of LDH released in the media and can give an estimation of cytotoxicity generated by external factors. The LDH assay is a commonly used technique for cytotoxicity assessment [308,309].

LDH assay was performed according to manufacturer instructions on days 1 and 3 after elution treatment. Briefly, equal volumes of cell supernatant were mixed with the prepared lactate dehydrogenase (LDH) reaction mixture and incubated for 15 mins. The suspension was quickly mixed with the stop solution and fluorescence was measured at 560nm/590nm. Positive cytotoxic controls were prepared by adding the lysis solution to control cells.

2.2.6 Scanning Electron Microscopy (SEM)

In this experiment, we used scanning electron microscopy (SEM) to check the effect CNTs on keratinocyte cell growth and attachment. HaCaTs were grown on 1 cm × 1 cm scaffolds placed in 12-well plates. Cells were grown for 3 days and 7 days. The cells were then washed twice with PBS and fixed using 4% paraformaldehyde for 1 hour. Scaffolds were then washed twice with PBS for 10 minutes followed by 10-minute ethanol dehydration treatments in increasing concentrations: 25%, 50%, 75%,

95%, 100%. The purpose of the gradual dehydration steps is to preserve the structure of cells to be visualized under vacuum and it is a commonly used technique when performing SEM with biological samples [310,311]. Scaffolds were then air-dried and sputter-coated with gold particles [310,311] for 10 seconds to make the samples electrically conductive, improve the signal-to-noise ratio and protect samples from the heating effect of the electron beam. Samples were finally visualized on SEM using ~3 kV accelerating voltage and a working distance of ~8 mm.

2.2.7 UVB and TCDD Treatment

To determine the toxicity and antiproliferative effects of UVB on cell number and viability, we seeded HaCaT cells on 35mm^2 plates, cultured them for 24 hours for cell attachment, and treated them with varying doses of UVB. Prior to UVB treatment, we removed the culture media from the plates as it can induce toxicity with the UVB treatment [312] and added 400µl of PBS to avoid drying of cells. The lids were also removed before UVB exposure to ensure the cells are directly exposed to the UVB and none of the radiation is blocked in the process. Immediately after treatment, we washed cells two times with PBS and added 2ml complete media to each 35mm^2 plate.

For the TCDD study, after allowing 24 hours for cell attachment, the keratinocytes were then treated with complete media with 30nM TCDD (treatment group) or 0.01% DMSO (vehicle group), respectively. For cell number assessment, cells were trypsinized with 0.25% Trypsin-EDTA and counted on Vi-Cell cell Counter (Beckman Coulter).

2.2.8 Cell Proliferation

Cell proliferation while growing on various carbon scaffolds was determined using the CellTiter 96® Aqueous One Solution Cell Proliferation Assay kit (Promega). In this assay, 3-(4,5-dimethylthiazol-2-yl)-5-(3-carboxymethoxyphenyl)-2H tetrazolium (MTS) is bio-reduced into a formazan product by dehydrogenase enzymes, which are active in living cells. Sample blanks were prepared using culture media with or without scaffolds and without any cells. After the cells were grown for the appropriate duration, samples were washed twice with PBS before being incubated in MTS colorimetric reagent.

The incubation time of the MTS reagent with U87MG and HaCaT was 3 and 1.5 hours, respectively. After the incubation, 100µl of the solution was transferred to a 96-well plate, and absorbance was measured at 490 nm using a BioTek Synergy H1 hybrid multi-mode fluorescence microplate reader. Cell proliferation was expressed as (OD_{test} – OD_{blank}) and represented as OD values for glioblastoma study and cell control normalized values were presented for the keratinocyte study. Cell culture media was replaced every two days.

2.2.9 DNA Quantification

DNA concentrations were measured using Quant-iT™ PicoGreen® dsDNA Reagent (Thermo Fisher, USA). PicoGreen binds to dsDNA and forms a luminescent complex and gives an estimation of the DNA content present in the cell lysate. Picogreen assay for DNA quantification is a commonly used technique to estimate cell proliferation on biomaterials [313,314]. After the cells were grown for 1 day, 3 days, 7 days, or 14 days on scaffolds in 12 well plates, samples were washed twice with PBS

and stored in lysis buffer at −80 °C overnight. Samples were then thawed, homogenized, and centrifuged. DNA quantification was done according to the manufacturer's protocol. DNA standard provided in the kit was used as a positive control and culture media without cells was used as a negative control. Fluorescence intensity was measured at an excitation wavelength of 480 nm and an emission wavelength of 520 nm using a BioTek Synergy H1 hybrid multi-mode fluorescence microplate reader.

2.2.10 Cytotoxicity Analysis

To check whether the scaffolds contributed to cytotoxicity on growing keratinocytes, we performed cytotoxicity analysis using LDH on HaCaTs grown on different bioscaffolds on days 1, 3, and 5. At each time point, plates were first incubated at room temperature for 20 minutes, the supernatant was collected and mixed with an equal volume of LDH assay reagent mix according to manufacturer instructions. After 15 minutes of incubation, stop solution was added to stop the reaction, and fluorescence was measured at 560nm/590nm. For positive controls, to account for the maximum possible LDH release, cells were lysed using the LDH positive control.

2.2.11 Cell Labeling

When noted, cells were stained with cell tracking dyes, CellTracker™ Red CMTPX, or CellTrace™ CFSE using the manufacturer’s instructions. Briefly, for labeling, the cells were trypsinized, counted and the cell suspension was centrifuged. The pellet was resuspended in PBS with appropriate dye staining solution and cells

were incubated in the dark for either 15 minutes (CMTPX, CFSE) and mixed with an equal volume of complete culture media. After 15 minutes of incubation, the suspension was again centrifuged, pellets were resuspended in the complete media, and plating was performed. For calcein-AM staining, cells were incubated with calcein-AM green (Thermo Fisher) for 1.5 hours. For fixing cells with paraformaldehyde, cells were first washed 2 times with PBS and incubated with 4% paraformaldehyde for 1 hour. For nuclear staining, cells were first washed 2 times with PBS and stained with 4',6-diamidino-2-phenylindole (DAPI) for 10 minutes.

2.2.12 Cell Migration from CNT-coated Scaffolds

2.2.12.1.1 Assessing Intrascaffold Cellular Migration

To understand if the cells can migrate within the scaffolds, we cut 3 cm x 1 cm CNT-coated scaffolds into three 1 cm x 1 cm scaffolds to ensure that the scaffolds could have a compatible planar alignment. We then transferred two scaffolds to wells of a 12-well plate and seeded 0.25×10^6 cells/scaffold. After 24 hours, the scaffolds were transferred to a 100mm cell culture plate and aligned so as the unseeded scaffold stays in the center and the pre-seeded scaffolds will be adjacent to the center scaffold. We incubated the plate for 3 days and then transferred the scaffolds to a 12-well plate. The scaffolds were then washed 3X with 1X PBS, fixed with 4% paraformaldehyde for 1 hour, and cell nuclei were stained using DAPI. Images were captured using an AMEFC4300 EVOS™ Digital Color Fluorescence Microscope.

2.2.12.1.2 Modified Scratch Wound Assay

To understand the role of the CNT-coated scaffolds in wound healing, we first used a modified scratch wound assay which was quite similar to a traditional scratch wound method. We first seeded 0.25×10^6 or 0.125×10^6 HaCaTs in a 12 or 24 well plate, respectively, and allowed them to become confluent. Once confluent, a vertical scratch was made using a 200ul pipet tip and a pre-seeded scaffold with Red CMTPX fluorescent dye loaded HaCaTs (0.25×10^6 for 12 well or 0.125×10^6 for 24 well) was placed on top of the scratch. The scratch plates were then incubated for 48 or 72 hours and image analysis was performed using BioTek Cytation5 or AMEFC4300 EVOS™.

2.2.12.1.3 Cell Migration assay using PDMS Cell barriers

In this experiment, we prepared and used PDMS cell barriers to block the center of the 35mm plates similar to the Oris™ Cell Migration Assay platform which is traditionally used to perform barrier-based migration assays in 96 well plates [315,316]. The PDMS barriers were provided by Dr. Tyler Nelson at WPAFB. The barriers were cut to be 10mm in diameter and were treated with 70% ethanol for sterilization. They were then placed in the center of 35mm plates to block cell growth in the region. HaCaTs were first treated with CMTPX fluorescent dye and seeded at 0.6×10^6 cells/plate. At the same time, HaCaTs were seeded on the 35mm plates, 1×10^6 cells were also seeded on the scaffolds. The cells seeded on the scaffolds were treated with CFSE green fluorescent dye. Once the center barriers were removed, the scaffolds were placed in the center and the plates were incubated for 3 days. After the end of the incubation, scaffolds were transferred to a fresh plate. Both plates were washed 3X with 1X PBS, fixed with 4% paraformaldehyde, and observed under Olympus BX51.

2.2.12.1.4 Cell Migration From and Towards CNT-coated Scaffolds

To understand the cell migration from the scaffolds, all the carbon bioscaffolds used in the study were placed in a 12-well plate and seeded with 1×10^6 cells/scaffold for HaCaTs and 0.5×10^6 cells/scaffold for NHF1 cells. After 24 hour incubation, the scaffolds were then washed with 2X PBS and transferred to an empty well, and fresh media was added to the scaffolds. The cells were allowed to proliferate on the scaffolds for up to 10 days and cell migration towards the empty plate was observed to understand how keratinocytes and fibroblasts migrate from the scaffolds. To analyze cell migration towards the scaffolds, 0.75×10^5 NHF1 or 1.5×10^6 HaCaT cells were seeded per well in 12-well plates, and 24 hour after incubation, scaffolds were placed in the wells with pre-seeded cells. The scaffolds were removed on day 5 and stained with calcein-AM, fixed with 4% paraformaldehyde, stained with DAPI, and visualized under AMEFC4300 EVOS™ microscope.

2.2.13 Photodynamic Therapy (PDT)

HaCaTs were seeded in a 35mm plate at 0.15×10^6 cells/plate. Once the cells were near confluent, they were treated with PDT as previously described [317]. Briefly, cells were first treated with a photosensitizing agent, 5-Aminolevulinic acid hydrochloride (5-ALA) for 4 hours in the dark. It was then removed and replenished by a mixture of Hank's balanced salt solution (HBSS, Sigma Aldrich) and 1.5mM Bovine Serum Albumin solution (BSA, Millipore Sigma). For the scaffold groups, 1 cm × 1 cm scaffolds were placed in the center, and cells were then treated with blue light (415 nm) at 20 J/cm^2 doses in Dr. Jeffery Travers' Lab at Wright State University. Scaffolds

were then removed, cells were washed with 2X PBS to remove the dead cells, and then trypsinized and counted on the Vi-Cell cell counter.

2.2.14 Cytokine Analysis

The inflammatory cytokine profile was analyzed by Dr. Tyler Nelson's lab at WPAFB. Briefly, cytokines were measure in cell culture supernatants of HaCaTs grown for 5 days on the scaffolds as well as SKW and CL-01 cells grown in presence of the scaffold for 4 days by using a 25-Plex Human ProcartaPlex™ Panel 1B (Invitrogen). The reads were performed using a Luminex FLEXMAP 3D® System. The heatmaps were generated using Prism 8.r

2.2.15 Sandwich Enzyme-linked Immunosorbent Assay (ELISA)

ELISA was performed as described previously [318] to measure IgM and IgG secretion from B cell lines. For analyzing antibody secretion, the cell suspension was collected, centrifuged at 680xg for 5 minutes and the supernatant was stored at -80°C for later ELISA analysis. Briefly, 96-well ELISA plates were coated with 100 µl/well of capture antibody and incubated overnight at 4°C. For IgG capture antibody, goat anti-human IgG Fc (Abcam ab97221) was used at 1:500 and for IgM capture, Goat Anti-Human Ig-UNLB (SouthernBiotech, 2010-01) was used at 1:1500. Dilutions were made using 0.1M sodium carbonate bicarbonate buffer, pH 9.6. Following the overnight incubation, plates were washed twice with 1X PBS + 0.05% Tween-20 and thrice with ddH_2O and then blocked by adding a blocking solution of 1X PBS + 3% Bovine Serum Albumin (BSA, Millipore Sigma). Blocking solution (200 µl) was added to all the wells and plates were either left overnight at 4°C or for 2 hours at room

temperature. Plates were again washed twice with 1X PBS + 0.05% Tween-20 and thrice with ddH2O.

Standards for IgG and IgM were diluted in RPMI complete media and 100 µl of standards were added to the plates. IgG standard was purchased from Bethyl Laboratories (A80-105) and IgM antibody was purchased from SouthernBiotech (0158L-01). The concentration range used for IgG standard curve was from 0.104 ng/ml to 6 ng/ml and 1.172 ng/ml to 150 ng/ml for IgM. Along with standards, 100 µl of samples were also added to the ELISA plate and incubated for 1.5 hours at 37°C. Once the incubation was over, plates were then washed thrice with PBS + 0.05% Tween-20 and four times with ddH_2O. Secondary antibodies conjugated with HRP were added to all of the wells. HRP-conjugated goat anti-human IgG (Bethyl Laboratories, A80-104P) was diluted at 1:10,000 and HRP-conjugated goat anti-human IgM (SouthernBiotech, 2020-05) diluted at 1:4000, and 100 µl of secondary antibody solution was added to each well and incubated for 1.5 hours at 37°C. Plates were then again washed thrice with PBS + 0.05% Tween-20 and four times with ddH_2O. Finally, 100 µl TMB substrate (Millipore) was added to each well in the dark and incubated for 30 minutes for IgG or 5 minutes for IgM. The stop solution (4N H_2SO_4, Fisher Scientific) was added (100 µl/well) after the appropriate time frame and the absorbance values were read at 450nm using a SpectraMax Plus 384 UV/VIS microplate spectrophotometer (Molecular Devices). SoftMax Pro was used to process the standard curves and to do the calculations of the secreted IgG and IgM.

2.2.16 Data Analysis

All experiments were performed 2-3 times in triplicates. For experiments replicated three times, endpoints from the triplicates were averaged and counted as a single n for statistical analysis. Data is reported as the mean ± standard error of the mean (SE) for the keratinocyte study and mean ± standard deviation for the glioma study. Statistical analysis was carried out using GraphPad prism. Statistical significance between CNT and pristine group was measured by one-way ANOVA and Tukey post-hoc analysis by comparing both groups. Statistical significance in the fold-effect between scaffold groups and the controls was measured by two-way ANOVA analysis followed by Bonferroni post-tests or Dunnett's multiple comparisons test by comparing each sample to the corresponding cell controls and/ or CFC controls. Statistical differences between fold-effect between TCDD treatment group and cell control group or their respective vehicle control groups were measured by one-way ANOVA analysis followed by Bonferroni post-test comparing each sample to the cell control vehicle group or by comparing each TCDD treatment group to their respective vehicle controls. Statistical significance in the fold-effect between UVB groups and control groups was measured by one-way ANOVA with Tukey post-hoc analysis by comparing all groups to cell controls. Statistical analyses were performed with a 95% confidence interval ($p<0.05$).

2.3 Results

2.3.1 Effects of Surface Wettability of Carbon Nanotube-coated Scaffolds on Glioblastoma Cell Growth

Our first study focused on investigating the bio-interaction between CNT-coated and surface-modified 2D or 3D hierarchical scaffolds and glioblastoma (GBM) cells. This was done to understand the potential viability of the scaffolds as possible implant structures for glioblastoma postresection therapy. To understand the interaction between GBM and scaffolds, we used the U87MG cell line, which is a commonly used GBM cell line in brain cancer research [290,291].

In this study, we nano-functionalized two different carbon supports, 1) rigid porous foams that could potentially fill surgical voids and 2) flexible carbon fiber cloths that can be applied as sheets. These supports were also used without the CNT nano-functionalization as the respective foam or fiber controls and referred to as ‘pristine’ supports.

U87MG Cell Proliferation on CNT-coated Scaffolds is Modulated by Surface Wettability

To correlate GBM cell growth to material characteristics, we first visualized cells for nano-interaction using immunofluorescence. U87MG GBM cells were grown for 3 or 14 days on carbon fiber scaffolds with or without CNT-coating. U87MG cellular morphology and cytostructure were visualized using Glial Fibrillary Acidic Protein (GFAP, 1:500), and all cells were stained with DAPI to confirm staining and aid with cell counting (Figure 23 *A*). GFAP/DAPI cell counts for each image were performed using ImageJ. U87MG cell counts were significantly decreased on CNT-coated

scaffolds after 3 days of growth when compared to those grown on pristine controls (*Figure 23 B*). However, after 14 days of growth, U87MG cells show a significantly higher cell count on CNT-coated scaffolds when compared to pristine supports *(Figure 23 B*). Therefore, growth on CNT-coated scaffolds induced bi-phasic cellular growth in U87MG cells when compared to the growth curve shown for pristine supports. Immunofluorescence to visualize cells grown upon carbon foam scaffolds (pristine or CNT-coated) was also performed. However, due to carbon's opaque nature and the 3D morphology of the foam scaffolds, reliable imaging using confocal microscopy was not adequate for quantification and this data is therefore not presented.

The inherent wettability of the CNT scaffolds is superhydrophobic and with sodium hypochlorite-based bleach treatment, they were made hydrophilic to evaluate the effect of surface wettability on cell growth. No significant changes between pristine carbon fibers and CNT-coated carbon fiber scaffolds in U87MG cell counts were noted post sodium hypochlorite-based bleach-treatment at any given time point of cell growth (Figure 24 *B*).

Alongside IF, we also utilized MTS colorimetric assay to measure the cell proliferation of U87MG cells grown on carbon foam or fiber supports with or without CNT-coating. MTS colorimetric assay measures tetrazolium, an electron coupling agent which is then reduced by metabolically active cells. This assay is commonly used as a correlative measure of cell proliferation and viability. Cell proliferation was significantly decreased in CNT-coated scaffolds when compared to pristine substrates after 3 or 7 days (Figure 25). The change in nanomaterial hydrophilicity after sodium hypochlorite-based bleach treatment resulted in increased cell proliferation of the CNT group and no significant differences were noted between the pristine and CNT-coated groups for the foam scaffolds (Figure 25 *B*). A significant decrease in U87MG cell

proliferation was still noted in the CNT-coated fiber scaffolds on days 3 and 14, which were not seen on days 1 and 7 (Figure 25 *B*).

To further explore the effects of nanotubes on cell growth and to understand the differences between cell counts and MTS colorimetric assay data, we measured the amount of DNA, which directly correlates with cell numbers [319]. U87MG cells were grown for 1, 3, 7, or 14 days before cells were lysed and DNA measured. No significant differences in DNA concentration were noted between the pristine and CNT-coated carbon foam structures with or without sodium hypochlorite-based bleach treatment (Figure 26). For the shorter time points, similar to that noted in the MTS colorimetric assay and immunofluorescence, there was a significant reduction in U87MG DNA concentration suggesting a decrease in cell number with the CNT-coated fiber compared to pristine fiber structures (Figure 26 *A*). This reduction was nullified after bleach treatment (Figure 26 *B*).

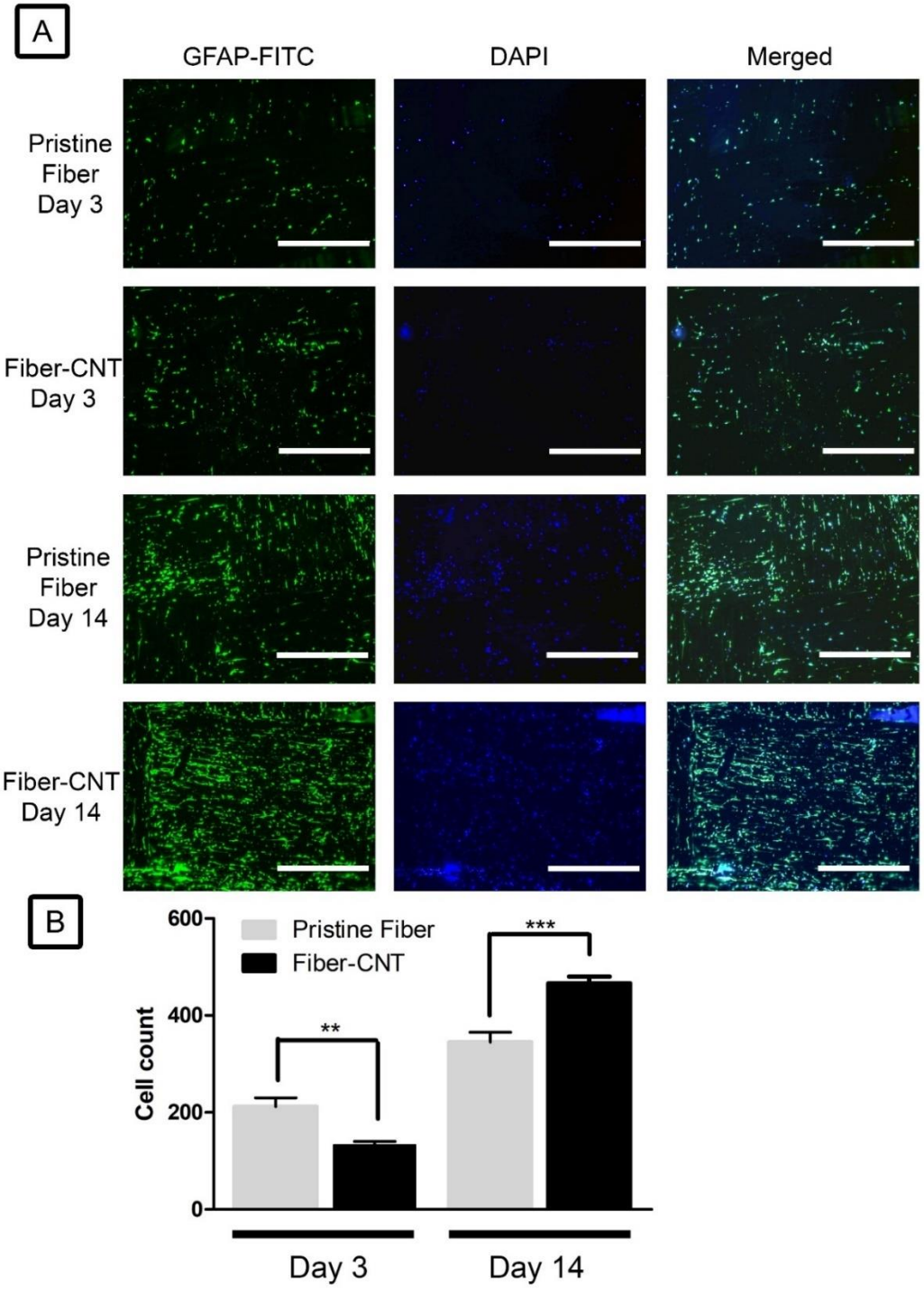

Figure 23 ***Bi-phasic U87MG cell proliferation on CNT-coated carbon fiber scaffolds.***

Representative Immunofluorescence images of cell-seeded carbon fiber scaffolds with or without CNT-coating (A). Cells are labeled with GFAP (green) and cell nuclei with DAPI (blue). Scale bar represents 1000µm. Cell counts performed via ImageJ

*from 4x images (n=3/sample) (B). Statistical significance was measured by one-way ANOVA and Tukey post-hoc analysis by comparing both groups. Error bars denote SD, ** denotes p < 0.01, *** denotes p < 0.005. Reprinted from "Multi-walled carbon nanotube carpets as scaffolds for U87MG glioblastoma multiforme cell growth" by Parikh, S. D., Dave, S., Huang, L., Wang, W., Mukhopadhyay, S. M., & Mayes, D. A. (2020). Materials Science and Engineering: C, 108, 110345. Copyright by Elsevier*

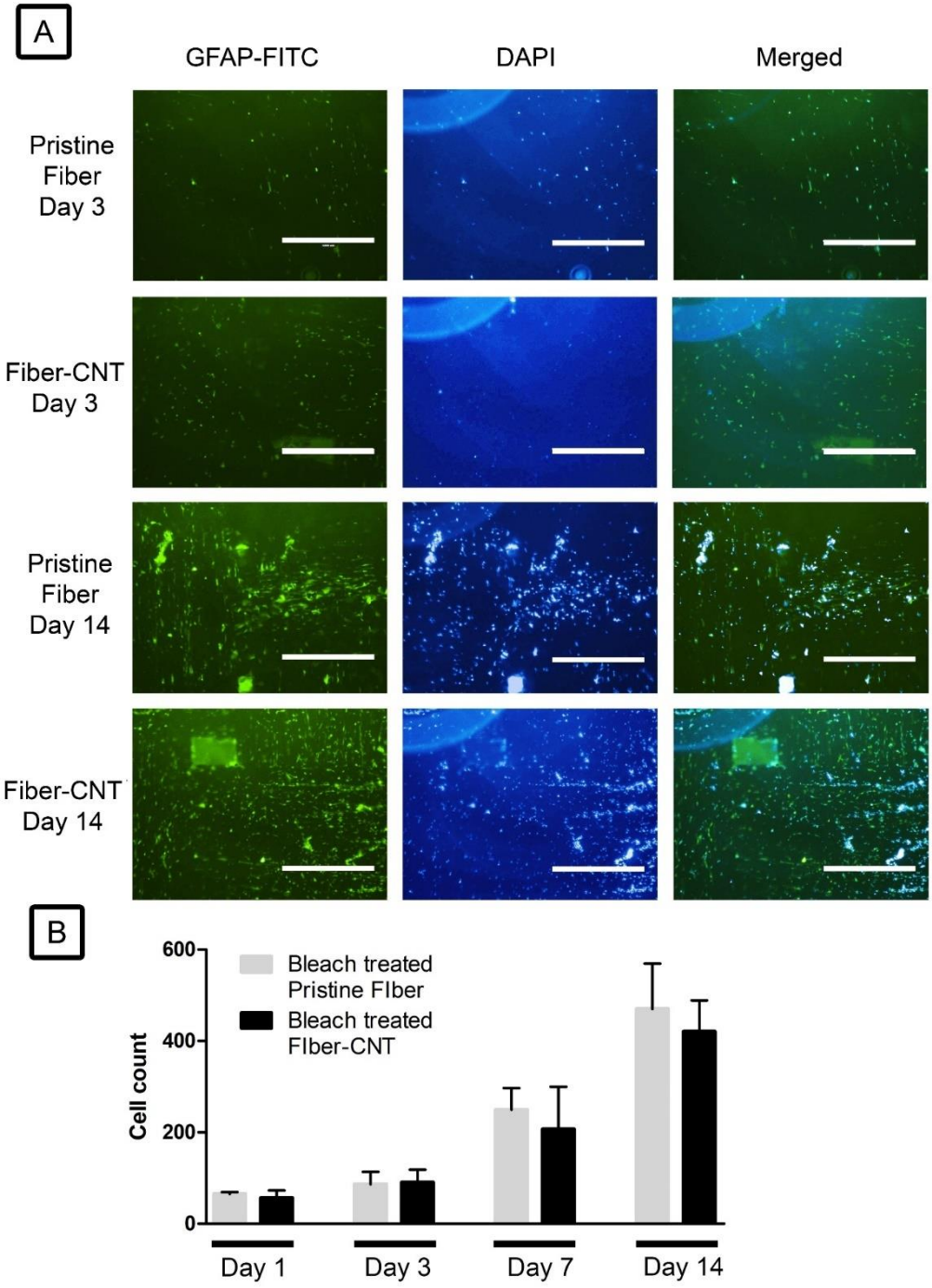

Figure 24 ***U87MG cell proliferation is comparable between CNT-coated hydrophilic scaffolds and pristine supports.***

Representative Immunofluorescence images of U87MG cells seeded on bleach-treated carbon fiber scaffolds with or without CNT-coating (A) Cells are labeled with GFAP (green) and cell nuclei with DAPI (blue). Scale bar represents 1000μm. Cell

counts performed via ImageJ from 4x images (n=3/sample) (B). Statistical significance was measured by one-way ANOVA and Tukey post-hoc analysis by comparing both groups. Error bars denote SD. Reprinted from "Multi-walled carbon nanotube carpets as scaffolds for U87MG glioblastoma multiforme cell growth" by Parikh, S. D., Dave, S., Huang, L., Wang, W., Mukhopadhyay, S. M., & Mayes, D. A. (2020). Materials Science and Engineering: C, 108, 110345. Copyright by Elsevier

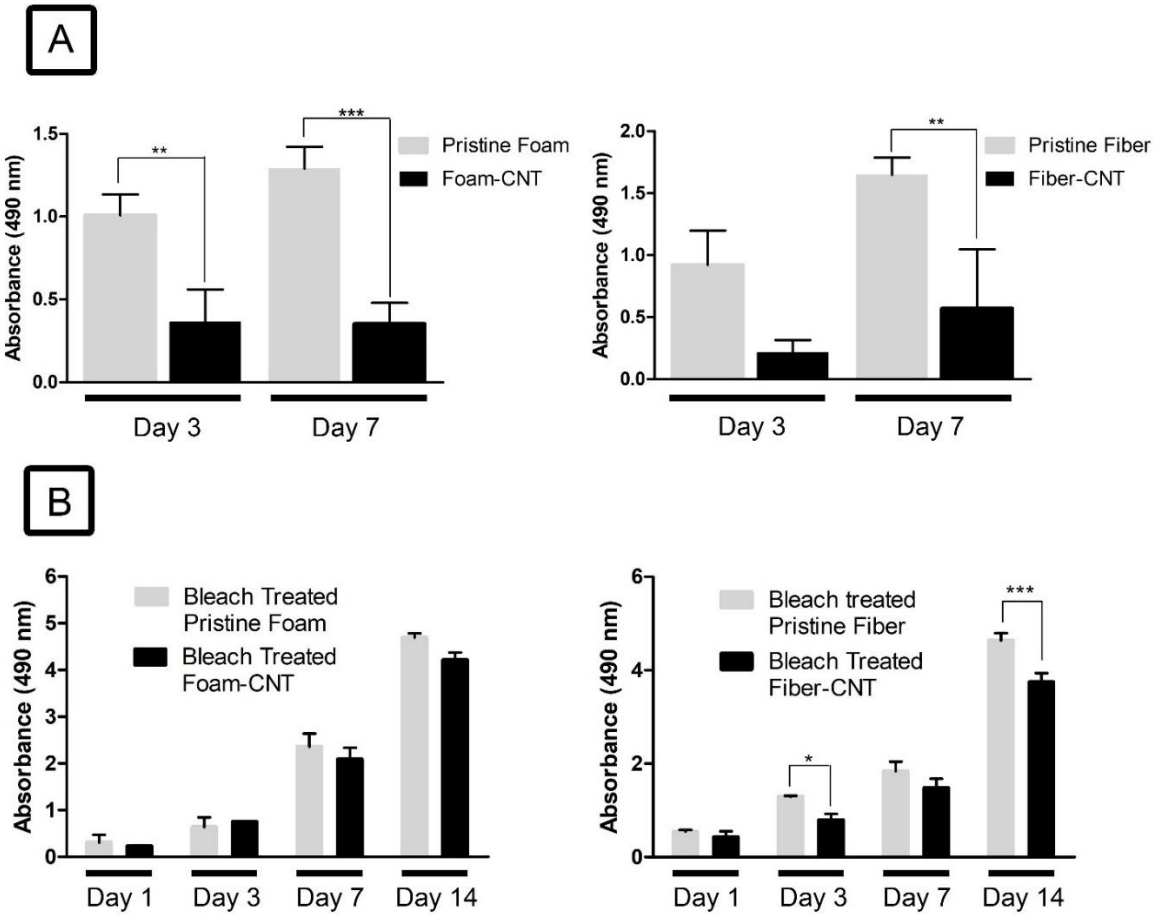

Figure 25 ***U87MG Cell Proliferation is significantly low on hydrophobic CNT-coated scaffolds as compared to pristine controls.***

*Cells were seeded on carbon foam or carbon fiber scaffolds with or without CNT-coating (A) or after bleach oxidation treatment (B). The X-axis in each graph depicts the number of days U87MG cells were grown on the scaffolds. Cell proliferation was evaluated by the MTS Assay. Statistical significance was measured by one-way ANOVA with Tukey post-hoc analysis by comparing both groups. Error bars denote SD. **, *** denote $p < 0.01$, $p < 0.005$, respectively. n=3/group/experiment. Reprinted from "Multi-walled carbon nanotube carpets as scaffolds for U87MG glioblastoma multiforme cell growth" by Parikh, S. D., Dave, S., Huang, L., Wang, W., Mukhopadhyay, S. M., & Mayes, D. A. (2020). Materials Science and Engineering: C, 108, 110345. Copyright by Elsevier*

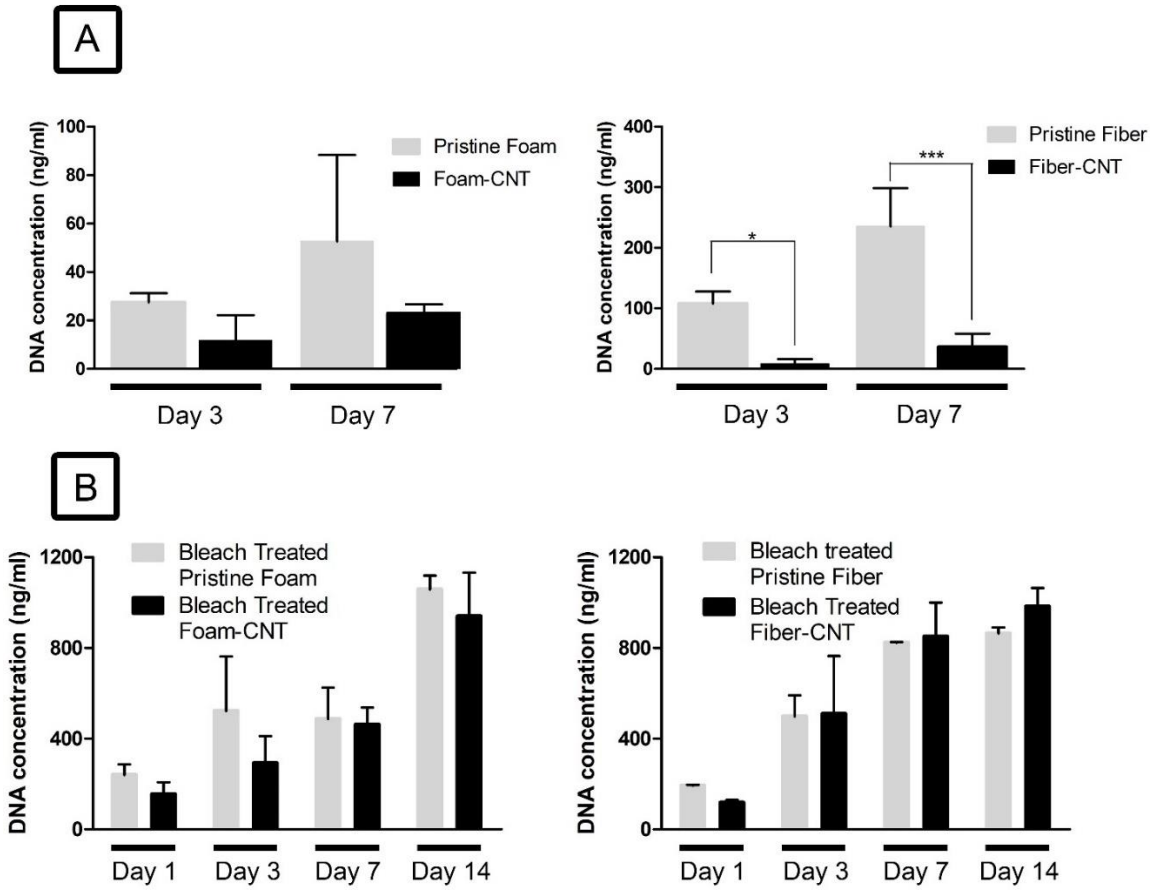

Figure 26 ***U87MG DNA Quantification is comparable between CNT-coated hydrophilic scaffolds and pristine supports.***

*DNA quantification of cells on carbon foam or carbon fiber scaffolds with or without CNT-coating (A) or after bleach oxidation treatment (B) measured with Quant-iT™ PicoGreen™ dsDNA Assays. The X-axis in each graph depicts the number of days the U87MG cells were grown on the scaffolds. Statistical significance was measured by one-way ANOVA with Tukey post-hoc analysis by comparing both groups. Error bars denote SD. *, ** denote $p < 0.05$, or $p < 0.01$, respectively. n=3/group/experiment. Reprinted from "Multi-walled carbon nanotube carpets as scaffolds for U87MG glioblastoma multiforme cell growth" by Parikh, S. D., Dave, S., Huang, L., Wang, W., Mukhopadhyay, S. M., & Mayes, D. A. (2020). Materials Science and Engineering: C, 108, 110345. Copyright by Elsevier*

2.3.2 Evaluation of the Effect of Length and Surface Wettability of CNT-coated Scaffolds on Biocompatibility and Cell Growth of Keratinocytes

Current wound healing scaffolds lack effectiveness in varied wound types and also have limitations with handling, preparation, sterilization, and shelf life [192]. The CNT-coated scaffolds due to their unique properties could be a suitable material for wound healing scaffolds that can address the limitations of the current scaffolds. Hence, in this study, we focused on investigating how surface functionalization and lengths of CNT-coating can alter the bio-interaction between the hierarchical scaffolds and keratinocyte cells. We used the HaCaT cell line for this study, which is a commonly used immortalized keratinocyte cell line in skin research [320,321].

In this study, we nano-functionalized flexible carbon fiber cloths (CFC) that could be applied as wound healing sheets at the injury site. Such CFCs were nano-functionalized with short or long lengths of nanotubes and were denoted by Short CNT-CFC or Long CNT-CFCs, respectively. We propose that these hierarchical scaffolds would provide unique micro as well as nanoscale cell interactions for promoting cell growth and wound healing without the probable toxicity risks linked with isolated and free CNTs. Therefore, the materials were evaluated for the ability to support cell proliferation of keratinocytes, and cell migration of keratinocyte and fibroblast cells.

2.3.2.1 Extract prepared from CNT-coated scaffolds does not induce cytotoxicity in keratinocytes

Since our objective in this study was to evaluate the CNT-coated scaffolds for their wound healing capability, we first checked for toxicity effects on keratinocyte cell

growth. Carbon scaffolds could potentially induce cellular toxicity in a variety of ways including disassociation of CNTs from the material [153–156], residual metallic impurities [159,160], length [309,322]. surface defects [22], unintentional moieties such as remnant sodium hypochlorite or nitric acid due to inadequate washing steps, and/or extractables [323]. Extractables are compounds that could release from scaffold surfaces under aggressive conditions, such as extended exposure times or gamma-irradiation [324]. Carbon nanotubes have also been known to cause toxicity as well as oxidative stress in keratinocytes [325,326]. To determine if the scaffolds are biocompatible and safe for tissue engineering, we followed the FDA-recommended guidelines for biocompatibility testing of external materials and performed an elution test [327]. Elution tests can help predict the short-term as well as long-term cytotoxicity risks associated with the implant material based on its proposed use and the potential for the release of extractables from implant materials [323].

To evaluate the indirect cytotoxicity effects of the scaffolds, we prepared extracts by incubating the scaffolds with simulated wound fluid (SWF). SWF was chosen for the elution analysis because it is physiologically relevant and has been used to imitate the natural wound healing process [306,328]. The prepared scaffolds were incubated with SWF for 14 days at 37°C in a humidified 5% CO_2 environment. The SWF eluent was then in turn diluted at various concentrations with cell culture media (Figure 27).

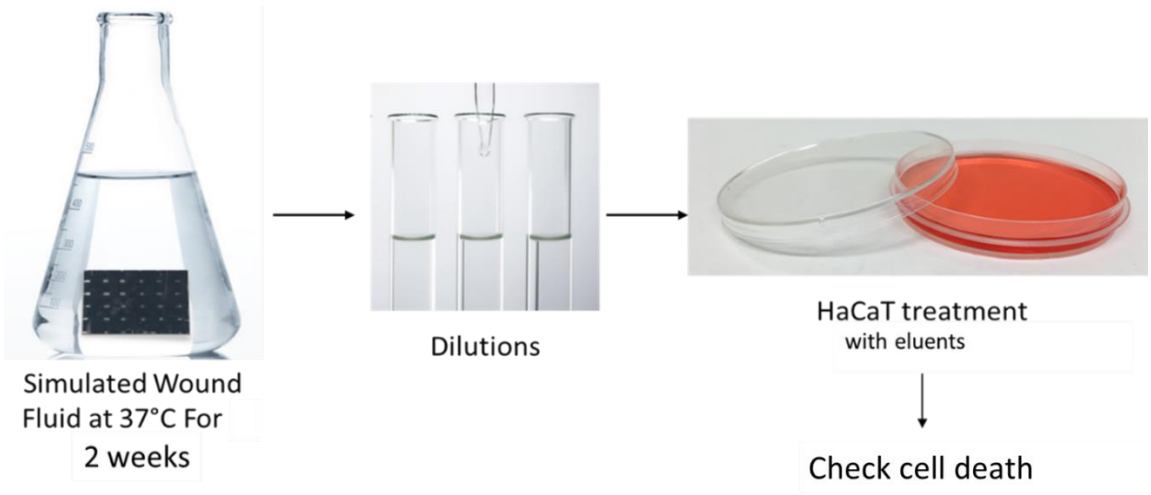

Figure 27 ***Graphical representation of the elution test assay.***

Through the elution test, the scaffolds used in the study were evaluated for their cytotoxicity profile before initiating cell-culture work to assert their non-toxic nature. The scaffolds were first soaked in the simulated wound fluid (SWF) for 14 days at 37°C for 5% CO_2 to prepare an extract. These prepared extracts from the scaffolds were further diluted to 25%, 50%, and 75% in the complete cell culture media as well as quiescent cell culture media to evaluate short term as well as long term cytotoxicity effects on growing HaCaTs as well as quiescent HaCaTs. The cytotoxicity analysis of the prepared extracts was done through brightfield microscopy as well as CytoTox-ONE™ Homogeneous Membrane Integrity Assay (LDH assay).

In addition to normally dividing cells, we also evaluated quiescent cells. Quiescent cells are less prone to toxic effects and stress exerted on them [329,330]. In case the scaffolds were highly cytotoxic, we wanted to analyze if the scaffolds can potentiate toxic effects that could supersede the stress-resistant nature of the quiescent cells. Quiescent cells were prepared by first incubating the cells in complete culture media until the cells reached near-confluency and then culturing the cells for 24 hour with quiescent media, which is a commonly used approach to achieve quiescence [234,331]. For our quiescent media preparation, we used 1% serum instead of 10% for the complete media.

There was no change in the pH with any prepared extracts with an average pH of around 8.57 for all prepared extracts. Extract dilutions with complete or quiescent media were prepared and cells were incubated with the extracts for 1 and 3 days to assess any short-term or long-term cytotoxic effects. From visual examination through brightfield microscopy, we did not observe any noticeable differences in the HaCaTs for any of the dilutions or time points. We also performed an LDH assay to assess cell viability. Cell death did not increase after 24 hours of incubation with the extracts at any concentrations both in presence of complete and quiescent media (Figure 28 *A* and Figure 29 *A*). This is noteworthy considering that not only was there no cytotoxicity induced after all extract treatments but the CFC and Long CNT-coated scaffolds also exhibited significantly less toxicity as compared to the cell controls. These results suggest a non-cytotoxic nature of all scaffolds used in this study at shorter time frames.

For the 3-day treatment of the eluents (Figure 28 *B* and Figure 29 *B*), we did not observe any cytotoxicity for up to 50% concentrations of the extracts. However, at 75% extract concentration, there was noticeable cell death in all the groups including the controls. The increase in cytotoxicity at such high concentrations of the extracts was not surprising due to the lack of nutrients for the actively dividing cells. The 75% extract concentration is usually not attempted in elution-based studies due to its limitations. The purpose of including a 75% group was to assess if the CNT-coated scaffolds have any extractables, which can exaggerate cell death in nutrient-deprived conditions. All the extracts prepared from CNT nano functionalization of the CFCs did not show any increase in cell death compared to cell controls and the Long CNT-CFC hydrophilic group showed significantly reduced cell death when compared to the control. Again, in the quiescent media study at 3 days (Figure 29 *B*) with 75% extract concentration, we saw a trend of decreasing cell death of HaCaTs with extracts

prepared from scaffolds as compared to the control. Both short CNT groups, as well as the long CNT-CFC hydrophilic group, showed significantly less cytotoxicity as compared to the SWF control group. This test followed established guidelines by the FDA and the U.S. Pharmacopoeia for tests on biomaterials [332] and the results from the test unveiled the non-cytotoxic nature of the extract of various bioscaffolds used in the study on HaCaTs.

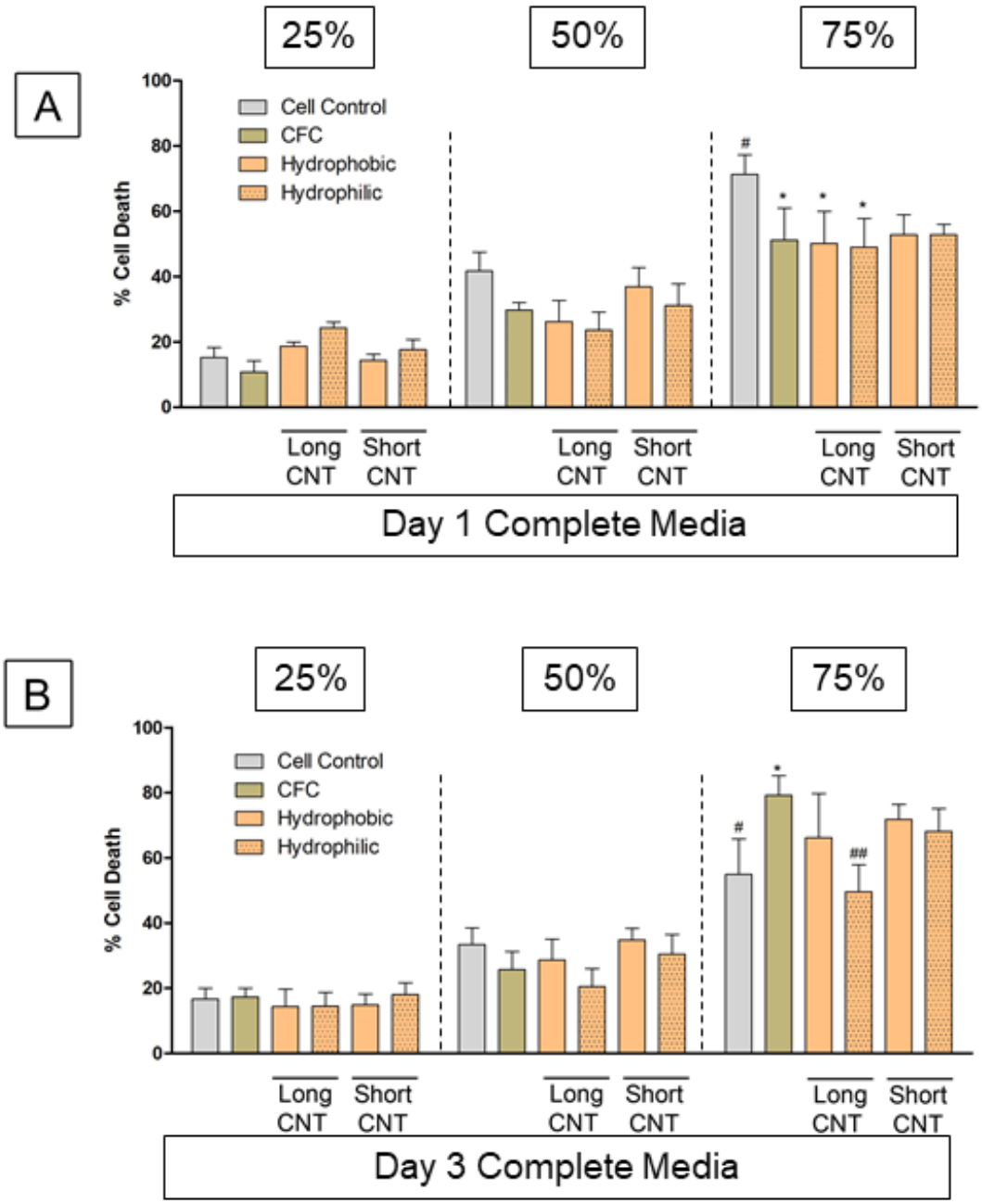

Figure 28 ***Evaluation of indirect cytotoxicity of scaffolds on keratinocytes (HaCaTs).***

Cytotoxic effects of the eluted solution of scaffolds used in the study (Carbon fiber cloth (CFC), Long CNT-CFC, and Short CNT-CFC) with or without sodium hypochlorite-based bleach treatment on normally dividing HaCaT cells were measured on Day 1 (A) and Day 3 (B). Extracts were prepared from different scaffolds by incubating scaffolds with SWF for 14 days and the extracts were evaluated for their potential cytotoxic effects on HaCaTs by LDH assay. The Y-axis represents the quantification of mean formazan-correlated cytotoxicity results normalized to positive

*cytotoxic controls. The X-axis represents the treatment groups. CNT-coated scaffolds did not induce cytotoxicity in HaCaTs. Statistical significance was measured by two-way ANOVA analysis followed by Bonferroni post-tests by comparing each sample to the corresponding cell controls as well as CFC controls. Significant differences from the cell controls were denoted by *, which represents significance at $p<0.05$. Significant differences from the appropriate CFC controls were denoted by # and ##, which represent significance at $p<0.05$ and $p<0.01$, respectively. Results are representative of two independent experiments ($n = 3$ for each treatment group). Error bars denote SE.*

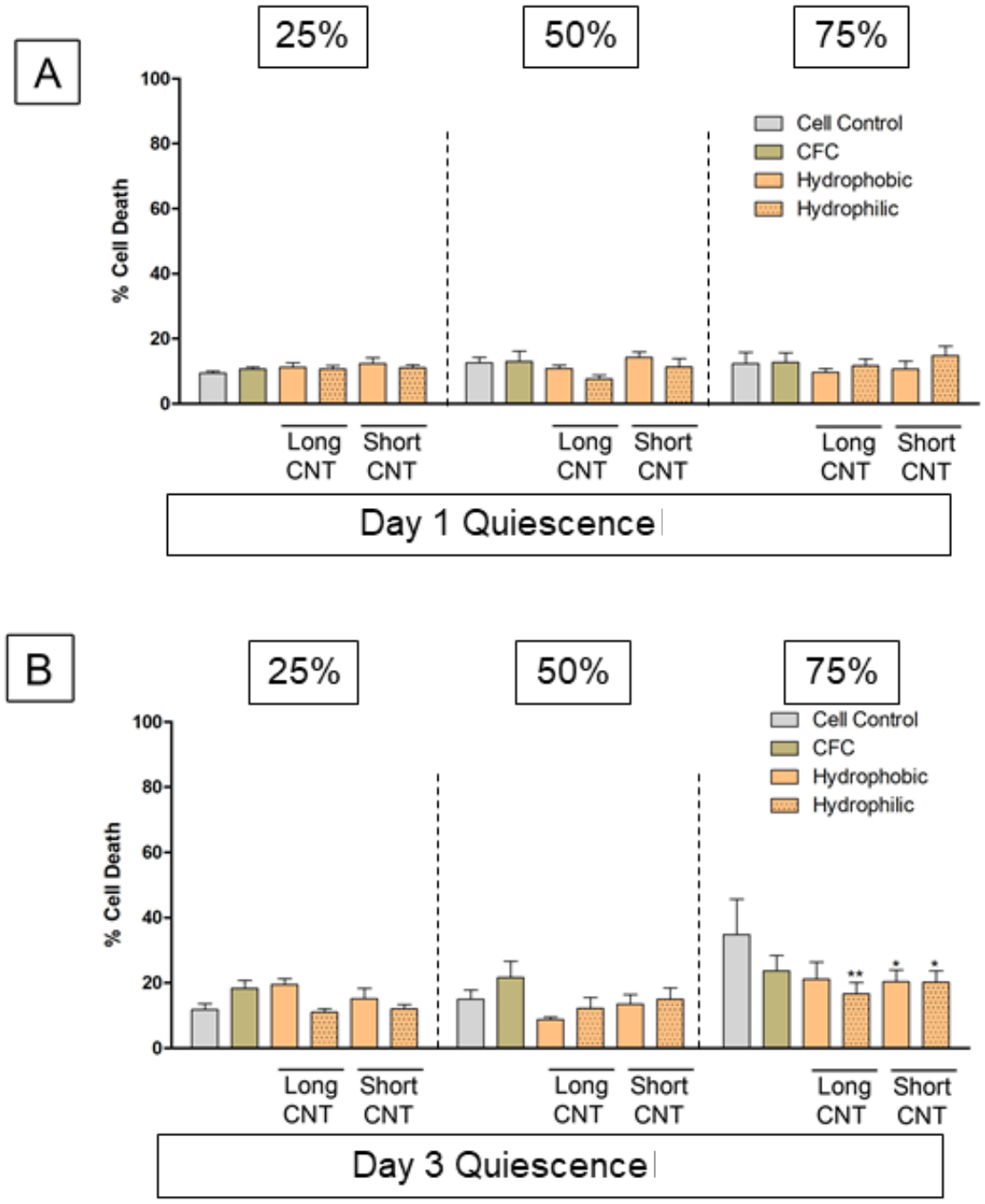

Figure 29 ***Evaluation of indirect cytotoxicity of scaffolds on quiescent keratinocytes (HaCaTs).***

Cytotoxic effects of the eluted solution of scaffolds used in the study (Carbon fiber cloths (CFC), Long CNT-CFC, and Short CNT-CFC) with or without sodium hypochlorite-based bleach treatment were assessed on quiescent HaCaT cells on Day 1 (A) and Day 3 (B). Extracts were prepared from different scaffolds by incubating scaffolds with SWF for 14 days and the effects of extracts on quiescent HaCaTs were analyzed by LDH assay. The Y-axis represents the quantification of mean formazan-

*correlated cytotoxicity normalized to positive cytotoxic controls. The X-axis in each graph represents the treatment groups. Scaffolds did not induce cytotoxicity in quiescent HaCaTs. Statistical significance was measured by two-way ANOVA analysis followed by Bonferroni post-tests by comparing each sample to the corresponding cell controls as well as CFC controls. Significant differences from the cell controls were denoted by * and **, which represent significance at $p<0.05$ and $p<0.01$, respectively. Results are representative of two independent experiments (n = 3 for each treatment group). Error bars denote SE.*

2.3.2.2 CNT-coated scaffolds do not induce cytotoxicity in keratinocytes upon direct contact

To further evaluate the toxicity profile of the scaffolds, we performed cytotoxicity analysis of cells growing directly on the prepared scaffolds. This was done by adhering to non-standard direct contact study guidelines as per ISO 10993-5 by FDA [327]. HaCaT cells were directly grown on the scaffolds and their cytotoxicity was measured using an LDH assay. No significant cytotoxicity of HaCaT cells was observed at short, intermediate, or long-term time points with any of the bioscaffolds (Figure 30). On Day 1, not all seeded cells may have attached to the culture plate and hence we saw relatively higher cytotoxicity values compared to other time points.

The comparable cytotoxicity results for different scaffolds imply that the bioscaffolds are non-cytotoxic for keratinocyte cell growth. The results also suggest that the varying length or water wettability of the CNT layer does not cause any unexpected cytotoxicity in HaCaTs. This was consistent with our hypothesis that the covalently bound CNTs will not contribute to cytotoxicity *in vitro*.

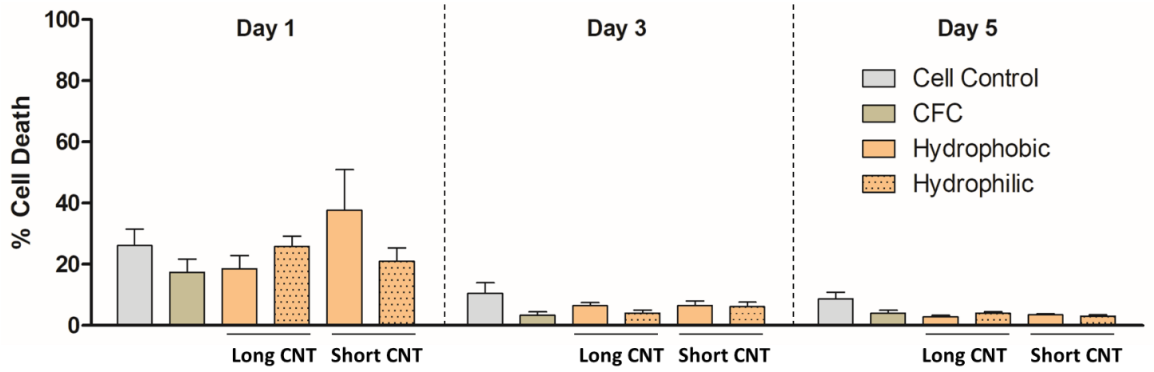

Figure 30 ***Alteration of CNT length and wettability does not induce cytotoxicity in keratinocytes (HaCaTs).***

Cytotoxicity evaluation in HaCaTs growing on scaffolds was performed by LDH assay. The Y-axis represents the quantification of mean formazan-correlated cytotoxicity results normalized to the positive cytotoxic controls. The X-axis represents the treatment groups. Statistical significance was measured by two-way ANOVA analysis followed by Bonferroni post-test comparing each sample to the corresponding carbon fiber cloth (CFC) controls. Results are representative of three separate experiments (n = 3 for each treatment group). Error bars denote SE.

2.3.2.3 Short CNTs can effectively support keratinocyte cell proliferation

The effects of CNT length, as well as surface wettability of the nanomaterials on keratinocytes cell growth over time, was evaluated via MTS. Cell proliferation on all scaffolds was not significantly different from the control cell groups at Day 1 (Figure 31). However, we did see negligible cell proliferation on Long CNT-coated scaffolds. Also, relative cell proliferation on all CNT-coated scaffolds was noticeably low, hinting that cell attachment on CNT-coated scaffolds could have been slower on Day 1. This was consistent with our previous observations with the glioblastoma studies [67]. Slower proliferation rates could be associated with the substantially high surface area and 3D nanostructure provided by the CNTs, which can slow down cell attachment as compared to flat, tissue culture-treated plates.

On Day 3, cell proliferation between the CFC group and Short CNT-coated scaffolds was comparable and not significantly different (Figure 31). This implies that cell growth was well supported on the short CNT surfaces. The Long CNT-coated scaffolds showed significantly less cell proliferation as compared to the other groups. On Day 5, cell proliferation between the cell control group, CFC group, and Short CNT-coated hydrophilic scaffolds was comparable and not significantly different (Figure 31) This implies that cell growth was well supported on Short CNT-coated hydrophilic scaffolds. In general, Short CNT-coated scaffolds showed higher cell proliferation than Long CNT-coated scaffolds and hydrophilic scaffolds showed increased cell proliferation than their hydrophobic counterparts.

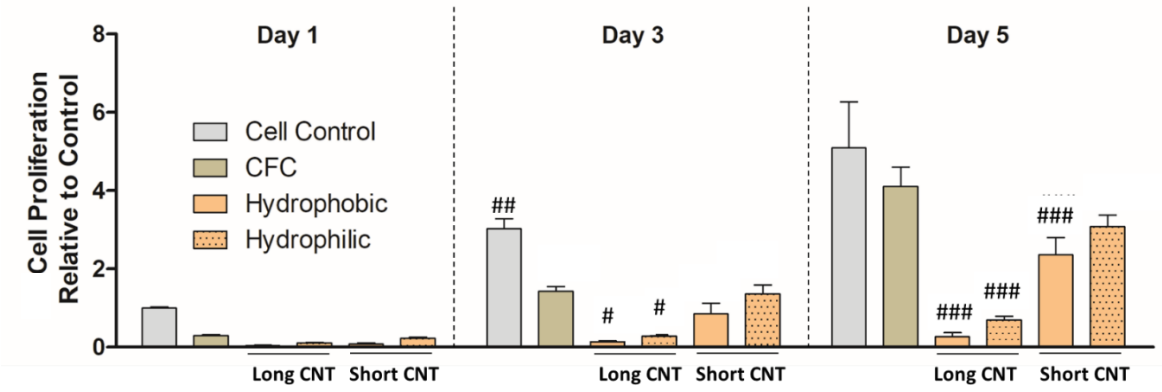

Figure 31 ***Short CNTs can effectively support keratinocyte (HaCaT) cell proliferation.***

HaCaTs were cultured on different scaffolds and cell proliferation was measured by MTS assay. The Y-axis represents the quantification of mean tetrazolium-correlated cell proliferation results normalized to cell control values on Day 1. The X-axis in each graph represents the scaffolds on which the HaCaTs were cultured. On Days 3 and 5, the Long CNT-CFC scaffolds showed significantly lower cell proliferation as compared to carbon fiber cloth (CFC) groups. HaCaTs cultured on Short CNT-coated scaffolds showed similar cell proliferation as CFC controls. Statistical significance was measured by two-way ANOVA analysis and Bonferroni post-test. Significant differences from the corresponding CFC controls were denoted by # and ###, which represents significance at $p<0.05$ and $p<0.001$, respectively. Results are

representative of three independent experiments (n = 3 for each treatment group). Error bars denote SE.

2.3.3 Assessment of Cell Migration with CNT-coated Scaffolds to Check their Potential as a Future Wound Healing Scaffold

Cell migration is a critical process in order to understand whether the scaffolds are suitable for wound healing applications. Hence, to understand the full extent of the feasibility of the scaffolds used in this study, apart from their potential to aid cell proliferation, we also checked their effects on cell migration.

CNT-coated Scaffolds Effectively Support HaCaT Migration

Keratinocyte and fibroblast migration and proliferation are key steps involved in the wound healing process. Therefore, determining the effect of CNT-coated scaffolds on cell migration is important to assess whether these scaffolds are suitable for wound healing applications. From the cell proliferation study (Figure 31), it was identified that hydrophilic CNT-coated scaffolds were more effective for keratinocyte cell growth and only hydrophilic scaffolds were used for migration analyses. Several approaches were employed to evaluate cell migration as described below.

2.3.3.1.1 Modified Scratch Wound Assay

We utilized a modified scratch wound model to evaluate cell migration from the CNT-coated scaffolds. In this method, just like a traditional scratch wound assay, a scratch was made on a confluent layer of HaCaTs using a 200ul pipette tip. We then covered the scratches with 1x1 cm carbon bioscaffolds with dye-loaded HaCaTs to visualize and evaluate if the cells can migrate from the scaffolds towards the scratch

and facilitate the wound healing process. We observed very few labeled cells migrating from the scaffolds towards the wound site (results not shown), but we had difficulty in getting reproducible results and unfortunately, the results from this study were inconclusive due to experimental limitations.

2.3.3.1.2 Intrascaffold Cellular Migration Experiment

In this preliminary study, we checked if the scaffolds by themselves can facilitate intrascaffold cellular migration. A simple experimental set-up was used where we cultured HaCaTs on two different Long CNT-coated hydrophilic scaffolds and placed a scaffold without any cells in between those two pre-seeded scaffolds. This was done to understand if the scaffold nano-interaction of the pre-seeded cells allows for the migration towards the center scaffold, which mimics a no-cell zone within the scaffold (Figure 32 *A*). After 3 days, cells were visualized in the center scaffold (Figure 32 *B*), supporting cell migration from the cell-seeded scaffolds using AMEFC4300 EVOS™ Digital Color Fluorescence Microscope. This study validated that the scaffolds are capable to support cell migration on their surface and can be further explored for keratinocyte cell migration.

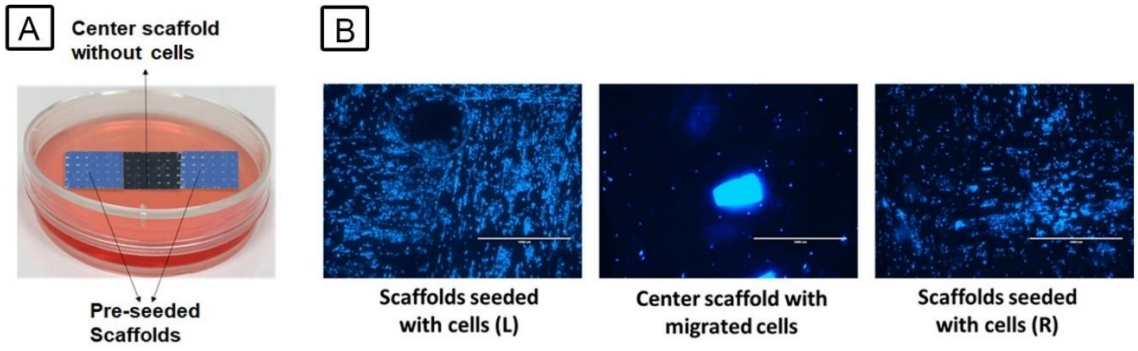

Figure 32 ***Keratinocytes (HaCaTs) can migrate within the CNT-coated scaffold.***

HaCaT seeded Long CNT-coated hydrophilic scaffolds were placed on either end of a scaffold without any cells and incubated for 3 days. All cell nuclei were stained with DAPI (blue). Fluorescent pictures were captured using AMEFC4300 EVOS™ Digital Color Fluorescence Microscope. Representative graphic of the intrascaffold cell migration set-up (A). Representative image showing HaCaT cell migration towards the central CNT-coated scaffold (B). Images are representative of one experiment (n = 3). Scale bar represents 1000µm.

2.3.3.1.3 Keratinocyte and Fibroblast cells can Effectively Migrate from CNT-coated Scaffolds

To further evaluate cell migration, we determined if cells grown on the CNT-coated scaffolds will leave the nanostructures and migrate towards an area with no cells (Figure 34). These scaffolds provide a customizable surface that is highly flexible and easy to functionalize with growth factors as a split-thickness skin graft or as dermo-epidemal substitutes which can contain fibroblasts as well as keratinocytes as they are also one of the critical cell types required for the wound healing process [333].

To evaluate cell migration from the scaffolds, scaffolds were pre-seeded with cells in a plate for 1 day to give the cells enough time to attach to the nano and microarchitecture of the scaffolds. Scaffolds were then transferred to a fresh cell culture plate and migration from the scaffolds evaluated (Figure 33). This was done to gain a qualitative insight into whether the cells grown onto the nanostructures can

effectively leave the area to test their potential as wound healing scaffolds. The results showed that both keratinocytes (HaCaT cells) and fibroblasts (NHF1 cells) migrated from the CFC, Long CNT, and Short CNT scaffolds (Figure 34 and Figure 35).

The results from this test are qualitative as the number of cells migrating from the scaffolds varied depending on the scaffold movement inside the tissue culture plates. As the scaffolds could not be taped to the plates and were submerged in the cell culture media, routine steps such as media exchange and moving plates from the incubator to the cell culture hood tended to perturb the cellular migration as the scaffolds moved. Enough precautions were taken to limit the disturbance; however, it could not be completely avoided. Hence, the results for this test are not quantified for cell counts.

To further verify the keratinocyte cell migration from the scaffolds, we designed another method using PDMS polymer-based cell barriers to analyze cell migration. In the first preliminary test, a confluent layer of cells was grown with a circular no cell zone (simulated wound region) in the center. A Long as well as Short CNT-coated hydrophilic scaffold pre-seeded with CellTracker™ Red CMTPX-loaded HaCaT cells was placed in the wound region and incubated for 4 days (Figure 36 *A*). Dye-loaded cells were observed throughout the wound edge (Figure 36 *C*), which suggested that keratinocyte cells migrate from the scaffolds toward the wound edge.

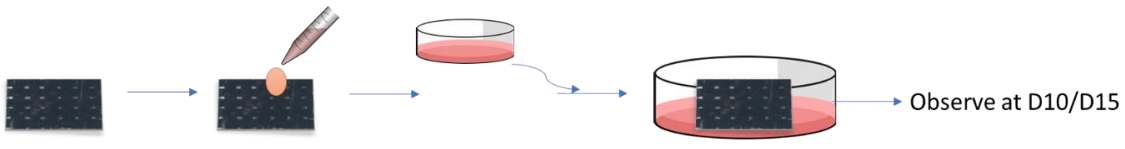

Figure 33 ***Graphical representation of set-up used to assess keratinocyte and fibroblast cell migration from the cell-seeded scaffolds.***

Keratinocytes (HaCaT cells) or fibroblasts (NHF1 cells) were seeded on the scaffolds and the cell-seeded scaffolds were transferred to an empty plate the next day. Cell migration from the scaffolds to the plate was observed through phase-contrast microscopy at day 15 for HaCaTs and day 10 for NHF1s.

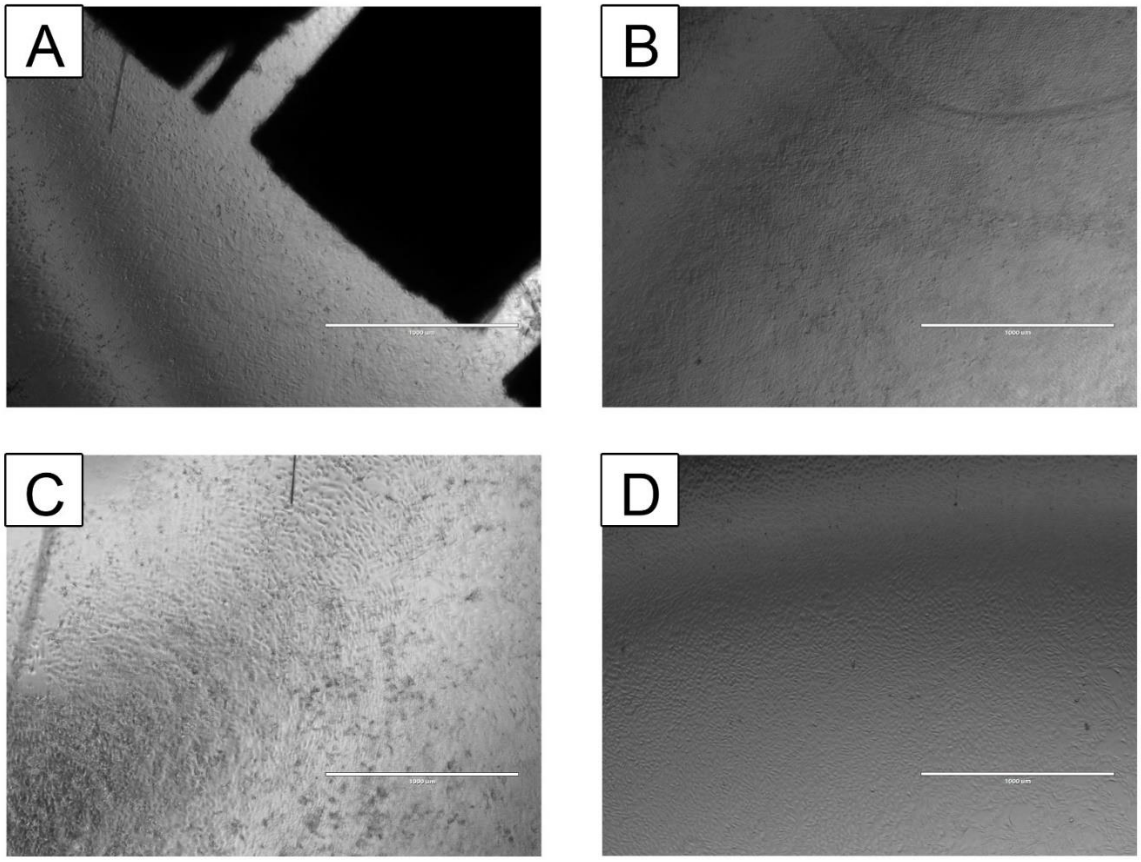

Figure 34 ***Keratinocytes migrate from the CNT-coated scaffolds.***

HaCaTs were seeded on scaffolds and the cell-seeded scaffolds were transferred to a fresh well plate and incubated for 15 days. Plates were then observed for cell migration by phase-contrast microscopy using AMEFC4300 EVOS™. A representative image showing the HaCaT-seeded Short CNT-coated hydrophilic scaffold (black image) on the tissue culture plate and the migrated cells from the scaffold (bright field) (A). Representative images of HaCaTs migrated from carbon fiber cloth (CFC) (B), Long CNT-coated hydrophilic scaffold (C), and Short CNT-coated hydrophilic scaffold (D). Scale bar represents 1000μm. Representative images are from 3 independent experiments (n=3, 10 images analyzed per sample for each experiment).

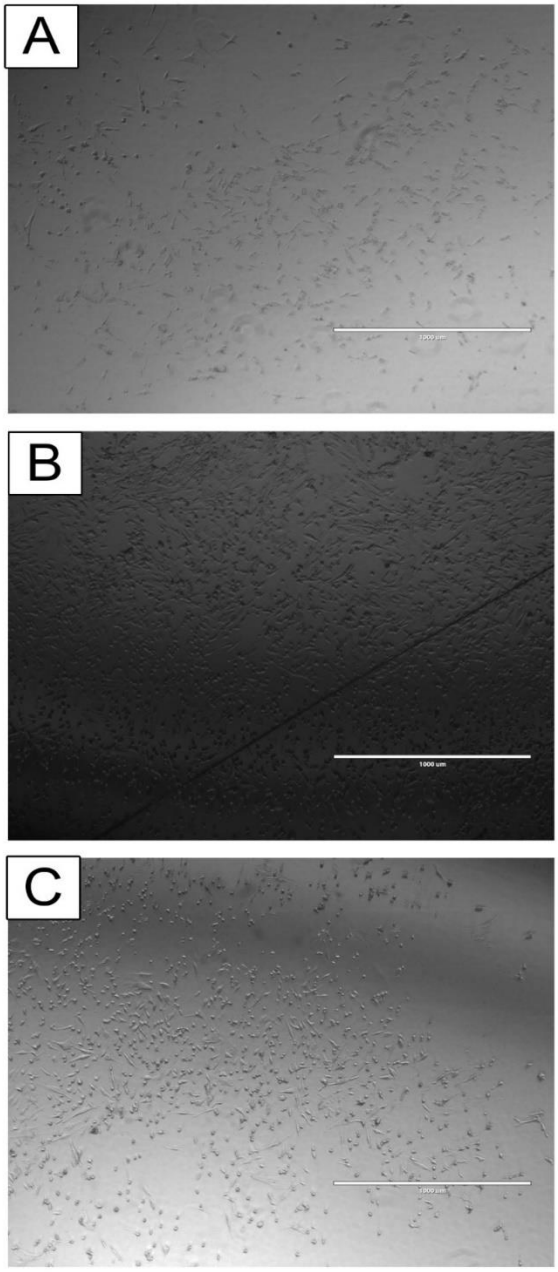

Figure 35 ***Fibroblasts migrate from CNT-coated scaffolds.***

NHF1s were seeded on scaffolds and the cell-seeded scaffolds were transferred to a fresh well plate and incubated for 10 days. Plates were then observed for cell migration by phase-contrast microscopy using AMEFC4300 EVOS™. Representative images of NHF1 cells migrated from carbon fiber cloth (CFC) (A), Long CNT-coated hydrophilic scaffold (B), and Short CNT-coated hydrophilic scaffold (C). Scale bar represents 1000µm. Representative images are from 3 independent experiments (n=3, 10 images analyzed per sample for each experiment).

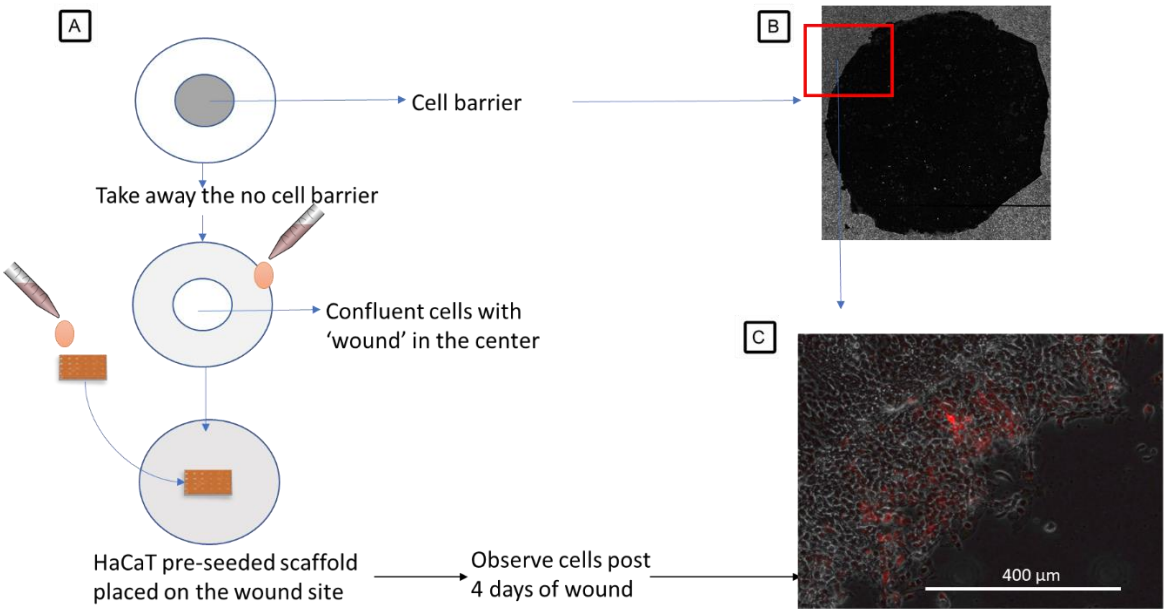

Figure 36 ***Keratinocyte cells (HaCaTs) migrate from the CNT-coated scaffolds towards the wound edge.***

Cell migration of HaCaT cells (red) from the Long CNT-coated hydrophilic scaffolds towards the wound edge after 4 days. Cell migration study set-up using PDMS no-cell barrier (A). Representative image of the no cell zone created by the PDMS cell barrier imaged by BioTek Cytation5 using image stitching at 4x (B). Migrated CellTracker™ Red CMTPX-loaded HaCaT cells (red) from the CNT-coated scaffold towards the wound edge (C). Nonfluorescent cells are HaCaT cells grown to confluency around the PDMS barrier. Scale bar in (B) represents 10000µm and (C) represents 400µm. The image is representative of one independent experiment (n=3, 10 images analyzed per sample per group for each experiment).

2.3.3.1.4 Keratinocyte and Fibroblast cells can Effectively Migrate Towards the CNT-coated Scaffolds

To further validate the cell migration findings, we performed this study to check if the cells grown on the culture plates can migrate towards the scaffolds. This was done to check if the scaffolds can attract cell migration to be able to support the wound healing at the injury site. The set-up for the test is illustrated in Figure 37.

Cells effectively migrate towards the CNT-coated scaffolds through the leading weaves and fibrils (Figure 38-Figure 39). We also observed the migrated cells towards the central region of the scaffolds and migrated cells throughout the scaffold surface implying that once attached, the cells can continue their migration on these CNT carpets. This study also suggests that the scaffolds provide directionality of the migrating keratinocytes and fibroblasts and this property can be exploited to use these materials as wound healing or tissue scaffolds.

CNT-coated scaffolds were further evaluated for keratinocyte cell migration from the wound edge to the scaffold. HaCaT cells loaded with CellTracker™ Red CMTPX dye were grown to a confluent layer around the PDMS barrier. A CNT-coated scaffold pre-seeded with HaCaTs loaded with CellTrace™ CFSE dye was then placed in the wound area and incubated for 4 days (Figure 40 *A*). HaCaT cells migrated from the plate to the scaffold (Figure 40 *B*, signifying that the cells from the wound edge had successfully migrated towards the pre-seeded scaffolds and the scaffolds were capable to retain seeded cells and facilitate cell migration into the scaffold.

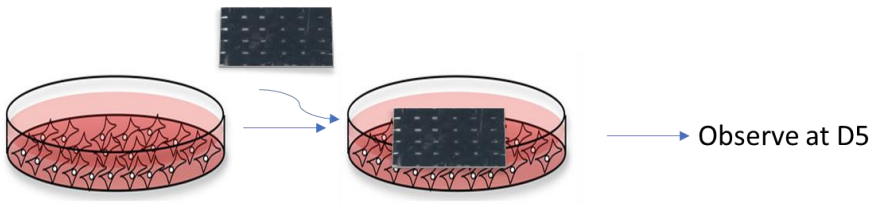

Figure 37 ***Graphical representation of set-up used to assess cell migration towards the CNT-coated scaffolds.***

HaCaTs or NHF1 cells were seeded in 12 well plates and incubated for a day. CNT-coated scaffolds were then transferred to the cell-seeded wells and allowed to incubate for 5 days. Cell migration on CNT-coated scaffolds was analyzed by staining the cells with Calcein-AM after the 5-day incubation.

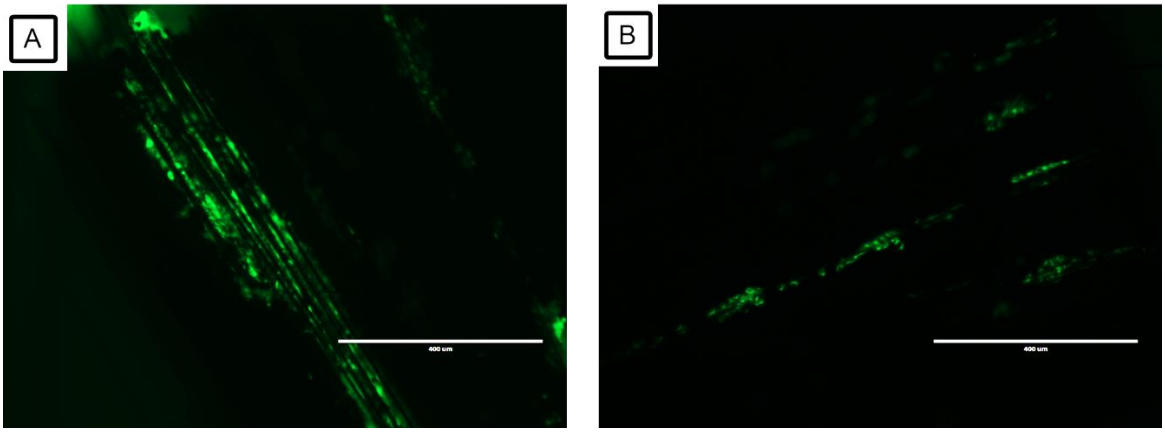

Figure 38 ***Keratinocytes migrate towards the CNT-coated scaffolds.***

HaCaTs were seeded in 12 well plates and incubated for a day. Scaffolds were then placed and incubated for 5 days and observed for cell migration by staining the cells with Calcein-AM (green) before imaging them with AMEFC4300 EVOS™. Representative fluorescence images show migrated HaCaTs on Long CNT-coated hydrophilic scaffolds (A) and Short CNT- hydrophilic coated scaffolds (B). The scale bar represents 400µm. Representative images are from 3 independent experiments (n=3, 10 images analyzed per sample for each experiment).

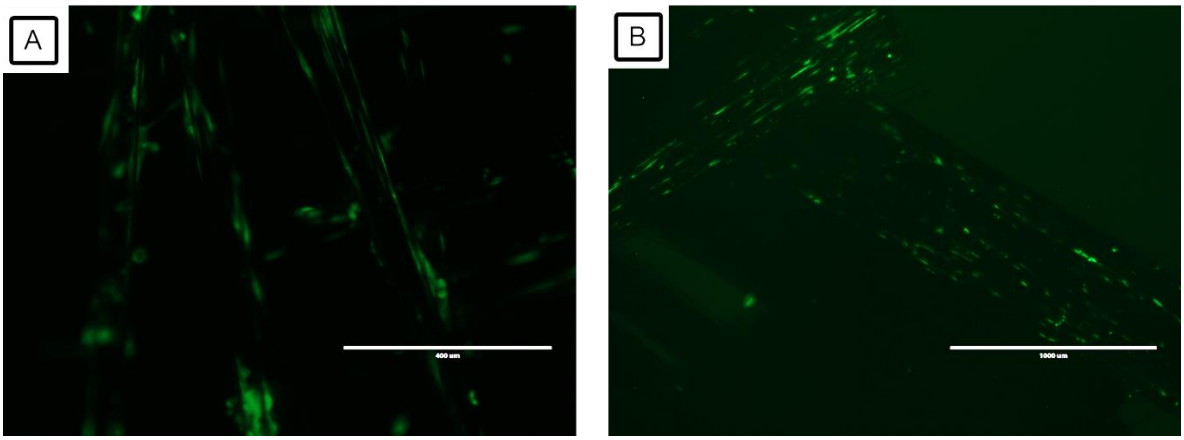

Figure 39 ***Fibroblasts migrate towards the CNT-coated scaffolds.***

NHF1 cells were seeded in 12 well plates and incubated for a day. Scaffolds were then placed and incubated for 5 days and observed for cell migration by staining the cells with Calcein-AM (green) before imaging them with AMEFC4300 EVOS™. Representative fluorescence images show migrated NHF1 cells on Long CNT-coated hydrophilic scaffolds (A) and Short CNT-coated hydrophilic scaffolds (B). Scale bar in (A) represents 400µm and (B) represents 1000µm. Representative images are from 3 independent experiments (n=3, 10 images analyzed per sample for each experiment).

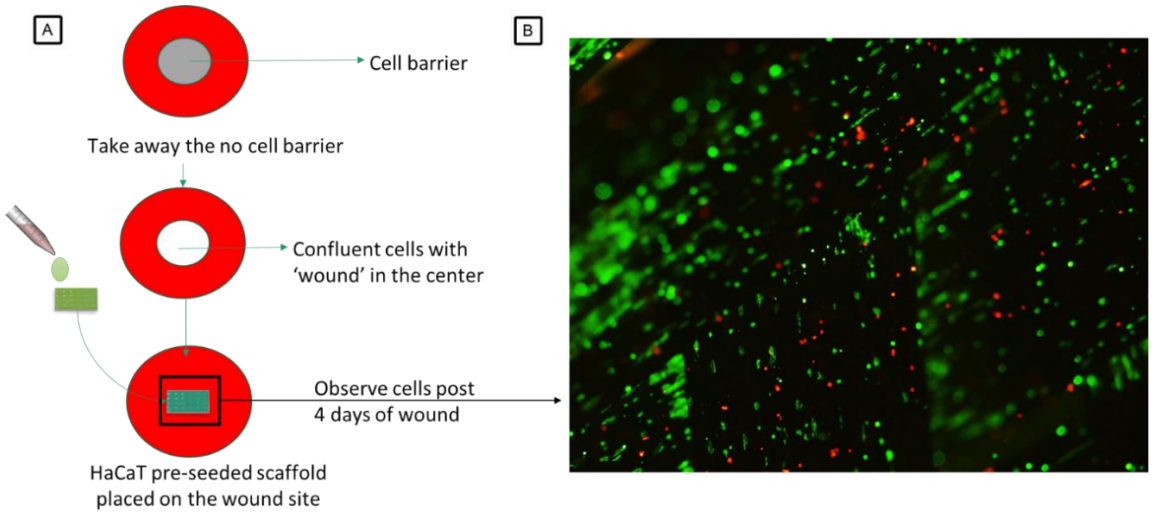

Figure 40 ***Keratinocytes migrate towards the CNT-coated scaffolds.***

Cell migration of HaCaT cells (red) from the Short and Long CNT-coated hydrophilic scaffolds towards the wound edge after 4 days imaged using Olympus BX51. Cell migration study set-up using PDMS no-cell barriers (A). Red cells are CellTracker™ Red CMTPX-loaded HaCaT cells grown to confluency around the PDMS barrier. Green cells are HaCaT cells loaded with CellTrace™ CFSE that were pre-seeded on the Short and Long CNT-coated scaffolds (B). The image is of a Short CNT-coated hydrophilic scaffold and is representative of two independent experiments (n=3, 10 images analyzed per sample for each experiment).

2.3.4 Effects of Environmental Stressors on Cells Grown on CNT-coated Scaffolds

We tested the potential cytoprotective effects of the CNT-coated scaffolds in presence of environmental stressors TCDD and UVB.

2.3.4.1 TCDD does not Impact HaCaT cell Proliferation or Cytotoxicity

Our lab's previous work on CNT scaffolds with aromatic compounds [61] and lipid molecules [63] insinuate that the CNT-coated scaffolds can potentially adsorb TCDD on their surface. In this study, we wanted to determine whether the CNT-coated

scaffolds due to their adsorbent nature could provide cytoprotective effects against TCDD. TCDD is also shown to decrease cell proliferation of HaCaTs, particularly at higher concentrations [231,234], and slows down the cell migration during wound healing [235]. Therefore, we hypothesized that CNT-coated scaffolds could preferentially minimize the anti-proliferative effects of TCDD. However, in our hands, TCDD treatment did not inhibit HaCaT cell proliferation and was not cytotoxic. Similarly, TCDD had no significant effect on proliferation and showed a modest protective effect on cell death for HaCaT cells seeded on the CNT-coated scaffolds (*Figure 41* and Figure 42).

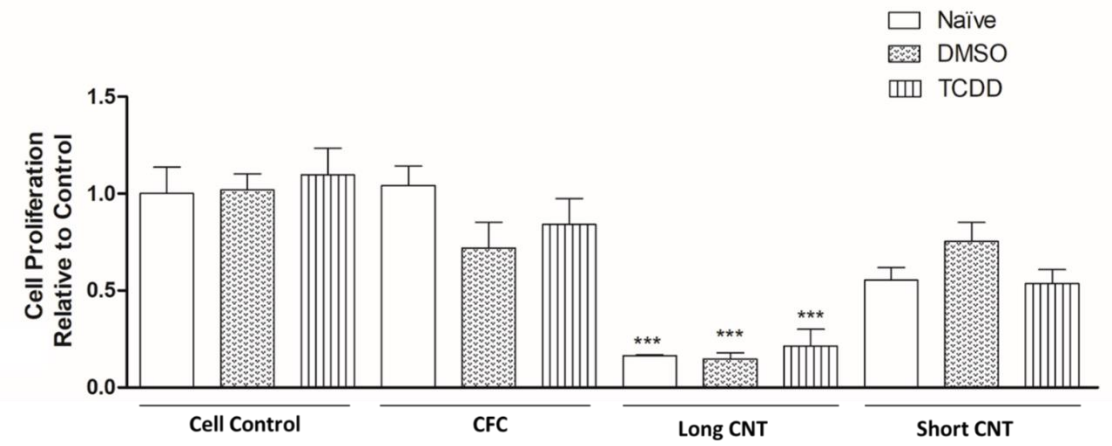

Figure 41 ***TCDD does not impact keratinocyte (HaCaT) cell proliferation.***

*TCDD-treated HaCaT cells were either cultured in the absence of any additional treatment (naïve) or treated with 0.01% DMSO (vehicle) or 30nM TCDD and grown on different CNT-coated scaffolds for 4 days. Cell proliferation of HaCaTs growing on different surfaces was measured by MTS assay. The Y-axis represents the quantification of mean tetrazolium-correlated cell proliferation normalized to cell control values on Day 4. The X-axis in each graph represents the scaffolds on which the HaCaTs were cultured. Cell control represents cells grown in the absence of scaffolds. CFC is the carbon fiber control. Statistical significance was measured by one-way ANOVA analysis followed by Bonferroni post-test comparing each sample to the cell control vehicle group and by comparing each TCDD treatment group to their respective vehicle controls. Significant difference from the naïve cell control is denoted by *** which represents significance at $p < 0.001$. Results are representative of two separate experiments ($n = 3$ for each treatment group). Error bars denote SE.*

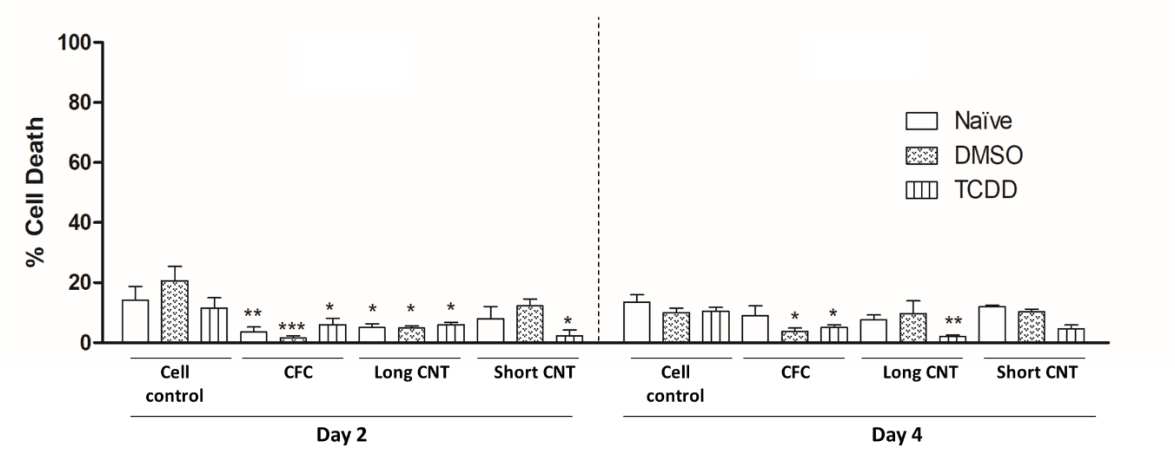

Figure 42 ***TCDD does not induce cytotoxicity in HaCaTs.***

*TCDD-treated HaCaT cells were either cultured in the absence of any additional treatment (naïve) or treated with 0.01 % DMSO (vehicle) or 30nM TCDD and grown on different scaffolds for 2 or 4 days. Cytotoxicity evaluation in HaCaTs growing on scaffolds was performed by LDH assay. The Y-axis represents the quantification of mean formazan-correlated cytotoxicity normalized to the positive cytotoxic controls. The X-axis represents the treatment groups. Cell control represents cells grown in the absence of scaffolds. CFC is the carbon fiber control. Statistical significance was measured by two-way ANOVA analysis followed by Bonferroni post-test. Significant difference from the naïve cell control is denoted by *, **, and *** which represents significance at p <0.05, p<0.01, and 0.001, respectively. Results are representative of two separate experiments (n = 3 for each treatment group). Error bars denote SE.*

2.3.4.2 UVB Significantly Decreases HaCaT Cell Viability

Keratinocytes are highly vulnerable to UVB radiation. UVB light substantially slows down skin cell growth and induces cell death and skin cancer in addition to substantially slowing down wound healing [249,251]. HaCaT cell viability was measured at increasing doses of UVB. All the treatments of UVB significantly decreased the number of viable cells (Figure 43).

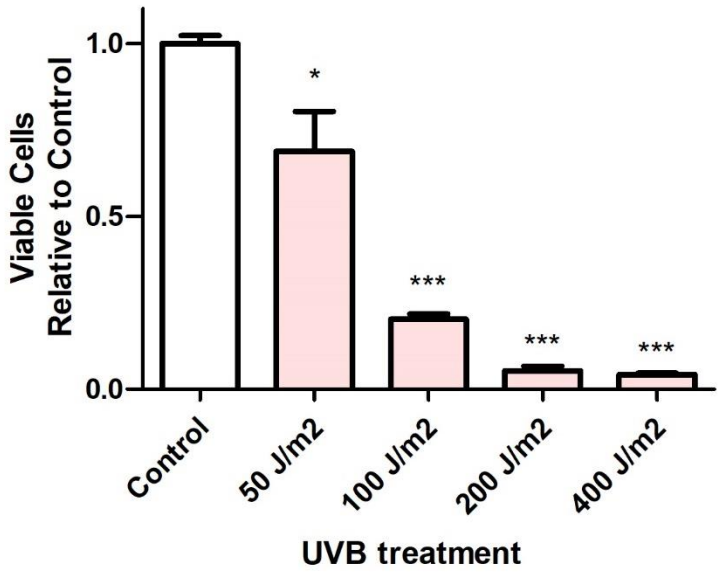

Figure 43 ***UVB treatment significantly inhibits keratinocyte cell viability.***

*HaCaT cells were either cultured in 35mm plates for 1 day. The cells were then treated with 50-400 J/m^2 UVB and grown for 3 days. Cell counts were measured by Vi-Cell Cell Counter (Beckman Coulter). The Y-axis represents a viable cell number normalized to control cells. The X-axis in each graph depicts the dosage of UVB treatment. Statistical significance was measured by one-way ANOVA with Tukey post-hoc analysis. Significant difference from the cell control is denoted by * and ***, which represents significance at p<0.05 and p<0.001, respectively. Results are representative of a single experiment with each treatment in triplicate. Error bars denote SE.*

2.3.4.2.1 Scaffolds Protect Keratinocytes Against UVB-induced Cell Death

In the next series of experiments, we wanted to explore the cytoprotective potential of CNT-coated scaffolds against UVB light. To analyze that, we treated cells with a wide range of UVB doses including 100, 200, 400, 700, 1000, 2000, and 3000 J/m^{2,} and evaluated the change in cell confluency to confirm the hypothesis that the CNT-coated scaffolds form a protective barrier. We selected to use doses up to 3000 J/m^2 as that is one of the highest exposures observed [334]. Keratinocytes (HaCaT cells) were stained with CellTracker™ Red CMTPX and one day after cell seeding, cells were

covered with either Long CNT-coated hydrophilic scaffolds, Short CNT-coated hydrophilic scaffolds, or CFC before treating the cells with UVB doses (Figure 44). Post-UVB treatment, the covered scaffolds were removed, cells were incubated for 3 days and cell viability, as well as confluency, were determined by visual examination as well as through phase-contrast microscopy by AMEFC4300 EVOS™ Digital Color Fluorescence Microscope. With increasing UVB doses, we saw detrimental effects on cell confluency in the control groups as they started exhibiting rounded morphology and increased cell death, and reduced confluency. On the contrary, both CNT and CFC-covered cells had no visual signs of cell death at any of the doses.

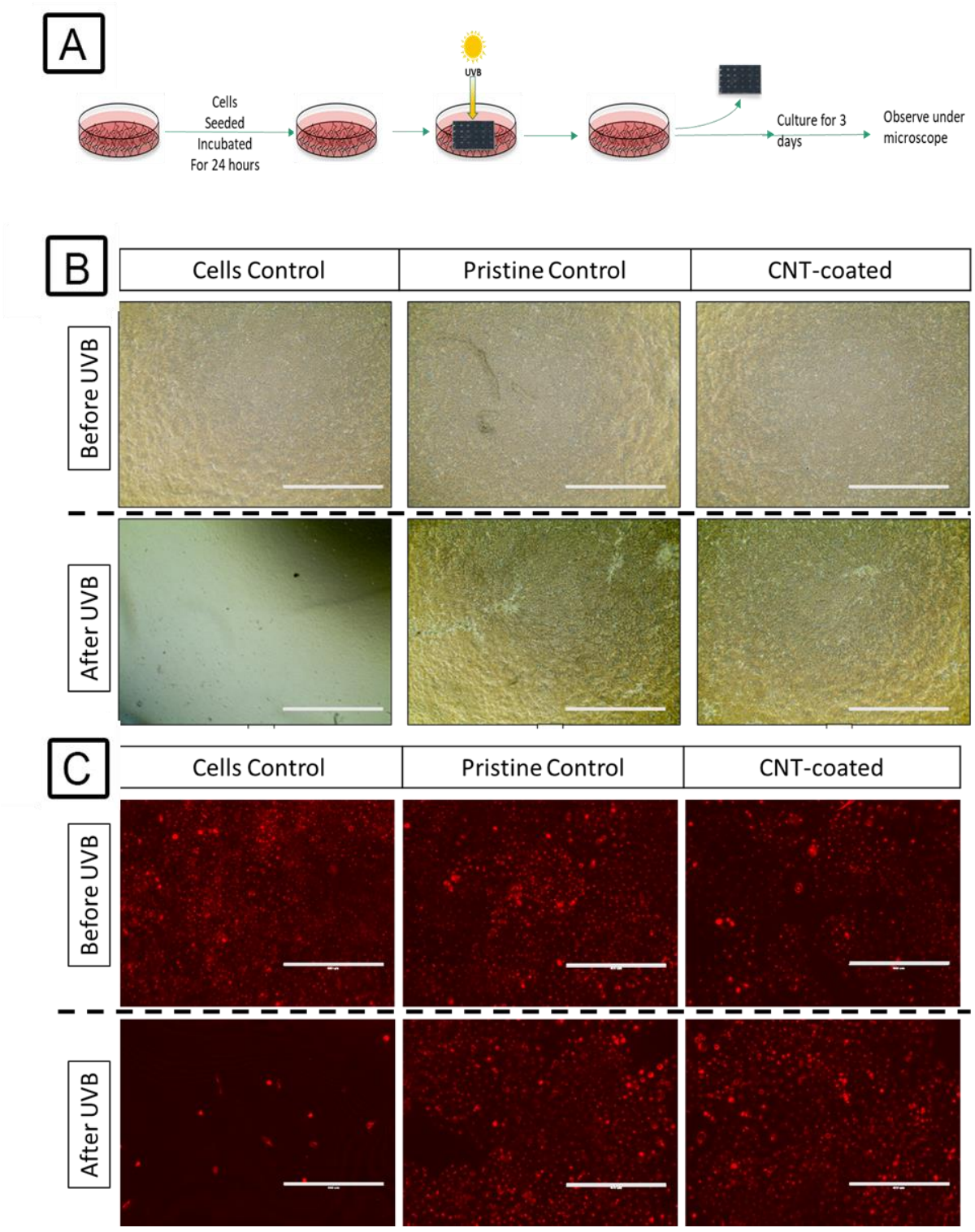

Figure 44 ***Keratinocytes covered with CNT-coated scaffolds are protected against UVB.***

Graphical representation of the set-up used to evaluate the effect of UVB on cells covered with carbon-coated scaffolds (A). HaCaTs were cultured in 35mm plates and

incubated for 1 day. The cells were then covered with CNT-coated scaffolds and treated with UVB. Scaffolds were immediately removed after the treatment and grown for 3 days and observed for cell growth and viability by phase contrast and fluorescent microscopy. HaCaTs were treated with UVB and cultured for 3 days. Representative images show phase-contrast (B) and fluorescent images of HaCaTs (C) after 3000 J/m^2 and 400 J/m^2 UVB, respectively. For fluorescent visualization, HaCaTs were stained with CellTracker™ Red CMTPX. The upper and lower rows show representative images of control cells, cells covered with carbon fiber cloth (CFC), and CNT-coated scaffolds before and after the UVB treatment, respectively. Scale bar represents 1000μm in (B) and in (C) 400μm. Representative images are from 3 independent experiments (n=3, 10 images analyzed per sample for each experiment).

We next evaluated the cytoprotective capacity of CNT-coated scaffolds when seeded with cells. Keratinocytes loaded with CellTrace™ CFSE were grown on the scaffolds and the scaffolds were inverted during the 400 J/m^2 UVB treatment so that the seeded cells do not receive direct UVB light (Figure 45 *A*). All cells were also stained with DAPI post UVB treatment to have an additional measure to validate the cell counting done using CellTrace™ CFSE (images not shown). Cell confluency and viability were evaluated visually after 72 hours and all scaffold groups provided protection against UVB. Direct UVB treatment of cells seeded on CNT-coated scaffolds was also protective (Figure 46). Taken together, the CNT-coated scaffolds were protective against UVB-induced toxicity. Additionally, we discovered that the Long CNT-coated scaffolds exhibited substantially increased cells compared to the cell control and the other scaffolds (Figure 46 *C*). Such scaffolds due to their longer CNTs and increased growth times of CNTs produce dense nanotube carpet forests and provide extensively intertwined nanostructures for cell growth, which appears to provide greater protection against UVB as compared with short CNTs.

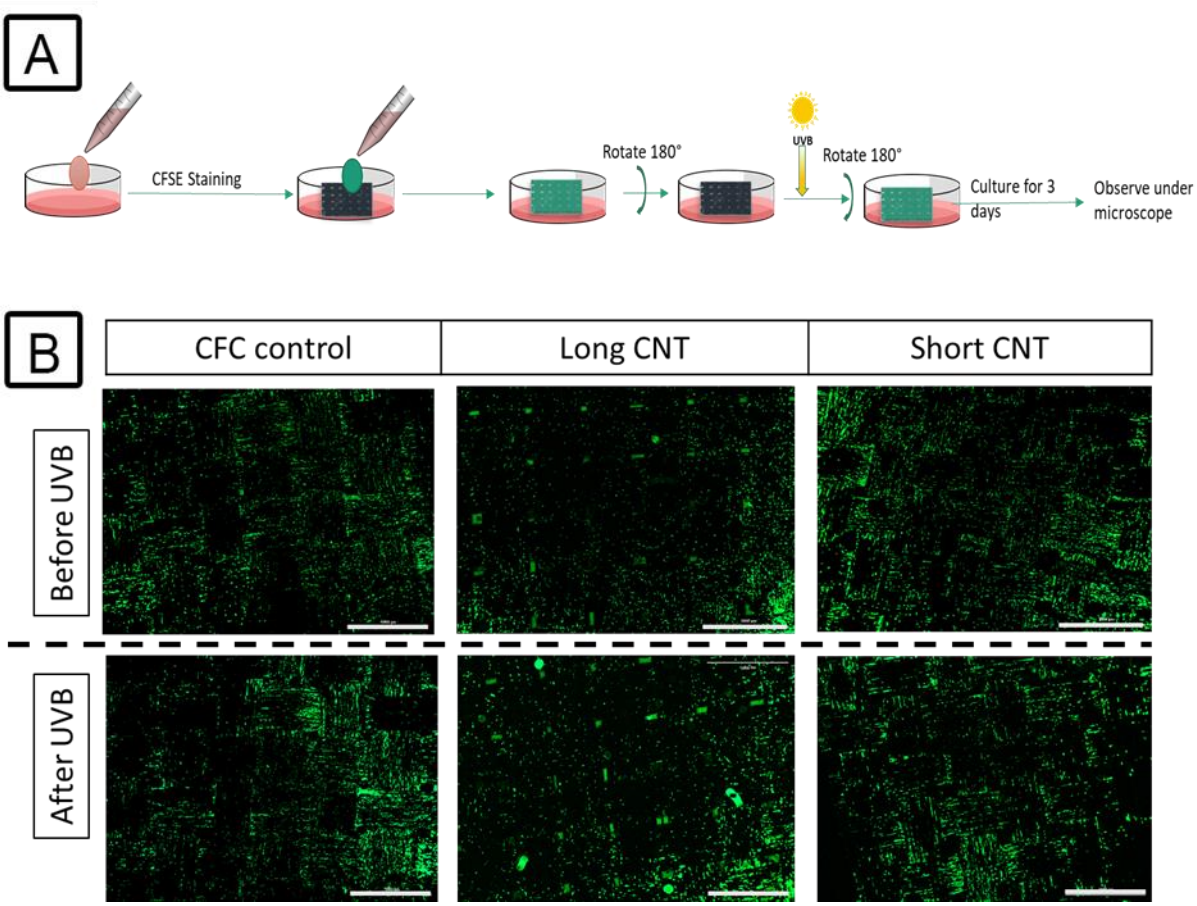

Figure 45 ***CNT-coated scaffolds provide protection from indirect exposure to UVB.***

Graphical representation of the indirect UVB treatment set-up (A). Cells were labeled with CellTrace™ CFSE and cultured on scaffolds and incubated for 1 day. Scaffolds were then imaged by capturing 6x6 stitched images using BioTek Cytation5 to get an assessment of cellular seeding of scaffolds. Scaffolds were flipped upside down for the 400 J/m^2 UVB treatment. Scaffolds were then flipped right side up and grown for 3 days. Cell growth and cell counts were evaluated by phase contrast and fluorescent microscopy via BioTek Cytation5 and Gen5 software. The upper and lower rows represent the fluorescent images of cells grown on carbon fiber cloth (CFC), Long CNT-coated scaffolds, and Short CNT-coated scaffolds before and after the UVB treatment, respectively (B). No visual changes in cell confluency were seen after the UVB exposure for cells grown on carbon fiber cloth (CFC) and CNT-covered cells. Scale bar represents 3000µm. Results are representative images of two repeats with each treatment in triplicate, each image being a stitched image of 36 images.

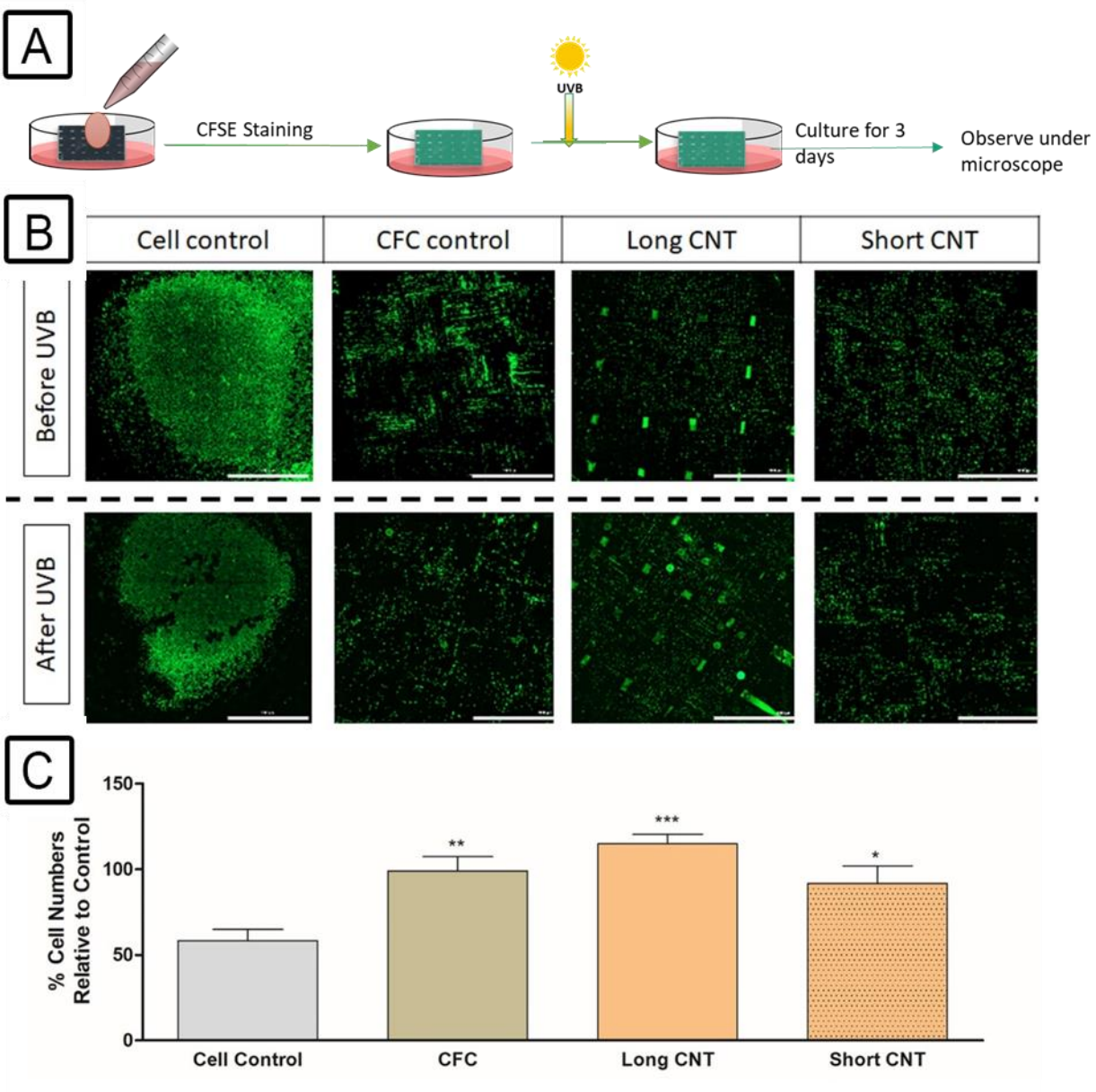

Figure 46 ***CNT-coated scaffolds provide protection from direct exposure to UVB.***

Graphical representation of the direct UVB treatment set-up (A). Cells were labeled with CellTrace™ CFSE and cultured on scaffolds and incubated for one day. Scaffolds were then imaged by capturing 6x6 stitched images using BioTek Cytation5 to get an assessment of cellular seeding of scaffolds. Scaffolds were then treated with 100 J/m^2 UVB and further incubated for 3 days. Cell growth and viability were evaluated by phase contrast and fluorescent microscopy via BioTek Cytation5 and Gen5 software. The upper and lower rows are fluorescent images of cells grown on cover slides and represent cell control, carbon fiber cloth (CFC) control, Long CNT-coated scaffold, and Short CNT-coated scaffold before and after UVB treatment, respectively (B). Scale bar represents 3000μm. Y-axis represents the relative cell number per each group after UVB treatment as compared to the cell numbers of the same group before UVB

*treatment (C). Statistical significance was measured by one-way ANOVA with Tukey post-hoc analysis. Significant difference from the cell control is denoted by *, **, and *** which represents significance at p <0.05, p<0.01, and 0.001, respectively. Results are representative of three separate experiments (n = 3 for each treatment group). Error bars denote SE.*

2.3.5 CNT-coated Scaffolds do not Improve the Effects of Photodynamic Therapy Treatment (PDT)

This preliminary test aimed to check the efficacy of CNT-coated scaffolds as photosensitizers for the PDT therapy treatment. PDT works on the principle that a specific wavelength of light activates a photosensitizing agent which produces reactive oxygen species (ROS) that causes cellular toxicity in the targeted cells. PDT has been in use for the past four decades for cancer cell ablation and in different chemotherapeutic applications [335]. Due to their substantially high surface area, thermal conductivity, and electrical properties; carbon nanotubes have been successfully implemented to use with a photosensitizer (PS) [336] or as the sole photosensitizing agent for PDT-based chemotherapeutic systems [337].

In this study, we wanted to understand if the CNT-coated scaffolds can potentially aid in the PDT therapy or can serve as the sole photosensitizer (PS) without the 5-ALA, the PS used in the study. The results from this study indicated that the scaffolds used in the study do not play a significant role in the PDT treatment. The cell numbers with PDT treatment did not reduce for the CNT treatment group (Figure 47).

Although the CNT-coated scaffold was not effective in modulating the PDT effects, this could have been due to the hierarchical structure of the overall scaffold which may have blocked the blue light used in the PDT treatment. Also, the source we used in this study was 415nm (specific to the 5-ALA excitation) and this would have

not been ideal to promote ROS shuffling by the nanotubes. From the knowledge gained from this study, we believe that the CNT-coated scaffolds can be functionalized with the PS to produce a synergistic effect in the redox cycling process and to help aid in localized PDT or they can be alternatively used with near-infrared light sources (NIR; 750-2500 nm) without any agents as the CNTs produce excessive heat with NIR which could be very effective for photothermal therapy (PTT).

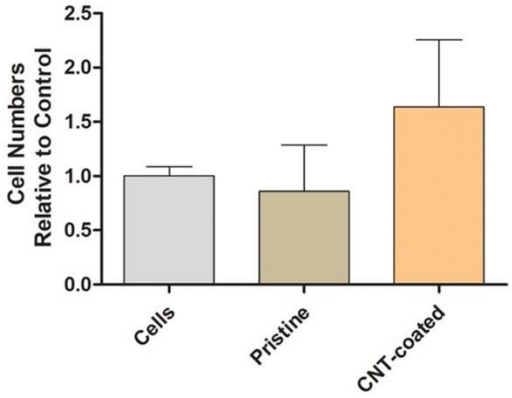

Figure 47 ***CNT-coated scaffolds do not improve the effects of Photodynamic Therapy Treatment (PDT).***

HaCaTs were treated with a photosensitizing agent and covered with CNT-coated scaffolds during the PDT treatment. The Y-axis represents the relative cell numbers post PDT treatment normalized to the cell control. We did not see a reduction in CNT-coated groups after PDT treatment, implying that CNT did not aid in the process.

2.3.6 Evaluation of Immunoreactivity of CNT-coated Scaffolds

After evaluating the cell proliferation, migration, and inflammatory cytokine release for the keratinocytes, which are adherent in nature; to further understand the immunoreactivity of the scaffolds, we evaluated them with B-lymphocytes. These B-lymphocytes are also suspension cells and were tested with the scaffolds for their function as well as the inflammatory markers.

2.3.6.1.1 Long CNT-coated Scaffolds may modulate B-lymphocyte Function

To gain insights into the potential immunogenic nature of the CNT-coated scaffolds, we evaluated the effect of the scaffolds on B lymphocyte function using two human B cell lines (SKW and CL-01). B lymphocytes secrete antibodies and are the primary mediators of humoral immunity against extracellular pathogens. Primary B lymphocytes and B cell lines are also non-adherent cells, unlike the adherent cell lines that have been evaluated thus far. For evaluating the effects of scaffolds, the SKW and CL-01 cells, originally derived from different Burkitt lymphoma patients, were incubated with scaffolds for 4 and 8 days and evaluated for changes in cell proliferation through cell counts and interaction with scaffolds through microscopy, as well as IgM and IgG antibody secretion through ELISA. IgM is the first antibody secreted by B lymphocytes in the humoral immune response [338] and IgG is the most abundantly secreted antibody [339].

After 4 days of incubating the scaffolds with the B lymphocytes, we observed an increasing number of cells interacting and attaching to the scaffolds through phase-contrast microscopy (Figure 48). Compared to the CFC group, both CNT-coated groups expressed increased scaffold attached cells. The cell scaffold interaction was further evaluated through fluorescence microscopy, which demonstrated a markedly increased number of surface-attached B lymphocytes on CNT-coated scaffolds on days 4 and 8 (*Figure 49-Figure 52 (A)*). The Long CNT-coated scaffolds showed a substantially higher number of cells attached to them at Day 8 compared to the CFC and Short CNT-coated groups.

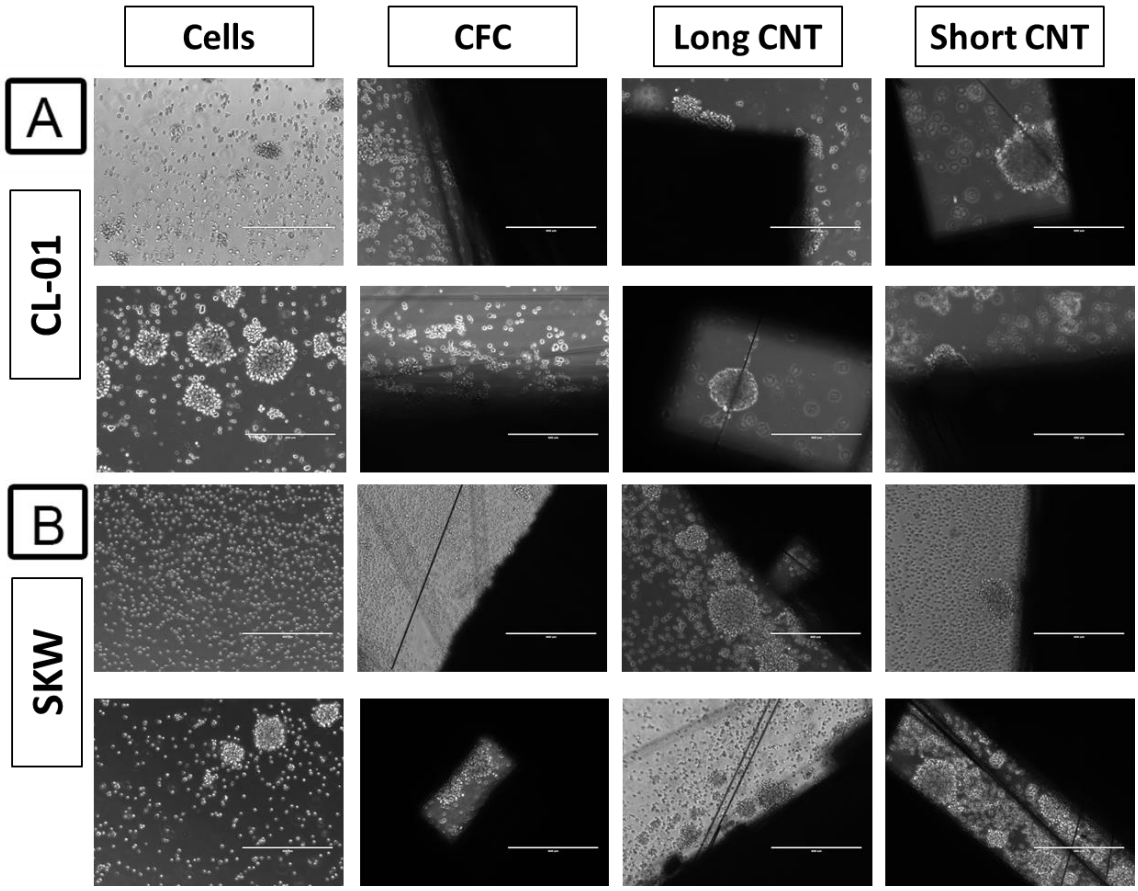

Figure 48 ***B lymphocyte interaction with scaffolds.***

CL-01 (A) or SKW (B) cells were incubated for 4 days with various scaffolds or without any scaffolds. Representative phase-contrast images showing the interaction of cells with carbon fiber cloth (CFC) (B), Long CNT-coated scaffolds (C), and Short CNT-coated scaffolds (D). The scale bar represents 400μm. The opaque structures are scaffolds used for the study. Surface-attached B lymphocytes on CNT-coated scaffolds can be observed. Images are representative images of one experiment with each treatment in triplicate.

Such bio-nano interactions could potentially alter the cellular function of these cells. Hence, antibody secretion from both B-cell lines was evaluated after incubation with the scaffolds for 4 or 8 days. Since B cells must be activated to produce antibodies, we stimulated the cells on Day 0 with CD40 ligand and IL-4 to mimic T cell-dependent stimulation of B-cells. Previous studies have identified optimal induction of antibody secretion by Day 4 of stimulation [296]. We also evaluated a longer

incubation period (Day 8) for naïve cells because of the increased surface area that the scaffolds provide for cell interaction and growth, which may lead to effects over time. Simulation induced IgG secretion.

At 4 days, in the stimulated group, we observed a more than two-fold increase in IgG secretion and a slight increase in IgM secretion in CL-01 cells *Figure 49,* which is consistent with previous work with these cells (Bhakta *et al.*, unpublished work). Interestingly, all of the scaffolds enhanced stimulation-induced IgG secretion from CL-01 cells on Day 4. Only the Long CNT-coated scaffolds increased IgM secretion from stimulated cells (*Figure 49 C*). Long CNT-coated scaffolds increased IgM secretion in unstimulated CL-01 cells after 8 days of incubation (*Figure 50 C*). The effect of CNT-coated scaffolds on antibody secretion was evaluated in another human B-cell line (SKW) isolated from a different patient. Unlike the CL-01 cells, CD40 ligand and IL-4 stimulation induced IgM but IgG was negligible (*Figure 51 B*). This corresponds to our previous studies and suggests either unknown cellular differences or different maturation phases of the SKW cells compared to the CL-01 cells (Bhakta *et al.*, unpublished work). The scaffolds had no impact on IgM secretion in the SKW cell line at Day 4 (*Figure 51 B*). However, following 8 days of incubation, all scaffolds appeared to non-significantly lower IgM secretion as compared to the cell control (*Figure 52 B*). We did not observe any significant changes in cell numbers with scaffolds as compared to the cell control group. These results suggest that antibody secretion could be modulated depending on the B-cell maturation stage and should be evaluated when designing a bioscaffold-based implant.

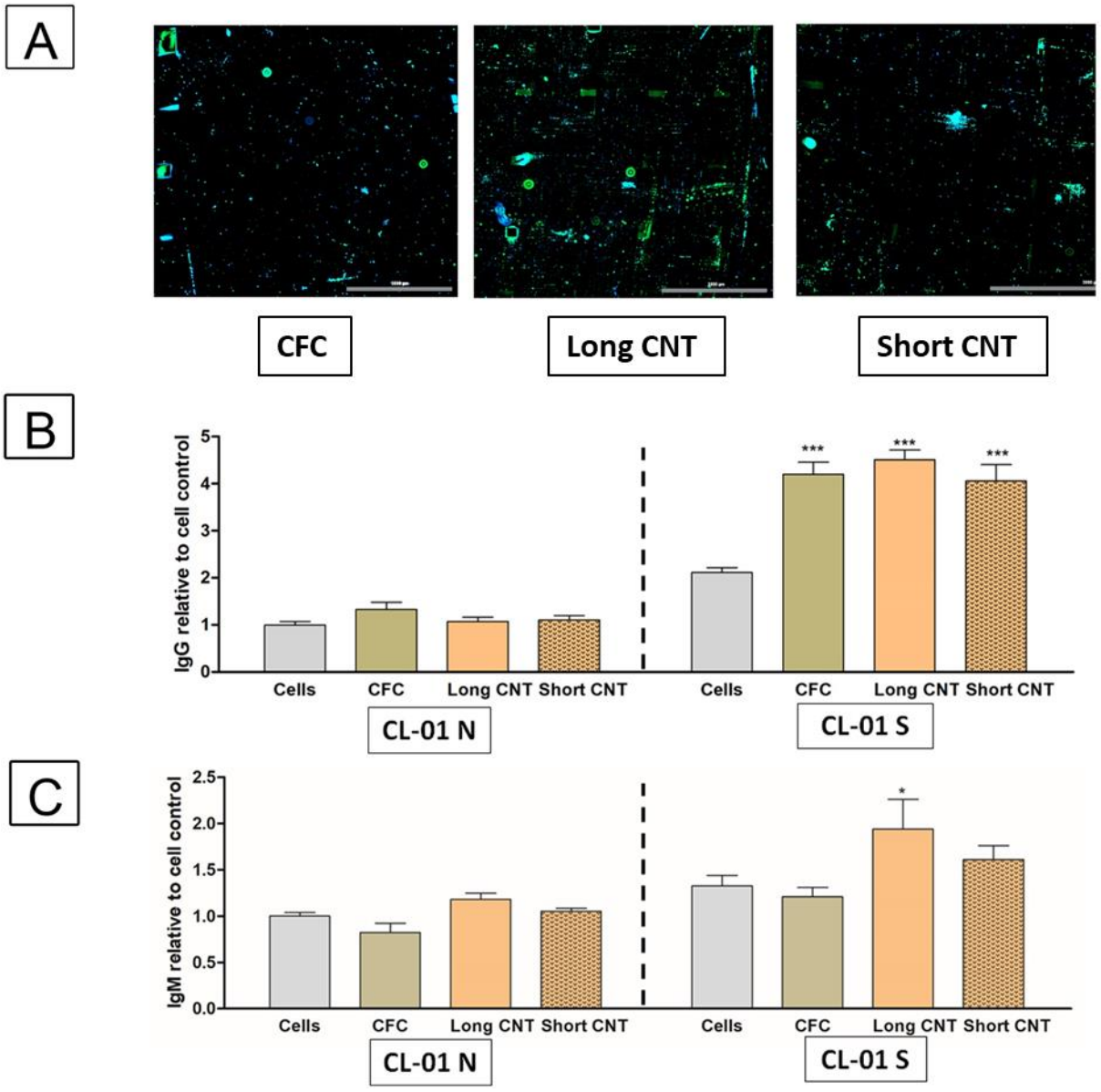

Figure 49 ***Scaffolds enhance IgG and IgM secretion in stimulated CL-01 cells.***

*CL-01 cells were incubated for 4 days with the various scaffolds or in the absence of any scaffolds (cells). Representative fluorescent images showing scaffold interaction of CL-01 cells labeled with Calcein-AM (green) and cell nuclei with DAPI (blue) (A). Scale bar represents 3000μm. Supernatant for IgG (B) and IgM (C) ELISA analysis was collected from unstimulated (N) or CD40L+IL-4 stimulated (S) CL-01 cells after 4 days of incubation. The Y-axis represents the antibody levels normalized to the naïve cell control (denoted cells, CL-01 N). Statistical significance was measured by two-way ANOVA analysis and Bonferroni post-test. Significant differences from the corresponding cell controls (denoted cells) were denoted by * and *** which represents significance at $p<0.05$ and $p<0.001$, respectively. Results are representative of three independent experiments (n = 3 for each treatment group). Error bars denote SE.*

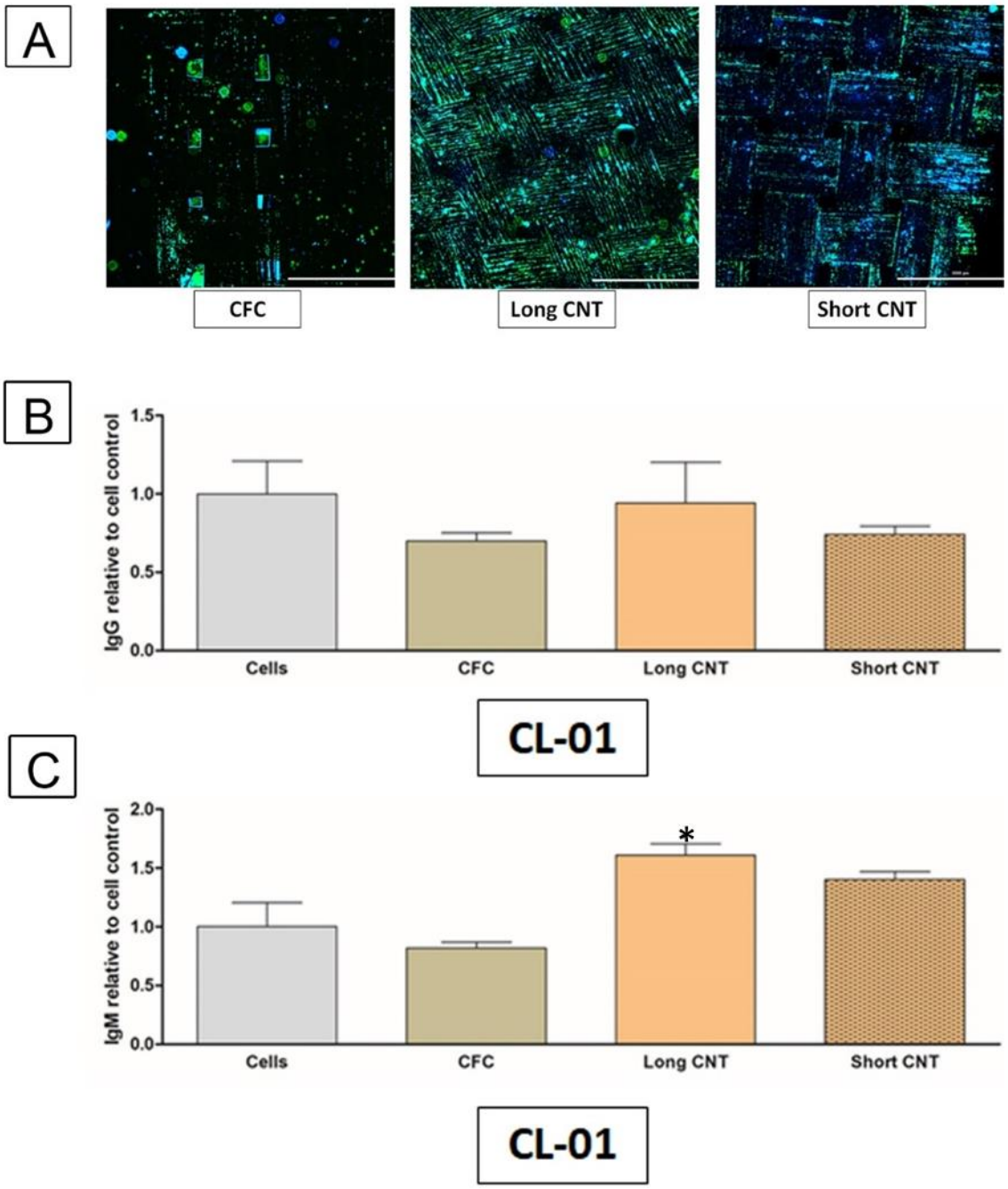

Figure 50 ***Preliminary study: Long CNT-coated scaffolds induced IgM secretion in CL-01 cells on day 8.***

CL-01 cells were incubated for 8 days with appropriate scaffolds or as is (cells). Representative fluorescent images showing the interaction and cell attachment of CL-01 cells with scaffolds (A). Scale bar represents 3000µm. Cells are labeled with Calcein-AM (green) and cell nuclei with DAPI (blue). After a 4-day incubation period, the supernatant was analyzed using an IgG or IgM ELISA for IgG and IgM concentration, respectively (B, C). The Y-axis represents the antibody levels normalized to the naïve cell control. Naïve CL-01 cells incubated with Long CNT-

*coated scaffolds exhibited significantly increased IgM secretion. Statistical significance was measured by two-way ANOVA analysis and Bonferroni post-test. Significant differences from the corresponding cell controls were denoted by * which represents significance at p<0.05. Results are representative of a single experiment with each treatment in triplicate. Error bars denote SE values.*

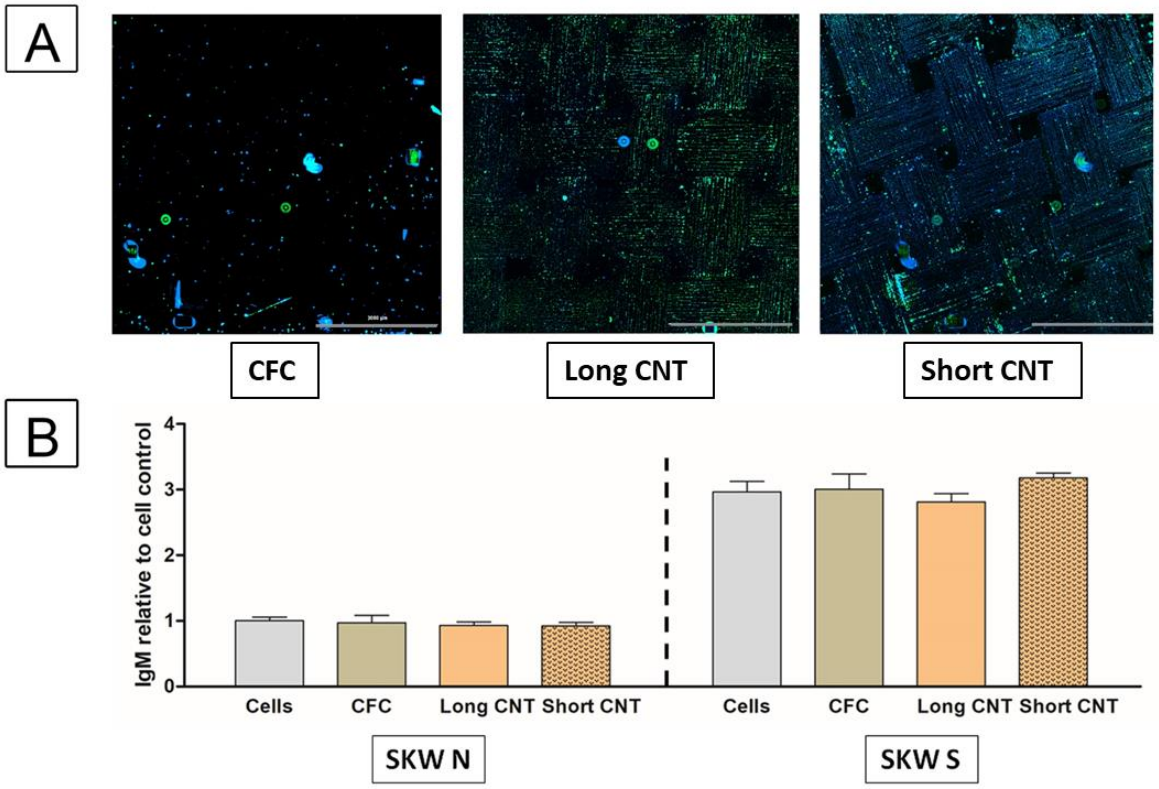

Figure 51 ***CNT-coated scaffolds do not affect IgM secretion in SKW cells.***

*SKW cells were incubated for 4 days with the various scaffolds or in the absence of any scaffolds (cells). Representative fluorescent images showing scaffold interaction of SKW cells labeled with Calcein-AM (green) and cell nuclei with DAPI (blue) (A). Scale bar represents 3000μm. Supernatant for IgM (B) ELISA analysis was collected from unstimulated (N) or CD40L+IL-4 stimulated (S) SKW cells after 4 days of incubation. The Y-axis represents the antibody levels normalized to the naïve cell control (denoted cells, SKW N). Statistical significance was measured by two-way ANOVA analysis and Bonferroni post-test. Significant differences from the corresponding cell controls (denoted cells) were denoted by * and *** which represents significance at p<0.05 and <0.001, respectively. Results are representative of three independent experiments (n = 3 for each treatment group). Error bars denote SE.*

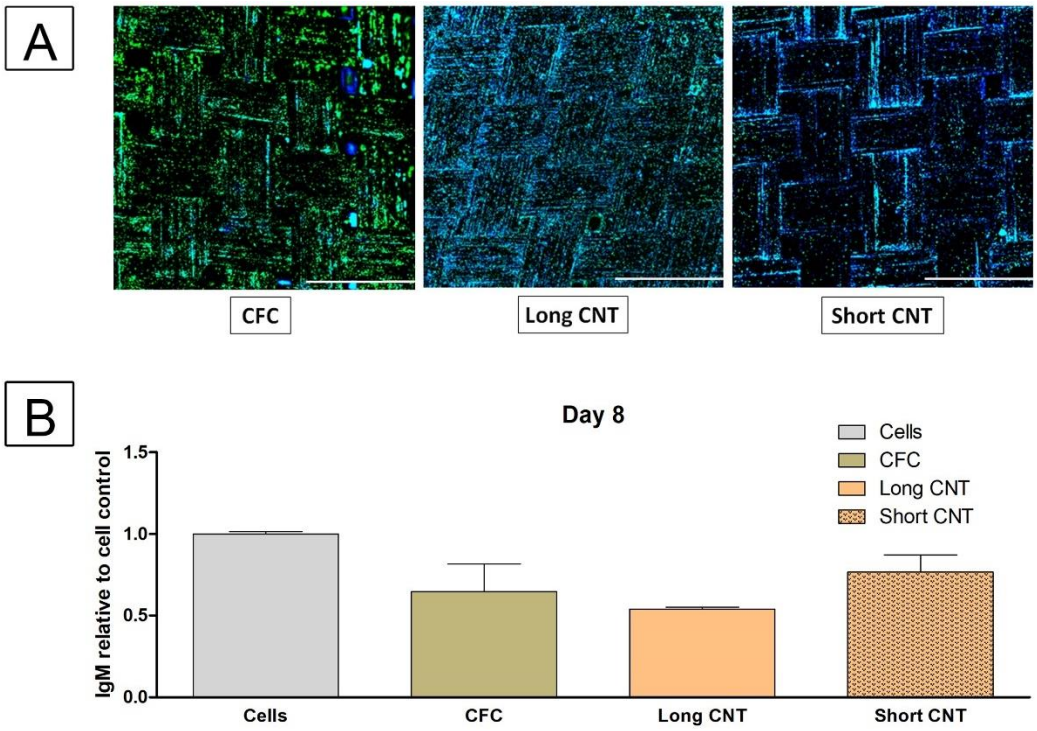

Figure 52 ***Preliminary study: Scaffolds may decrease IgM secretion in SKW cells on day 8.***

SKW cells were incubated for 8 days with appropriate scaffolds or as is. (A) Representative fluorescent images showing the interaction and cell attachment of CL-01 cells with scaffolds. Scale bar represents 3000µm. Cells are labeled with Calcein-AM (green) and cell nuclei with DAPI (blue). After an 8-day incubation period, the supernatant was analyzed for IgM concentration using an IgM ELISA (B). The Y-axis represents the antibody levels normalized to the naïve cell control. Statistical significance was measured by two-way ANOVA analysis and Bonferroni post-test by comparing each sample to the corresponding cell control. Results are representative of a single experiment with each treatment in triplicate. Error bars denote SE values.

2.3.6.1.2 CNT-coated Scaffolds may modulate Cytokine Secretion

All scaffolds used in the study were checked for their cytokine secretion after seeding HaCaTs on the scaffolds for 5 days. Long CNT-Coated hydrophobic scaffolds significantly increased IL-4. CFC scaffolds significantly induced secretion of IL-6, Il12P70, GM-CSF, and TNG-a; some of the pro-inflammatory cytokines were tested in the assay. Both short CNT-coated scaffolds also significantly increased GM-CSF

secretion. Short CNT-coated hydrophobic scaffolds also increased the amount of IL-17a, and Short CNT-coated hydrophilic scaffolds significantly increased IL-12P70 levels.

The cytokine secretion profile from the CL-01 and SKW B-lymphocyte cell lines was evaluated with or without CD40 ligand plus IL-4 stimulation after a 4-day incubation with either the carbon fiber cloth control or Long or Short CNT-coated hydrophilic scaffolds. From the 25 tested cytokines, in the CL-01 cells, only IL-4 showed any variation in secretion (*Figure 56*). IL-4 secretion was significantly increased in the presence of carbon fiber cloths and trended toward an increase with Long and Short CNT-coated hydrophilic scaffolds in naïve, unstimulated CL-01 cells (*Figure 57*). However, in stimulated CL-01 cells, IL-4 was significantly reduced in cells exposed to Short CNT-coated hydrophilic scaffolds. With the SKW cells, IL-4 and IL-10 were the only cytokines modulated by exposure to the scaffolds (*Figure 59*). IL-10 secretion significantly increased in SKW cells exposed to Short CNT-coated hydrophilic scaffolds and significantly decreased with the carbon fiber cloth as compared to cell controls. For stimulated SKW cells, IL-4 secretion was significantly reduced in cells exposed to short CNT-coated hydrophilic scaffolds, which was similar to the CL-01 cells. Additionally, IL-10 secretion significantly increased in cells treated with carbon fiber cloths. Overall, the changes in cytokines are relatively minimal and do not suggest an autocrine effect since these cytokine changes do not correspond to the effects of the scaffolds on antibody secretion.

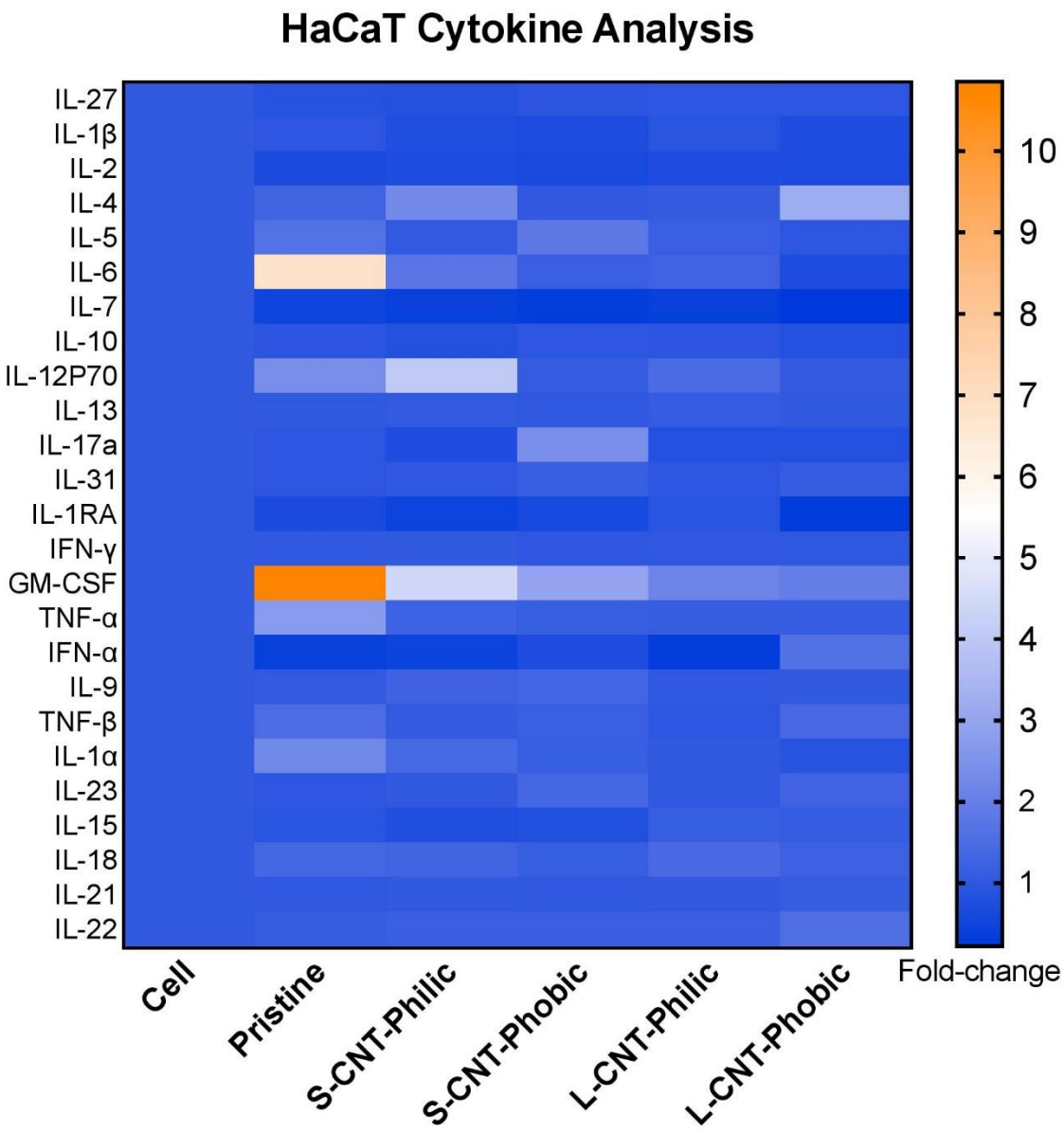

Figure 53 ***Analysis of inflammatory mediators released by HaCaT cells cultured for 5 days on scaffolds.***

Anti-inflammatory cytokine IL-4 was significantly increased in presence of Long CNT-Coated hydrophobic scaffolds. CFC scaffolds significantly induced secretion of IL-6, Il12P70, GM-CSF, and TNG-a; some of the pro-inflammatory cytokines were tested in the assay. Both short CNT-coated scaffolds also significantly increased GM-CSF secretion. Short CNT-coated hydrophobic scaffolds also increased the amount of IL-17a, and Short CNT-coated hydrophilic scaffolds significantly increased IL-12P70 levels. Statistical significance was measured by two-way ANOVA analysis followed by Dunnett's multiple comparisons test comparing each sample to the corresponding cell control.

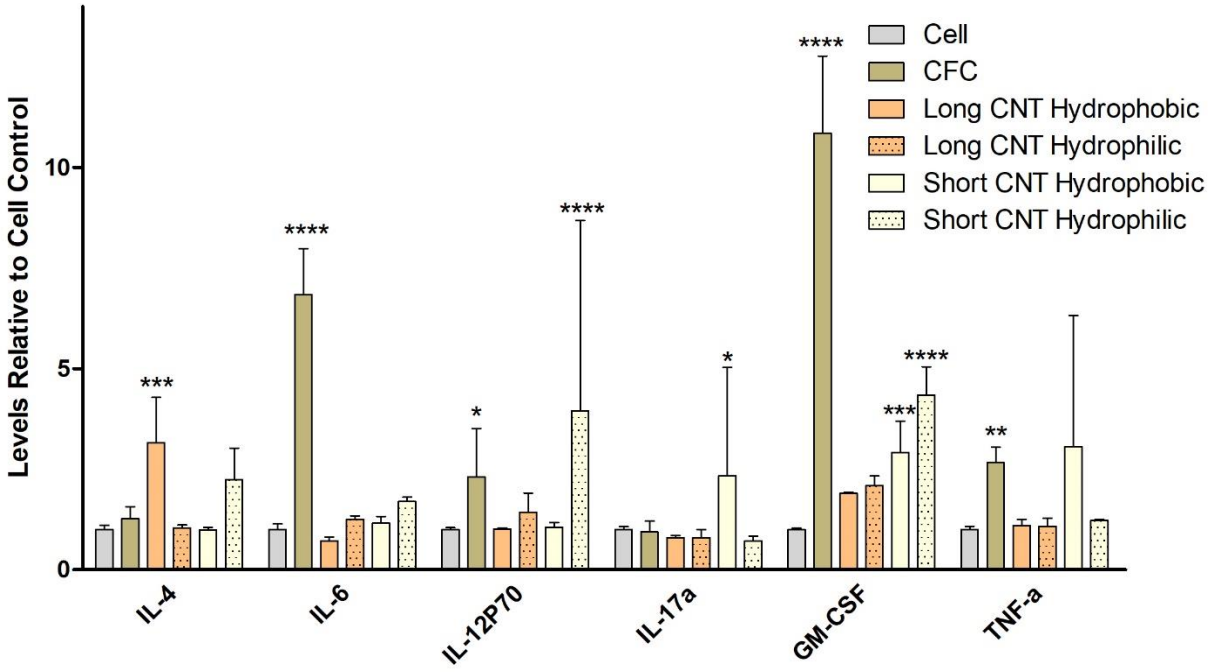

Figure 54 ***Some Inflammatory mediators are increased by culturing HaCaT cells on scaffolds.***

*Anti-inflammatory cytokine IL-4 was significantly increased in presence of Long CNT-Coated hydrophobic scaffolds. CFC scaffolds significantly induced secretion of pro-inflammatory cytokines IL-6, Il12P70, GM-CSF, and TNG-a. Short CNT-coated scaffolds significantly increased GM-CSF secretion. Short CNT-coated hydrophobic scaffolds also increased the amount of IL-17a, and Short CNT-coated hydrophilic scaffolds significantly increased IL-12P70 levels. Statistical significance was measured by two-way ANOVA analysis followed by Dunnett's multiple comparisons test comparing each sample to the corresponding cell control. Significant difference from the cell control is denoted by *, **, *** and **** which represents significance at p <0.05, p<0.01, p<0.001 and p<0.0001, respectively. Results are representative of one experiment (n = 3 for each treatment group). Error bars denote SD.*

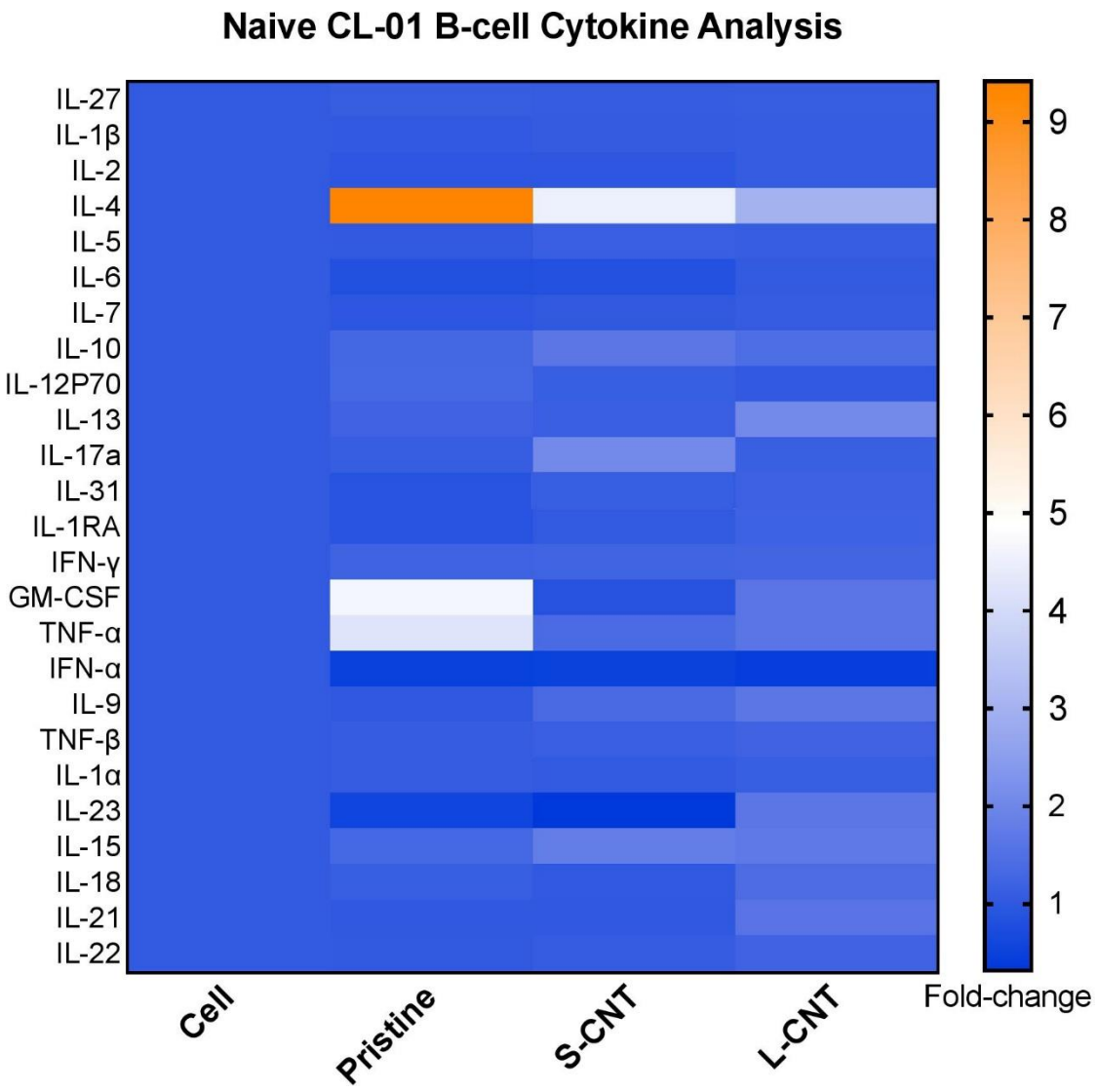

Figure 55 ***Analysis of inflammatory mediators released by naïve CL-01 cells cultured for 4 days on scaffolds.***

IL-4 secretion significantly increased in cells treated with carbon fiber cloths. Statistical significance was measured by two-way ANOVA analysis followed by Dunnett's multiple comparisons test comparing each sample to the corresponding cell control.

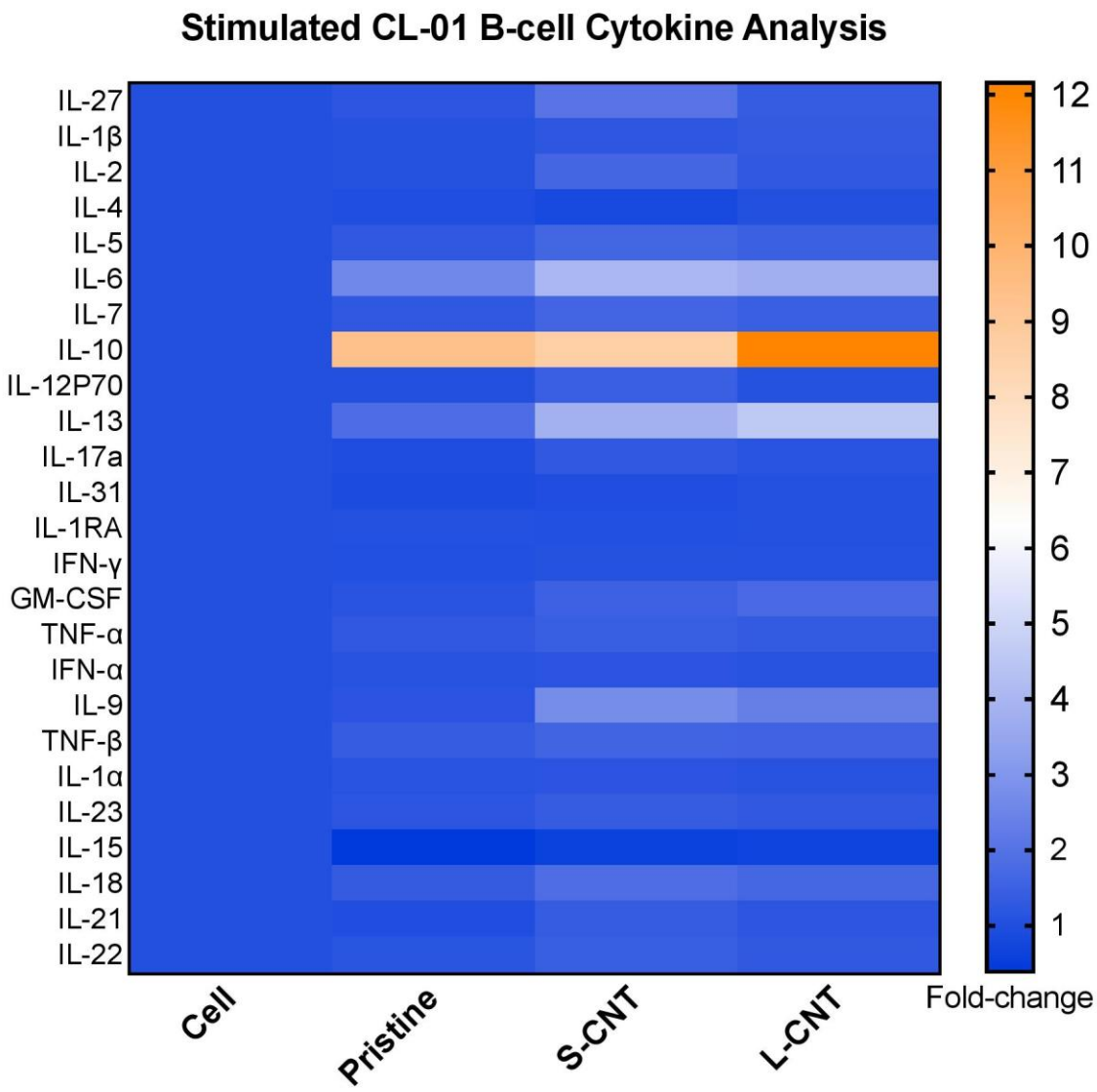

Figure 56 ***Analysis of inflammatory mediators released by stimulated CL-01 cells cultured for 4 days on scaffolds.***

IL-4 secretion significantly decreased in cells treated with Short CNT-coated hydrophilic scaffolds and carbon fiber cloths compared to cell controls. Statistical significance was measured by two-way ANOVA analysis followed by Dunnett's multiple comparisons test comparing each sample to the corresponding cell control.

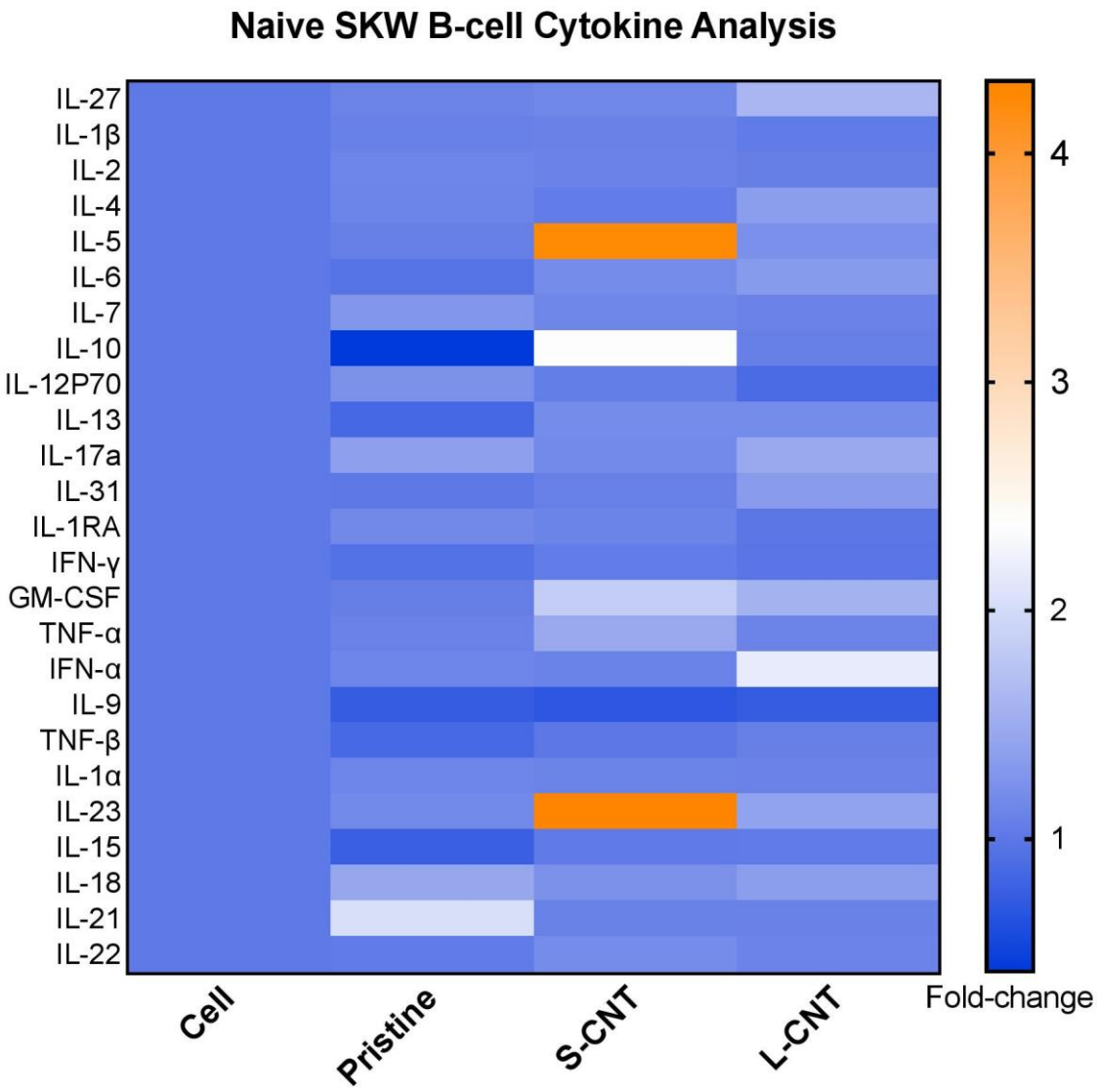

Figure 57 ***Analysis of inflammatory mediators released by naïve SKW cells cultured for 4 days on scaffolds.***

IL-10 secretion significantly increased in cells treated with Short CNT-coated hydrophilic scaffolds and significantly decreased in carbon fiber cloths. Statistical significance was measured by two-way ANOVA analysis followed by Dunnett's multiple comparisons test comparing each sample to the corresponding cell control.

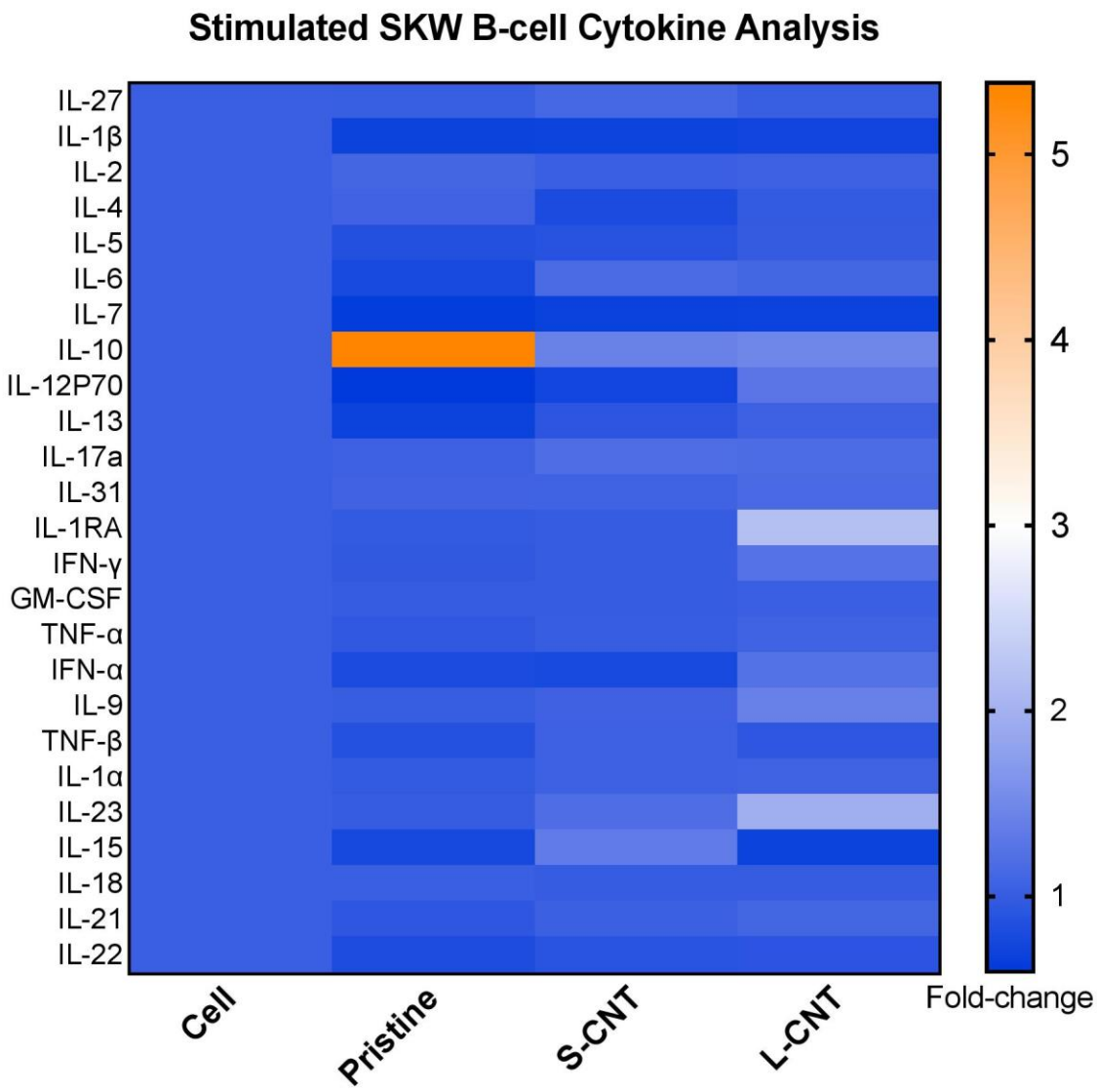

Figure 58 ***Analysis of inflammatory mediators released by stimulated SKW cells cultured for 4 days on scaffolds.***

IL-4 secretion significantly reduced in cells treated with Short CNT-coated hydrophilic scaffolds and IL-10 secretion significantly increased in cells treated with carbon fiber cloths. Statistical significance was measured by two-way ANOVA analysis followed by Dunnett's multiple comparisons test comparing each sample to the corresponding cell control.

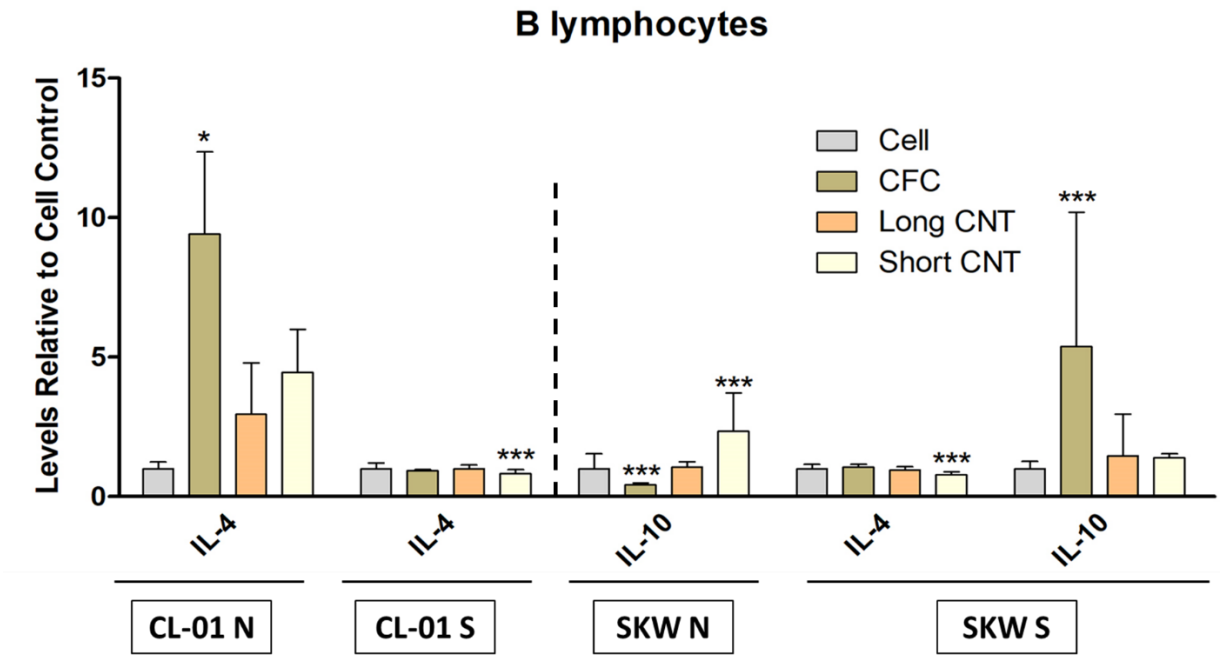

Figure 59 ***IL-4 and IL-10 are modulated by culturing B lymphocyte cells with scaffolds.***

*Naïve Cl-01 (CL-01 N), stimulated CL-01 (CL-01S), naïve SKW (SKW N), or stimulated SKW cells (SKW S) were cultured for 4 days on scaffolds, and levels of inflammatory cytokines were measured. Carbon fiber cloths (CFC) significantly increased anti-inflammatory cytokine IL-4 levels in naïve CL-01 cells and anti-inflammatory IL-10 in stimulated SKW cells. Short CNT-coated scaffolds significantly increased IL-10 levels in naïve SKW cells. Interestingly CFC significantly decreased IL-10 levels in naïve SKW cells and Short CNT-coated scaffolds significantly reduced IL-4 in stimulated SKW and CL-01 cells. Statistical significance was measured by two-way ANOVA analysis followed by Dunnett's multiple comparisons test comparing each sample to the corresponding cell control. Significant difference from the cell control is denoted by *, ***, and **** which represents significance at p <0.05, p<0.001, and p<0.0001, respectively. Results are representative of one experiment (n = 3 for each treatment group). Error bars denote SD.*

Discussion

Bioscaffolds have been increasingly used for constructive remodeling applications by providing cell delivery and supporting cell growth. Natural biological scaffolds, synthetic scaffolds, composite scaffolds, and nanostructure scaffolds are four major classes of scaffolds, each of which provides unique advantages depending on the specialized tissue regeneration applications. Since the past two decades, there has been a growing trend of using CNTs for bioscaffold applications [340] as they can provide unique advantages in addition to the majority of the properties attainable through other scaffold types. CNTs are relatively simple to manufacture and functionalize [120] and easy to sterilize [341]. They also robust mechanical properties [121], elasticity [122], electrical conductivity [11], and modifiable wettability [123]. Due to such properties, 3D structures with cross-linked CNTs have been successful in supporting tissue formation [65,66,342]. Despite these unique advantages for regenerative medicine, the biggest limitation of studies with CNTs is that free, detached, or disintegrated CNTs used in extensively investigated approaches are susceptible to intracellular uptake and can cause *in vitro* and *in vivo* cytotoxicity [153–156].

The current study addresses this issue in that we prepared unique hierarchical scaffolds with covalently attached CNTs. These CNT nanocarpets can provide the

advantages of nanoscale cellular and molecular interactions seen with CNTs without the potential toxicity risks associated with isolated, non-bound nanomaterials. We have prepared such scaffolds by covalently linking carbon nanotubes with flexible carbon fiber cloths or porous 3D carbon foams. Using these foam or fiber substrate materials also provides an additional advantage of flexible material architecture which can be customized according to the tissue characteristics and ultrastructure.

Our project focused on using these novel hierarchical CNT scaffolds whose activity and role in cell growth applications is relatively unknown. We characterized our materials for key surface properties (i.e. nanoroughness, wettability, and morphology) that could influence cell growth. Using glioblastoma and keratinocyte cell lines as a proof of concept, we evaluated cell growth on our hierarchical scaffolds to understand the bio-nano interaction. The knowledge gained from understanding the cellular toxicity, attachment, and proliferation mechanism(s) between the cells and these nanocarpets could be a key to future designing of CNT-coated scaffolds applicable for various applications including skin grafts, surgical resection of glioma, and other tissue engineering applications.

In the first study, we aimed to understand the glioblastoma cell interaction with these scaffolds. We assessed the viability of the scaffolds for the development of a possible chemotherapy-containing implant for GBM patients. We used carbon fibers and carbon foams as substrate materials for CNT-coating in this study. Carbon fibers tested in these studies are highly flexible 2D structures that also have interconnected spaces allowing fluid movement. These interwoven structures along with CNTs can also be used as flexible, non-degradable microfiber material with multilayered structural arrangements as a tissue-engineered graft or implant. Carbon fiber scaffolds

can also incorporate drugs onto the structure surface which can be used for fast release applications for therapeutic development. We also used carbon foam structures due to their easy-to-manipulate 3D structure, porosity, and high surface area. These foams can be easily made to mimic the tumor-specific size and shape necessary to fill the GBM resection area [177], which would increase the tumor-chemotherapy interaction. The 3D structure of carbon foam combined with the additional surface area of the nanostructured CNT carpets allows for the possibility of sustained drug release applications. The porous nature of these structures also allows for cell and fluid infiltration, possibly decreasing the pressurized fluid buildup which has been a concern in previous implant studies [343].

Cell growth on the scaffold can be modulated by a wide variety of factors such as material surface roughness, composition, conformation, orientation, functionalization, wettability, surface area, and porosity [65,66,99,123,313,344–350]. Through the glioblastoma study, we discovered that the wettability of the scaffolds could be a critical element controlling the cellular response of GBM cells. When the superhydrophobic CNT scaffolds were used, cell growth of GBM was observed where the initial cell growth on CNT scaffolds was inhibited. Once the surfaces were functionalized to be hydrophilic, alteration in wettability resulted in a standard growth curve pattern over time instead of the initial slow growth patterns noted in non-treated superhydrophobic scaffolds. The insights gained from this study on bio-nano interaction, particularly the impact of hydrophobic surfaces on GBM growth could be key to designing a future treatment option for glioblastoma as the hydrophobic CNT in presence of chemotherapy may produce a synergistic effect in slowing down glioma proliferation. From the knowledge gained from this study about the impact of wettability

on cellular growth, we also wanted to further evaluate if such an effect is consistent with different cell types.

To assess the universal applicability of these scaffolds, we identified wound healing as another area where the usage of CNT bioscaffolds could be very advantageous. These scaffolds provide a customizable surface that is highly flexible and easy to functionalize with growth factors as a split-thickness skin graft or as dermo-epidemal substitutes which can contain multiple cell types and can cover a large area. Current scaffolds for wound healing have major limitations in terms of their sterilization, storage, and proliferative capacities [267]. Keratinocyte cell sheets are too delicate to be transferred by themselves and require a scaffold that can provide mechanical strength as well as biomimetic cues [351,352]. Additionally, the effectiveness of CNT-coated hierarchical materials for wound healing is still poorly understood. The role of the carbon nanotube lengths on cell growth is also not known. Therefore, in our study, we evaluated bio-interaction between the hierarchical scaffolds and keratinocyte cells by varying surface wettability as well as the lengths of CNTs to assess the possible applicability of our materials as wound healing scaffolds. Till now, the evaluation of CNT lengths on cell growth has only been focused on toxicity evaluation of the unbound nanotubes [309,322,353]. We hypothesized that shorter CNTs due to their directionality can significantly aid keratinocyte and fibroblast growth. We chose to use the CNT-coated fiber cloth scaffolds for this study as they can provide a customizable surface that is highly flexible and easy to functionalize with growth factors as a split-thickness skin graft. To our knowledge, this is one of the first studies exploring the efficacy of varying CNT lengths on such hierarchical CNT-coated materials for cell growth applications.

We first followed established guidelines by the FDA and the U.S. Pharmacopoeia for tests on biomaterials [261] and the results from the test unveiled the non-cytotoxic nature of the extract of various bioscaffolds used in the study on HaCaTs. We found out that cell death is comparable and not significantly different between extracts prepared from the scaffolds and the control groups. Therefore, the indirect contact test validates that these hierarchical nanostructures could be considered safe for keratinocyte cell growth and can be tested further for their tissue engineering applications.

We discovered that CNT-coated scaffolds are not only biocompatible and non-cytotoxic but also hold promise in supporting skin cell growth and proliferation for wound healing applications. The results from this work give us insight into differences between preferential cell attachment and proliferation of keratinocytes (HaCaTs) on different surfaces, i.e., increased cell proliferation on short vs. long CNT growth. This study also determined that surface hydrophilicity did not play a major role in cell proliferation. We also evaluated the ability of the scaffolds to protect skin cells from external stressors like UVB. This study focused on evaluating the cytoprotective capacity of CNT-coated scaffolds towards the indirect treatment of UVB. This was done to check the capacity of the scaffolds as a split-thickness skin graft where scaffold cultured cells are not directly exposed to the external environment. Both the CFC and the CNT-coated scaffolds successfully blocked UVB exposure. We also found that longer, more densely connected CNTs are more cytoprotective against UVB. Another environmental stressor tested in the study, TCDD did not induce cell death in HaCaTs and hence the potential cytoprotective effects of CNT-coated scaffolds were thus could not be validated in this study.

Lastly, to check the compatibility of the scaffolds for implant-based applications, we evaluated them for their preliminary biocompatibility and immunogenic evaluation. Interestingly, in the CL-01 B-lymphocyte cell line stimulated with T-cell-derived factors, all of the scaffolds increased IgG secretion, including the carbon fiber cloth controls, while IgM secretion was only enhanced by the long CNT-coated scaffolds. Stimulation used in the study was done via CD40 ligand and IL-4 treatment, which binds to the surface CD40 and IL-4 receptor on the B-cell surface, mimicking T cell-dependent stimulation of B-cells. Prolonged incubation with scaffolds with no stimulation treatment also yielded increased IgM secretion with Long CNT-coated scaffolds. However, these effects on antibody secretion were not seen in the SKW B-lymphocyte cell line. Both SKW and CL-01 cells are derived from different Burkitt lymphoma patients and are EBV-transformed cell lines. However, they both could be at a different cellular stage which could explain the variability in antibody secretion profiles. The potential effects of the scaffolds on the modulation of antibody production could have been due to specific interaction of the CL-01 cells or a non-specific interaction due to the nature of nanotubes or both. The extensive surface area of CNTs has been exploited as antigen-presenting cells for T-cell activation [354] and activated B and T lymphocytes have also been shown to modulate increased uptake of loose CNTs as compared to resting lymphocytes [355]. B Cells get activated when B-cell receptors are cross-linked by foreign particles. Due to the extensively high surface area, B-cells could have non-specifically interacted with the nanotubes, and through B-cell receptor cross-linking, antibody response of the stimulated cells could have been induced. Alternatively, B-cells could have interacted with the 3D structures of nanotubes as they could mimic lymph nodes by bringing the cells closer together and perhaps providing interactions that mimic cell-cell contact and promoting the

stimulatory effect of the T-cell-derived factors, CD40L and IL-4. We had chosen IL-4 and CD40 ligand as T-cell-derived factors to mimic T cell-dependent stimulation of B-cells as it is well known that the CL-01 cells start secreting significant amounts of antibodies and start the class switch recombination process in presence of it [296]. Although cytotoxicity and cell growth capabilities of the CNT-linked supports have been extensively studied, a very limited amount of focus has been paid to the immune response, particularly to B-lymphocytes [356].

The cytokine profiles of B-cells greatly depend on the activation conditions and differentiation stages [357]. Assessment of cytokine profiles of two different B lymphocyte cell lines revealed that changes in cytokines are relatively minimal and point towards the non-immunogenic nature of the scaffolds used. Even after the stimulation conditions contained IL-4, we observed significantly decreased IL-4 levels in both SKW and CL-01 cell lines with short CNT-coated scaffolds. This was an interesting observation as IL-4 was externally added as a treatment. The mechanism of this alteration is not yet understood but one of the possibilities could be that CNT structures could be non-specifically attaching with the secreted antibodies. If that is true, it can completely skew our interpretation of the scaffolds being non-immunoreactive and needs to be studied in detail.

Surface roughness is an important factor that can regulate cell adhesion. Our lab has already shown that nanocarpet functionalization increases nanoroughness by several orders of magnitude which improves cellular attachment [65,66]. In superhydrophobic surfaces, surface roughness has been positively associated with cell adhesion [349,350]. Scaffold hydrophilicity is another important material property that is capable of altering cell adhesion and cell growth. For example, increased

hydrophilicity can increase fibroblast cell growth and attachment upon smooth and rough PLLA poly(L-lactic acid) surfaces, thought to be due to increases in cellular adhesion capabilities [358,359]. The Oliveira group studied the effectiveness of polystyrene surface roughness and hydrophilicity using osteosarcoma (Saos-2) cells and found that rough superhydrophobic and smooth, highly hydrophilic surfaces have better cell attachment short-term; however, over time cell proliferation upon hydrophilic surfaces was significantly enhanced independently of surface roughness [313].

Similar to previous studies on hydrophilicity, this increase in cell proliferation with glioblastoma and keratinocyte cells may be explained by cell adhesion capability. While the CNT-coated scaffolds provide a significant increase in available surface area, the superhydrophobic nature of these structures could initially inhibit this interaction. The Cassie–Baxter model may explain this phenomenon (*Figure 5*). In this model, when surfaces are highly hydrophobic, the presence of air pockets in the surface may avert cellular and/or culture medium contact with the full surface. Over time, increased cell secretion of ECM could allow for increased cell-structure interaction, increasing cell proliferation capacity. This environmental shift in cell-nano-matrix interaction could shift the cell's ability to integrate and divide. This could be one of the explanations of the limited cell adhesion and proliferation on our CNT-coated scaffolds with their hydrophobic nature short term. Long-term, there may be a partial transition switch to a Wenzel state (*Figure 4*), where cells can be in immediate contact with the surface, accelerating cell proliferation [359] and resulting in biphasic growth. Thus, shifts in cell proliferation in GBM cell growth for superhydrophobic surfaces may be explained by a probable transition from the Cassie-Baxter model to a Wenzel state in which the culture media and cellular adhesion transition to more immediate contact

with the structure surface. The keratinocyte study was mainly focused on the log phase of the cell growth as we wanted to characterize the cell growth pattern on different CNT lengths. So, we did not acquire proliferation data at near-confluency points, which could have been able to provide more insights about the biphasic growth pattern if any.

It has also been shown that moderately hydrophilic surfaces facilitate better attachment and provide excellent cell growth on the scaffolds through strong binding of cellular adhesion proteins [344–348]. Similarly, the increased scaffold hydrophilicity found post-sodium hypochlorite-based bleach treatment would increase cell attachment to the scaffolds concomitant with our cell proliferation findings. This could explain the comparable cell growth between pristine supports and sodium hypochlorite-based bleach treated samples, where hydrophilicity and not nanoroughness could be a more important aspect controlling the cell growth of glioma. This alteration in wettability resulted in significant proliferation of cells on the carpets, changing the growth pattern to a standard growth curve over time instead of the biphasic development noted on non-treated hydrophobic scaffolds. These data mirror studies by Oliveira *et al.* that displayed time-dependent changes in the osteosarcoma (Saos-2) cell line when grown on rough superhydrophobic or smooth, highly hydrophilic surfaces [313]. In their study, cells displayed better cell attachment short-term when grown on rough surfaces, but long-term cell proliferation was higher when cells were grown on hydrophilic surfaces with water contact angles ranging from 13 to 30°, independent of roughness. Our data show that the hydrophobic/hydrophilic nature of structures as a component of cell attachment and adhesion may be a critical material property for cell growth of glioblastoma cells. However, our previous reports

using similar scaffolds involving stem cell differentiation and growth did not show exaggerated differences in cell proliferation depending on the hydrophilicity profile of the materials [66]. Moreover, with the keratinocytes, the CFC fiber controls, and the hydrophilic short CNT-coated scaffolds exerted comparable cell proliferation. This may indicate that hydrophilicity was one of the regulating factors for cell growth, however, the effects on cell proliferation were not as drastic as with GBM cells. This implies that the differences for cell proliferation on these nanocarpets are cell-type specific and need to be understood in detail before using it as implant materials.

Numerous studies have been conducted to assess toxicity profiles of CNTs based on their lengths but less is known regarding how the length of CNT can modulate cell proliferation. Free, short CNTs are more effective and less cytotoxic for cellular growth due to their potential internalization and removal than longer CNTs or clusters of CNTs, which cannot be engulfed by macrophages/reticuloendothelial system and thus cannot be degraded and/or removed [309,322]. The Meng group also observed that cellular uptake of short CNTs is higher as compared to longer CNTs and shows higher degrees of cell differentiation in pheochromocytoma cells [360]. CNTs due to their size and functionalization show varying degrees of *in vivo* distribution and thus show altered cytotoxicity [353]. However, since our CNTs are covalently attached to the underlying materials, we did not observe any associated toxicity in the short CNT-coated scaffolds.

The previous studies had explored the role of nanoroughness [66] and wettability [67] of the CNT-coated scaffolds and had evaluated their effects on cell growth. The alterations of the CNT lengths allowed us to understand the varying CNT lengths and not necessarily the hydrophilicity or nanoroughness would be the key

aspect controlling the keratinocytes cellular response on our hierarchical materials. Results from our study also indicate that cell growth for keratinocytes on CNT-coated surfaces is modulated by the length of the nanotubes spanning through the carbon fiber cloth. Both, hydrophilic and hydrophobic long CNT-coated scaffolds had significantly lower proliferating cells as compared to both short CNT-coated surfaces. Controllable CNT length over these surfaces (optimized in our lab) change the surface area available for cell growth, which makes long CNT-coated scaffolds distinctively different from short CNT-coated scaffolds (*Table 2*). Long CNTs provide more randomness, extremely high surface area, and substantially interconnected structures. Keratinocyte cells may not be able to attach and start ECM secretion on the longer CNTs as easily due to their randomized orientation and denser clusters of nanotubes. However, the long CNT-coated scaffolds were more effective for cytoprotection against UVB, which can also be associated with its substantially increased surface area as it can absorb and block the UVB more effectively [273].

Short CNT surfaces can provide less nanoroughness and have relatively less dense forests of CNTs. They do not completely cover the fiber cloth surface underneath and also do not create a randomized cluster of tubes as seen with long CNTs (*Figure 15*). This more uniform and less heightened structure of the short CNTs (*Figure 12*) can be more receptive to cell attachment, ECM secretion and provide increased directionality to cells through the weaves of the underlying fiber cloths. This could imply that keratinocyte cell growth is more regulated by available surface area and structural directionality of the CNTs than surface wettability. This also suggests that surface nanoroughness may not be a key controlling factor for HaCaT growth on such surfaces since the cell proliferation was comparable between short CNT-coated

scaffolds, CFC group, and control cells. We observed the scaffolds for the potential cell migration from the wound edge and discovered that the scaffolds expressed a significant number of dye-loaded cells on their surface, signifying that the cells from the wound edge had successfully migrated towards the pre-seeded scaffolds. Lastly, we performed similar experiments to understand the cell migration profiles towards the scaffolds and from cell-loaded scaffolds towards an area with no cells to understand the suitability of such scaffolds as surface grafts. The cell migration results were really promising and successfully point towards the assessment of further exploration of these scaffolds as would healing grafting material.

The keratinocytes (HaCaTs) were also tested for their inflammatory cytokines in presence of scaffolds to understand if the scaffolds can promote the release of pro-inflammatory markers and to better understand the biocompatibility. We observed that carbon fiber cloth controls (CFC) mediated a significant increase in TNF-α which is a major pro-inflammatory cytokine and regulates initial inflammation and injury [361–363]. Upregulation of TNF-α can also mediate the NF-kB pathway and could result in the upregulation of other pro-inflammatory cytokines [364,365]. That could potentially explain the significant increases of IL-6 and GM-CSF in the CFC group. Increased upregulation of IL-12P70 has been linked with psoriasis [366] and the effects of Short CNT-coated hydrophilic CNT scaffolds on skin function needs to be studied further. Lastly, damage of keratinocytes is strongly linked with the release of IL-1α [367] and we did not observe any upregulation of IL-1α in any scaffold groups. Long CNT-coated hydrophobic scaffolds significantly increased IL-4 levels, which was an interesting observation as IL-4 is linked with increased cell proliferation [287] and cytoprotection

[368]. Overall, Long CNT-coated scaffolds did not modulate the cytokine profile of the keratinocytes.

Based on the glioma work, we can propose that the hydrophobic CNT-coated foam scaffolds can be particularly useful for glioblastoma post-surgical resection implant studies. We also propose that scaffolds with shorter CNT growth on hydrophilic surfaces could be useful for the commercial development of future wound healing scaffolds. However, further evaluation is necessary. For both studies, their interaction and attachment with the cells and how it affects the cell cycle need to be completely understood to uncover the underlying mechanism of cell growth on such surfaces. It would also be valuable to further understand the mechanism of how the scaffolds with or without the functionalization can modulate pro and anti-inflammatory cytokines to understand the effects on innate immunity. Such scaffolds also need to be extensively characterized for their immunogenic profile and studied with T-cell lines and macrophages.

How neurons and brain glia can attach and grow with such scaffolds also will give key insights for designing the CNT-based surgical implants intended for GBM. Effects of CNT lengths and the surface functionalization properties and their subsequent effects on cellular retention, invasion as well as migration also need to be further evaluated before attempting such materials as chemotherapy attaining implants. From the wound healing study, we also evaluated the scaffolds for fibroblast cell migration because keratinocytes and fibroblasts play a vital role in the wound healing process. We had implemented migration strategies where physical stimuli (i.e. scratch) are not introduced with the wound creation. There were inconsistencies in terms of the manual scratching of the wounds. Modified scratch wound assays can

address that limitation and adding a similar condition can significantly improve our understanding to use such materials as grafts. One of the limitations of our experiments was that the scaffolds could not retain a fixed position. The cell migration process could have been perturbed due to this and could have resulted in varying healing rates. Also, the dye used in the study could not be retained by the cells for more than the experimental duration. To further investigate cellular migration, scaffolds could also be embedded in hydrogels. A co-culture model of keratinocytes with fibroblasts and monocytes can also be studied for evaluating cell proliferation and migration and to understand how the scaffolds behave in physiological conditions. Furthermore, understanding the cell migration from hydrophobic scaffolds can further uncover cellular mechanisms that were beyond the scope of the current study. Using stable, fluorescently labeled cells and quantifying the migrated cell numbers and insights about the rate of the cell migration from the scaffolds can also extensively bolster our understanding of the skin-scaffold interaction and can lead to their future therapeutic development. The scaffolds can also be used with artificial or reconstructed skin models and checked for their bio-nano interaction and cytoprotection against UVB.

The results from this study combined with previous work with our scaffolds [65,66] provide comprehensive knowledge about these bioscaffolds that can be translatable for tissue engineering approaches utilizing other cell types as well. CNTs are electrically conductive that can circumvent the limitations of prosthetics which have significant challenges in transmitting the electrical stimuli. Researchers have also shown that CNTs as scaffolds can improve neuronal signaling [369]. Due to their conductive nature, CNTs could be incorporated in bioscaffolds that require the propagation of electrical stimuli at sites, such as cardiomyocyte cells for synchronous

beating behavior. These CNT-containing materials due to their conductivity can also be utilized to control and regulate cell growth, migration and aid in cell directionality [370] for various applications and can be further explored for electrical stimulation procedures. The porous morphology of a scaffold also plays an important role in nutrient and waste exchange and can also promote cell infiltration through the scaffolds [371]. The CNT-coated foams can be tested for bone cell regeneration due to their porous and robust structural properties.

In summary, this study provides significant knowledge on important considerations when designing a bioscaffold. The two-step chemical vapor deposition (CVD) method used in our study can be employed to prepare hierarchical CNT-coatings on desired substrates which can supersede the toxicity risks associated with free CNTs.

Summary

While loose carbon nanotubes have previously been shown to modify cell growth in culture, the influence of vertically aligned CNT carpets covalently bonded to structurally stable carbon scaffolds on cells is unknown. In our previous studies, we had evaluated these scaffolds in multipotent progenitor cell lines and the nanoroughness of these structures was the major factor influencing cellular growth. However, in this study, we wanted to check the effect of the scaffolds on differentiated cells to assess if the effects of CNTs remain consistent through different cell types. To do that, we tested the scaffolds for two cell lines: glioblastoma and keratinocytes. We observed that the glioblastoma cells followed a biphasic growth pattern when the scaffolds were hydrophobic and the wettability of carbon scaffolds coated with CNTs was an important regulator of U87MG cellular growth. For the keratinocyte study, we first confirmed the prepared scaffolds are non-toxic and safe through elution test and cytotoxicity analysis. We were further able to understand preferential cell proliferation of HaCaTs on surfaces with different water wettability as well as different CNT lengths and found that shorter CNT-coatings may be better suited for bioscaffolds for keratinocyte cell growth. We also observed that the hydrophilic scaffolds are more effective at promoting the cell proliferation of keratinocytes than hydrophobic scaffolds. Furthermore, the scaffolds were capable to retain, attract as well as facilitate cell migration towards their surface for the effective wound healing process. The scaffolds

also provided cytoprotection against UVB and this could prove to be an important property when designing a wound healing graft. To further explore their immunoreactivity, we tested the scaffolds for B lymphocyte antibody secretion and found that long CNT scaffolds may promote antibody secretion. Lastly, for assessing their biocompatibility, we measured the cytokine levels of keratinocytes and B lymphocytes with carbon nanotubes and observed that the CNT-coated scaffolds relatively minimal changes in the cytokine production of B lymphocytes, however, they do promote some pro-inflammatory markers and it needs to be characterized further in detail before utilizing these scaffolds for potential implant-based applications. Overall, the results strongly support the future potential of these bio-mimetic scaffolds in tissue engineering, and the findings of this work give valuable insight for choosing substrate materials and designing future bioscaffolds for diverse tissue engineering approaches.

References

[1] S. Iijima, Helical microtubules of graphitic carbon, Nature. 354 (1991) 56.

[2] P. Couvreur, C. Vauthier, Nanotechnology: intelligent design to treat complex disease, Pharmaceutical Research. 23 (2006) 1417–1450.

[3] A.L. Alpatova, W. Shan, P. Babica, B.L. Upham, A.R. Rogensues, S.J. Masten, E. Drown, A.K. Mohanty, E.C. Alocilja, V.V. Tarabara, Single-walled carbon nanotubes dispersed in aqueous media via non-covalent functionalization: effect of dispersant on the stability, cytotoxicity, and epigenetic toxicity of nanotube suspensions, Water Research. 44 (2010) 505–520.

[4] J. Ezzati Nazhad Dolatabadi, Y. Omidi, D. Losic, Carbon Nanotubes as an Advanced Drug and Gene Delivery Nanosystem, Current Nanoscience. 7 (2011) 297–314. https://doi.org/10.2174/157341311795542444.

[5] S. Hampel, D. Kunze, D. Haase, K. Krämer, M. Rauschenbach, M. Ritschel, A. Leonhardt, J. Thomas, S. Oswald, V. Hoffmann, B. Büchner, Carbon nanotubes filled with a chemotherapeutic agent: a nanocarrier mediates inhibition of tumor cell growth, Nanomedicine. 3 (2008) 175–182. https://doi.org/10.2217/17435889.3.2.175.

[6] D. Pantarotto, C.D. Partidos, J. Hoebeke, F. Brown, E. Kramer, J.-P. Briand, S. Muller, M. Prato, A. Bianco, Immunization with Peptide-Functionalized Carbon Nanotubes Enhances Virus-Specific Neutralizing Antibody Responses, Chemistry & Biology. 10 (2003) 961–966. https://doi.org/10.1016/j.chembiol.2003.09.011.

[7] X. Chen, A. Kis, A. Zettl, C.R. Bertozzi, A cell nanoinjector based on carbon nanotubes, Proceedings of the National Academy of Sciences. 104 (2007) 8218–8222. https://doi.org/10.1073/pnas.0700567104.

[8] B. Pei, W. Wang, N. Dunne, X. Li, Applications of Carbon Nanotubes in Bone Tissue Regeneration and Engineering: Superiority, Concerns, Current Advancements, and Prospects, Nanomaterials (Basel). 9 (2019). https://doi.org/10.3390/nano9101501.

[9] Z. Xin, Z. Jianjun, O.-Y. Zhong-can, Strain energy and Young's modulus of single-wall carbon nanotubes calculated from electronic energy-band theory, Phys. Rev. B. 62 (2000) 13692–13696. https://doi.org/10.1103/PhysRevB.62.13692.

[10] J.-P. Salvetat, G. Briggs, J.-M. Bonard, R. Bacsa, A. Kulik, T. Stöckli, N. Burnham, L. Forró, Elastic and Shear Moduli of Single-Walled Carbon Nanotube Ropes, Phys. Rev. Lett. 82 (1999) 944–947. https://doi.org/10.1103/PhysRevLett.82.944.

[11] H. Dai, A. Javey, E. Pop, D. Mann, W. Kim, Y. Lu, ELECTRICAL TRANSPORT PROPERTIES AND FIELD EFFECT TRANSISTORS OF

CARBON NANOTUBES, NANO. 01 (2006) 1–13. https://doi.org/10.1142/S1793292006000070.
[12] S. Hong, S. Myung, A flexible approach to mobility, Nature Nanotechnology. 2 (2007) 207–208. https://doi.org/10.1038/nnano.2007.89.
[13] E. Joselevich, C.M. Lieber, Vectorial Growth of Metallic and Semiconducting Single-Wall Carbon Nanotubes, Nano Lett. 2 (2002) 1137–1141. https://doi.org/10.1021/nl025642u.
[14] Q. Liu, W. Ren, Z.-G. Chen, L. Yin, F. Li, H. Cong, H.-M. Cheng, Semiconducting properties of cup-stacked carbon nanotubes, Carbon. 47 (2009) 731–736. https://doi.org/10.1016/j.carbon.2008.11.005.
[15] L.-M. Peng, Z. Zhang, C. Qiu, Carbon nanotube digital electronics, Nature Electronics. 2 (2019) 499–505. https://doi.org/10.1038/s41928-019-0330-2.
[16] G. Hills, C. Lau, A. Wright, S. Fuller, M.D. Bishop, T. Srimani, P. Kanhaiya, R. Ho, A. Amer, Y. Stein, D. Murphy, Arvind, A. Chandrakasan, M.M. Shulaker, Modern microprocessor built from complementary carbon nanotube transistors, Nature. 572 (2019) 595–602. https://doi.org/10.1038/s41586-019-1493-8.
[17] A.A. Balandin, Thermal properties of graphene and nanostructured carbon materials, Nature Materials. 10 (2011) 569–581. https://doi.org/10.1038/nmat3064.
[18] P. Kim, L. Shi, A. Majumdar, P.L. McEuen, Thermal Transport Measurements of Individual Multiwalled Nanotubes, Phys. Rev. Lett. 87 (2001) 215502. https://doi.org/10.1103/PhysRevLett.87.215502.
[19] E. Pop, D. Mann, Q. Wang, K. Goodson, H. Dai, Thermal Conductance of an Individual Single-Wall Carbon Nanotube above Room Temperature, Nano Lett. 6 (2006) 96–100. https://doi.org/10.1021/nl052145f.
[20] A.M. Marconnet, M.A. Panzer, K.E. Goodson, Thermal conduction phenomena in carbon nanotubes and related nanostructured materials, Rev. Mod. Phys. 85 (2013) 1295–1326. https://doi.org/10.1103/RevModPhys.85.1295.
[21] B.T. Quinton, L. Elston, J.D. Scofield, S.M. Mukhopadhyay, Aligned Carbon Nanotube Arrays Bonded to Solid Graphite Substrates: Thermal Analysis for Future Device Cooling Applications, C. 4 (2018) 28.
[22] J. Li, C. Chen, S. Zhang, X. Wang, Surface functional groups and defects on carbon nanotubes affect adsorption–desorption hysteresis of metal cations and oxoanions in water, Environ. Sci.: Nano. 1 (2014) 488–495. https://doi.org/10.1039/C4EN00044G.
[23] L. Xu, J. Li, M. Zhang, Adsorption Characteristics of a Novel Carbon-Nanotube-Based Composite Adsorbent toward Organic Pollutants, Ind. Eng. Chem. Res. 54 (2015) 2379–2384. https://doi.org/10.1021/ie5041379.
[24] F. Su, C. Lu, Adsorption kinetics, thermodynamics and desorption of natural dissolved organic matter by multiwalled carbon nanotubes, Journal of Environmental Science and Health, Part A. 42 (2007) 1543–1552. https://doi.org/10.1080/10934520701513381.
[25] S.-G. Wang, X.-W. Liu, W.-X. Gong, W. Nie, B.-Y. Gao, Q.-Y. Yue, Adsorption of fulvic acids from aqueous solutions by carbon nanotubes, Journal of Chemical Technology & Biotechnology. 82 (2007) 698–704. https://doi.org/10.1002/jctb.1708.
[26] M. Sweetman, S. May, N. Mebberson, P. Pendleton, K. Vasilev, S. Plush, J. Hayball, Activated Carbon, Carbon Nanotubes and Graphene: Materials and

Composites for Advanced Water Purification, C. 3 (2017) 18. https://doi.org/10.3390/c3020018.
[27] N.P. Shetti, S.J. Malode, D.S. Nayak, C.V. Reddy, K.R. Reddy, Novel biosensor for efficient electrochemical detection of methdilazine using carbon nanotubes-modified electrodes, Mater. Res. Express. 6 (2019) 116308. https://doi.org/10.1088/2053-1591/ab4471.
[28] X. Xu, C. Liu, W. Zhang, X. Zou, Active Temperature Regulation and Teamed Boronate Affinity-Facilitated Microelectrode Module for Blood Glucose Detection in Physiological Environment, Sensors and Actuators B: Chemical. 324 (2020) 128720. https://doi.org/10.1016/j.snb.2020.128720.
[29] J. Bhardwaj, S. Devarakonda, S. Kumar, J. Jang, Development of a paper-based electrochemical immunosensor using an antibody-single walled carbon nanotubes bio-conjugate modified electrode for label-free detection of foodborne pathogens, Sensors and Actuators B: Chemical. 253 (2017) 115–123. https://doi.org/10.1016/j.snb.2017.06.108.
[30] H. Vijwani, M.N. Nadagouda, V. Namboodiri, S.M. Mukhopadhyay, Hierarchical hybrid carbon nano-structures as robust and reusable adsorbents: Kinetic studies with model dye compound, Chemical Engineering Journal. 268 (2015) 197–207.
[31] A.K. Karumuri, D.P. Oswal, H.A. Hostetler, S.M. Mukhopadhyay, Silver nanoparticles attached to porous carbon substrates: robust materials for chemical-free water disinfection, Materials Letters. 109 (2013) 83–87.
[32] W. Wang, Hierarchical Hybrid Materials from Flexible Fabric Substrates, Wright State University, 2020. https://etd.ohiolink.edu/apexprod/rws_olink/r/1501/10?clear=10&p10_accession_num=wright1590083299625317 (accessed January 2, 2021).
[33] J.S. Says, Applications of Carbon Nanotubes, AZoNano.Com. (2018). https://www.azonano.com/article.aspx?ArticleID=4842 (accessed January 2, 2021).
[34] O. Gohardani, M.C. Elola, C. Elizetxea, Potential and prospective implementation of carbon nanotubes on next generation aircraft and space vehicles: A review of current and expected applications in aerospace sciences, Progress in Aerospace Sciences. 70 (2014) 42–68. https://doi.org/10.1016/j.paerosci.2014.05.002.
[35] M.D. Yadav, K. Dasgupta, A.W. Patwardhan, J.B. Joshi, High Performance Fibers from Carbon Nanotubes: Synthesis, Characterization, and Applications in Composites—A Review, Ind. Eng. Chem. Res. 56 (2017) 12407–12437. https://doi.org/10.1021/acs.iecr.7b02269.
[36] IBM builds first IC around a single carbon nanotube, (n.d.). https://phys.org/news/2006-03-ibm-ic-carbon-nanotube.html (accessed January 2, 2021).
[37] J. Tang, Q. Cao, G. Tulevski, K.A. Jenkins, L. Nela, D.B. Farmer, S.-J. Han, Flexible CMOS integrated circuits based on carbon nanotubes with sub-10 ns stage delays, Nature Electronics. 1 (2018) 191–196. https://doi.org/10.1038/s41928-018-0038-8.
[38] A. Graf, C. Murawski, Y. Zakharko, J. Zaumseil, M.C. Gather, Infrared Organic Light-Emitting Diodes with Carbon Nanotube Emitters, Advanced Materials. 30 (2018) 1706711. https://doi.org/10.1002/adma.201706711.

[39] D.S. Hecht, L. Hu, G. Irvin, Emerging Transparent Electrodes Based on Thin Films of Carbon Nanotubes, Graphene, and Metallic Nanostructures, Advanced Materials. 23 (2011) 1482–1513. https://doi.org/10.1002/adma.201003188.
[40] J. Han, S. Wang, S. Zhu, C. Huang, Y. Yue, C. Mei, X. Xu, C. Xia, Electrospun Core–Shell Nanofibrous Membranes with Nanocellulose-Stabilized Carbon Nanotubes for Use as High-Performance Flexible Supercapacitor Electrodes with Enhanced Water Resistance, Thermal Stability, and Mechanical Toughness, ACS Appl. Mater. Interfaces. 11 (2019) 44624–44635. https://doi.org/10.1021/acsami.9b16458.
[41] R.L.V. Wal, T.M. Ticich, V.E. Curtis, Substrate-support interactions in metal-catalyzed carbon nanofiber growth, CARBON. 39 (2001) 2277–2289. https://doi.org/10.1016/S0008-6223(01)00047-1.
[42] A. Cao, P.M. Ajayan, G. Ramanath, R. Baskaran, K. Turner, Silicon oxide thickness-dependent growth of carbon nanotubes, Appl. Phys. Lett. 84 (2003) 109–111. https://doi.org/10.1063/1.1636826.
[43] M. Hu, P. Keblinski, J.-S. Wang, N. Raravikar, Interfacial thermal conductance between silicon and a vertical carbon nanotube, Journal of Applied Physics. 104 (2008) 083503. https://doi.org/10.1063/1.3000441.
[44] T. Guo, P. Nikolaev, A. Thess, D.T. Colbert, R.E. Smalley, Catalytic growth of single-walled manotubes by laser vaporization, Chemical Physics Letters. 243 (1995) 49–54. https://doi.org/10.1016/0009-2614(95)00825-O.
[45] M. Kumar, Y. Ando, Chemical Vapor Deposition of Carbon Nanotubes: A Review on Growth Mechanism and Mass Production, Journal of Nanoscience and Nanotechnology. 10 (2010) 3739–3758. https://doi.org/10.1166/jnn.2010.2939.
[46] R.V. Pulikollu, S.M. Mukhopadhyay, Nanoscale coatings for control of interfacial bonds and nanotube growth, Applied Surface Science. 253 (2007) 7342–7352.
[47] W. Qian, T. Liu, F. Wei, Z. Wang, G. Luo, H. Yu, Z. Li, The evaluation of the gross defects of carbon nanotubes in a continuous CVD process, Carbon. 41 (2003) 2613–2617. https://doi.org/10.1016/S0008-6223(03)00341-5.
[48] T. Young, III. An essay on the cohesion of fluids, Philosophical Transactions of the Royal Society of London. 95 (1805) 65–87. https://doi.org/10.1098/rstl.1805.0005.
[49] R.N. Wenzel, RESISTANCE OF SOLID SURFACES TO WETTING BY WATER, Ind. Eng. Chem. 28 (1936) 988–994. https://doi.org/10.1021/ie50320a024.
[50] A.B.D. Cassie, S. Baxter, Wettability of porous surfaces, Trans. Faraday Soc. 40 (1944) 546–551. https://doi.org/10.1039/TF9444000546.
[51] L. He, A. Karumuri, S.M. Mukhopadhyay, Wettability tailoring of nanotube carpets: morphology-chemistry synergy for hydrophobic–hydrophilic cycling, RSC Advances. 7 (2017) 25265–25275.
[52] Y. Zhang, Y. Bai, B. Yan, Functionalized carbon nanotubes for potential medicinal applications, Drug Discovery Today. 15 (2010) 428–435.
[53] R. Shvartzman-Cohen, Y. Levi-Kalisman, E. Nativ-Roth, R. Yerushalmi-Rozen, Generic approach for dispersing single-walled carbon nanotubes: the strength of a weak interaction, Langmuir. 20 (2004) 6085–6088.
[54] W. Yang, P. Thordarson, J.J. Gooding, S.P. Ringer, F. Braet, Carbon nanotubes for biological and biomedical applications, Nanotechnology. 18 (2007) 412001.

[55] S.M. Mukhopadhyay, A. Karumuri, I.T. Barney, Hierarchical nanostructures by nanotube grafting on porous cellular surfaces, Journal of Physics D: Applied Physics. 42 (2009) 195503.
[56] S.M. Mukhopadhyay, A.K. Karumuri, Nanotube attachment for prevention of interfacial delamination, Journal of Physics D: Applied Physics. 43 (2010) 365301.
[57] B.T. Quinton, Aligned Carbon Nanotube Carpets on Carbon Substrates for High Power Electronic Applications, Mechanical and Thermal Systems Branch, Power and Control Division Wright-Patterson Air Force Base United States, 2016.
[58] H. Vijwani, HIGHLY ACTIVE POROUS CATALYSTS FABRICATED BY ATTACHMENT OF PALLADIUM NANOPARTICLES ON HIERARCHICAL CARBON STRUCTURES, Wright State University, 2011. https://etd.ohiolink.edu/apexprod/rws_olink/r/1501/10?p10_etd_subid=86127&clear=10 (accessed March 31, 2021).
[59] I.T. Barney, Fabrication and testing of hierarchical carbon nanostructures for multifunctional applications, (2012).
[60] A.K. Karumuri, D.P. Oswal, H.A. Hostetler, S.M. Mukhopadhyay, Silver nanoparticles supported on carbon nanotube carpets: Influence of surface functionalization, Nanotechnology. 27 (2016) 145603.
[61] H. Vijwani, Hierarchical Porous Structures with Aligned Carbon Nanotubes as Efficient Adsorbents and Metal-Catalyst Supports, (2015).
[62] L. He, A thesis submitted in partial fulfillment of the requirements for the degree of Master of Science in Engineering, (n.d.) 102.
[63] K. Kiaei, Hierarchical carbon structures with vertically- aligned nanotube carpets for oil-water separation under different conditions, (n.d.) 97.
[64] I. Barney, S. Ganguli, A. Roy, S.M. Mukhopadhyay, Improved thermal response in encapsulated phase change materials by nanotube attachment on encapsulating solid, Journal of Nanotechnology in Engineering and Medicine. 3 (2012) 031005.
[65] E. Maurer, S. Hussain, S.M. Mukhopadhyay, Cell growth in a porous microcellular structure: influence of surface modification and nanostructures, Nanoscience and Nanotechnology Letters. 3 (2011) 110–113.
[66] A. Patel, S. Mukundan, W. Wang, A. Karumuri, V. Sant, S.M. Mukhopadhyay, S. Sant, Carbon-based hierarchical scaffolds for myoblast differentiation: Synergy between nano-functionalization and alignment, Acta Biomaterialia. 32 (2016) 77–88.
[67] S.D. Parikh, S. Dave, L. Huang, W. Wang, S.M. Mukhopadhyay, D.A. Mayes, Multi-walled carbon nanotube carpets as scaffolds for U87MG glioblastoma multiforme cell growth, Materials Science and Engineering: C. 108 (2020) 110345. https://doi.org/10.1016/j.msec.2019.110345.
[68] A.K. Karumuri, A.A. Maleszewski, D.P. Oswal, H.A. Hostetler, S.M. Mukhopadhyay, Fabrication and characterization of antibacterial nanoparticles supported on hierarchical hybrid substrates, Journal of Nanoparticle Research. 16 (2014) 2346.
[69] C. Itthichaisri, M. Wiedmann-Al-Ahmad, U. Huebner, A. Al-Ahmad, R. Schoen, R. Schmelzeisen, N.-C. Gellrich, Comparative in vitro study of the proliferation and growth of human osteoblast-like cells on various biomaterials, Journal of Biomedical Materials Research Part A: An Official Journal of The Society for

Biomaterials, The Japanese Society for Biomaterials, and The Australian Society for Biomaterials and the Korean Society for Biomaterials. 82 (2007) 777–787.
[70] T.P. Kunzler, T. Drobek, M. Schuler, N.D. Spencer, Systematic study of osteoblast and fibroblast response to roughness by means of surface-morphology gradients, Biomaterials. 28 (2007) 2175–2182.
[71] C.M. Sayes, F. Liang, J.L. Hudson, J. Mendez, W. Guo, J.M. Beach, V.C. Moore, C.D. Doyle, J.L. West, W.E. Billups, K.D. Ausman, V.L. Colvin, Functionalization density dependence of single-walled carbon nanotubes cytotoxicity in vitro, Toxicology Letters. 161 (2006) 135–142. https://doi.org/10.1016/j.toxlet.2005.08.011.
[72] A.R. Murray, E. Kisin, S.S. Leonard, S.H. Young, C. Kommineni, V.E. Kagan, V. Castranova, A.A. Shvedova, Oxidative stress and inflammatory response in dermal toxicity of single-walled carbon nanotubes, Toxicology. 257 (2009) 161–171. https://doi.org/10.1016/j.tox.2008.12.023.
[73] S. Koyama, Y.A. Kim, T. Hayashi, K. Takeuchi, C. Fujii, N. Kuroiwa, H. Koyama, T. Tsukahara, M. Endo, In vivo immunological toxicity in mice of carbon nanotubes with impurities, Carbon. 47 (2009) 1365–1372. https://doi.org/10.1016/j.carbon.2009.01.028.
[74] R.F. Hamilton, C. Xiang, M. Li, I. Ka, F. Yang, D. Ma, D.W. Porter, N. Wu, A. Holian, Purification and sidewall functionalization of multiwalled carbon nanotubes and resulting bioactivity in two macrophage models, Inhalation Toxicology. 25 (2013) 199–210. https://doi.org/10.3109/08958378.2013.775197.
[75] P.P.D.K. Wulan, S.H. Ulwani, H. Wulandari, W.W. Purwanto, K. Mulia, The effect of hydrochloric acid addition to increase carbon nanotubes dispersibility as drug delivery system by covalent functionalization, IOP Conf. Ser.: Mater. Sci. Eng. 316 (2018) 012013. https://doi.org/10.1088/1757-899X/316/1/012013.
[76] V. Datsyuk, M. Kalyva, K. Papagelis, J. Parthenios, D. Tasis, A. Siokou, I. Kallitsis, C. Galiotis, Chemical oxidation of multiwalled carbon nanotubes, Carbon. 46 (2008) 833–840. https://doi.org/10.1016/j.carbon.2008.02.012.
[77] N. Saifuddin, A.Z. Raziah, A.R. Junizah, Carbon Nanotubes: A Review on Structure and Their Interaction with Proteins, Journal of Chemistry. 2013 (2013) 1–18. https://doi.org/10.1155/2013/676815.
[78] A.K. Karumuri, L. He, S.M. Mukhopadhyay, Tuning the surface wettability of carbon nanotube carpets in multiscale hierarchical solids, Applied Surface Science. 327 (2015) 122–130.
[79] R.V. Pulikollu, S.R. Higgins, S.M. Mukhopadhyay, Model nucleation and growth studies of nanoscale oxide coatings suitable for modification of microcellular and nano-structured carbon, Surface and Coatings Technology. 203 (2008) 65–72.
[80] S.M. Mukhopadhyay, P. Joshi, S. Datta, J. Macdaniel, Plasma assisted surface coating of porous solids, Applied Surface Science. 201 (2002) 219–226.
[81] S.M. Mukhopadhyay, P. Joshi, R. Pulikollu, Thin films for coating nanomaterials, Tsinghua Science and Technology. 10 (2005) 709–717.
[82] H. Kim, W. Sigmund, Iron particles in carbon nanotubes, Carbon. 43 (2005) 1743–1748. https://doi.org/10.1016/j.carbon.2005.02.019.
[83] K.C. Jha, Z. Liu, H. Vijwani, M. Nadagouda, S.M. Mukhopadhyay, M. Tsige, Carbon Nanotube Based Groundwater Remediation: The Case of Trichloroethylene, Molecules. 21 (2016) 953.

[84] J.-W. Kim, E.I. Galanzha, E.V. Shashkov, H.-M. Moon, V.P. Zharov, Golden carbon nanotubes as multimodal photoacoustic and photothermal high-contrast molecular agents, Nature Nanotechnology. 4 (2009) 688.
[85] S. Xu, R. Sheng, Y. Cao, J. Yan, Reversibly switching water droplets wettability on hierarchical structured Cu 2 S mesh for efficient oil/water separation, Scientific Reports. 9 (2019) 12486. https://doi.org/10.1038/s41598-019-48952-1.
[86] S.B. Kulkarni, U.M. Patil, R.R. Salunkhe, S.S. Joshi, C.D. Lokhande, Temperature impact on morphological evolution of ZnO and its consequent effect on physico-chemical properties, Journal of Alloys and Compounds. 509 (2011) 3486–3492. https://doi.org/10.1016/j.jallcom.2010.12.036.
[87] Y.-N. Zhou, J.-J. Li, Q. Zhang, Z.-H. Luo, Light-Responsive Smart Surface with Controllable Wettability and Excellent Stability, Langmuir. 30 (2014) 12236–12242. https://doi.org/10.1021/la501907w.
[88] A. Khademhosseini, J.P. Vacanti, R. Langer, Progress in tissue engineering, Sci Am. 300 (2009) 64–71. https://doi.org/10.1038/scientificamerican0509-64.
[89] Biomaterials Market Size, Share, Analysis | Industry Report, 2027, (n.d.). https://www.grandviewresearch.com/industry-analysis/biomaterials-industry (accessed January 3, 2021).
[90] I.V. Yannas, E. Lee, D.P. Orgill, E.M. Skrabut, G.F. Murphy, Synthesis and characterization of a model extracellular matrix that induces partial regeneration of adult mammalian skin, PNAS. 86 (1989) 933–937. https://doi.org/10.1073/pnas.86.3.933.
[91] R. Schimming, R. Schmelzeisen, Tissue-engineered bone for maxillary sinus augmentation, Journal of Oral and Maxillofacial Surgery. 62 (2004) 724–729. https://doi.org/10.1016/j.joms.2004.01.009.
[92] A. Atala, S.B. Bauer, S. Soker, J.J. Yoo, A.B. Retik, Tissue-engineered autologous bladders for patients needing cystoplasty, The Lancet. 367 (2006) 1241–1246. https://doi.org/10.1016/S0140-6736(06)68438-9.
[93] P. Macchiarini, P. Jungebluth, T. Go, M.A. Asnaghi, L.E. Rees, T.A. Cogan, A. Dodson, J. Martorell, S. Bellini, P.P. Parnigotto, S.C. Dickinson, A.P. Hollander, S. Mantero, M.T. Conconi, M.A. Birchall, Clinical transplantation of a tissue-engineered airway, The Lancet. 372 (2008) 2023–2030. https://doi.org/10.1016/S0140-6736(08)61598-6.
[94] T.B.F. Woodfield, J. Malda, J. de Wijn, F. Péters, J. Riesle, C.A. van Blitterswijk, Design of porous scaffolds for cartilage tissue engineering using a three-dimensional fiber-deposition technique, Biomaterials. 25 (2004) 4149–4161. https://doi.org/10.1016/j.biomaterials.2003.10.056.
[95] B.P. Chan, K.W. Leong, Scaffolding in tissue engineering: general approaches and tissue-specific considerations, Eur Spine J. 17 (2008) 467–479. https://doi.org/10.1007/s00586-008-0745-3.
[96] F.J. O'Brien, Biomaterials & scaffolds for tissue engineering, Materials Today. 14 (2011) 88–95. https://doi.org/10.1016/S1369-7021(11)70058-X.
[97] F. Rosso, G. Marino, A. Giordano, M. Barbarisi, D. Parmeggiani, A. Barbarisi, Smart materials as scaffolds for tissue engineering, Journal of Cellular Physiology. 203 (2005) 465–470. https://doi.org/10.1002/jcp.20270.
[98] A. Gilpin, Y. Yang, Decellularization Strategies for Regenerative Medicine: From Processing Techniques to Applications, BioMed Research International. 2017 (2017) e9831534. https://doi.org/10.1155/2017/9831534.

[99] M. Setayeshmehr, E. Esfandiari, M. Rafieinia, B. Hashemibeni, A. Taheri-Kafrani, A. Samadikuchaksaraei, D.L. Kaplan, L. Moroni, M.T. Joghataei, Hybrid and Composite Scaffolds Based on Extracellular Matrices for Cartilage Tissue Engineering, Tissue Engineering Part B: Reviews. 25 (2019) 202–224. https://doi.org/10.1089/ten.teb.2018.0245.
[100] P. KC, Y. Hong, G. Zhang, Cardiac tissue-derived extracellular matrix scaffolds for myocardial repair: advantages and challenges, Regen Biomater. 6 (2019) 185–199. https://doi.org/10.1093/rb/rbz017.
[101] D. Lam, H.A. Enright, J. Cadena, S.K.G. Peters, A.P. Sales, J.J. Osburn, D.A. Soscia, K.S. Kulp, E.K. Wheeler, N.O. Fischer, Tissue-specific extracellular matrix accelerates the formation of neural networks and communities in a neuron-glia co-culture on a multi-electrode array, Scientific Reports. 9 (2019) 4159. https://doi.org/10.1038/s41598-019-40128-1.
[102] Y.S. Kim, M. Majid, A.J. Melchiorri, A.G. Mikos, Applications of decellularized extracellular matrix in bone and cartilage tissue engineering, Bioeng Transl Med. 4 (2018) 83–95. https://doi.org/10.1002/btm2.10110.
[103] M.C. Cramer, S.F. Badylak, Extracellular Matrix-Based Biomaterials and Their Influence Upon Cell Behavior, Ann Biomed Eng. 48 (2020) 2132–2153. https://doi.org/10.1007/s10439-019-02408-9.
[104] L. Lu, S.J. Peter, M.D. Lyman, H.L. Lai, S.M. Leite, J.A. Tamada, S. Uyama, J.P. Vacanti, R. Langer, A.G. Mikos, In vitro and in vivo degradation of porous poly(DL-lactic-co-glycolic acid) foams, Biomaterials. 21 (2000) 1837–1845. https://doi.org/10.1016/s0142-9612(00)00047-8.
[105] F.N. Alaribe, S.L. Manoto, S.C.K.M. Motaung, Scaffolds from biomaterials: advantages and limitations in bone and tissue engineering, Biologia. 71 (2016) 353–366. https://doi.org/10.1515/biolog-2016-0056.
[106] H. Liu, E.B. Slamovich, T.J. Webster, Less harmful acidic degradation of poly(lactic-co-glycolic acid) bone tissue engineering scaffolds through titania nanoparticle addition, Int J Nanomedicine. 1 (2006) 541–545.
[107] J.M. Anderson, A. Rodriguez, D.T. Chang, Foreign body reaction to biomaterials, Seminars in Immunology. 20 (2008) 86–100. https://doi.org/10.1016/j.smim.2007.11.004.
[108] P. Cravedi, S. Farouk, A. Angeletti, L. Edgar, R. Tamburrini, J. Dusuit, L. Perin, G. Orlando, REGENERATIVE IMMUNOLOGY: THE IMMUNOLOGICAL REACTION TO BIOMATERIALS, Transpl Int. 30 (2017) 1199–1208. https://doi.org/10.1111/tri.13068.
[109] S. Kalita, J. Finley, S. Bose, H. Hosick, A. Bandyopadhyay, Development of Porous Polymer-Ceramic Composites as Bone Grafts, MRS Online Proceedings Library (OPL). 726 (2002). https://doi.org/10.1557/PROC-726-Q5.8.
[110] I.O. Smith, X.H. Liu, L.A. Smith, P.X. Ma, Nano-structured polymer scaffolds for tissue engineering and regenerative medicine, Wiley Interdiscip Rev Nanomed Nanobiotechnol. 1 (2009) 226–236. https://doi.org/10.1002/wnan.26.
[111] H. Yi, F. Ur Rehman, C. Zhao, B. Liu, N. He, Recent advances in nano scaffolds for bone repair, Bone Res. 4 (2016) 16050. https://doi.org/10.1038/boneres.2016.50.
[112] G. Balasundaram, D.M. Storey, T.J. Webster, Novel nano-rough polymers for cartilage tissue engineering, Int J Nanomedicine. 9 (2014) 1845–1853. https://doi.org/10.2147/IJN.S55865.

[113] J.V. Veetil, K. Ye, Tailored Carbon Nanotubes for Tissue Engineering Applications, Biotechnol Prog. 25 (2009) 709–721. https://doi.org/10.1002/bp.165.
[114] M. Yang, M. Zhang, Biodegradation of Carbon Nanotubes by Macrophages, Front. Mater. 6 (2019). https://doi.org/10.3389/fmats.2019.00225.
[115] C.H. Villa, T. Dao, I. Ahearn, N. Fehrenbacher, E. Casey, D.A. Rey, T. Korontsvit, V. Zakhaleva, C.A. Batt, M.R. Philips, D.A. Scheinberg, Single-walled carbon nanotubes deliver peptide antigen into dendritic cells and enhance IgG responses to tumor-associated antigens, ACS Nano. 5 (2011) 5300–5311. https://doi.org/10.1021/nn200182x.
[116] G.M. Mutlu, G.R.S. Budinger, A.A. Green, D. Urich, S. Soberanes, S.E. Chiarella, G.F. Alheid, D.R. McCrimmon, I. Szleifer, M.C. Hersam, Biocompatible Nanoscale Dispersion of Single Walled Carbon Nanotubes Minimizes in vivo Pulmonary Toxicity, Nano Lett. 10 (2010) 1664–1670. https://doi.org/10.1021/nl9042483.
[117] K. Kostarelos, A. Bianco, M. Prato, Promises, facts and challenges for carbon nanotubes in imaging and therapeutics, Nat Nanotechnol. 4 (2009) 627–633. https://doi.org/10.1038/nnano.2009.241.
[118] K. Kostarelos, L. Lacerda, G. Pastorin, W. Wu, S. Wieckowski, J. Luangsivilay, S. Godefroy, D. Pantarotto, J.-P. Briand, S. Muller, M. Prato, A. Bianco, Cellular uptake of functionalized carbon nanotubes is independent of functional group and cell type, Nature Nanotech. 2 (2007) 108–113. https://doi.org/10.1038/nnano.2006.209.
[119] D. Pantarotto, R. Singh, D. McCarthy, M. Erhardt, J. Briand, M. Prato, K. Kostarelos, A. Bianco, Functionalized carbon nanotubes for plasmid DNA gene delivery, Angewandte Chemie International Edition. 43 (2004) 5242–5246.
[120] A. Bianco, K. Kostarelos, C.D. Partidos, M. Prato, Biomedical applications of functionalised carbon nanotubes, Chemical Communications. (2005) 571–577.
[121] X. Wang, Q. Li, J. Xie, Z. Jin, J. Wang, Y. Li, K. Jiang, S. Fan, Fabrication of ultralong and electrically uniform single-walled carbon nanotubes on clean substrates, Nano Letters. 9 (2009) 3137–3141.
[122] H. Mao, N. Kawazoe, G. Chen, Uptake and intracellular distribution of collagen-functionalized single-walled carbon nanotubes, Biomaterials. 34 (2013) 2472–2479.
[123] T. Sun, G. Wang, H. Liu, L. Feng, L. Jiang, D. Zhu, Control over the wettability of an aligned carbon nanotube film, Journal of the American Chemical Society. 125 (2003) 14996–14997.
[124] H. Vijwani, S.M. Mukhopadhyay, Palladium nanoparticles on hierarchical carbon surfaces: a new architecture for robust nano-catalysts, Applied Surface Science. 263 (2012) 712–721.
[125] E.I. Maurer, K.K. Comfort, S.M. Hussain, J.J. Schlager, S.M. Mukhopadhyay, Novel platform development using an assembly of carbon nanotube, nanogold and immobilized RNA capture element towards rapid, selective sensing of bacteria, Sensors. 12 (2012) 8135–8144.
[126] M. Zhang, Y. Deng, M. Yang, H. Nakajima, M. Yudasaka, S. Iijima, T. Okazaki, A Simple Method for Removal of Carbon Nanotubes from Wastewater Using Hypochlorite, Scientific Reports. 9 (2019) 1284. https://doi.org/10.1038/s41598-018-38307-7.

[127] H. Cui, Y. Yu, X. Li, Z. Sun, J. Ruan, Z. Wu, J. Qian, J. Yin, Direct 3D printing of a tough hydrogel incorporated with carbon nanotubes for bone regeneration, J. Mater. Chem. B. 7 (2019) 7207–7217. https://doi.org/10.1039/C9TB01494B.
[128] G. Cirillo, M. Curcio, U.G. Spizzirri, O. Vittorio, P. Tucci, N. Picci, F. Iemma, S. Hampel, F.P. Nicoletta, Carbon nanotubes hybrid hydrogels for electrically tunable release of Curcumin, European Polymer Journal. 90 (2017) 1–12.
[129] S. Taghavi, A.H. Nia, K. Abnous, M. Ramezani, Polyethylenimine-functionalized carbon nanotubes tagged with AS1411 aptamer for combination gene and drug delivery into human gastric cancer cells, International Journal of Pharmaceutics. 516 (2017) 301–312. https://doi.org/10.1016/j.ijpharm.2016.11.027.
[130] T. Dvir, B.P. Timko, D.S. Kohane, R. Langer, Nanotechnological strategies for engineering complex tissues, Nature Nanotechnology. 6 (2011) 13.
[131] E. Hirata, M. Uo, Y. Nodasaka, H. Takita, N. Ushijima, T. Akasaka, F. Watari, A. Yokoyama, 3D collagen scaffolds coated with multiwalled carbon nanotubes: initial cell attachment to internal surface, Journal of Biomedical Materials Research Part B: Applied Biomaterials. 93 (2010) 544–550.
[132] M.P. Mattson, R.C. Haddon, A.M. Rao, Molecular functionalization of carbon nanotubes and use as substrates for neuronal growth, J Mol Neurosci. 14 (2000) 175–182. https://doi.org/10.1385/JMN:14:3:175.
[133] E. Lizundia, J.R. Sarasua, F. D'Angelo, A. Orlacchio, S. Martino, J.M. Kenny, I. Armentano, Biocompatible Poly (L-lactide)/MWCNT Nanocomposites: Morphological Characterization, Electrical Properties, and Stem Cell Interaction, Macromolecular Bioscience. 12 (2012) 870–881.
[134] J. Ren, Q. Xu, X. Chen, W. Li, K. Guo, Y. Zhao, Q. Wang, Z. Zhang, H. Peng, Y.-G. Li, Superaligned Carbon Nanotubes Guide Oriented Cell Growth and Promote Electrophysiological Homogeneity for Synthetic Cardiac Tissues, Advanced Materials. 29 (2017) 1702713. https://doi.org/10.1002/adma.201702713.
[135] N.W. Shi Kam, M. O'Connell, J.A. Wisdom, H. Dai, Carbon nanotubes as multifunctional biological transporters and near-infrared agents for selective cancer cell destruction, Proceedings of the National Academy of Sciences. 102 (2005) 11600–11605. https://doi.org/10.1073/pnas.0502680102.
[136] G. Lalwani, M. D'agati, A. Gopalan, S.C. Patel, Y. Talukdar, B. Sitharaman, Three-dimensional carbon nanotube scaffolds for long-term maintenance and expansion of human mesenchymal stem cells, Journal of Biomedical Materials Research Part A. 105 (2017) 1927–1939.
[137] T. Akasaka, A. Yokoyama, M. Matsuoka, T. Hashimoto, F. Watari, Thin films of single-walled carbon nanotubes promote human osteoblastic cells (Saos-2) proliferation in low serum concentrations, Materials Science and Engineering: C. 30 (2010) 391–399.
[138] A. Abarrategi, M.C. Gutierrez, C. Moreno-Vicente, M.J. Hortigüela, V. Ramos, J.L. Lopez-Lacomba, M.L. Ferrer, F. del Monte, Multiwall carbon nanotube scaffolds for tissue engineering purposes, Biomaterials. 29 (2008) 94–102.
[139] E. Hirata, M. Uo, H. Takita, T. Akasaka, F. Watari, A. Yokoyama, Multiwalled carbon nanotube-coating of 3D collagen scaffolds for bone tissue engineering, Carbon. 49 (2011) 3284–3291.

[140] S. Baoukina, L. Monticelli, D.P. Tieleman, Interaction of Pristine and Functionalized Carbon Nanotubes with Lipid Membranes, J. Phys. Chem. B. 117 (2013) 12113–12123. https://doi.org/10.1021/jp405732k.
[141] A.A. Skandani, R. Zeineldin, M. Al-Haik, Effect of Chirality and Length on the Penetrability of Single-Walled Carbon Nanotubes into Lipid Bilayer Cell Membranes, Langmuir. 28 (2012) 7872–7879. https://doi.org/10.1021/la3011162.
[142] P.M. Costa, M. Bourgognon, J.T.-W. Wang, K.T. Al-Jamal, Functionalised carbon nanotubes: From intracellular uptake and cell-related toxicity to systemic brain delivery, Journal of Controlled Release. 241 (2016) 200–219. https://doi.org/10.1016/j.jconrel.2016.09.033.
[143] H. Nagai, Y. Okazaki, S.H. Chew, N. Misawa, Y. Yamashita, S. Akatsuka, T. Ishihara, K. Yamashita, Y. Yoshikawa, H. Yasui, L. Jiang, H. Ohara, T. Takahashi, G. Ichihara, K. Kostarelos, Y. Miyata, H. Shinohara, S. Toyokuni, Diameter and rigidity of multiwalled carbon nanotubes are critical factors in mesothelial injury and carcinogenesis, Proceedings of the National Academy of Sciences. 108 (2011) E1330–E1338. https://doi.org/10.1073/pnas.1110013108.
[144] H. Wang, J. Wang, X. Deng, H. Sun, Z. Shi, Z. Gu, Y. Liu, Y. Zhaoc, Biodistribution of Carbon Single-Wall Carbon Nanotubes in Mice, J. Nanosci. Nanotech. 4 (2004) 1019–1024. https://doi.org/10.1166/jnn.2004.146.
[145] V.E. Kagan, N.V. Konduru, W. Feng, B.L. Allen, J. Conroy, Y. Volkov, I.I. Vlasova, N.A. Belikova, N. Yanamala, A. Kapralov, Y.Y. Tyurina, J. Shi, E.R. Kisin, A.R. Murray, J. Franks, D. Stolz, P. Gou, J. Klein-Seetharaman, B. Fadeel, A. Star, A.A. Shvedova, Carbon nanotubes degraded by neutrophil myeloperoxidase induce less pulmonary inflammation, Nat Nanotechnol. 5 (2010) 354–359. https://doi.org/10.1038/nnano.2010.44.
[146] F.T. Andón, A.A. Kapralov, N. Yanamala, W. Feng, A. Baygan, B.J. Chambers, K. Hultenby, F. Ye, M.S. Toprak, B.D. Brandner, A. Fornara, J. Klein-Seetharaman, G.P. Kotchey, A. Star, A.A. Shvedova, B. Fadeel, V.E. Kagan, Biodegradation of Single-Walled Carbon Nanotubes by Eosinophil Peroxidase, Small. 9 (2013) 2721–2729. https://doi.org/10.1002/smll.201202508.
[147] N. Lu, J. Li, R. Tian, Y.-Y. Peng, Binding of Human Serum Albumin to Single-Walled Carbon Nanotubes Activated Neutrophils to Increase Production of Hypochlorous Acid, the Oxidant Capable of Degrading Nanotubes, Chem. Res. Toxicol. 27 (2014) 1070–1077. https://doi.org/10.1021/tx5001317.
[148] A. Nunes, C. Bussy, L. Gherardini, M. Meneghetti, M.A. Herrero, A. Bianco, M. Prato, T. Pizzorusso, K.T. Al-Jamal, K. Kostarelos, In vivo degradation of functionalized carbon nanotubes after stereotactic administration in the brain cortex, Nanomedicine. 7 (2012) 1485–1494. https://doi.org/10.2217/nnm.12.33.
[149] A.A. Shvedova, A.A. Kapralov, W.H. Feng, E.R. Kisin, A.R. Murray, R.R. Mercer, C.M.S. Croix, M.A. Lang, S.C. Watkins, N.V. Konduru, B.L. Allen, J. Conroy, G.P. Kotchey, B.M. Mohamed, A.D. Meade, Y. Volkov, A. Star, B. Fadeel, V.E. Kagan, Impaired Clearance and Enhanced Pulmonary Inflammatory/Fibrotic Response to Carbon Nanotubes in Myeloperoxidase-Deficient Mice, PLOS ONE. 7 (2012) e30923. https://doi.org/10.1371/journal.pone.0030923.

[150] V.E. Kagan, A.A. Kapralov, C.M. St. Croix, S.C. Watkins, E.R. Kisin, G.P. Kotchey, K. Balasubramanian, I.I. Vlasova, J. Yu, K. Kim, W. Seo, R.K. Mallampalli, A. Star, A.A. Shvedova, Lung Macrophages “Digest” Carbon Nanotubes Using a Superoxide/Peroxynitrite Oxidative Pathway, ACS Nano. 8 (2014) 5610–5621. https://doi.org/10.1021/nn406484b.
[151] M. Yang, M. Zhang, H. Nakajima, M. Yudasaka, S. Iijima, T. Okazaki, Time-dependent degradation of carbon nanotubes correlates with decreased reactive oxygen species generation in macrophages , International Journal of Nanomedicine. 14 (2019) 2797–2807. https://doi.org/10.2147/IJN.S199187.
[152] J. Hou, B. Wan, Y. Yang, X.-M. Ren, L.-H. Guo, J.-F. Liu, Biodegradation of Single-Walled Carbon Nanotubes in Macrophages through Respiratory Burst Modulation, International Journal of Molecular Sciences. 17 (2016) 409. https://doi.org/10.3390/ijms17030409.
[153] C. Lin, B. Fugetsu, Y. Su, F. Watari, Studies on toxicity of multi-walled carbon nanotubes on Arabidopsis T87 suspension cells, Journal of Hazardous Materials. 170 (2009) 578–583.
[154] A. Simon-Deckers, B. Gouget, M. Mayne-L’Hermite, N. Herlin-Boime, C. Reynaud, M. Carriere, In vitro investigation of oxide nanoparticle and carbon nanotube toxicity and intracellular accumulation in A549 human pneumocytes, Toxicology. 253 (2008) 137–146.
[155] J. Muller, F. Huaux, N. Moreau, P. Misson, J.-F. Heilier, M. Delos, M. Arras, A. Fonseca, J.B. Nagy, D. Lison, Respiratory toxicity of multi-wall carbon nanotubes, Toxicology and Applied Pharmacology. 207 (2005) 221–231.
[156] S. Sachar, R.K. Saxena, Cytotoxic effect of poly-dispersed single walled carbon nanotubes on erythrocytes in vitro and in vivo, PLoS One. 6 (2011) e22032.
[157] T.I. Vitkina, V.I. Yankova, T.A. Gvozdenko, V.L. Kuznetsov, D.V. Krasnikov, A.V. Nazarenko, V.V. Chaika, S.V. Smagin, A.M. Tsatsakis, A.B. Engin, S.P. Karakitsios, D.A. Sarigiannis, K.S. Golokhvast, The impact of multi-walled carbon nanotubes with different amount of metallic impurities on immunometabolic parameters in healthy volunteers, Food and Chemical Toxicology. 87 (2016) 138–147. https://doi.org/10.1016/j.fct.2015.11.023.
[158] B.C. Palmer, S.J. Phelan-Dickenson, L.A. DeLouise, Multi-walled carbon nanotube oxidation dependent keratinocyte cytotoxicity and skin inflammation, Part Fibre Toxicol. 16 (2019) 3. https://doi.org/10.1186/s12989-018-0285-x.
[159] X. Wang, R. Qu, J. Liu, Z. Wei, L. Wang, S. Yang, Q. Huang, Z. Wang, Effect of different carbon nanotubes on cadmium toxicity to Daphnia magna: The role of catalyst impurities and adsorption capacity, Environmental Pollution. 208 (2016) 732–738. https://doi.org/10.1016/j.envpol.2015.10.053.
[160] G. Visalli, A. Facciolà, D. Iannazzo, A. Piperno, A. Pistone, A. Di Pietro, The role of the iron catalyst in the toxicity of multi-walled carbon nanotubes (MWCNTs), Journal of Trace Elements in Medicine and Biology. 43 (2017) 153–160. https://doi.org/10.1016/j.jtemb.2017.01.005.
[161] S.H. Lin, L.R. Kleinberg, Carmustine wafers: localized delivery of chemotherapeutic agents in CNS malignancies, Expert Review of Anticancer Therapy. 8 (2008) 343–359.
[162] P. Kleihues, L.H. Sobin, World Health Organization classification of tumors, Cancer. 88 (2000) 2887–2887.

[163] S. Zimm, G.L. Wampler, D. Stablein, T. Hazra, H.F. Young, Intracerebral metastases in solid-tumor patients: natural history and results of treatment, Cancer. 48 (1981) 384–394.
[164] L.J. Schouten, J. Rutten, H.A. Huveneers, A. Twijnstra, Incidence of brain metastases in a cohort of patients with carcinoma of the breast, colon, kidney, and lung and melanoma, Cancer. 94 (2002) 2698–2705.
[165] J.D. Cox, R.A. Yesner, Adenocarcinoma of the lung: recent results from the Veterans Administration Lung Group, American Review of Respiratory Disease. 120 (1979) 1025–1029.
[166] A. Omuro, L.M. DeAngelis, Glioblastoma and other malignant gliomas: a clinical review, Jama. 310 (2013) 1842–1850.
[167] R.W. Chakroun, P. Zhang, R. Lin, P. Schiapparelli, A. Quinones-Hinojosa, H. Cui, Nanotherapeutic systems for local treatment of brain tumors, Wiley Interdisciplinary Reviews: Nanomedicine and Nanobiotechnology. 10 (2018) e1479.
[168] R. Stupp, W.P. Mason, M.J. Van Den Bent, M. Weller, B. Fisher, M.J. Taphoorn, K. Belanger, A.A. Brandes, C. Marosi, U. Bogdahn, Radiotherapy plus concomitant and adjuvant temozolomide for glioblastoma, New England Journal of Medicine. 352 (2005) 987–996.
[169] J. Loeffler, E. Alexander, F.H. Hochberg, P.Y. Wen, J.H. Morris, W.C. Schoene, R.L. Siddon, R.H. Morse, P.M. Black, Clinical patterns of failure following stereotactic interstitial irradiation for malignant gliomas, International Journal of Radiation Oncology• Biology• Physics. 19 (1990) 1455–1462.
[170] D.R. Groothuis, J.M. Fischer, G. Lapin, D.D. Bigner, N.A. Vick, Permeability of different experimental brain tumor models to horseradish peroxidase, Journal of Neuropathology & Experimental Neurology. 41 (1982) 164–185.
[171] H.-L. Liu, M.-Y. Hua, P.-Y. Chen, P.-C. Chu, C.-H. Pan, H.-W. Yang, C.-Y. Huang, J.-J. Wang, T.-C. Yen, K.-C. Wei, Blood-brain barrier disruption with focused ultrasound enhances delivery of chemotherapeutic drugs for glioblastoma treatment, Radiology. 255 (2010) 415–425.
[172] D.R. Groothuis, The blood-brain and blood-tumor barriers: a review of strategies for increasing drug delivery, Neuro-Oncology. 2 (2000) 45–59.
[173] L.W. Pinto, M.B.M. Araújo, A.L. Vettore, L. Wernersbach, A.C.C. Leite, L.M.C. Chimelli, F.A. Soares, Glioblastomas: correlation between oligodendroglial components, genetic abnormalities, and prognosis, Virchows Archiv. 452 (2008) 481–490.
[174] S.H. Ranganath, C.-H. Wang, Biodegradable microfiber implants delivering paclitaxel for post-surgical chemotherapy against malignant glioma, Biomaterials. 29 (2008) 2996–3003.
[175] N.A. Ochekpe, P.O. Olorunfemi, N.C. Ngwuluka, Nanotechnology and drug delivery part 2: nanostructures for drug delivery, Tropical Journal of Pharmaceutical Research. 8 (2009).
[176] M. Zhao, F. Danhier, C. Bastiancich, N. Joudiou, L.P. Ganipineni, N. Tsakiris, B. Gallez, A. des Rieux, A. Jankovski, J. Bianco, Post-resection treatment of glioblastoma with an injectable nanomedicine-loaded photopolymerizable hydrogel induces long-term survival, International Journal of Pharmaceutics. 548 (2018) 522–529.

[177] M. Westphal, D.C. Hilt, E. Bortey, P. Delavault, R. Olivares, P.C. Warnke, I.R. Whittle, J. Jääskeläinen, Z. Ram, A phase 3 trial of local chemotherapy with biodegradable carmustine (BCNU) wafers (Gliadel wafers) in patients with primary malignant glioma., Neuro Oncol. 5 (2003) 79–88. https://doi.org/10.1215/S1522-8517-02-00023-6.
[178] H. Brem, S. Piantadosi, P.C. Burger, M. Walker, R. Selker, N.A. Vick, K. Black, M. Sisti, S. Brem, G. Mohr, P. Muller, R. Morawetz, S.C. Schold, Placebo-controlled trial of safety and efficacy of intraoperative controlled delivery by biodegradable polymers of chemotherapy for recurrent gliomas, The Lancet. 345 (1995) 1008–1012. https://doi.org/10.1016/S0140-6736(95)90755-6.
[179] W. Xiao, Bioengineered scaffolds for 3D culture demonstrate extracellular matrix-mediated mechanisms of chemotherapy resistance in glioblastoma, (n.d.) 19.
[180] W. Xiao, A. Sohrabi, S.K. Seidlits, Integrating the glioblastoma microenvironment into engineered experimental models, Future Sci OA. 3 (2017). https://doi.org/10.4155/fsoa-2016-0094.
[181] F. van Zijl, G. Krupitza, W. Mikulits, Initial steps of metastasis: Cell invasion and endothelial transmigration, Mutat Res. 728 (2011) 23–34. https://doi.org/10.1016/j.mrrev.2011.05.002.
[182] J.B. Kim, R. Stein, M.J. O'Hare, Three-dimensional in vitro tissue culture models of breast cancer — a review, Breast Cancer Res Treat. 85 (2004) 281–291. https://doi.org/10.1023/B:BREA.0000025418.88785.2b.
[183] B.M. Baker, C.S. Chen, Deconstructing the third dimension – how 3D culture microenvironments alter cellular cues, J Cell Sci. 125 (2012) 3015–3024. https://doi.org/10.1242/jcs.079509.
[184] M. Zhang, P. Boughton, B. Rose, C.S. Lee, A.M. Hong, The Use of Porous Scaffold as a Tumor Model, International Journal of Biomaterials. 2013 (2013) e396056. https://doi.org/10.1155/2013/396056.
[185] Z. Liu, K. Yang, S.-T. Lee, Single-walled carbon nanotubes in biomedical imaging, Journal of Materials Chemistry. 21 (2011) 586–598.
[186] Z. Ou, B. Wu, D. Xing, F. Zhou, H. Wang, Y. Tang, Functional single-walled carbon nanotubes based on an integrin $\alpha_v\beta_3$ monoclonal antibody for highly efficient cancer cell targeting, Nanotechnology. 20 (2009) 105102. https://doi.org/10.1088/0957-4484/20/10/105102.
[187] Z. Liu, W. Cai, L. He, N. Nakayama, K. Chen, X. Sun, X. Chen, H. Dai, In vivo biodistribution and highly efficient tumour targeting of carbon nanotubes in mice, Nature Nanotechnology. 2 (2007) 47.
[188] P. Martin, Wound healing--aiming for perfect skin regeneration, Science. 276 (1997) 75–81.
[189] A.J. Singer, R.A. Clark, Cutaneous wound healing, New England Journal of Medicine. 341 (1999) 738–746.
[190] D. Nguyen, D. Orgill, G. Murphy, The pathophysiologic basis for wound healing and cutaneous regeneration, in: Biomaterials for Treating Skin Loss, Elsevier, 2009: pp. 25–57.
[191] G. Han, R. Ceilley, Chronic Wound Healing: A Review of Current Management and Treatments, Adv Ther. 34 (2017) 599–610. https://doi.org/10.1007/s12325-017-0478-y.

[192] A. Kaur, S. Midha, S. Giri, S. Mohanty, Functional Skin Grafts: Where Biomaterials Meet Stem Cells, Stem Cells International. 2019 (2019) e1286054. https://doi.org/10.1155/2019/1286054.
[193] J.F. Burke, I.V. Yannas, W.C. Quinby, C.C. Bondoc, W.K. Jung, Successful use of a physiologically acceptable artificial skin in the treatment of extensive burn injury., Ann Surg. 194 (1981) 413–428.
[194] C.A. Brohem, L.B. da S. Cardeal, M. Tiago, M.S. Soengas, S.B. de M. Barros, S.S. Maria-Engler, Artificial skin in perspective: concepts and applications, Pigment Cell & Melanoma Research. 24 (2011) 35–50. https://doi.org/10.1111/j.1755-148X.2010.00786.x.
[195] H.A. Wallace, B.M. Basehore, P.M. Zito, Wound Healing Phases, in: StatPearls, StatPearls Publishing, Treasure Island (FL), 2020. http://www.ncbi.nlm.nih.gov/books/NBK470443/ (accessed February 17, 2021).
[196] L.G. Bowden, H.M. Byrne, P.K. Maini, D.E. Moulton, A morphoelastic model for dermal wound closure, Biomech Model Mechanobiol. 15 (2016) 663–681. https://doi.org/10.1007/s10237-015-0716-7.
[197] J. Moores, Vitamin C: a wound healing perspective, Br J Community Nurs. Suppl (2013) S6, S8-11. https://doi.org/10.12968/bjcn.2013.18.sup12.s6.
[198] R.A.F. Clark, Wound Repair, in: R.A.F. Clark (Ed.), The Molecular and Cellular Biology of Wound Repair, Springer US, Boston, MA, 1988: pp. 3–50. https://doi.org/10.1007/978-1-4899-0185-9_1.
[199] M. Toriseva, V.-M. Kähäri, Proteinases in cutaneous wound healing, Cell Mol Life Sci. 66 (2009) 203–224. https://doi.org/10.1007/s00018-008-8388-4.
[200] B. Hinz, D. Mastrangelo, C.E. Iselin, C. Chaponnier, G. Gabbiani, Mechanical Tension Controls Granulation Tissue Contractile Activity and Myofibroblast Differentiation, The American Journal of Pathology. 159 (2001) 1009–1020. https://doi.org/10.1016/S0002-9440(10)61776-2.
[201] S. Guo, L.A. DiPietro, Factors Affecting Wound Healing, J Dent Res. 89 (2010) 219–229. https://doi.org/10.1177/0022034509359125.
[202] W.K. Stadelmann, A.G. Digenis, G.R. Tobin, Impediments to wound healing, The American Journal of Surgery. 176 (1998) 39S-47S. https://doi.org/10.1016/S0002-9610(98)00184-6.
[203] Y.S. Choi, I.-H. Sung, J.Y. Lim, A.H. Kyun, E.D. Yeo, S.G. Lee, Y.K. Lee, Evaluation of the Effects of Air Pollutants on Diabetic Wounds, Wounds. 29 (2017) 65–70.
[204] S. Ejaz, I. Chekarova, M. Ahmad, A. Nasir, M. Ashraf, C.W. Lim, Pollution dilemma in Asian population: CNG and wound healing, Environmental Toxicology and Pharmacology. 28 (2009) 323–332. https://doi.org/10.1016/j.etap.2009.05.005.
[205] C. Parrado, S. Mercado-Saenz, A. Perez-Davo, Y. Gilaberte, S. Gonzalez, A. Juarranz, Environmental Stressors on Skin Aging. Mechanistic Insights, Front. Pharmacol. 10 (2019). https://doi.org/10.3389/fphar.2019.00759.
[206] Y. Lim, A.D. Phung, A.M. Corbacho, H.H. Aung, E. Maioli, A.Z. Reznick, C.E. Cross, P.A. Davis, G. Valacchi, Modulation of cutaneous wound healing by ozone: differences between young and aged mice, Toxicology Letters. 160 (2006) 127–134.
[207] M. Pollet, S. Shaik, M. Mescher, K. Frauenstein, J. Tigges, S.A. Braun, K. Sondenheimer, M. Kaveh, A. Bruhs, S. Meller, B. Homey, A. Schwarz, C. Esser,

T. Douki, C.F.A. Vogel, J. Krutmann, T. Haarmann-Stemmann, The AHR represses nucleotide excision repair and apoptosis and contributes to UV-induced skin carcinogenesis, Cell Death & Differentiation. 25 (2018) 1823–1836. https://doi.org/10.1038/s41418-018-0160-1.

[208] P.K. Mandal, Dioxin: a review of its environmental effects and its aryl hydrocarbon receptor biology, J Comp Physiol B. 175 (2005) 221–230. https://doi.org/10.1007/s00360-005-0483-3.

[209] J. Mimura, Y. Fujii-Kuriyama, Functional role of AhR in the expression of toxic effects by TCDD, Biochimica et Biophysica Acta (BBA) - General Subjects. 1619 (2003) 263–268. https://doi.org/10.1016/S0304-4165(02)00485-3.

[210] E. Fritsche, C. Schafer, C. Calles, T. Bernsmann, T. Bernshausen, M. Wurm, U. Hubenthal, J.E. Cline, H. Hajimiragha, P. Schroeder, L.-O. Klotz, A. Rannug, P. Furst, H. Hanenberg, J. Abel, J. Krutmann, Lightening up the UV response by identification of the arylhydrocarbon receptor as a cytoplasmatic target for ultraviolet B radiation, Proceedings of the National Academy of Sciences. 104 (2007) 8851–8856. https://doi.org/10.1073/pnas.0701764104.

[211] M. Furue, A. Hashimoto-Hachiya, G. Tsuji, Aryl Hydrocarbon Receptor in Atopic Dermatitis and Psoriasis, Int J Mol Sci. 20 (2019). https://doi.org/10.3390/ijms20215424.

[212] C. Vogeley, C. Esser, T. Tüting, J. Krutmann, T. Haarmann-Stemmann, Role of the Aryl Hydrocarbon Receptor in Environmentally Induced Skin Aging and Skin Carcinogenesis, Int J Mol Sci. 20 (2019). https://doi.org/10.3390/ijms20236005.

[213] T. Haarmann-Stemmann, C. Esser, J. Krutmann, The Janus-Faced Role of Aryl Hydrocarbon Receptor Signaling in the Skin: Consequences for Prevention and Treatment of Skin Disorders, J Invest Dermatol. 135 (2015) 2572–2576. https://doi.org/10.1038/jid.2015.285.

[214] K. Frauenstein, U. Sydlik, J. Tigges, M. Majora, C. Wiek, H. Hanenberg, J. Abel, C. Esser, E. Fritsche, J. Krutmann, T. Haarmann-Stemmann, Evidence for a novel anti-apoptotic pathway in human keratinocytes involving the aryl hydrocarbon receptor, E2F1, and checkpoint kinase 1, Cell Death & Differentiation. 20 (2013) 1425–1434. https://doi.org/10.1038/cdd.2013.102.

[215] M. Tauchi, A. Hida, T. Negishi, F. Katsuoka, S. Noda, J. Mimura, T. Hosoya, A. Yanaka, H. Aburatani, Y. Fujii-Kuriyama, H. Motohashi, M. Yamamoto, Constitutive Expression of Aryl Hydrocarbon Receptor in Keratinocytes Causes Inflammatory Skin Lesions, MOL. CELL. BIOL. 25 (2005) 10.

[216] R. Kapp, TCDD (2,3,7,8-Tetrachlorodibenzo-p-Dioxin), in: P. Wexler (Ed.), Encyclopedia of Toxicology (Second Edition), Elsevier, New York, 2005: pp. 136–139. https://doi.org/10.1016/B0-12-369400-0/00921-2.

[217] B.A. Vorderstrasse, L.B. Steppan, A.E. Silverstone, N.I. Kerkvliet, Aryl hydrocarbon receptor-deficient mice generate normal immune responses to model antigens and are resistant to TCDD-induced immune suppression, Toxicol Appl Pharmacol. 171 (2001) 157–164. https://doi.org/10.1006/taap.2000.9122.

[218] J.Q. Rose, J.C. Ramsey, T.H. Wentzler, R.A. Hummel, P.J. Gehring, The fate of 2,3,7,8-tetrachlorodibenzo-p-dioxin following single and repeated oral doses to the rat, Toxicology and Applied Pharmacology. 36 (1976) 209–226. https://doi.org/10.1016/0041-008X(76)90001-6.

[219] J.L. Pirkle, W.H. Wolfe, D.G. Patterson, L.L. Needham, J.E. Michalek, J.C. Miner, M.R. Peterson, D.L. Phillips, Estimates of the half-life of 2,3,7,8-tetrachlorodibenzo-p-dioxin in Vietnam veterans of operation ranch hand, Journal of Toxicology and Environmental Health. 27 (1989) 165–171. https://doi.org/10.1080/15287398909531288.
[220] Dioxins and their effects on human health, (n.d.). https://www.who.int/news-room/fact-sheets/detail/dioxins-and-their-effects-on-human-health (accessed April 15, 2020).
[221] D.W. Nebert, T.P. Dalton, A.B. Okey, F.J. Gonzalez, Role of Aryl Hydrocarbon Receptor-mediated Induction of the CYP1 Enzymes in Environmental Toxicity and Cancer, J. Biol. Chem. 279 (2004) 23847–23850. https://doi.org/10.1074/jbc.R400004200.
[222] J. Yin, B. Sheng, Y. Qiu, K. Yang, W. Xiao, H. Yang, Role of AhR in positive regulation of cell proliferation and survival, Cell Prolif. 49 (2016) 554–560. https://doi.org/10.1111/cpr.12282.
[223] E.H. van den Bogaard, J.G.M. Bergboer, M. Vonk-Bergers, I.M.J.J. van Vlijmen-Willems, S.V. Hato, P.G.M. van der Valk, J.M. Schröder, I. Joosten, P.L.J.M. Zeeuwen, J. Schalkwijk, Coal tar induces AHR-dependent skin barrier repair in atopic dermatitis, J. Clin. Invest. (2013) JCI65642. https://doi.org/10.1172/JCI65642.
[224] A. Poland, J.C. Knutson, 2,3,7,8-tetrachlorodibenzo-p-dioxin and related halogenated aromatic hydrocarbons: examination of the mechanism of toxicity, Annu Rev Pharmacol Toxicol. 22 (1982) 517–554. https://doi.org/10.1146/annurev.pa.22.040182.002505.
[225] A.S. Phadnis-Moghe, W. Chen, J. Li, R.B. Crawford, A. Bach, S. D'Ingillo, N. Kovalova, J.E. Suarez-Martinez, B.L.F. Kaplan, J.A. Harrill, R. Budinsky, J.C. Rowlands, R.S. Thomas, N.E. Kaminski, Immunological characterization of the aryl hydrocarbon receptor (AHR) knockout rat in the presence and absence of 2,3,7,8-tetrachlorodibenzo-p-dioxin (TCDD), Toxicology. 368–369 (2016) 172–182. https://doi.org/10.1016/j.tox.2016.08.019.
[226] F. Fiorito, R. Santamaria, C. Irace, L. De Martino, G. Iovane, 2,3,7,8-tetrachlorodibenzo-p-dioxin and the viral infection, Environmental Research. 153 (2017) 27–34. https://doi.org/10.1016/j.envres.2016.11.004.
[227] K. Yoshizawa, A. Heatherly, D.E. Malarkey, N.J. Walker, A. Nyska, A Critical Comparison of Murine Pathology and Epidemiological Data of TCDD, PCB126, and PeCDF, Toxicol Pathol. 35 (2007) 865–879. https://doi.org/10.1080/01926230701618516.
[228] D.W. Nebert, A. Puga, V. Vasiliou, Role of the Ah Receptor and the Dioxin-Inducible [Ah] Gene Battery in Toxicity, Cancer, and Signal Transduction, Ann NY Acad Sci. 685 (1993) 624–640. https://doi.org/10.1111/j.1749-6632.1993.tb35928.x.
[229] C.J. Molloy, M.A. Gallo, J.D. Laskin, Alterations in the expression of specific epidermal keratin markers in the hairless mouse by the topical application of the tumor promoters 2,3,7,8-tetrachlorodibenzo- p -dioxin and the phorbol ester 12-O -tetradecanoylphorbol-13-acetate, Carcinogenesis. 8 (1987) 1193–1199. https://doi.org/10.1093/carcin/8.9.1193.
[230] V. Moirangthem, W.S. Katz, W. Su, E.-Y. Choi, R.C. Dingle, G.M. Zeigler, W.V. Everson, C.D. Jennings, M. Gong, H.I. Swanson, Impact of 2, 3, 7, 8-

tetrachlorodibenzo-p-dioxin on cutaneous wound healing, Experimental and Toxicologic Pathology. 65 (2013) 61–67.
[231] D.N. Das, P.K. Panda, N. Sinha, S. Mukhopadhyay, P.P. Naik, S.K. Bhutia, DNA damage by 2,3,7,8-tetrachlorodibenzo-p-dioxin-induced p53-mediated apoptosis through activation of cytochrome P450/aryl hydrocarbon receptor, Environmental Toxicology and Pharmacology. 55 (2017) 175–185. https://doi.org/10.1016/j.etap.2017.08.012.
[232] S. Perumal Kuppusamy, Telomerase and telomere dysregulation in Polychlorinated Biphenyl (PCB) exposed human skin keratinocytes, Doctor of Philosophy, University of Iowa, 2012. https://doi.org/10.17077/etd.854f3htg.
[233] A. Puga, J. Marlowe, S. Barnes, C. Chang, A. Maier, Z. Tan, J.K. Kerzee, X. Chang, M. Strobeck, E.S. Knudsen, Role of the aryl hydrocarbon receptor in cell cycle regulation, Toxicology. 181–182 (2002) 171–177. https://doi.org/10.1016/s0300-483x(02)00276-7.
[234] H.R. Kim, S.Y. Kang, H.O. Kim, C.W. Park, B.Y. Chung, Role of Aryl Hydrocarbon Receptor Activation and Autophagy in Psoriasis-Related Inflammation, IJMS. 21 (2020) 2195. https://doi.org/10.3390/ijms21062195.
[235] J.M. Carvajal-Gonzalez, A.C. Roman, M.I. Cerezo-Guisado, E.M. Rico-Leo, G. Martin-Partido, P.M. Fernandez-Salguero, Loss of dioxin-receptor expression accelerates wound healing in vivo by a mechanism involving TGF, Journal of Cell Science. 122 (2009) 1823–1833. https://doi.org/10.1242/jcs.047274.
[236] E.L. Woodward, Crosstalk of lysosomes, autophagy and apoptosis in dioxin-induced chloracne in vitro., (n.d.) 238.
[237] 엄미옥, Effects of TCDD on micronucleus formation and cellular factors responsible for toxicity in human cell lines, (2005). http://dspace.ewha.ac.kr/handle/2015.oak/191433 (accessed April 8, 2020).
[238] A. Zamarrón, E. Morel, S. Lucena, M. Mataix, A. Pérez-Davó, C. Parrado, S. González, Extract of Deschampsia antarctica (EDA) Prevents Dermal Cell Damage Induced by UV Radiation and 2,3,7,8-Tetrachlorodibenzo-p-dioxin, IJMS. 20 (2019) 1356. https://doi.org/10.3390/ijms20061356.
[239] S.S. Ray, H.I. Swanson, Alteration of keratinocyte differentiation and senescence by the tumor promoter dioxin☆, Toxicology and Applied Pharmacology. 192 (2003) 131–145. https://doi.org/10.1016/S0041-008X(03)00277-1.
[240] S.S. Ray, H.I. Swanson, Dioxin-induced Immortalization of Normal Human Keratinocytes and Silencing of p53 and p16INK4a, J. Biol. Chem. 279 (2004) 27187–27193. https://doi.org/10.1074/jbc.M402771200.
[241] J.A. Guerrero-Beltr·n, G.V. Barbosa-C·novas, Advantages and Limitations on Processing Foods by UV Light, Food Sci. Technol. Int. 10 (2004) 137–147. https://doi.org/10.1177/1082013204044359.
[242] F. de Gruijl, J. Leun, Environment and health: 3. Ozone depletion and ultraviolet radiation, CMAJ. 163 (2000) 851–855.
[243] J.H. Shim, J.H. Shim, Anti-aging Effects of P7C3 in UVA-irradiated Human Dermal Fibroblasts, Asian J Beauty Cosmetol. 15 (2017) 45–53. https://doi.org/10.20402/ajbc.2016.0094.
[244] Y. Sola, J. Lorente, Contribution of UVA irradiance to the erythema and photoaging effects in solar and sunbed exposures, Journal of Photochemistry

and Photobiology B: Biology. 143 (2015) 5–11. https://doi.org/10.1016/j.jphotobiol.2014.10.024.
[245] J. D'Orazio, S. Jarrett, A. Amaro-Ortiz, T. Scott, UV Radiation and the Skin, Int J Mol Sci. 14 (2013) 12222–12248. https://doi.org/10.3390/ijms140612222.
[246] O. Engelsen, The Relationship between Ultraviolet Radiation Exposure and Vitamin D Status, Nutrients. 2 (2010) 482–495. https://doi.org/10.3390/nu2050482.
[247] IARC, Exposure to Artificial UV Radiation and Skin Cancer, n.d. https://publications.iarc.fr/Book-And-Report-Series/Iarc-Working-Group-Reports/Exposure-To-Artificial-UV-Radiation-And-Skin-Cancer-2006 (accessed January 7, 2021).
[248] K. Biniek, K. Levi, R.H. Dauskardt, Solar UV radiation reduces the barrier function of human skin, PNAS. 109 (2012) 17111–17116. https://doi.org/10.1073/pnas.1206851109.
[249] Y. Matsumura, H.N. Ananthaswamy, Toxic effects of ultraviolet radiation on the skin, Toxicology and Applied Pharmacology. 195 (2004) 298–308.
[250] B.A. Gilchrest, J. Krutmann, Skin Aging, Springer Science & Business Media, 2006.
[251] K.S. Lee, H.J. Cha, G.T. Lee, K.K. Lee, J.T. Hong, K.J. Ahn, I.-S. An, S. An, S. Bae, Troxerutin induces protective effects against ultraviolet B radiation through the alteration of microRNA expression in human HaCaT keratinocyte cells, International Journal of Molecular Medicine. 33 (2014) 934–942.
[252] L. Yildirimer, N.T. Thanh, A.M. Seifalian, Skin regeneration scaffolds: a multimodal bottom-up approach, Trends in Biotechnology. 30 (2012) 638–648.
[253] A. Hassanshahi, M. Hassanshahi, S. Khabbazi, Z. Hosseini-Khah, Y. Peymanfar, S. Ghalamkari, Y.-W. Su, C.J. Xian, Adipose-derived stem cells for wound healing, Journal of Cellular Physiology. 234 (2019) 7903–7914. https://doi.org/10.1002/jcp.27922.
[254] S.T. Boyce, R.J. Kagan, D.G. Greenhalgh, P. Warner, K.P. Yakuboff, T. Palmieri, G.D. Warden, Cultured skin substitutes reduce requirements for harvesting of skin autograft for closure of excised, full-thickness burns, J Trauma. 60 (2006) 821–829. https://doi.org/10.1097/01.ta.0000196802.91829.cc.
[255] S. Dixit, D.R. Baganizi, R. Sahu, E. Dosunmu, A. Chaudhari, K. Vig, S.R. Pillai, S.R. Singh, V.A. Dennis, Immunological challenges associated with artificial skin grafts: available solutions and stem cells in future design of synthetic skin, Journal of Biological Engineering. 11 (2017) 49. https://doi.org/10.1186/s13036-017-0089-9.
[256] M.E. Braza, M.P. Fahrenkopf, Split-Thickness Skin Grafts, in: StatPearls, StatPearls Publishing, Treasure Island (FL), 2020. http://www.ncbi.nlm.nih.gov/books/NBK551561/ (accessed February 17, 2021).
[257] R.E. Horch, M.G. Jeschke, G. Spilker, D.N. Herndon, J. Kopp, Treatment of second degree facial burns with allografts—preliminary results, Burns. 31 (2005) 597–602. https://doi.org/10.1016/j.burns.2005.01.011.
[258] K.H. Lee, Tissue-engineered human living skin substitutes: development and clinical application, Yonsei Med J. 41 (2000) 774–779. https://doi.org/10.3349/ymj.2000.41.6.774.

[259] L. Alrubaiy, K.K. Al-Rubaiy, Skin Substitutes: A Brief Review of Types and Clinical Applications, Oman Med J. 24 (2009) 4–6. https://doi.org/10.5001/omj.2009.2.
[260] D.M. Supp, S.T. Boyce, Engineered skin substitutes: practices and potentials, Clinics in Dermatology. 23 (2005) 403–412.
[261] C.E. Butler, D.P. Orgill, Simultaneous in vivo regeneration of neodermis, epidermis, and basement membrane, in: Regenerative Medicine II, Springer, 2005: pp. 23–41.
[262] M. Romanelli, E. Kaha, H. Stege, J. Wnorowski, P. Vowden, H. Majamaa, J. Lazaro, Effect of amelogenin extracellular matrix protein and compression on hard-to-heal venous leg ulcers: follow-up data, Journal of Wound Care. 17 (2008) 17–23.
[263] U. Mirastschuski, D. Konrad, E. Lundberg, S.P. Lyngstadaas, L.N. Jorgensen, M.S. Ågren, Effects of a topical enamel matrix derivative on skin wound healing, Wound Repair and Regeneration. 12 (2004) 100–108.
[264] E.N. Mostow, G.D. Haraway, M. Dalsing, J.P. Hodde, D. King, OASIS Venus Ulcer Study Group, Effectiveness of an extracellular matrix graft (OASIS Wound Matrix) in the treatment of chronic leg ulcers: a randomized clinical trial, Journal of Vascular Surgery. 41 (2005) 837–843.
[265] L.T. Smith, K.A. Holbrook, J.A. Madri, Collagen types I, III, and V in human embryonic and fetal skin, American Journal of Anatomy. 175 (1986) 507–521.
[266] S.A. Brigido, The use of an acellular dermal regenerative tissue matrix in the treatment of lower extremity wounds: a prospective 16-week pilot study, International Wound Journal. 3 (2006) 181–187.
[267] N.J. Turner, S.F. Badylak, The use of biologic scaffolds in the treatment of chronic nonhealing wounds, Advances in Wound Care. 4 (2015) 490–500.
[268] Y. Har-el, J.A. Gerstenhaber, R. Brodsky, R.B. Huneke, P.I. Lelkes, Electrospun soy protein scaffolds as wound dressings: Enhanced reepithelialization in a porcine model of wound healing, Wound Medicine. 5 (2014) 9–15. https://doi.org/10.1016/j.wndm.2014.04.007.
[269] M. Bravo-Sanchez, T.J. Simmons, M. Vidal, Liquid crystal behavior of single wall carbon nanotubes, Carbon. 48 (2010) 3531–3542.
[270] R.A. MacDonald, B.F. Laurenzi, G. Viswanathan, P.M. Ajayan, J.P. Stegemann, Collagen–carbon nanotube composite materials as scaffolds in tissue engineering, Journal of Biomedical Materials Research Part A: An Official Journal of The Society for Biomaterials, The Japanese Society for Biomaterials, and The Australian Society for Biomaterials and the Korean Society for Biomaterials. 74 (2005) 489–496.
[271] E. Jan, N.A. Kotov, Successful differentiation of mouse neural stem cells on layer-by-layer assembled single-walled carbon nanotube composite, Nano Letters. 7 (2007) 1123–1128.
[272] J.A. Matthews, G.E. Wnek, D.G. Simpson, G.L. Bowlin, Electrospinning of collagen nanofibers, Biomacromolecules. 3 (2002) 232–238.
[273] P.J. Glatkowski, J.W. Piché, J.L. Conroy, R. Bolduc, P. LaBlanc, (54) NANOTUBE BASED SUNSCREEN, (n.d.) 13.
[274] K. Murphy, C. Weaver, Janeway's Immunobiology, Garland Science, 2016.

[275] C.-A. Siegrist, Chapter 2 - Vaccine immunology, in: S.A. Plotkin, W.A. Orenstein, P.A. Offit (Eds.), Vaccines (Fifth Edition), W.B. Saunders, Edinburgh, 2008: pp. 17–36. https://doi.org/10.1016/B978-1-4160-3611-1.50006-4.
[276] M. Seifert, R. Küppers, Human memory B cells, Leukemia. 30 (2016) 2283–2292. https://doi.org/10.1038/leu.2016.226.
[277] F.C. USHER, S.A. WALLACE, Tissue Reaction to Plastics: A Comparison of Nylon, Orlon, Dacron, Teflon, and Marlex, A.M.A. Archives of Surgery. 76 (1958) 997–999. https://doi.org/10.1001/archsurg.1958.01280240155026.
[278] J. Cohen, Assay of Foreign-Body Reaction, The Journal of Bone & Joint Surgery. 41 (1959) 152–166.
[279] R. Marchant, A. Hiltner, C. Hamlin, A. Rabinovitch, R. Slobodkin, J.M. Anderson, In vivo biocompatibility studies. I. The cage implant system and a biodegradable hydrogel, Journal of Biomedical Materials Research. 17 (1983) 301–325. https://doi.org/10.1002/jbm.820170209.
[280] S. Jhunjhunwala, S. Aresta-DaSilva, K. Tang, D. Alvarez, M.J. Webber, B.C. Tang, D.M. Lavin, O. Veiseh, J.C. Doloff, S. Bose, A. Vegas, M. Ma, G. Sahay, A. Chiu, A. Bader, E. Langan, S. Siebert, J. Li, D.L. Greiner, P.E. Newburger, U.H. von Andrian, R. Langer, D.G. Anderson, Neutrophil Responses to Sterile Implant Materials, PLOS ONE. 10 (2015) e0137550. https://doi.org/10.1371/journal.pone.0137550.
[281] G. Niccoli, C. Calvieri, S. Minelli, G. Copponi, R.A. Montone, A. Imaeva, M. Roberto, N. Cosentino, F. Crea, Permanent polymer of drug eluting stents increases eosinophil cationic protein levels following percutaneous coronary intervention independently of C-reactive protein, Atherosclerosis. 237 (2014) 816–820. https://doi.org/10.1016/j.atherosclerosis.2014.11.002.
[282] Z. Wang, Y. Cui, J. Wang, X. Yang, Y. Wu, K. Wang, X. Gao, D. Li, Y. Li, X.-L. Zheng, Y. Zhu, D. Kong, Q. Zhao, The effect of thick fibers and large pores of electrospun poly(ε-caprolactone) vascular grafts on macrophage polarization and arterial regeneration, Biomaterials. 35 (2014) 5700–5710. https://doi.org/10.1016/j.biomaterials.2014.03.078.
[283] J.C. Sunshine, J.J. Green, Nanoengineering approaches to the design of artificial antigen-presenting cells, Nanomedicine. 8 (2013) 1173–1189. https://doi.org/10.2217/nnm.13.98.
[284] W. Bai, Y. Chen, P. Sun, A. Gao, Downregulation of B-cell lymphoma/leukemia-2 by overexpressed microRNA 34a enhanced titanium dioxide nanoparticle-induced autophagy in BEAS-2B cells, International Journal of Nanomedicine. 11 (2016) 1959–1971. https://doi.org/10.2147/IJN.S99945.
[285] J.E. Vela Ramirez, L.T. Tygrett, J. Hao, H.H. Habte, M.W. Cho, N.S. Greenspan, T.J. Waldschmidt, B. Narasimhan, Polyanhydride Nanovaccines Induce Germinal Center B Cell Formation and Sustained Serum Antibody Responses, Journal of Biomedical Nanotechnology. 12 (2016) 1303–1311. https://doi.org/10.1166/jbn.2016.2242.
[286] Y.P.S. Goh, N.C. Henderson, J.E. Heredia, A.R. Eagle, J.I. Odegaard, N. Lehwald, K.D. Nguyen, D. Sheppard, L. Mukundan, R.M. Locksley, A. Chawla, Eosinophils secrete IL-4 to facilitate liver regeneration, PNAS. 110 (2013) 9914–9919. https://doi.org/10.1073/pnas.1304046110.
[287] V. Salmon-Ehr, L. Ramont, G. Godeau, P. Birembaut, M. Guenounou, P. Bernard, F.-X. Maquart, Implication of Interleukin-4 in Wound Healing,

Laboratory Investigation. 80 (2000) 1337–1343. https://doi.org/10.1038/labinvest.3780141.
[288] J. Pontén, E.H. Macintyre, Long Term Culture of Normal and Neoplastic Human Glia, Acta Pathologica Microbiologica Scandinavica. 74 (1968) 465–486. https://doi.org/10.1111/j.1699-0463.1968.tb03502.x.
[289] G. Beckman, L. Beckman, J. Pontén, B. Westermark, G-6-PD and PGM Phenotypes of 16 Continuous Human Tumor Cell Lines, HHE. 21 (1971) 238–241. https://doi.org/10.1159/000152408.
[290] A. Das, N.L. Banik, S.K. Ray, Flavonoids activated caspases for apoptosis in human glioblastoma T98G and U87MG cells but not in human normal astrocytes, Cancer. 116 (2010) 164–176. https://doi.org/10.1002/cncr.24699.
[291] S. Puli, J.C.K. Lai, A. Bhushan, Inhibition of matrix degrading enzymes and invasion in human glioblastoma (U87MG) Cells by isoflavones, J Neurooncol. 79 (2006) 135–142. https://doi.org/10.1007/s11060-006-9126-0.
[292] P. Boukamp, R.T. Petrussevska, D. Breitkreutz, J. Hornung, A. Markham, N.E. Fusenig, Normal keratinization in a spontaneously immortalized aneuploid human keratinocyte cell line., The Journal of Cell Biology. 106 (1988) 761–771.
[293] N.E. Fusenig, P. Boukamp, D. Breitkreutz, A. Hülsen, S. Petrusevska, P. Cerutti, E. Stanbridge, In vitro transformation of human skin epithelial cells: Role of RAS oncogene in malignant progression, Toxicology in Vitro. 4 (1990) 627–634. https://doi.org/10.1016/0887-2333(90)90132-D.
[294] J.C. Boyer, W.K. Kaufmann, M. Cordeiro-Stone, Role of Postreplication Repair in Transformation of Human Fibroblasts to Anchorage Independence, (n.d.) 6.
[295] T.P. Heffernan, D.A. Simpson, A.R. Frank, A.N. Heinloth, R.S. Paules, M. Cordeiro-Stone, W.K. Kaufmann, An ATR- and Chk1-Dependent S Checkpoint Inhibits Replicon Initiation following UVC-Induced DNA Damage, MCB. 22 (2002) 8552–8561. https://doi.org/10.1128/MCB.22.24.8552-8561.2002.
[296] A. Cerutti, H. Zan, A. Schaffer, L. Bergsagel, N. Harindranath, E.E. Max, P. Casali, CD40 Ligand and Appropriate Cytokines Induce Switching to IgG, IgA, and IgE and Coordinated Germinal Center and Plasmacytoid Phenotypic Differentiation in a Human Monoclonal IgM+IgD+ B Cell Line, J Immunol. 160 (1998) 2145–2157.
[297] R.M. Bernstein, F.C. Mills, M. Mitchell, E.E. Max, Complex mechanisms for inhibition of immunoglobulin gene expression in a germinal center B cell line, Molecular Immunology. 41 (2004) 63–72. https://doi.org/10.1016/j.molimm.2004.01.005.
[298] O. Saiki, P. Ralph, Clonal differences in response to T cell replacing factor (TRF) for IgM secretion and TRF receptors in a human B lymphoblast cell line, Eur. J. Immunol. 13 (1983) 31–34. https://doi.org/10.1002/eji.1830130108.
[299] P. Ralph, O. Saiki, D.H. Maurer, K. Welte, IgM and IgG secretion in human B-cell lines regulated by B-cell-inducing factors (BIF) and phorbol ester, Immunology Letters. 7 (1983) 17–23. https://doi.org/10.1016/0165-2478(83)90049-4.
[300] P. Ralph, G. Jeong, K. Welte, R. Mertelsmann, H. Rabin, L.E. Henderson, L.M. Souza, T.C. Boone, R.J. Robb, Stimulation of immunoglobulin secretion in human B lymphocytes as a direct effect of high concentrations of IL 2., The Journal of Immunology. 133 (1984) 2442–2445.
[301] C.-M. Chen, M. Chen, Y.-W. Peng, C.-H. Lin, L.-W. Chang, C.-F. Chen, Microwave digestion and acidic treatment procedures for the purification of

multi-walled carbon nanotubes, Diamond and Related Materials. 14 (2005) 798–803.
[302] S.M. Mukhopadhyay, R.V. Pulikollu, E. Ripberger, A.K. Roy, Surface modification of graphitic foam, Journal of Applied Physics. 93 (2003) 878–882.
[303] G. Jones, S.H. Cartmell, Optimization of Cell Seeding Efficiencies on a Three-Dimensional Gelatin Scaffold for Bone Tissue Engineering, Journal of Applied Biomaterials and Biomechanics. 4 (2006) 172–180. https://doi.org/10.1177/228080000600400306.
[304] D. DONJERKOVIć, D.W. Scott, Activation-induced cell death in B lymphocytes, Cell Research. 10 (2000) 179–192. https://doi.org/10.1038/sj.cr.7290047.
[305] W. Jia, X. Jiang, W. Liu, L. Wang, B. Zhu, H. Zhu, X. Liu, M. Zhong, D. Xie, W. Huang, Effects of three-dimensional collagen scaffolds on the expression profiles and biological functions of glioma cells, International Journal of Oncology. 52 (2018) 1787–1800.
[306] C. Bradford, R. Freeman, S.L. Percival, In Vitro Study of Sustained Antimicrobial Activity of a New Silver Alginate Dressing, The Journal of the American College of Certified Wound Specialists. 1 (2009) 117–120. https://doi.org/10.1016/j.jcws.2009.09.001.
[307] L. Mu, J. Tang, H. Liu, C. Shen, M. Rong, Z. Zhang, R. Lai, A potential wound-healing-promoting peptide from salamander skin, FASEB J. 28 (2014) 3919–3929. https://doi.org/10.1096/fj.13-248476.
[308] J. Miao, R.C. Pangule, E.E. Paskaleva, E.E. Hwang, R.S. Kane, R.J. Linhardt, J.S. Dordick, Lysostaphin-functionalized cellulose fibers with antistaphylococcal activity for wound healing applications, Biomaterials. 32 (2011) 9557–9567. https://doi.org/10.1016/j.biomaterials.2011.08.080.
[309] K. Cendrowski, M. Jedrzejczak-Silicka, Carbon nanotubes with controlled length – preparation, characterization and their cytocompatibility effects, Polish Journal of Chemical Technology. 20 (2018) 71–79. https://doi.org/10.2478/pjct-2018-0025.
[310] M. Markovic, J. Van Hoorick, K. Hölzl, M. Tromayer, P. Gruber, S. Nürnberger, P. Dubruel, S. Van Vlierberghe, R. Liska, A. Ovsianikov, Hybrid Tissue Engineering Scaffolds by Combination of Three-Dimensional Printing and Cell Photoencapsulation, Journal of Nanotechnology in Engineering and Medicine. 6 (2015) 021001. https://doi.org/10.1115/1.4031466.
[311] H.-M. Wang, Y.-T. Chou, Z.-H. Wen, Z.-R. Wang, C.-H. Chen, M.-L. Ho, Novel Biodegradable Porous Scaffold Applied to Skin Regeneration, PLoS ONE. 8 (2013) e56330. https://doi.org/10.1371/journal.pone.0056330.
[312] L. Tang, W. Wu, W. Fu, Y. Hu, The effects of phototherapy and melanocytes on keratinocytes, Exp Ther Med. 15 (2018) 3459–3466. https://doi.org/10.3892/etm.2018.5807.
[313] S.M. Oliveira, W. Song, N.M. Alves, J.F. Mano, Chemical modification of bioinspired superhydrophobic polystyrene surfaces to control cell attachment/proliferation, Soft Matter. 7 (2011) 8932–8941.
[314] S. Bhowmick, D. Scharnweber, V. Koul, Co-cultivation of keratinocyte-human mesenchymal stem cell (hMSC) on sericin loaded electrospun nanofibrous composite scaffold (cationic gelatin/hyaluronan/chondroitin sulfate) stimulates epithelial differentiation in hMSCs: In vitro study, Biomaterials. 88 (2016) 83–96. https://doi.org/10.1016/j.biomaterials.2016.02.034.

[315] Y.-J. Lee, W.-W. Chang, C.-P. Chang, T.-Y. Liu, C.-Y. Chuang, K. Qian, Y.G. Zheng, C. Li, Downregulation of PRMT1 promotes the senescence and migration of a non- MYCN amplified neuroblastoma SK-N-SH cells, Scientific Reports. 9 (2019) 1771. https://doi.org/10.1038/s41598-018-38394-6.
[316] A. Kanda, K. Noda, I. Hirose, S. Ishida, TGF-β-SNAIL axis induces Müller glial-mesenchymal transition in the pathogenesis of idiopathic epiretinal membrane, Scientific Reports. 9 (2019) 673. https://doi.org/10.1038/s41598-018-36917-9.
[317] O.A. Oyebanji, Topical Photodynamic Therapy Generates Microvesicle Particles, Wright State University, 2020. https://etd.ohiolink.edu/apexprod/rws_olink/r/1501/10?clear=10&p10_accession_num=wright1591035785031408 (accessed February 8, 2021).
[318] C.E.W. Sulentic, M.P. Holsapple, N.E. Kaminski, Aryl Hydrocarbon Receptor-Dependent Suppression by 2,3,7,8-Tetrachlorodibenzo-p-dioxin of IgM Secretion in Activated B Cells, Mol Pharmacol. 53 (1998) 623–629. https://doi.org/10.1124/mol.53.4.623.
[319] W.R. Otto, Fluorimetric DNA Assay of Cell Number, in: K. Turksen (Ed.), Epidermal Cells: Methods and Protocols, Humana Press, Totowa, NJ, 2005: pp. 251–262. https://doi.org/10.1385/1-59259-830-7:251.
[320] M.K. Trivedi, A. Branton, D. Trivedi, G. Nayak, M. Gangwar, S. Jana, Wound Healing Potential of Biofield Energy Treatment in HaCaT Cell Line Using Scratch Assay, (n.d.) 8.
[321] P. Bhushan, Y. Umasankar, J.D. Hutcheson, S. Bhansali, Toxicity assessment of wearable wound sensor constituents on keratinocytes, Toxicology in Vitro. 58 (2019) 170–177. https://doi.org/10.1016/j.tiv.2019.03.034.
[322] K. Kostarelos, The long and short of carbon nanotube toxicity, Nat Biotechnol. 26 (2008) 774–776. https://doi.org/10.1038/nbt0708-774.
[323] B. Mendoza-Novelo, J.L. Mata-Mata, A. Vega-González, J.V. Cauich-Rodríguez, Á. Marcos-Fernández, Synthesis and characterization of protected oligourethanes as crosslinkers of collagen-based scaffolds, J. Mater. Chem. B. 2 (2014) 2874–2882. https://doi.org/10.1039/C3TB21832E.
[324] N.P. Shah, N.M. Patel, P.K. Patel, Impact of Steam and Gamma Processing on Extractable, International Journal for Scientific Research and Development. 1 (2013) 527–528.
[325] S.K. Manna, S. Sarkar, J. Barr, K. Wise, E.V. Barrera, O. Jejelowo, A.C. Rice-Ficht, G.T. Ramesh, Single-Walled Carbon Nanotube Induces Oxidative Stress and Activates Nuclear Transcription Factor-κB in Human Keratinocytes, Nano Lett. 5 (2005) 1676–1684. https://doi.org/10.1021/nl0507966.
[326] N.A. Monteiro-Riviere, A.O. Inman, Y.Y. Wang, R.J. Nemanich, Surfactant effects on carbon nanotube interactions with human keratinocytes, Nanomedicine: Nanotechnology, Biology and Medicine. 1 (2005) 293–299. https://doi.org/10.1016/j.nano.2005.10.007.
[327] Use of International Standard ISO 10993-1, “Biological evaluation of medical devices - Part 1: Evaluation and testing within a risk management process” - Guidance for Industry and Food and Drug Administration Staff, (n.d.) 68.
[328] J.B. Lutz, C.L. Zehrer, S.E. Solfest, S.-A. Walters, A new in vivo test method to compare wound dressing fluid handling characteristics and wear time, Ostomy Wound Manage. 57 (2011) 28–36.
[329] J. Naderi, M. Hung, S. Pandey, Oxidative stress-induced apoptosis in dividing fibroblasts involves activation of p38 MAP kinase and over-expression of Bax:

Resistance of quiescent cells to oxidative stress, Apoptosis. 8 (2003) 91–100. https://doi.org/10.1023/A:1021657220843.
[330] T.J. Mitchison, The proliferation rate paradox in antimitotic chemotherapy, Mol Biol Cell. 23 (2012) 1–6. https://doi.org/10.1091/mbc.E10-04-0335.
[331] J.-P. Boissel, D. Ohly, M. Bros, U. Gödtel-Armbrust, U. Förstermann, S. Frank, The Neuronal Nitric Oxide Synthase Is Upregulated in Mouse Skin Repair and in Response to Epidermal Growth Factor in Human HaCaT Keratinocytes, Journal of Investigative Dermatology. 123 (2004) 132–139. https://doi.org/10.1111/j.0022-202X.2004.22731.x.
[332] U. Pharmacopeia, 87> Biological reactivity tests, Vitro. USP, Rockville, MD, USA. (2015).
[333] P. Bainbridge, Wound healing and the role of fibroblasts, Journal of Wound Care. 22 (2013) 407–411. https://doi.org/10.12968/jowc.2013.22.8.407.
[334] M. Ichihashi, H. Ando, The maximal cumulative solar UVB dose allowed to maintain healthy and young skin and prevent premature photoaging, Experimental Dermatology. 23 (2014) 43–46. https://doi.org/10.1111/exd.12393.
[335] R.R. Allison, H.C. Mota, C.H. Sibata, Clinical PD/PDT in North America: An historical review, Photodiagnosis and Photodynamic Therapy. 1 (2004) 263–277. https://doi.org/10.1016/S1572-1000(04)00084-5.
[336] P. Huang, J. Lin, D. Yang, C. Zhang, Z. Li, D. Cui, Photosensitizer-loaded dendrimer-modified multi-walled carbon nanotubes for photodynamic therapy, Journal of Controlled Release. 152 (2011). https://doi.org/10.1016/j.jconrel.2011.08.105.
[337] L. Wang, J. Shi, R. Liu, Y. Liu, J. Zhang, X. Yu, J. Gao, C. Zhang, Z. Zhang, Photodynamic effect of functionalized single-walled carbon nanotubes: a potential sensitizer for photodynamic therapy, Nanoscale. 6 (2014) 4642–4651. https://doi.org/10.1039/C3NR06835H.
[338] J. Charles A Janeway, P. Travers, M. Walport, M.J. Shlomchik, The distribution and functions of immunoglobulin isotypes, Immunobiology: The Immune System in Health and Disease. 5th Edition. (2001). https://www.ncbi.nlm.nih.gov/books/NBK27162/ (accessed February 1, 2021).
[339] M.J. Feige, S. Groscurth, M. Marcinowski, Y. Shimizu, H. Kessler, L.M. Hendershot, J. Buchner, An Unfolded CH1 Domain Controls the Assembly and Secretion of IgG Antibodies, Molecular Cell. 34 (2009) 569–579. https://doi.org/10.1016/j.molcel.2009.04.028.
[340] J. Simon, E. Flahaut, M. Golzio, Overview of Carbon Nanotubes for Biomedical Applications, Materials (Basel). 12 (2019). https://doi.org/10.3390/ma12040624.
[341] S. Bellucci, M. Chiaretti, P. Onorato, F. Rossella, M.S. Grandi, P. Galinetto, I. Sacco, F. Micciulla, Micro-Raman study of the role of sterilization on carbon nanotubes for biomedical applications, Https://Doi.Org/10.2217/Nnm.09.100. (2010). https://doi.org/10.2217/nnm.09.100.
[342] M.A. Correa-Duarte, N. Wagner, J. Rojas-Chapana, C. Morsczeck, M. Thie, M. Giersig, Fabrication and biocompatibility of carbon nanotube-based 3D networks as scaffolds for cell seeding and growth, Nano Letters. 4 (2004) 2233–2236.
[343] S. Kuramitsu, K. Motomura, A. Natsume, T. Wakabayashi, Double-edged Sword in the Placement of Carmustine (BCNU) Wafers along the Eloquent Area: A

Case Report, NMC Case Rep J. 2 (2014) 40–45. https://doi.org/10.2176/nmccrj.2014-0025.
[344] W. Song, D.D. Veiga, C.A. Custódio, J.F. Mano, Bioinspired degradable substrates with extreme wettability properties, Advanced Materials. 21 (2009) 1830–1834.
[345] S. Bauer, J. Park, K. von der Mark, P. Schmuki, Improved attachment of mesenchymal stem cells on super-hydrophobic TiO2 nanotubes, Acta Biomaterialia. 4 (2008) 1576–1582.
[346] N.M. Alves, J. Shi, E. Oramas, J.L. Santos, H. Tomás, J.F. Mano, Bioinspired superhydrophobic poly (L-lactic acid) surfaces control bone marrow derived cells adhesion and proliferation, Journal of Biomedical Materials Research Part A: An Official Journal of The Society for Biomaterials, The Japanese Society for Biomaterials, and The Australian Society for Biomaterials and the Korean Society for Biomaterials. 91 (2009) 480–488.
[347] Y. Arima, H. Iwata, Effect of wettability and surface functional groups on protein adsorption and cell adhesion using well-defined mixed self-assembled monolayers, Biomaterials. 28 (2007) 3074–3082.
[348] A. Martins, E.D. Pinho, S. Faria, I. Pashkuleva, A.P. Marques, R.L. Reis, N.M. Neves, Surface modification of electrospun polycaprolactone nanofiber meshes by plasma treatment to enhance biological performance, Small. 5 (2009) 1195–1206.
[349] Y. Koc, A.J. de Mello, G. McHale, M.I. Newton, P. Roach, N.J. Shirtcliffe, Nano-scale superhydrophobicity: suppression of protein adsorption and promotion of flow-induced detachment, Lab on a Chip. 8 (2008) 582–586.
[350] M. Lampin, R. Warocquier-Clérout, C. Legris, M. Degrange, M. Sigot-Luizard, Correlation between substratum roughness and wettability, cell adhesion, and cell migration, Journal of Biomedical Materials Research: An Official Journal of The Society for Biomaterials and The Japanese Society for Biomaterials. 36 (1997) 99–108.
[351] S. MacNeil, Progress and opportunities for tissue-engineered skin, Nature. 445 (2007) 874–880. https://doi.org/10.1038/nature05664.
[352] I.V. Yannas, J.F. Burke, D.P. Orgill, E.M. Skrabut, Wound tissue can utilize a polymeric template to synthesize a functional extension of skin, Science. 215 (1982) 174–176. https://doi.org/10.1126/science.7031899.
[353] F.A. Murphy, C.A. Poland, R. Duffin, K. Donaldson, Length-dependent pleural inflammation and parietal pleural responses after deposition of carbon nanotubes in the pulmonary airspaces of mice, Nanotoxicology. 7 (2012) 1157–1167. https://doi.org/10.3109/17435390.2012.713527.
[354] T.R. Fadel, F.A. Sharp, N. Vudattu, R. Ragheb, J. Garyu, D. Kim, E. Hong, N. Li, G.L. Haller, L.D. Pfefferle, S. Justesen, K.C. Herold, T.M. Fahmy, A carbon nanotube–polymer composite for T-cell therapy, Nature Nanotech. 9 (2014) 639–647. https://doi.org/10.1038/nnano.2014.154.
[355] T.S. Dutt, R.K. Saxena, Activation of T and B lymphocytes Induces Increased Uptake of Poly-Dispersed Single-Walled Carbon Nanotubes and Enhanced Cytotoxicity, 4 (2019) 11.
[356] M. Orecchioni, D. Bedognetti, F. Sgarrella, F.M. Marincola, A. Bianco, L. Delogu, Impact of carbon nanotubes and graphene on immune cells, J Transl Med. 12 (2014) 138. https://doi.org/10.1186/1479-5876-12-138.

[357] M.I. Vazquez, J. Catalan-Dibene, A. Zlotnik, B cells responses and cytokine production are regulated by their immune microenvironment, Cytokine. 74 (2015) 318–326. https://doi.org/10.1016/j.cyto.2015.02.007.
[358] J.H. Lee, G. Khang, J.W. Lee, H.B. Lee, Interaction of different types of cells on polymer surfaces with wettability gradient, Journal of Colloid and Interface Science. 205 (1998) 323–330.
[359] W. Song, J.F. Mano, Interactions between cells or proteins and surfaces exhibiting extreme wettabilities, Soft Matter. 9 (2013) 2985–2999.
[360] L. Meng, R. Chen, A. Jiang, L. Wang, P. Wang, C. Li, R. Bai, Y. Zhao, H. Autrup, C. Chen, Short Multiwall Carbon Nanotubes Promote Neuronal Differentiation of PC12 Cells via Up-Regulation of the Neurotrophin Signaling Pathway, Small. 9 (2013) 1786–1798. https://doi.org/10.1002/smll.201201388.
[361] C.H. Arnott, K.A. Scott, R.J. Moore, S.C. Robinson, R.G. Thompson, F.R. Balkwill, Expression of both TNF-alpha receptor subtypes is essential for optimal skin tumour development, Oncogene. 23 (2004) 1902–1910. https://doi.org/10.1038/sj.onc.1207317.
[362] H. Bachelez, Immunopathogenesis of psoriasis: recent insights on the role of adaptive and innate immunity, J Autoimmun. 25 Suppl (2005) 69–73. https://doi.org/10.1016/j.jaut.2005.09.025.
[363] K. Bahar-Shany, A. Ravid, R. Koren, Upregulation of MMP-9 production by TNFalpha in keratinocytes and its attenuation by vitamin D, J Cell Physiol. 222 (2010) 729–737. https://doi.org/10.1002/jcp.22004.
[364] M. Pasparakis, I. Haase, F.O. Nestle, Mechanisms regulating skin immunity and inflammation, Nat Rev Immunol. 14 (2014) 289–301. https://doi.org/10.1038/nri3646.
[365] Advances in Immunology, Academic Press, 1995.
[366] N. Yawalkar, G.G. Tscharner, R.E. Hunger, A.S. Hassan, Increased expression of IL-12p70 and IL-23 by multiple dendritic cell and macrophage subsets in plaque psoriasis, J Dermatol Sci. 54 (2009) 99–105. https://doi.org/10.1016/j.jdermsci.2009.01.003.
[367] L. Fusco, M. Pelin, S. Mukherjee, S. Keshavan, S. Sosa, C. Martín, V. González, E. Vázquez, M. Prato, B. Fadeel, A. Tubaro, Keratinocytes are capable of selectively sensing low amounts of graphene-based materials: Implications for cutaneous applications, Carbon. 159 (2020) 598–610. https://doi.org/10.1016/j.carbon.2019.12.064.
[368] H. Hwang, S.-Y. Choi, T.Y. Kim, IL-4 suppresses UVB-induced apoptosis in skin, J Biochem Mol Biol. 40 (2007) 36–43. https://doi.org/10.5483/bmbrep.2007.40.1.036.
[369] V. Lovat, D. Pantarotto, L. Lagostena, B. Cacciari, M. Grandolfo, M. Righi, G. Spalluto, M. Prato, L. Ballerini, Carbon nanotube substrates boost neuronal electrical signaling, Nano Letters. 5 (2005) 1107–1110.
[370] N. Saito, Y. Usui, K. Aoki, N. Narita, M. Shimizu, K. Hara, N. Ogiwara, K. Nakamura, N. Ishigaki, H. Kato, S. Taruta, M. Endo, Carbon nanotubes: biomaterial applications, Chem. Soc. Rev. 38 (2009) 1897. https://doi.org/10.1039/b804822n.
[371] C.M. Hwang, S. Sant, M. Masaeli, N.N. Kachouie, B. Zamanian, S.-H. Lee, A. Khademhosseini, Fabrication of three-dimensional porous cell-laden hydrogel for tissue engineering, Biofabrication. 2 (2010) 035003.